BAYESIAN BASED RISK STRATIFICATION OF ATRIAL FIBRILLATION IN CORONARY ARTERY BYPASS GRAFT PATIENTS

A Dissertation
Presented to
The Academic Faculty

By

Matthew Corbin Wiggins

In partial Fulfillment
Of the Requirements for the Degree
Doctor of Philosophy in Bioengineering

Georgia Institute of Technology

August, 2007

BAYESIAN BASED RISK STRATIFICATION OF ATRIAL FIBRILLATION IN CORONARY ARTERY BYPASS GRAFT PATIENTS

Approved By

Dr. George Vachtsevanos
School of Electrical and Computer Engineering
Georgia Institute of Technology

Dr. Brian Litt
Department of Bioengineering
Hospital of the University of Pennsylvania

Dr. Robert Butera
School of Electrical and Computer Engineering
Georgia Institute of Technology

Dr. A. Bruno Frazier
School of Electrical and Computer Engineering
Georgia Institute of Technology

Dr. Edward Gerstenfeld
Department of Medicine
Hospital of the University of Pennsylvania

Dr. William Hunt
School of Electrical and Computer Engineering
Georgia Institute of Technology

Date Approved: April 25th, 2007

Knowledge is not a series of self-consistent theories that converges toward an ideal view; it is rather an ever increasing ocean of mutually incompatible (and perhaps even incommensurable) alternatives, each single theory, each fairy tale, each myth that is part of the collection forcing the others into greater articulation and all of them contributing, via this process of competition, to the development of our consciousness.

-Paul Feyerabend

To my wife, parents, and sister,
without whom I am no one.

Acknowledgement

Although only a single name can go on the cover, I cannot convey my gratitude enough to those who have helped, either directly or indirectly, in the completion of this work. For their guidance and direction, I thank my advisors, George Vachtsevanos and Brian Litt. Without them, I might never have understood the potential and importance of one's work. I thank Edward Gerstenfeld and Samuel Dudley, who gave me a glimpse through the murky waters of cardiology through their time and expertise. For their infinite patience and countless hours of tutelage and proofing, I thank Hiram Firpi, George Georgoulas, and Lichu Zhao. After their numerous hours of collecting and cleaning data, I thank Muhammad Amer, Raul Blanco, and Lyndsey Darrow. MS Word gurus Romano Patrick and Abhinav Saxena, I thank for their help in formatting this document. I sincerely appreciate the guidance, friendship, and shared time from the members of the "Neurogroup", Lauren Burrell, Javier Echauz, Jackie Fairley, Andrew Gardner and Otis Smart.

This project would not have been possible without the gracious financial support of the DANA foundation. Additionally, I would like to acknowledge the hospital of the University of Pennsylvania and the Atlanta Veteran Affairs Medical Center for contributing the project's data.

I thank my wife, Heather Wiggins, (from whom I understand the true meaning of work ethic) for her understanding and unwavering support. She has been my Gibraltar. For unending friendship and a helping hand whenever I am in need, I thank my parents, John

and Debbie Wiggins. They have motivated me since my childhood to strive for the unreachable with dignity, honor, and compassion.

Table of Contents

List of Tables

List of Figures

List of Abbreviations

ACE angiotensin converting enzyme

AF – Atrial Fibrillation

AMP amiodarone prophylaxis

AUC – Area Under the Curve

BB – β-Blocker

BN – Bayesian Network

BPM Beats per minute

CABG – Coronary Artery Bypass Graft

ECG – Electrocardiogram

GA – Genetic Algorithm

IABP Intra-aortic balloon pump

IACD Intra-atrial conduction defect

IEI Isoelectric Interval

IRB Institutional Review Board

k-NN – *k*-Nearest Neighbor

LAV Left Atrial Volume

LOO – Leave-One-Out Validation

PAC Premature atrial contraction

ROC – Receiver Operating Characteristic

Summary

Roughly thirty percent of coronary artery bypass graft (CABG) patients develop atrial fibrillation (AF) in the five days following surgery, increasing the risk of stroke, prolonging hospital stay three to four days, and increasing the overall cost of the procedure. According to some studies, over $1 billion is spent annually on this problem in the US alone. Current pharmacologic and nonpharmacologic means of AF prevention are suboptimal, and their side effects, expense, and inconvenience limit their widespread application. An accurate method for identifying patients at high risk for postoperative AF would allow these methods to be focused on the patients on which its utility would be highest. Several identification approaches have been proposed for this purpose, but results have been unimpressive, with many studies investigating a relatively small variety of measurements and/or variables. These studies used simple univariate and/or greedily feature selection multivariate techniques that could have missed possible predictive optima among variables.

The main objective of this research was to develop a Bayesian Network (BN) and possibly other classifiers which could model/predict/assign risk of the occurrence of atrial fibrillation in coronary artery bypass graft patients through the incorporation of different types of patient data. Clinical data and electrocardiogram (ECG) derived features, both traditional and novel, are selected and combined using an evolutionary computing algorithm. A secondary objective was to develop an integrated framework for more advanced methods of feature selection and fusion for medical classification/prediction. To validate this novel methodology, we compare these advanced methods, specifically genetic algorithms and Bayesian networks, to current methods of data investigation.

We determined that the naïve Bayesian network classifier used with features selected by a genetic algorithm is a better classifier to use, given our cohort. The naïve BN allows for reasonable prediction despite being presented with patients with missing data points as might occur in the hospital. This classifier achieves a sensitivity of 0.63 and a specificity of 0.73 with an area under the receiver operating characteristic curve of 0.74. Furthermore, this system is based on probabilities that are well understood and easily incorporated into a clinical environment. These probabilities can be altered based on the cardiologists' prior knowledge through Bayesian statistics, allowing for online sensitivity analysis by doctors, to perceive the best treatment options. Additionally, we stress that with larger datasets a traditional Bayesian network built using the presented genetic algorithm would be preferable to the naïve BN.

Contributions of this research include:

- An accurate, physician-friendly, postoperative AF risk stratification system that performs even under missing data conditions, while outperforming the "state of the art" system,

- A thorough analysis of previously examined and novel pre- and postoperative clinical and ECG features for postoperative AF risk stratification,

- A new methodology for genetic algorithm-built traditional Bayesian network classifiers allowing dynamic structure through novel chromosome, operator, and fitness definitions, and

- An integrated methodology for inclusion of doctor's expert knowledge into a probabilistic diagnosis support system.

Chapter 1

Introduction

Imagine yourself preparing to buy a used car. You arrive at the dealership and look the car over, thinking of repair costs. The possibility of each car being a "lemon" looms at the forefront of your mind. You take the car to be inspected by an independent mechanic; it costs you a little money, and you have an educated opinion from someone who knows more about the system.

Now imagine that the inspection costs hundreds or even thousands of dollars, and there is the possibility of the inspection actually damaging the car in the process. At this point, you question the utility of the inspection and would most likely forgo it completely, hoping for the best. This is similar to situations that doctors face every day in hospitals around the nation when speculating on the occurrence of atrial fibrillation following coronary artery bypass graft, only the situation is more important than your personal transportation.

1.1 Motivation

Currently, roughly thirty percent of coronary artery bypass graft (CABG) patients develop atrial fibrillation (AF) in the five days following surgery, increasing the risk of stroke, prolonging hospital stay three to four days, and increasing the overall cost of the procedure[1, 2]. According to some studies, over $1 billion is spent annually on this problem in the US alone [1]. Current pharmacologic and nonpharmacologic means of AF prevention are suboptimal, and their side effects, expense, and inconvenience limit their

widespread use [3]. An accurate method for identifying patients at high risk for postoperative AF would allow these methods to be focused on the patients where its utility would be highest.

Several identification approaches have been proposed for this purpose, but results have been unimpressive [1-22]. Most clinical studies investigate a relatively small amount of measurements and/or variables after a significant amount of time and money have been invested. Then, simple univariate and multivariate techniques are used that can miss possible correlations between variables that may hold the answer to the problem. By simply collecting more data types and using more intelligent feature selection and classification techniques, we could shed more light on the problem being investigated.

This work illustrates the problem with the traditional approach and proposes a novel method for the creation of better classifiers based on the data that are already collected in many hospitals across the country. We present and test this method in this work and evaluate a methodology of electrocardiogram/electrogram (ECG) feature extraction to contribute to the risk stratification of AF following coronary bypass graft.

1.2 Objectives

The main objective of this research is to develop Bayesian networks (BN) and possibly other classifiers which could model/predict/assign risk of the occurrence of AF in CABG patients through the incorporation of different types of patient data. Clinical data and ECG derived features, both traditional and novel, are selected and combined using an evolutionary computing algorithm. We investigate profit or loss due to the inclusion of the following data types:

- Clinical Data: Risk factors and other medical indicators currently recorded in the hospital after CABG and

- ECG Features: Time, frequency, and wavelet domain features derived from the collected ECG signals showing AF prediction potential.

A secondary objective was to develop an integrated framework for more advanced methods of feature selection and fusion for medical classification/prediction. To validate this novel methodology, we compare current methods of data investigation to more advanced methodologies, specifically genetic programming and BNs.

1.3 Methods

Clinical data and ECG have been collected in two separate studies. The first, performed at the Hospital of the University of Pennsylvania, collected clinical data and ECG recordings following CABG and monitored which of these patients developed AF. The second study was performed at the Atlanta Veterans Affairs Medical Center, where presurgical ECGs were collected along with other clinical variables. Both studies are approved by each institution's respective Institutional Review Boards (IRB). ECG features include separation of the ECG into its individual waveforms with further analysis of these components, including wavelet, spectral, and time domain features. Using these two sets of data, characteristics of the ECG, as well as the clinical variables, are investigated singly and in combination to find their relationship to the onset of AF following CABG. Multivariate classifiers are created by selecting features with a genetic algorithm (GA) and by combining the variables using logistic regression or a BN. These classifiers are then validated and their results analyzed and compared.

1.4 Contributions

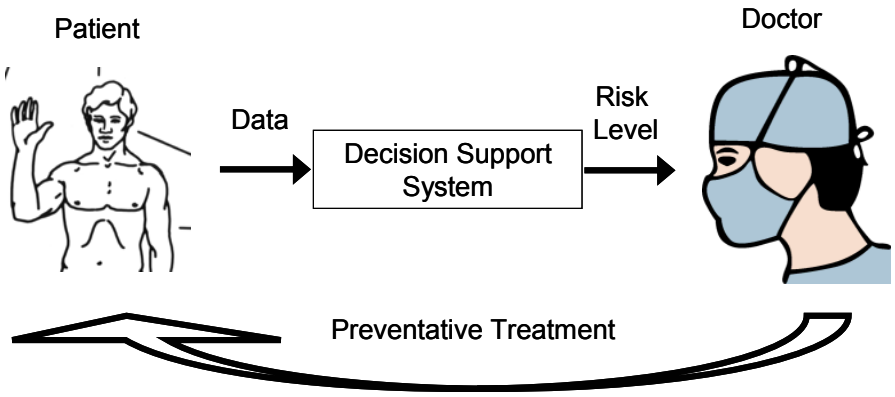

Figure 1.1 Block diagram of AF risk stratification system including the patient, the decision support system, and the cardiologist.

In order to more effectively prevent AF in CABG patients, high-risk patients must be identified and treated prophylactically through pharmacological or pacing means [3]. The overall system level approach to the control of postoperative AF consists of the patient, the decision system, and the physician that, based on the outcome of the decision system, prescribes the treatment. The contributions of this research focus on the decision system in this progression. The patient identification and treatment feedback control loop lends itself well to the application of intelligent control, possibly using automatic drug administration or electrical stimulation, though its implementation is beyond the scope of this research, due to the uncertainty behind the exact characteristics of these treatments. Contribution of this research to the decision system specifically includes:

- An accurate, physician-friendly, postoperative AF risk stratification system that performs even under missing data conditions, while outperforming the "state of the art" system,

- A thorough analysis of previously examined and novel pre- and postoperative clinical and ECG features for postoperative AF risk stratification,

- A new methodology for GA-built traditional BN classifiers allowing dynamic structure through novel chromosome, operator, and fitness definitions, and

- An integrated methodology for inclusion of doctor's expert knowledge into a probabilistic diagnosis support system.

Important medical problems have been "poked at" with limited feature selection/fusion methods for much too long, especially while there are advanced methods of data mining and decision-making to be applied. The BN is an excellent tool for making decisions based on collected information, and is even able to handle missing data points [23]. By combining more types of data and expert knowledge into a BN, better accuracy and healthier patients are the likely result.

1.5 Thesis Organization

This chapter serves as an introduction to the problem and its complexity. Additionally, the objectives of the research are outlined, as well as the exclusion of some topics. A basic overview of the methods is presented, and finally, the contributions made to the field of medical decision-making and ECG analysis are discussed.

Chapter 2 serves as more detailed background of AF following coronary bypass graft and previous work in the field. Tools used in this work for risk stratification are further described in detail.

Chapter 3 presents a typical methodology for the classification/prediction of AF following CABG using univariate classifiers on both the postoperative University of Pennsylvania dataset and the preoperativeVeterans Affairs dataset.

Chapter 4 presents an advanced method of feature selection with two traditional multivariate classification systems contrasting with the approach of the previous chapter's univariate classifier. This includes the usage of logistic regression and *k*-nearest neighbor classifiers.

Chapter 5 introduces the usage of BNs and a novel approach for their construction using genetic algorithms to find better classifiers than the previous methods. Several other methods for network structure discovery are also tested and compared using the pre- and postoperative AF risk stratification data. We then select the best classifier and compare and contrast the previous methods with the current state of the art. Finally, we explore the use of a physician's prior knowledge to influence the probabilities of the network offering an online sensitivity analysis of the predictive system.

Chapter 6 concludes this work by summarizing the classifiers developed and their benefits and drawbacks. We then offer suggestions for further work in this area.

Chapter 2

Background

When addressing a problem of this depth and breadth, spanning fields as diverse as cardiac electrophysiology and machine learning, the combination of tools from differing domains requires an understanding of the benefits and drawbacks associated with each. This chapter will discuss AF and its causes and how this relates to features taken from the ECG. Additionally, we will discuss the different approaches that have been taken toward risk stratification of AF using the ECG measures, as well as the traditional clinical characteristics. We will also address methods for combining a variety of variables into a predictive framework, beneficial for use in a clinical setting.

2.1 Electrocardiogram

From a bio-mechanical perspective, the human heart is a four-chamber pump, accepting deoxygenated blood from the body and oxygenated blood from the lungs. The blood arrives in the left and right atria, is moved into the respective ventricles, and is forced out to the lungs and body again. The timing for these events is instigated in the sino-atrial node, a self-excitatory group of cardiac cells that depolarizes spontaneously at a rate of sixty to seventy beats-per-minute (BPM). This wave front of depolarization moves through the atrial cardiac tissue in specially adapted tissue channels and reaches the atrio-ventricular node that then excites the ventricles. This excitation causes the cells to

contract, creating the heart's pumping action, which forces the blood out through the arteries [24].

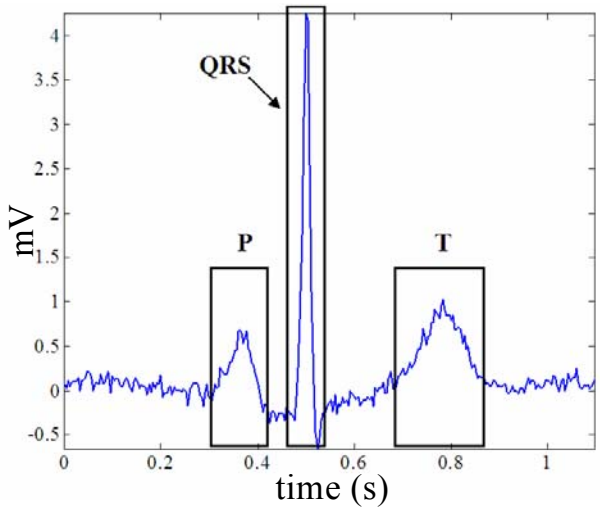

Figure 2.1 Basic ECG signal from a patient in normal sinus rhythm. The waveform components and their labels are shown.

The electrical activity in the heart can be recorded, resulting in the electrocardiogram (ECG) (Figure 2.1). This electrical signal is usually monitored with an electrode on the surface of the chest, which records the voltage at that point in relation to time. Surface electrodes, or leads, are placed on a patient in several different arrangements in order to record the electric information from several vantage points. The standard Einthoven arrangement is a set of three electrodes, one under the left and right clavicle as well as one below the left pectoral muscle as represented in Figure 2.2. These three electrodes are then designated as positive and negative in different combinations to create bipolar electrode pairs, measuring the potential across the chest. This allows recording of the heart's potential in the frontal plane (plane separating front from back). A second set of

chest leads also shown in Figure 2.2, designated V_1 through V_6, record electrical activity in the transverse or horizontal plane—depth-wise through the chest. Alternatively, during surgery, electrodes can be attached to the wall of the heart to monitor electrical activity in the muscle directly [25].

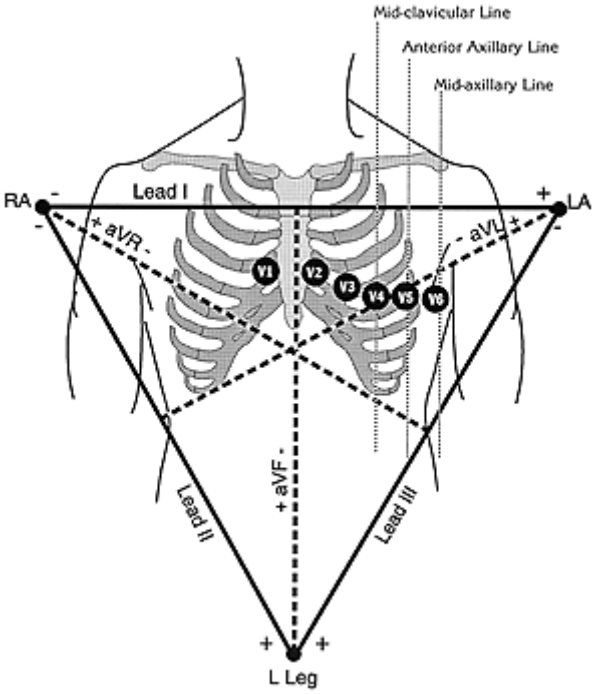

Figure 2.2 Standard ECG electrode placement.

The aforementioned electrodes each have a particular benefit for observing the heart in different stages in the contraction cycle. For instance, modified lead II records the R-wave well, due to its orientation to the depolarization direction of the heart muscle fibers during that stage. Lead V_1 is an excellent lead for observing the P wave. Therefore, it is important to select the correct electrode to observe the needed characteristic [25].

As the heart contraction cycle progresses, each part of the cycle has a characteristic waveform that appears in the chest ECG signal [25]. Figure 2.3 shows each of the portions, along with their contribution to the signal, and the sum of all parts. When there is an abnormality in the heart's conduction system, the ECG's shape changes, making it a useful tool for identifying the problem [25].

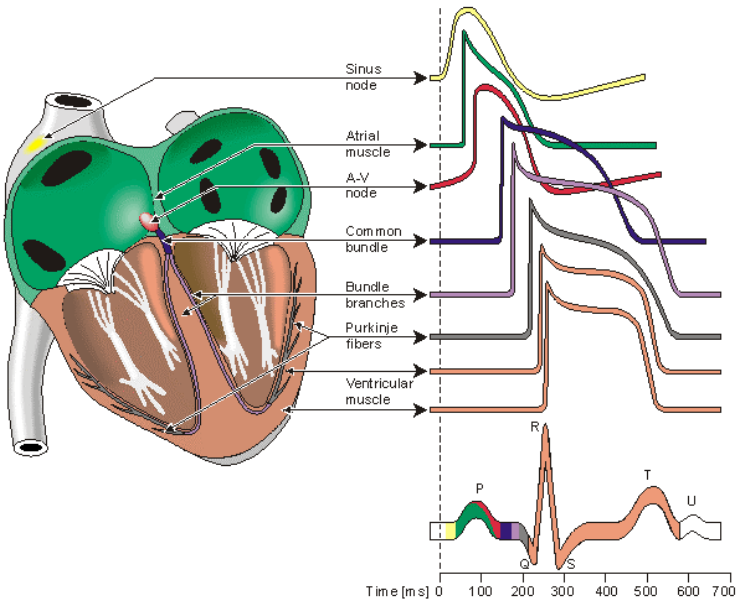

Figure 2.3. Cardiac excitatory structure and its associated ECG signal shape [25].

Unfortunately, the detection of an abnormality is more complicated than glancing at Figure 2.3 and determining if the patient's signal matches. Every person's heart structure is slightly different, with deviation in the muscle structure and orientation. Additionally, tissue densities and compositions differ, causing electrical conduction to change. The heart is also continuously adapting and remodeling in response to environmental stress. These factors alter the ECG recorded on the surface of the body [26]. Moreover, the

autonomic nervous system, through the vagus nerve, alters the pace and filling of the chambers, resulting in changes in cardiac output [27].

To complicate this, employing different machines, using different electrodes, on days with differing humidity, with patients breathing at different rates and depths will alter the measurement. There are many factors that change the signal slightly. Therefore, when comparing ECG waveforms between patients or among different recordings of the same patient, identifying markers of disease is extremely challenging [26, 28, 29]. All of these factors make the automation of this task difficult, given that a standard "template" is not known or does not exist.

2.2 Atrial Fibrillation

Atrial Fibrillation (AF) is the most commonly sustained cardiac arrhythmia, affecting over 2.2 million people [30] and roughly 5% of patients over the age of 65. It is characterized by erratic electrical activity of the atria as seen in Figure 2.4, causing erratic heart rate and fibrillatory P wave activity. This activity persists due to electrical wavelets, which in the presence of refractory tissue, reactivate previously depolarized heart muscle cells [31].

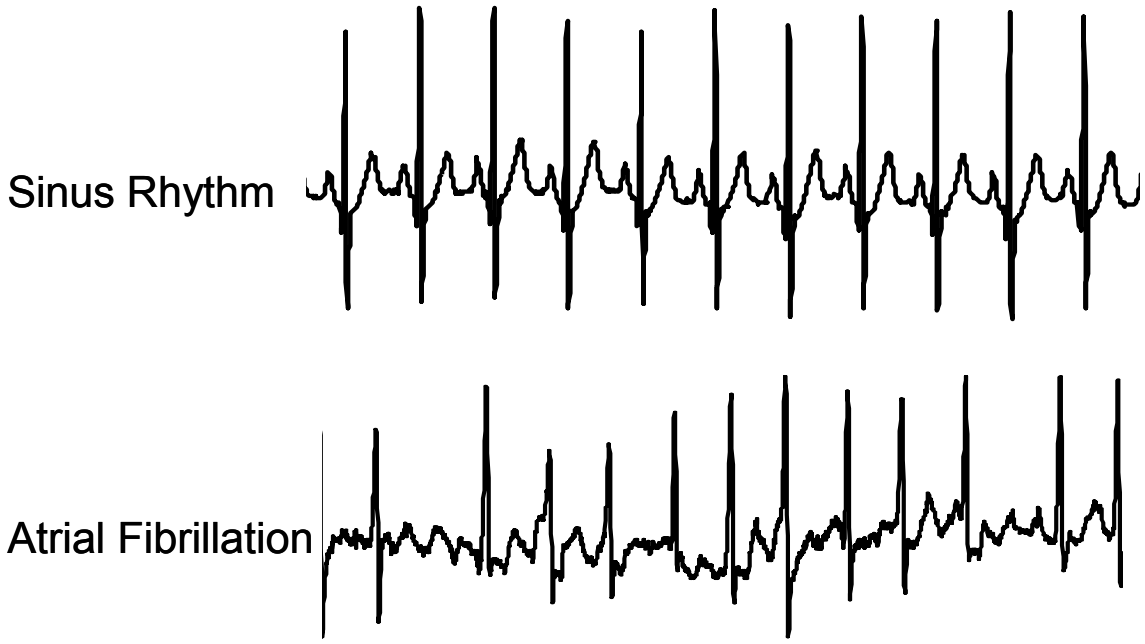

Figure 2.4 Normal sinus rhythm and AF ECG

Resulting in irregular heart pacing, AF is associated with, and can lead to congestive heart failure, cardiomyopathy [2], and mortality [32]. AF is also an independent risk factor for developing blood clots and strokes [33], increasing its risk five-fold according to the American Heart Association. AF's onset is highly correlated with age, sex, and the presence of coronary artery disease [34].

AF can be arrested in the short term through the use of medication or electrical cardioversion. Long-term solutions include medication, atrial pacemakers, and surgery such as the Maze procedure and radiofrequency ablation [31].

2.3 Coronary Artery Bypass Graft

Coronary artery bypass graft (CABG) is a procedure that allows the bypass of blood from the aorta around a blockage located on the surface of the heart. This blockage is the result of coronary artery disease that causes 37% of all deaths, nearly 500,000 Americans every year. The bypass conduit is usually the femoral vein, located in a patient's upper thigh, or a mammary artery from the patient's chest [35].

Roughly 30% of patients that undergo CABG surgery develop AF within the five days that follow [13], as seen in Figure 2.5. The risk of AF is highest in this period, and falls afterward. Postoperative AF is indistinguishable from other types of AF on the ECG and develops in both those patients who have and have not had this dysrhythmia previously. Though this is thought to be caused by the dramatic stress that is put on the body during surgery such as fluid loss, hormonal changes, inflammatory response, and possible ischemia, the actual mechanism is still unknown. This stress may *trigger* an individual's pre-existing substrate or the substrate, may have been created during the surgery, and/or while in recovery. The trigger mechanism itself may also be formed during the recovery, which then excites cells to start the ectopic beats [15].

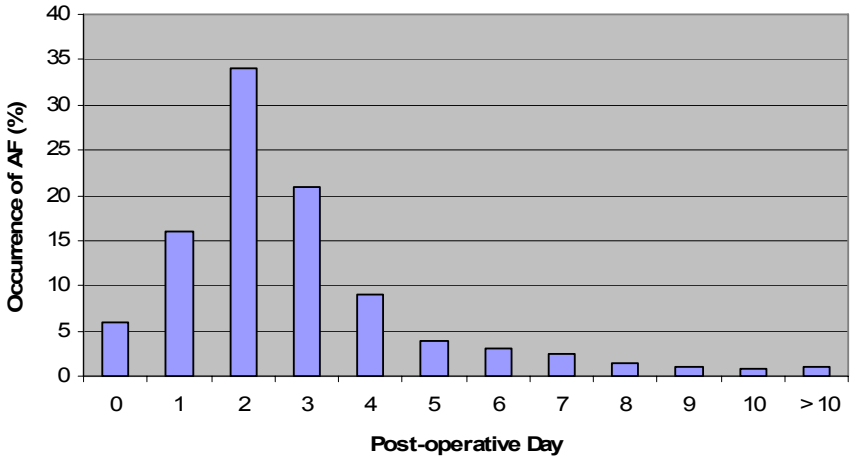

Figure 2.5 Day of onset of post-surgical AF [17].

It is thought that age contributes most significantly to the onset of postoperative AF by causing changes to the atrial myocardium, increased amounts of interstitial collagen, decreased myocytes, amyloid changes, dilation, fatty infiltration, and increased lipofuscin, which are all likely substrate components that would increase the occurrence of sustained AF. At age 75, roughly 10% of the original sinus node pacing cells still exist and 87% of postoperative AF patients have shown histological abnormalities, including myolysis and increased lipofuscin [36].

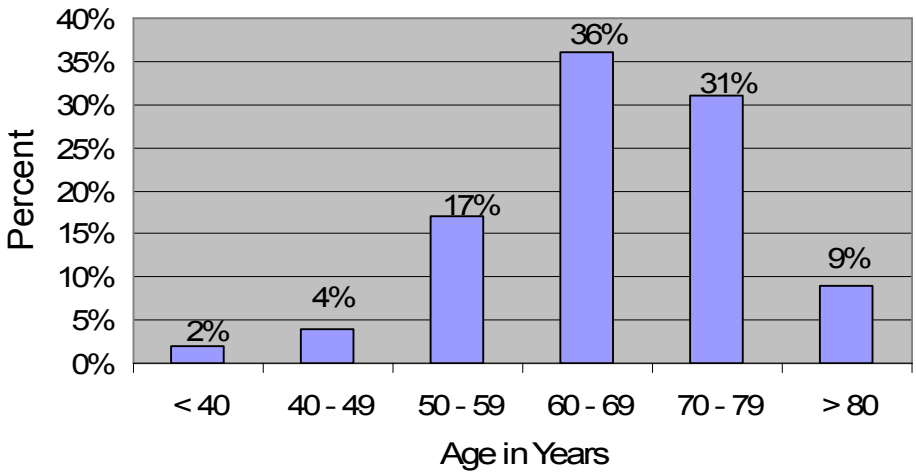

Figure 2.6 Age related to occurrence of post-surgical AF [5].

Once a patient develops AF, the treatment principles, in order of priority, are to restore sinus rhythm, control the ventricular rate if sinus rhythm is not restored, and administer antithrombotics. Reinitialization of sinus rhythm is important to prevent thromboembolisms and minimize the amount of atrial tissue remodeling that may promote continued AF, increase the chance of spontaneous conversion to sinus rhythm, and decrease the recurrence rate following termination. The downside of treating rhythm before rate is the significant side-effects and prodysrhythmic effects of antidysrhythmic medications. Despite this, there seems to be no significant difference in the long term mortality between rate and rhythm control [37], though there might be a reduction in the length of hospital stay when rhythm control is the initial treatment [38].

Several methods of prophylaxis of postoperative AF have been suggested. Pharmacologic methods include the use of β-blockers, sotalol, and amiodarone, while surgical recommendations include biatrial pacing. These methods' utilities are still not fully

quantified, but are generally accepted to be helpful in both reduction of occurrence and length of hospital stay when used appropriately [10, 39].

Many authors agree that a post-surgical AF risk stratification/prediction method would contribute greatly to the field [1-7, 13, 15, 17, 19, 22, 39-42].

2.4 AF Risk Stratification Research

Postoperative AF risk stratification has a basic trade-off that has been balanced throughout the research done to date: the balance between foresight and detection difficulty. Many investigators think that post-surgical AF is a multifactor problem that requires a prior tendency, that is then triggered by the stress imposed on the heart and its tissues by the surgery and healing [5]. If this is true, then risk could be assigned before the surgery, by identifying markers of this prior tendency, and prophylactic measures could be taken against AF's onset. This is best done before surgery while medications can be altered or preparations can be made to make alterations in the recovery plan itself.

Alternatively, by only trying to identify the patient's predisposition to develop AF, there is the risk of not finding the marker because it is a combination of a multitude of factors or simply a long train of events, which, without data, cannot be identified. Therefore, research has been conducted trying to identify more short-term markers that may be evident following the surgery, which are amplified due to both the predisposition and the insult due to the surgery.

In presurgical AF risk stratification, variables investigated include the patient's demographics, history, ECG, and any other information that would be gathered following

thoracic surgery. Post-surgical risk-stratification would include all of the presurgical variables previously mentioned as well as more variable indication changes that may have occurred in the heart due to the surgery, such as a certain morphology or frequency in the ECG.

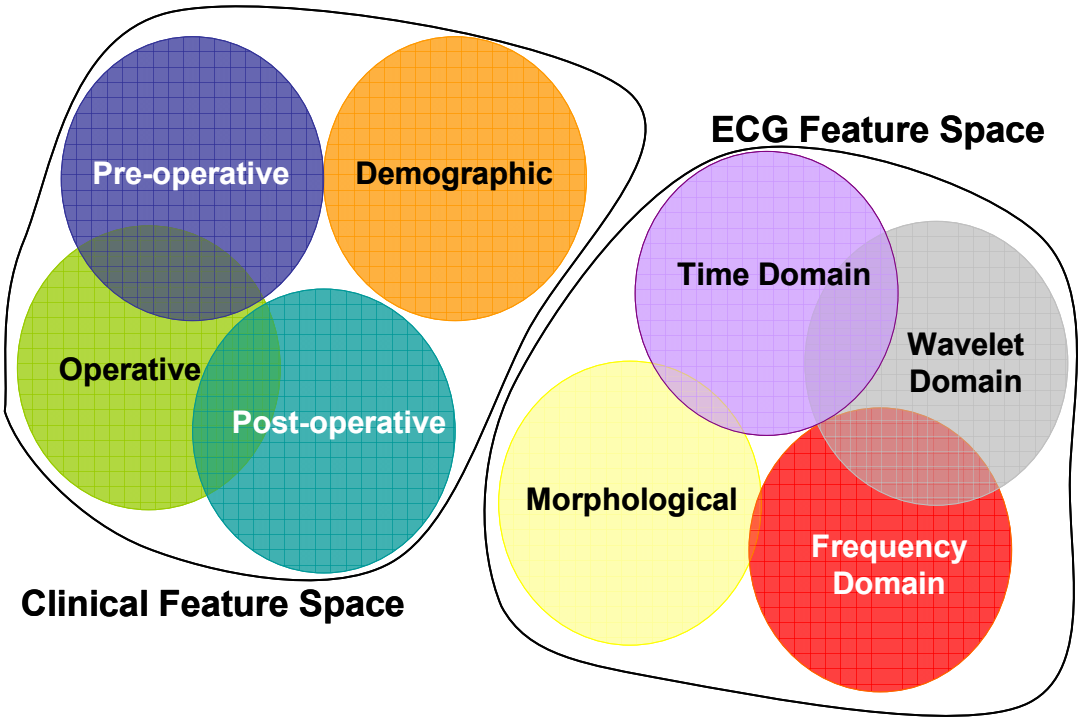

Figure 2.7 Clinical and ECG Feature Space Representations

2.4.1 Clinical Features

Typically, clinical data collected for these types of studies falls into four main groups:

- Demographic – age, race, sex, family history, etc.
- Preoperative – history of AF, beat blocker usage, etc.
- Operative – duration of cross clamp, temperature, etc.

- Postoperative – beat blocker withdrawal, hypokalemia, etc.

The actual data collected, as expected, vary by the study's purpose, the facility where it was conducted, and the facility's policies.

Clinical features are an excellent place to begin an investigation as they analyze information that is clearly linked to other issues within the hospital; otherwise, the data would never have been collected in the first place. Additionally, the infrastructure has already been established for its collection, and the data can be used for the investigation.

Chang et al. found age greater than 60 to be the best overall predictor of AF occurrence ($p < 0.01$) when they studied 120 patients. Those patients older than 60 had a 3.7-fold greater likelihood of developing the dysrhythmia. They also found gender to be another independent predictor, with males 3 times as likely to develop AF than women ($p = 0.03$) [9].

One study that focused entirely on clinical data was done by Mathew et al [17]. They studied 4,657 patients, of which, 1503 went into AF, to develop an AF risk index for postoperative patients. Demographic, preoperative, operative, and postoperative features were taken and combined into a weighted multivariable predictor. Simple t-, chi-squared, and rank-sum tests were used to select input variables and weights. They found important factors to be advanced age, history of AF or chronic obstructive pulmonary disease, valve surgery, and postoperative withdrawal of beta blockers (BB) or angiotensin-converting enzyme (ACE) inhibitor. Factors that reduced risk were BB administration, ACE inhibitors, potassium supplementation, and nonsteroidal anti-inflammatory drugs. Using their risk indicator, they achieved an area under the curve (AUC) of its receiver operating

characteristic (ROC) curve of 0.77 [17]. This risk factor was based on a cumulative point system, where the predictive factors were given a weighted score, and if a patient's additive score was beyond a threshold, he or she was at risk.

Following this study, Barnes et al. [7] performed a retrospective study on the use of amiodarone prophalaxis (AMP) using Mathew's risk stratification methodology. They classified 509 patients into either high or low risk and determined, from hospital records, which patients had received AMP. Overall, the AMP patients had less AF and shorter durations. It was not statistically significant that AMP reduced the occurrence of AF in high-risk patients, though [7].

Aranki et al. [5] reported that 189 of 570 patients developed AF following CABG. The major risk factors included age, male gender, history of hypertension, need for an intra aortic balloon pump (IABP), postoperative pneumonia, need for prolonged ventilation (>24 hours), and return to the intensive care unit. Simple t- and chi-squared tests were used to select input variables with a p-value < 0.1 which were then entered into a logistic regression model [5].

Auer and Lamm et al. [6, 43] performed a similar study in 2005 where 99 of 253 patients developed AF following CABG. They found advanced age, having valvular heart disease surgery, occurrence of other post surgical complications, elevated white blood cell count, and lack of administration of preoperative BB as risk factors. They stress that male gender was not an independent risk factor for AF, differing from the Aranki study.

Funk [13] reported that the most likely risk factors for postoperative AF were advanced age (65 years or greater), history of intermittent AF, atrial pacing, sex, race, and not

having hyperlipidemia. Risk factors for AF after hospital discharge up to 21 days following, included AF while hospitalized, valve surgery, and pulmonary hypertension. Of the 302 patients followed, 127 (42%) had AF; 41 had it after discharge, and for 10 it was their first episode.

Hakala and Hedman [3] created a logistic regression model retrospectively using age, left ventricle ejection fraction, body surface area, digoxin administration, need for a IABP and inotropic medication. With 3676 patients, the predictive results led to only a 0.69 AUC of the ROC.

Osranek et al. [18] report that an elevated echocardiographically determined left atrial volume (LAV), a marker for chronic high atrial filling pressure, is a risk factor for postoperative AF. Patients with left atrial volume > 32 ml had an almost five-fold increased risk of postoperative AF, independent of age and clinical risk factors. The area under the receiver-operator characteristic curve was 0.729 for LAV and 0.768 for the combination of LAV and age.

As a common thread through many studies, age continues to be a major contributing risk factor; possibly due to the physiological changes of that tissue we discussed earlier. The incidence of AF following cardiac surgery has been shown to increase 50% for every decade [44]. Members of the male sex seem to be generally more susceptible to postoperative AF [5, 22]. This is thought to be due to the differences in ion channel expression and autonomic tone. A previous history of AF is also indicative of risk, possibly due to the pre-existing substrate being already formed in the atrial tissue [15].

When β-blockers are abruptly halted before surgery, catecholamine levels increase, which has been a proposed risk factor for postoperative AF as well [3, 15].

There are many other risk factors that have been identified in study populations, but no predictor using these clinical risk factors have developed satisfactorily in a clinical setting [3]. So, further investigation has been performed to gain further understanding about the heart's state before and after surgery by observing patient's ECG.

Table 2.1 Summary of postoperative AF prediction studies.

Investigator	*Performance*	*Sample Size*	*Clinical Data Use*	*ECG Data Use*
Amar	AUC = 0.69	1553	Yes	Yes
Chandy	Not Validated	300	Yes	Yes
Chang	Not Validated	120	Yes	No
Fukunami	SN = 91% SP = 76%	92	No	Yes
Hakala	AUC = 0.69	3676	Yes	No
Hogue	Not Validated	31	No	Yes
Klein	SN = 69% SP = 79%	45	No	Yes
Mathew	AUC = 0.77	4675	Yes	No
Osranek	AUC = 0.77	205	Yes	No
Stafford	SN = 66% SP = 70%	20	No	Yes
Vassilikos	SN = 91% SP = 65%	50	Yes	Yes

2.4.2 ECG Features

The ECG can give more information about the immediate state of the heart, possibly showing any abnormal conduction patterns or variations. For this reason, the ECG has been investigated in a broad range of approaches [20]. The shape or widths of different morphological features have posed as a possible predictor, as has the variability of the

patient's heart rate. Frequency measures of both the heart rate and the components of the signal itself have also been experimented on. As mentioned before, here are various ECG leads as well as different ways of collecting and preprocessing the data that all of these approaches might be applied to.

It may seem like an impossible task to find the predictor amongst the noise, but fortunately, a significant amount of work has been done in this and related areas. In the following paragraphs, a summary of the features employed in these studies will be presented.

2.4.2.1 Morphology

Since atrial contractions are associated with the electrographic P wave, P waves' morphology is typically the focus in research when using ECG to determine indicators for AF. Many measures have been applied to the P wave including durations, deviations, dispersions, and slopes [8, 9, 11, 12, 16, 19, 21, 45-54].

The difficulty with P wave measures is their lack of standardization. Each research team makes slightly different decisions on where to mark the onset and offset and when a particular P wave is not considered acceptable, and thereby discarded from analysis. This makes comparison of different methods very difficult.

2.4.2.1.1 P wave duration

The P wave duration is the measure of the width of the P wave in milliseconds (ms). This can be done on any lead and varies greatly between researches as to how the onset and offset points are defined. For instance, some researchers say that 10% rise point defines

the onset, while others advocate the first sign of deflection from the baseline, and still others don't specify any particular method. Several studies found that a greater P wave duration is an indicator of abnormal atrial conduction, possibly showing substrate for AF. It seems to be a good indicator for the atrial conduction velocity [8]. The lengthening of the P wave and its associated electrical conduction through the heart can be thought of as water sounds in a clogged pipe; the longer the water sounds last, the longer it can be assumed the water is traveling due to the clog. If the water sounds are very short in overall time, there is probably not a clog, allowing smooth, quick flow with no chance of sedimentation fallout or the water finding its way through weak joints in the pipe. This could be analogous to action potential propagation through the electrical conduction pathways of the heart.

Buxton and Josephson [46] observed 99 patients undergoing bypass graft, in which 29 developed AF. They calculated the standard P wave duration on standard lead II as well as the simultaneous, three standard leads' P wave duration. The P wave duration on the single modified II lead had little predictive value, while the duration on the three simultaneous standard leads was significant ($p < 0.001$). They used the standard definition for intra-atrial conduction defect (IACD) being a P wave duration greater than 110 ms as defined by the New York Heart Association (NYHA). Passman et al. [19] studied the P wave durations of the standard leads I and II, as well as the V_1 lead in 152 patients finding them significantly predictive for AF ($p = 0.02$, $p = 0.04$, and $p < 0.01$, respectively).

Amar et al. [4] used a database of 1,553 CABG patients to develop a risk stratification metric including four risk factors: age, history of AF, P wave duration (>110 ms), and

low cardiac output. Each factor was assigned a point score developed through multiple logistic-regression: age (1 point per year), history of AF (12 points), P wave duration (3 points), and low cardiac output (10 points). The aggregate score was then transformed to a probability score using logistic regression and then thresholded into three risk classes. This score puts very little weight on ECG factors: three of roughly 125 possible points. The overall area under the ROC curve was 0.69, resulting in a fair overall classifier.

In addition to the duration on a single P wave, the signal's P waves can be averaged over many cycles to obtain the signal-averaged P wave. This requires the precise marking of many P wave onsets and offsets, lining them up, and doing an average. Some methods also use a template matching technique which also discards any "abnormal" morphologies. The only problem with this approach is how to determine abnormal.

Chang et al. [9] calculated the signal-averaged P wave duration on the standard lead II from a 12-lead system in 120 patients and found a P wave duration ($\geq$100 ms in lead II) to be an independent predictor of AF ($p = 0.04$). Steinberg et al. [21] performed a prospective study observing the relationship between the signal averaged P wave duration and the occurrence of AF with 130 patients, of which 33 developed AF. They used P wave template matching and cross correlation measures to select appropriate P waves for inclusion. They found the P wave duration significantly longer in the AF patients ($p < 0.001$) with a threshold of 140 ms giving a sensitivity of 77% and a specificity of 55%.

Klein et al. [16] developed a P wave triggered signal averaging method for P wave duration measurement using leads X, Y, and Z. The orthogonal leads were combined into a vector magnitude and roughly 350 beats per patient were averaged after template

matching. There were 45 patients included in the study and 16 developed AF. The two groups were highly separable using this P wave duration ($p < 0.005$). Given a threshold of 155 ms, classification yielded a sensitivity of 69% and a specificity of 79%.

Fukunami et al. performed a study using the same leads to determine whether a patient is at risk of paroxysmal AF. They compared 42 AF patients' signal-averaged P waves to 50 controls and found the P wave durations to be significantly longer in the AF patients ($p < 0.001$). They also found the root-mean-squared amplitude value of the descending P wave to be a significant predictor ($p < 0.0001$). By combining these two measures, a predictive classifier was determined, which yielded a sensitivity of 91% and a specificity of 76% [47].

Stafford et al. [50] performed a reproducibility analysis for signal averaged P waves taken four weeks apart. They analyzed 20 paroxysmal AF patients and 10 controls, recording the X, Y, and Z orthogonal leads. The P wave duration was the most reproducible of the measures, while P wave frequency components and spatial velocity were not consistent. Stafford suggests that some measures taken under signal averaging to predict AF are unreliable and questions their further utility if reproducibility concerns are not addressed.

Additionally, the variance of the P wave duration has been identified as a possible indicator of abnormalities in AF patients. Andrikopoulos et al. [45] found that the P wave variance combined with several other variables made a good predictor for 60 idiopathic paroxysmal AF patients and 50 controls.

2.4.2.1.2 Isoelectric interval

The isoelectric interval (IEI), shown in Figure 2.8, is determined by measuring the total onset to offset time across all channels of the ECG recording and subtracting from that, the maximum P wave duration seen on a single channel. This is difficult to do since it requires precise measurements of onsets and offsets on many channels, and slight mistakes make for large differences in value.

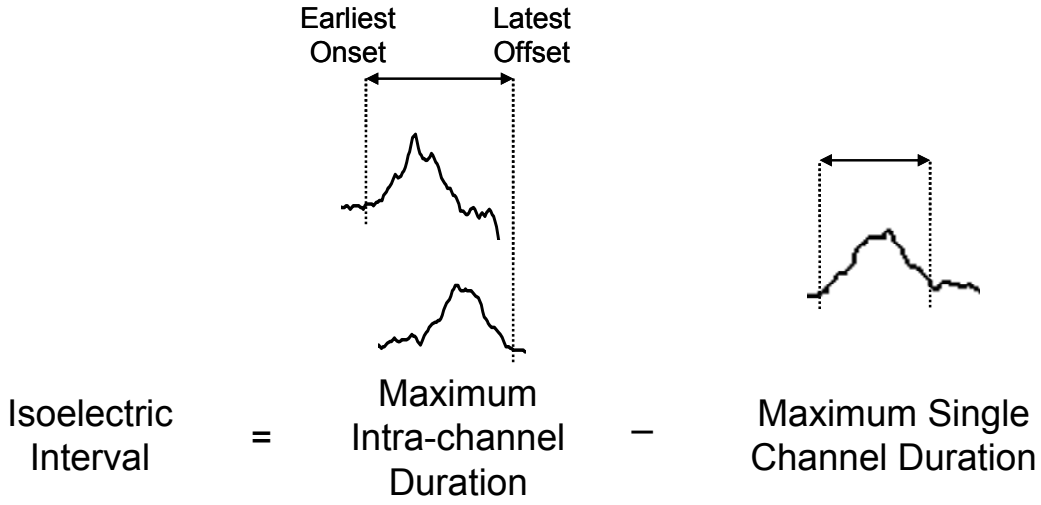

Figure 2.8 The Isoelectric Interval (IEI) is calculated as the difference of the maximum intra-channel P wave duration and the maximum single channel P wave duration.

Buxton and Josephson [46] tested this by subtracting the P wave duration on the standard II lead from the overall duration from the three standard simultaneous limb leads. Patients with AF had an IEI of 12.4 ms while the controls had 5.9 ms ($p < 0.001$). They propose that this measure could be useful in identifying asynchronous activation of atrial conduction tissue, thereby stretching the total P wave time on the entire set of ECG leads. Stafford et al. [51] performed a similar study and found IEI to not be significant alone,

but in a predictor combined with P duration, yielded a sensitivity of 66% and a specificity of 70%. Overall, IEI does not seem to be a useful predictor, unless combined with P wave duration.

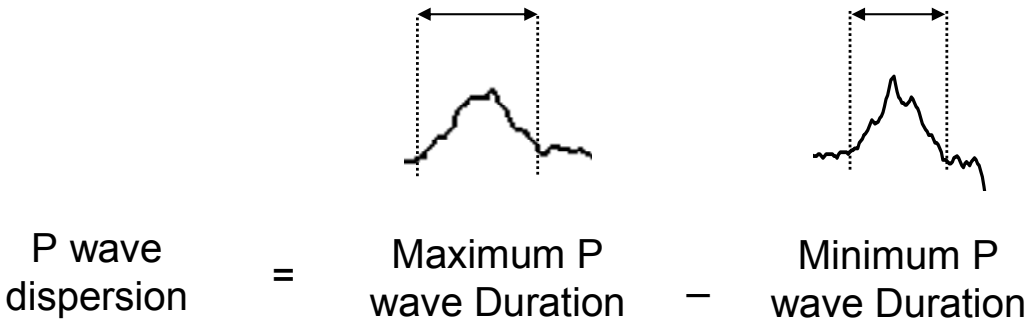

Figure 2.9 The P wave dispersion is measured as the difference of the maximum and minimum P wave durations.

2.4.2.1.3 P wave dispersion

P wave dispersion, shown in Figure 2.9, is measured as the difference of the longest and shortest P wave durations within a given period of time on a single lead. This is often done on the standard lead II, though other leads have been investigated. This is thought to be an indicator of the excitability of the atrial tissue surrounding the atrial conduction path [8]. If we think of the pipe analogy, this can be seen as the pipe's wall being cracked and releasing water into the surrounding space, while it should be traveling straight through the pipe.

Chandy et al. [8] collected both pre- and postoperative surface ECG signals from 300 patients undergoing CABG, and observed AF in 81. Their main hypothesis was that age-related structural and conduction changes of the atria, as well as surgical disruption, lead

to postoperative AF. Signs of these factors are hypothetically seen in the ECG. The usual demographic, medical condition, medication, surgical, and postoperative condition data were collected. P wave features were also calculated including P wave dispersion. Their analysis found a relationship between postoperative AF and age ($p < 0.0001$), body surface area ($p < 0.0001$), and an increase in postoperative P wave dispersion ($p < 0.01$). They used a multivariate logistic regression model to combine these predictors but did not report its performance metrics.

It is thought that changes in P wave dispersion could be caused by fluid overload, thereby stretching the atrium, and altering its excitability/conductivity. Studies have been conducted that show the pressure and fluid levels in the left atrium, as well as dehydration, change the P wave duration and dispersion [12, 53].

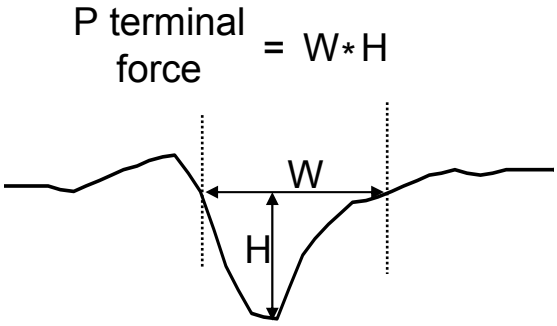

Figure 2.10 The P terminal force is calculated as the product of the width and depth under the baseline of the negative deflection of the P wave on the V1 lead.

2.4.2.1.4 P terminal force

The P terminal force, shown in Figure 2.10, is a measure of the V1 lead's negative deflection under the baseline following the P wave peak and the length of the P wave.

This is measured as the distance under the baseline, multiplied by the length of time it is below the baseline. Therefore, it is a combined measure of time and amplitude. Stafford et al. [51] investigated this measure with several other measures in a 189-patient study and found this variable to not have statistical significance. Hopkins and Barrett [48] found this measure to be a somewhat useful diagnostic means to determine a patient's left atrial enlargement.

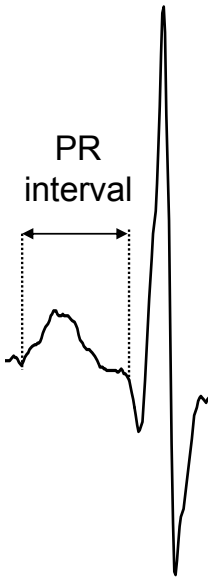

Figure 2.11 The PR interval is measured as the time interval from the beginning of the P wave to the beginning of the QRS complex.

2.4.2.1.5 PR interval

The PR interval, shown in Figure 2.11, is the length of time between the onset of the P wave and the beginning of the QRS complex. This can be interpreted as the time required

to excite the ventricle following the atrial activation, possibly giving insights into this activation pathway.

Chandy et al. [8] performed a study analyzing the pre- and postoperative ECG for several P wave features. The PR interval, as well as PR segment depression, had a very high P value, thereby having no significant relationship to the occurrence of AF. Passman [19] also found the PR interval to be a somewhat useful predictor of AF when above 180 ms ($p < 0.05$, age adjusted). This measure, along with age > 65 and increased P duration greater than 110 ms, yielded a somewhat useful predictor.

2.4.2.1.6 Premature atrial contractions

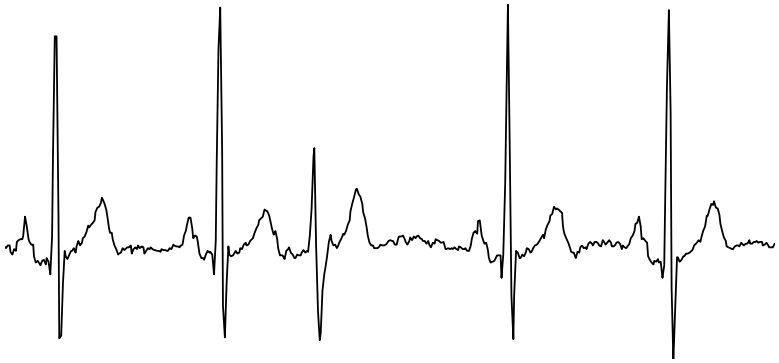

Figure 2.12 Premature Atrial Contraction

Premature atrial contractions (PACs) are the result of an activation of the atrium earlier than the typical cardiac cycle that propagates to make the ventricle contract early. The beat following the PAC is typically the traditional distance from this abnormal beat as seen in Figure 2.12. This shows a kind of resetting of the system. These PACs typically

have a differing morphology from the normal sinus beat, whose shape is determined by the location on the atrium it originated and spread to.

Kolb et al. [55] studied the apparent cause of onset of spontaneous AF in 33 patients and found that over 93% were caused by PACs. This is seen as a possible trigger of the predisposing substrate. It can be assumed, then, that a patient with greater numbers of isolated PACs could be at higher risk of developing AF since a probably trigger of its onset is present.

Although many of these studies of P wave characteristics had good data sets and thorough methods, the analysis of the P wave lacked some technological aspects. For instance, many P wave features were taken off of a paper ECG trace and measured with a magnifying glass, calipers, and/or metric ruler. Though definitions were clearly set individually for these measures, definitions varied greatly between studies.

2.4.2.2 Heart Rate Variability

Many investigators have also used the heart rate variability (HRV) as an indicator of sympathetic nervous system's activity and its relation to the refractory period of the atrial cells. The HRV is calculated by annotating the R waves or the QRS complex onset and creating a tachogram showing the times between each of these contractions. Therefore, a person beginning physical exercise would have heart rate values increasing through time. Many values can be observed from this trace including traditional statistical measures such as mean, standard deviation, and minimum.

Hogue et al. [14] have investigated the relationship between RR dynamics and AF prediction following CABG. They had 31 patients, of which 18 went into AF. They then used three 20-minute pre-onset chunks of data from each patient while in normal sinus rhythm to calculate features. The features were mean RR duration and its standard deviation, the percentage of successive RR intervals that deviated by > 50% from the previous RR interval, and the root-mean-square of successive RR intervals. Power features were computed in the following bands: total (0-0.5 Hz), VLF (0.0033-0.04 Hz), LF (0.04-0.15 Hz), and HF (0.15-0.4 Hz). Approximate Entropy, a nonlinear measure of variability, was calculated on a 2 Hz sampled HRV. The relationships between these features were analyzed with a basic multinomial logistic regression analysis. This study found that only low Approximate Entropy and heart rate were independently associated with AF. These two variables are correlated, so the conclusion of these variables being associated with AF is not surprising. A slightly higher or lower heart rate than the control group (5 BPM) was also found to be a good indicator of risk. However, this measure tends to vary widely within a single patient, and unless compared against a single patient's baseline rate, offers little information. No overall predictive accuracies or assessments were made. The small group of patients on which the study was based also leads us to have validation concerns.

Maier et al. [56] performed a study of 200 patients using data provided for the Computers in Cardiology 2001 challenge. They extracted HRV measures from several time windows ranging from 2 to 30 minutes before onset of AF. The HRV feature set included the means and standard deviations of the RR intervals (including ectopic beats) as well as between only normal beats and the relative number of successive normal beat pairs which

differ by 50 ms. The standard deviation of the RR intervals (including ectopics) was an interesting predictor as were the percentage of consecutive normal-to-normal beats which differed by more than 50 ms. This seemed to be more of an indicator of the prescience of ectopic beats than of the type of analysis. Though a well done study, the sample size was too small for any statistically significant results.

Vikman et al. [57] took a different approach by investigating the frequency content in the HRV signal. They investigated the significance of the HRV's low frequency (0.04 to 0.15 Hz), high frequency (0.15 to 0.4 Hz) and their relative relationship. They found that both of these frequency range magnitude decrease and the relationship between them stay relatively constant before AF onset. Additionally, they investigated an approximate entropy measure and a short-term detrended fluctuation analyses of the RR interval, measures of the repetitive and fractal natures of the signal. They found as AF onset approaches, there is increased repetition in the signal through the entropy measure and changes in the fratal characteristics of the signal.

2.4.2.3 Frequency Domain

Frequency domain analysis can be applied to the ECG data in many ways, both to the signal itself and the HRV data as Hogue did [14]. It has been observed that the fibrillatory frequency of a patient's arrhythmia ramps up following the onset and decreases prior to termination. Bollmann et al. [58, 59] also found a positive correlation between the fibrillatory frequency and AF duration, meaning a low frequency fibrillation tended to terminate in a shorter period of time. This could indicate a relationship between

the size and/or refractory period of the re-entrant atrial conduction pathway to the sustainability as well as initialization of AF.

Stafford et al. [52] observed the frequency content of the whole P wave and compared this with an analysis of its terminal portion. This was prompted by the discovery of the relationship between ventricular late potential activity and ventricular fibrillation and its possible extension to AF. They found that increased high frequency content in the third quarter of the P wave indicates a higher risk of AF.

2.4.2.4 Wavelet Domain

Wavelets are a useful tool to observe the time and frequency domain of the signal simultaneously. This is done by convolving the signal with a scaled version of a mother wavelet to arrive at the wavelet coefficients for that scale. These coefficients generally show greater amplitudes as the shape of the signal in the matching time frame correlates with the scaled wavelet. In this way we can see the given wavelet's frequency in that window in time. Because the ECG is such a nonstationary signal with small waves that resemble wavelets, wavelet analysis seems an obvious choice.

Vassilikos et al. [54] decomposed the high resolution ECG P wave using the Morlet wavelet on 50 patients after undergoing CABG, 17 of which went into AF. Prediction features such as hypertension, low ejection fraction, age, and power in the wavelet coefficients from several frequency bands were collected. Typical uni- and multivariate analyses were used for statistical significance. Overall, the regression yielded a sensitivity of 91% and a specificity of 65%. Again, this study uses a small sample size with few data types. Though this study begins to include clinical and ECG features in a

multivariable context, the max, min, and average P wave durations and Morlet wavelet decompositions do not show the short-term temporal information. More ECG features should be investigated in conjunction with the clinical features with attention to their location in time.

Maier et al. [56] also used the Daubechies wavelet to analyze the different possible scales of fluctuations of the HRV series. They used 10 different scales finding several to have interesting classification properties on the training set which did not hold on the testing set. Though the study was well planned resulting in interesting findings, the amount of data was low and any far reaching statements of utility of these measures would be overly bold.

2.4.3 ECG Feature Summary

As this research suggests, limited combinations of clinical characteristics and few ECG features have been investigated, and those that are, tend to be simple wave duration calculations. AF precursors could be hidden in the clutter between more prominent morphological features. Wavelet decompositions and novel feature calculations coupled with advanced search strategies like data-mining could result in new innovations. A more thorough look at the information contained in the ECG is certainly warranted.

2.5 Evolutionary Computing

Evolutionary computing [60] uses the principles of a) survival of the fittest, b) reproduction, and c) mutation to achieve a predetermined goal in computer algorithms. Its applications can be the matching of a curve, the design of the perfect antenna, or anything

in between as long as the problem can be encoded and a fitness function can be defined for its assessment. The solutions are found through many generations of evolving individuals which become more fit through Darwinian selection. A nice property of these evaluations is that they can often be done in parallel, allowing an entire generation to be calculated at once when employing enough processors. Genetic algorithms are a type of evolutionary computing used to address a number of complex engineering problems.

2.5.1 Genetic Algorithms

Genetic algorithms (GA) [61, 62] are a tool for problem solving in which an algorithm evolves an encoded chromosome through Darwinian evolution. The GA searches the space of possible solutions for the one that achieves its goals most satisfactorily. The basic sequence of a GA is seen in Figure 2.13. An initial population of individuals, encoded as chromosomes, is created through either prior knowledge or randomly. The individual's characteristics are encoded in the chromosome through many single quanta of information called nucleotides, just as they do in DNA. These individuals' fitness are assessed and a selection process follows where the more fit individuals breed and mutate to form new individuals in the next generation which are then once again tested, and the cycle continues. Once a fitness threshold or the maximum number of iterations has been reached, the evolution is halted and one is left with the best overall individual, assuming the use of elitist selection.

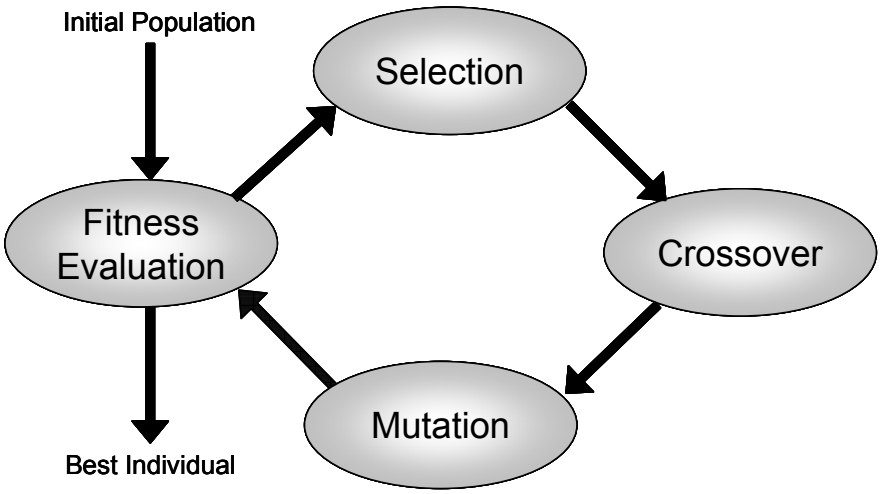

Figure 2.13 Genetic Algorithm (GA) Flow Chart

An important aspect of a GA is that the chromosome is of predetermined length that encodes the problem, usually in binary or continuous representations. For instance, this can be a vector of base-ten numbers or a string of bits. Very often, the chromosome encoded corresponds to a high dimensional problem where many combinations of a set are tested for the optimum set [63]. The alternative, genetic programming, allows for an ever changing chromosome length allowing greater control of the encoding through generations but with the drawback of added complexity.

There are three main operators which are performed while altering an individual's chromosome: selection, mutation, and crossover.

Elitism allows the selection of the overall best individual for inclusion in future generations. It essentially keeps the best gene pool in a population and does not allow the loss of the global maximum fitness earner until it has been beaten by another individual.

Mutation is the slight change in some part of the individual's chromosome ranging from a single nucleotide alteration to several nucleotides. This is done completely at random just as it might in biological mutations.

The crossover operator emulates chromosome creation following sexual reproduction in which a new individual's chromosome is a combination of both the original parents' chromosome. In the computational domain, this is achieved through an actual swapping of a section of chromosome creating two children with portions of each parents' chromosome and all nucleotides are preserved in the population.

2.6 Bayesian Networks

A Bayesian network (BN) is a relatively new tool that uses probabilistic correlations among multiple variables to make predictions or assessments of class membership based on past data [23]. The use of probabilities derived from past data is similar to how a doctor currently makes decisions [64]; A doctor assesses the past occurrences of these symptoms and test results, to determine a likely diagnosis for a current case. When a BN is used for risk stratification, classification results and probabilistic context can be output together, allowing the doctor to observe why the network made a suggestion, instead of the "black box" method where the doctor does not understand the inner-workings and therefore will not trust it in a clinical setting [64].

To understand the benefits of BNs, we first need a quick review of basic statistics. A conditional probability is the likelihood of some conclusion, C, given some evidence/observation, E, where a dependence relationship exists between C and E. This probability is denoted as $P(C \mid E)$ where

$$P(C \mid E) = \frac{P(E \mid C) \cdot P(C)}{P(E)} \tag{1}$$

Bayes' theorem is the method of finding the converse probability of the conditional,

$$P(E \mid C) = \frac{P(C \mid E) \cdot P(E)}{P(C)} = \frac{P(C, E)}{P(C)} \tag{2}$$

This conditional relationship allows an investigator to gain probability information about either *C* or *E* with the known outcome of the other. Now consider a complex problem with *n* binary variables, where the relationships among them are not clear for predicting a single class output variable (e.g., node 1 in Figure 2.14). If all variables were related using a single joint distribution, the equivalent of all nodes being first-level parents, the number of possible combinations of variables would be equal to 2^n-1, given each node has two possible outcomes. For each combination, a sufficient number of samples must occur to obtain a realistic likelihood estimate. This results in the need for a very large amount of data [23, 65]. If dependence relationships between these variables could be determined resulting in independent variables being removed, fewer nodes would be adjacent to the node of interest. This parent-node removal leads to a significant reduction in the number of variable combinations, thereby reducing the amount of needed data. Furthermore, variables that are directly conditional, not to the node of interest but to the parents of the node of interest (as nodes 4 and 5 are with respect to node 1 in Figure 2.14), can be related, which allows for a more robust system when dealing with missing data points. This property of requiring less information based on pre-existing understanding of the system's variable dependencies is a major benefit of BNs [65]. Some further theoretical underpinnings of the Bayesian approach for classification have been addressed in [66] and [67].

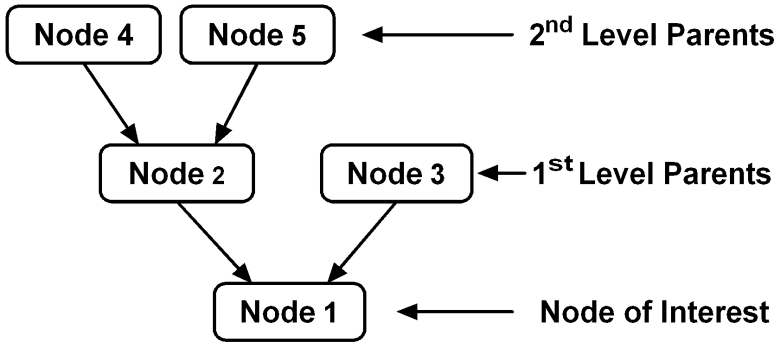

Figure 2.14 Basic BN Structure and Terminology.

To use a BN as a classifier, first, one must assume that data correlation is equivalent to statistical dependence. Though this is not true from a pure mathematical standpoint, for purposes of medical diagnosis when few dependencies can be determined with a high degree of certainty, correlation between the two variables is assumed to give similar information. We also must assume that the data gathered accurately portrays the system, and with small datasets, this can be a difficult idea to accept or cross validate.

In our work, we have investigated two types of BNs. The first type of network is the naïve BN, which makes an independence assumption, thereby reducing probability computation data requirements. The second type of network is the traditional network. The first traditional BNs were created with expert knowledge and usually dealt with fairly well understood principles and variable relationships. Currently, many complex problems exist where a researcher may have ample data for the variables of interest, but does not know the relationships between these variables in order to create the network. As the number of parents grows, the amount of data required to derive a conditional probability table of the BN grows exponentially. Therefore, the number of possible parents is limited by the size and composition of the data set available. Besides the data

requirement, the network must be built in a computationally viable way, while still producing accurate conditional variable dependencies [23, 65, 68].

Two methods of BN discovery are presented below, the first being a greedy hill-climb search and the second method based on evolutionary computing using a GA.

2.6.1 Naïve Bayesian Classifier

Given an evidence set $E = \{E_1, E_2, ..., E_n\}$, the joint probability, $P(C, E)$, can be expanded using the definition of conditional probability to

$$\begin{aligned} & P(C, E_1, ..., E_n) \\ & \quad = P(C) \cdot P(E_1, ..., E_n \mid C) \\ & \quad = P(C) \cdot P(E_1 \mid C) \cdot P(E_2, ...E_n \mid C, E_1) \\ & \quad = P(C) \cdot P(E_1 \mid C) \cdot P(E_2 \mid C, E_1) \cdot P(E_3, ...E_n \mid C, E_1, E_2) \\ & \quad = P(C) \cdot P(E_1 \mid C) \cdot P(E_2 \mid C, E_1) \cdot P(E_3 \mid C, E_1, E_2) \cdot P(E_4, ...E_n \mid C, E_1, E_2, E_3) \end{aligned} \tag{3}$$

This expansion requires the use of significant amounts of data to determine the many probabilities. In order to reduce the number of required data samples, an assumption of independence can be made for the components of *E,* letting the joint probability take the form of

$$\begin{aligned} & P(C, E_1, ..., E_n) \\ & \quad = P(C) \cdot P(E_1 \mid C) \cdot P(E_2 \mid C) \cdot P(E_3 \mid C) \cdots, \\ & \quad = P(C) \prod_{i=1}^{n} P(E_i \mid C) \end{aligned} \tag{4}$$

The use of this independence assumption is at the basis of the "naïve" Bayesian classifier. A network is created with only one node representing the class of interest and all other nodes as its first-level parents. The joint probability of the node of interest is then computed as in equation (4).

While the independence assumption may seem to simplify the situation and would therefore lead to less accurate classification, this has not been true in many applications. For instance, several datasets are classified in [69] using the naïve Bayesian classifier, decision tree induction, instance-based learning, and rule induction. These methods are compared showing the naïve classifier as the overall best method.

2.6.2 K2 Algorithm

Researchers have proposed various techniques for BN structure discovery without the above independence assumption, the most notable being Cooper and Herskovits, who developed the K2 algorithm, a greedy-hill climb algorithm [65]. This method starts with a graph and repetitively adds nodes/edges to maximize the following model-selection criterion,

$$K2\,criterion = \prod_{j=1}^{q} \frac{\Gamma\left(\sum_k a_{ijk}\right)}{\Gamma\left(\sum_k a_{ijk} + \sum_k s_{ijk}\right)} \prod_{k=1}^{r_i} \frac{\Gamma\left(a_{ijk} + s_{ijk}\right)}{\Gamma\left(a_{ijk}\right)}, \tag{5}$$

where

- *i, j,* and *k* are the indexes of the child node, of the parents of the child node, and of the possible values of the child node, respectively,
- q is the number of different instantiations of parent nodes,
- r_i is the number of values that the child node can assume,
- s is the number of times that the child node has the value of the k^{th} index value of the node,

- *a* is the number of times that the parents and the child correlate positively in discrete cases, and
- Γ (•) is the *Gamma* function which satisfies $\Gamma(x+1) = x\Gamma(x)$ and $\Gamma(1)=1$.

This selection criterion is basically a measure of how well the given graph correlates to the data. This method requires a complete dataset without any missing data points and a hierarchical causal ordering of nodes. This means that the nodes are listed so that any node preceding a given node can be its parent, while those following it cannot [23, 65, 68].

As a greedy-hill climb algorithm, the K2 algorithm suffers from a major limitation: it can terminate the search after encountering the first local maximum without finding the overall global maximum. Several methods for random restarts, such as simulated annealing and best-first search, have been proposed to eliminate this problem. Nonetheless, these methods are more computationally expensive, but in many cases, can still improve the network's accuracy when dealing with large data sets [23].

2.6.3 Genetic Algorithms for Network Structure Discovery

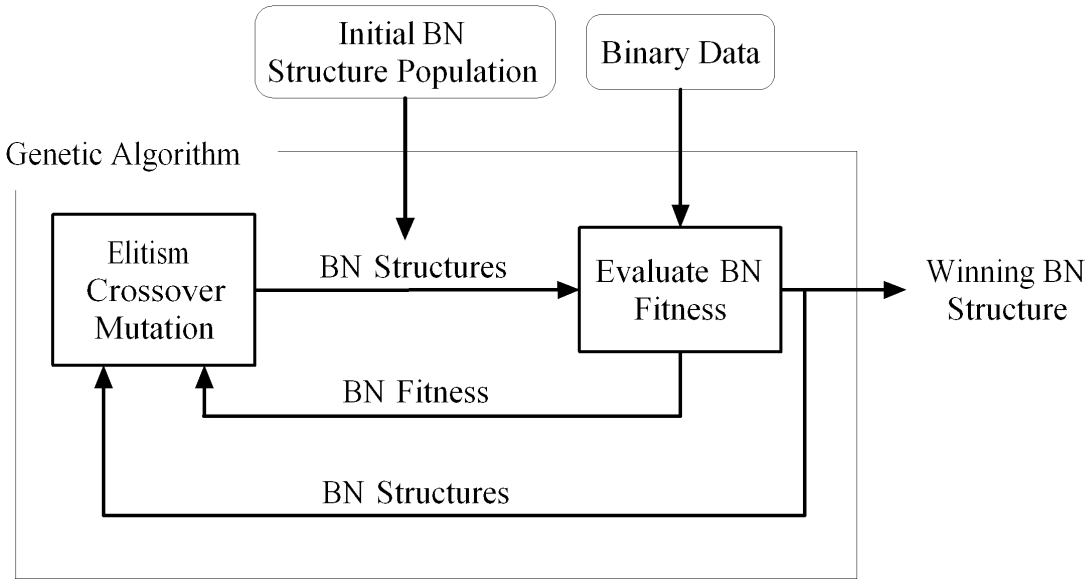

Figure 2.15. Flow diagram for the genetic algorithm based evolution of a BN.

A genetic algorithm (GA) is another tool that can be used to discover the BN structure [68]. The general GA-evolved BN algorithm framework is shown in Figure 2.15. The algorithm can be designed to begin with an initial BN structure population and then assesses fitness of these structures. Iteratively, random crossovers and mutations of networks within a population are tested, and the most fit of the population are kept for future generations. As generations pass, the population evolves, leaving the fitter structures while those performing poorly are discarded. This method is quite useful, due to the inherent randomness that alleviates the local maximum problem as seen in the K2 algorithm. An improvement is also gained since the structure of the resulting network is dynamic without regard to individual node-to-node fitness measures that have not been proven to be optimum or accurate [68]. These method characteristics allow intelligent

model construction without requiring an exhaustive search of all possible structure combinations of nodes.

2.7 Bayesian Networks in Medicine

Considering the many benefits of BNs and how they match in many cases with medical decision making, BNs have been under-used in a clinical setting. For instance, BNs combine data much as a physician does: combining past experience from other patients and combining different pieces of information based on relative probabilities. Medical decision making is also plagued by a lack of information or missing data points, something that BNs excel at dealing with. A BN's probability tables are very easily updated as well, ever increasing and improving the data set with which diagnoses are made.

There has been a recent thrust in using BNs to identify malignant versus benign tumors. Many of these networks have been constructed through expert knowledge but some have been learned from data. Kahn et al. used BNs to help in the diagnosis of breast cancer using a number of radiological features and several demographic features [70]. Though having a relatively large AUC of the ROC, there appeared to be no testing and training set and a huge number of features were used with very few patients, possibly indicating over-fitting. Following this, Wang et al. investigated the relationship of several types of variables to the development of breast cancer. They incorporated the breast cancer detection image features as well as non-image features into a BN. They also investigated using several feature sub-networks and combining the outcomes of each one versus the inclusion of all features in a single network. This proved a single network with more

features is more informative than less features or several combined sub-networks of fewer features. The final network, which took data from mammographies and other clinical data, yielded a better prediction accuracy than is the national average when done manually [64]. This shows the potential of Bayesian risk-stratification. This problem was fairly straightforward, though with dependencies that were practical and sometimes obvious. Also, the network was very small with a single layer of variables of the predicted value, making the complexity very low.

It is important to determine why a given classifier or system is good for given situations. Eisenstein et al. addressed this when they compared a BN, a Neural network, and logistic regression when used for patient myocardial infarction (MI) risk stratification. He compared the three learning systems with varying training sets and variable numbers with/without missing data points to determine which is better for a given situation. He found that with a BN, more variables included generally makes for better classification accuracy, plus the benefit of ease of understanding the outcomes of the BN. BNs, although not having the highest accuracy overall in all permutations of the experiment, were the most robust, given variation in missing data, small sample size, and number of input variables [71].

Other areas besides the diagnostic relationships have been modeled with BNs as well. Brogini et al. constructed a BN from 23,000 patients to access hospitalization satisfaction relationships. He used the Cooper-Herskovits K2 method, meaning he had complete information and an ordered set of nodes [72]. This resulted in a fairly complex network structure, though most of the relationships were previously understood. The paper did not

report on the accuracy or predictive value of the graph and offered little on the use of BNs except its ability to find interesting relationships among variables.

An interesting use of BNs in eastern medicine was presented by Pang et al. where they extracted textural and chromatic features from digital images of patients' tongues in order to predict disease using Chinese tongue diagnoses. These features were taken of healthy patients as well as patients with 13 different diseases. The variables were used to create a BN using a free PowerPredictor network program. The network was trained and tested using a k-fold validation resulting in over 75% sensitivity, which was significantly better than the nearest neighbor classifier to which it was compared [73]. This was an interesting study, and obviously shows some benefit from the use of quantitative features and BNs for diagnosis. However, there is ambiguity concerning the medical quality of the experiment's set-up as well as the lack of understanding of how the BN was built. Also, the analysis of 455 patients to discriminate fourteen different classes did not seem like enough data to populate the needed joint probability tables for the traditional full BNs that were built.

There have been other applications than those mentioned here [74], but this gives several examples of what has been done in the field where the experiments have been done with questionable statistical rigor and validation.

2.8 Bayesian Statistics

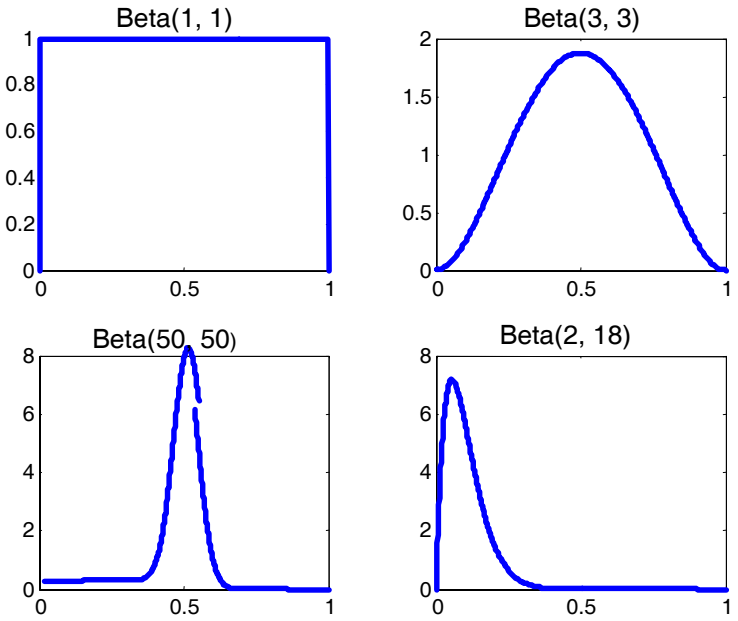

Figure 2.16. Sample beta distributions given several different α and β values.

In order to use the doctor's knowledge of the situation in a quantitative decision support system, the physician's opinions must be incorporated in a well defined, structured manner. Bayesian statistics is a structured method for the combination of objective data (experimentally collected) and other previously known information to predict future outcomes [23]. The inclusion of expert opinion with objective data is one of its uses. The objective data probabilities are easy to calculate, but the quantification of an expert opinion is a little more difficult. This must be made into a distribution with which it is easy to perform calculations. For example, if the data are binary, a binomial distribution is used for representation of the data's probabilities. When the data are modeled as

binomial, a beta distribution is both theoretically and intuitively rationalized for the quantification of the expert knowledge contribution [75].

The beta distribution has two input parameters, α and β, which both scale and shift the distribution. The uniform distribution is created when $\alpha=\beta=1$ as shown in Figure 2.16. When $\alpha=\beta>1$, the mass is concentrated around $\alpha/(\alpha+\beta)$. In this way, α and β can be thought of as the number of successes and failures, respectively. The more certain the expert is on a given distribution, the tighter the peak should be around that probability, and correspondingly, the higher the α and β values are relating to more statistical evidence of the probability estimate. By using these two parameters, an expert can make a multitude of different distribution shapes, which can then be combined with Bayes' theorem to determine a balanced prediction probability.

For example, we perform an experiment to deduce the probability of an unbiased coin landing on tails when flipped. In our experiment, we can only flip the coin four times and it lands on heads all four times (H=4) and none on tails (T=0). The traditional Frequentist approach to statistics might say the probability of getting tails with this coin is 0/4 = 0%.

The previous estimate might seem odd to the observer because we know the probability of tails and heads should be around 50%. This is considered our *prior* information and it can be derived through intuition, expert knowledge, or previous experiments. Usually, the *prior* probability is given with some statistical distribution showing the certainty of the prior knowledge. Here, since we are modeling a binary outcome, we use a *Beta(α,β)* distribution to model the probability of tails where $\alpha=2$ and $\beta=2$. Figure 2.17 shows the

Beta(2,2) distribution with a maximum probability at 50%, just like our instincts tell us about an unbiased coin.

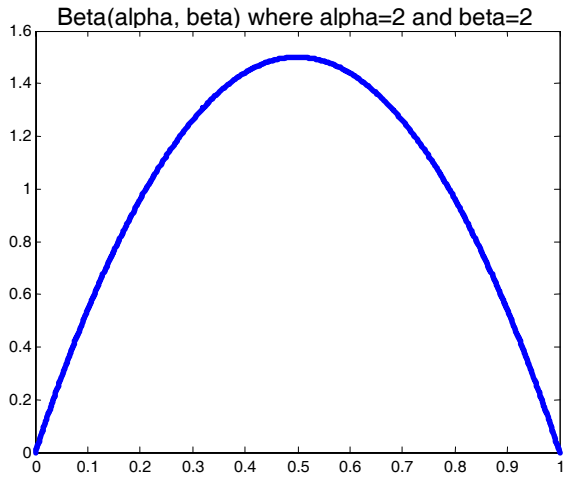

Figure 2.17 The beta(2,2) distribution.

Using the *prior* knowledge and the four coin flips we did earlier, a Bayesian would find a distribution of the probability of tails with a maximum at one-third. Although it is still not quite correct, a balance between observed data and expert knowledge often yields better results than data alone, especially when little data are available due to cost or difficulty of collection.

This example parallels how physicians' data would be incorporated into a single node in a BN, altering a single probability which is directly responsible for estimating the patient's risk of developing AF. It would of course be a little more complex than an unbiased coin toss, but the math is still the same. We need to use Bayesian statistics to help us use all pertinent information to solve the problem.

Table 2.2 Bayesian terminology and definitions

Name	Notation	Equivalent	Description
Model	$f(x \mid \theta)$		Data Distribution
Prior	$\pi(\theta)$		Expert Knowledge Distribution
Joint	$h(x,\theta)$	$f(x \mid \theta) \cdot \pi(\theta)$	Combined Model and Prior Distribution
Marginal	$m(x)$	$\int_{\Theta} f(x \mid \theta) \cdot \pi(\theta) d\theta$	Data Independent of Prior for Normalization
Posterior	$\pi(\theta \mid x)$	$\frac{f(x \mid \theta) \cdot \pi(\theta)}{\int_{\Theta} f(x \mid \theta) \cdot \pi(\theta) d\theta}$	Bayes' Theorem: Distribution of θ Given Data

Some further nomenclature should be explained for a better understanding of Bayesian statistics. There are several main pieces of information needed and arrived at when solving a Bayesian problem. We will explain these components in an example using a sequence of *Bernoulli trial* data $y_1,\ldots,y_n$, where each value is zero or one. This data set can be modeled using the binomial distribution, *Binomial(n,θ)* where n is the number of trials and θ is the proportion of successes in the entire population or, equivalently, the probability of success in each trial.

$$f(x \mid \theta) = p(x \mid \theta) = Binomial(x \mid n, \theta) = \binom{n}{x} \theta^x (1-\theta)^{n-x}$$

This distribution of the data is considered the *model* where x is the number of successes during the n trials such as the four heads or zero tails in the previous example.

Since the probability of success in each trial, or θ, is an unknown system wide parameter and can never be found exactly, we wish to estimate its value. In order to do this using Bayesian statistics, we also need some sort of previous knowledge of the variable to be

estimated. Our *prior* information distribution is notated as $\pi(\theta)$ where the distribution is a function of θ.

The *joint* probability, $h(x,\theta)$, is the probability of the value x and θ occurring at the same time, such as x=4 successes with an overall system probability of θ=0.5. The *joint* probability distribution is found by taking the product of the *likelihood* and the *prior,*

$$h(x,\theta) = f(x \mid \theta) \cdot \pi(\theta) .$$

Finally, the *posterior,* $\pi(\theta|x)$ is the probability of θ given the value x has occurred. This is found by dividing the *joint* by the *marginal*,

$$\pi(\theta \mid x) = \frac{h(x,\theta)}{\int_{\Theta} h(x,\theta) d\theta} = \frac{f(x \mid \theta) \cdot \pi(\theta)}{\int_{\Theta} f(x \mid \theta) \cdot \pi(\theta) d\theta}$$

This equation is the Bayes' theorem equivalent for use with probability distributions.

For instance, let's take our medical prediction problem of patients developing a heart arrhythmia following surgery. We have a population of 81 patients, N=81, where 28 of them develop an arrhythmia, x=28. A Frequentist might say the overall probability of developing an arrhythmia after surgery is 28/81=0.346, but we have more information that can be included in the estimate. We have hypothetically found an expert doctor who says that she believes the probability is more like 0.5 and gives a Beta distribution of Beta($\theta|\alpha$=30,β=30) as her certainty of this figure. This is our *prior.* We already have the *model* of the data as a Binomial(x|n,θ) distribution. We find the *posterior* to be

$$\pi(\theta|\text{x=28}) = \frac{\text{Binomial(x} \mid \text{n=81, } \theta) \cdot Beta(\theta \mid \alpha = 40, \beta = 41)}{\int_{\Theta} \text{Binomial(x} \mid \text{n=81, } \theta) \cdot Beta(\theta \mid \alpha = 40, \beta = 41) d\theta}$$
$$= Beta(\theta \mid \alpha + x, n - x + \beta)$$
$$= Beta(\theta \mid 40 + 28, 81 - 28 + 41)$$
$$= Beta(\theta \mid 68, 94).$$

The simplification of a Binomial and Beta distribution to a Beta posterior is a standard Bayesian conjugate pair and a proof will not be presented here.

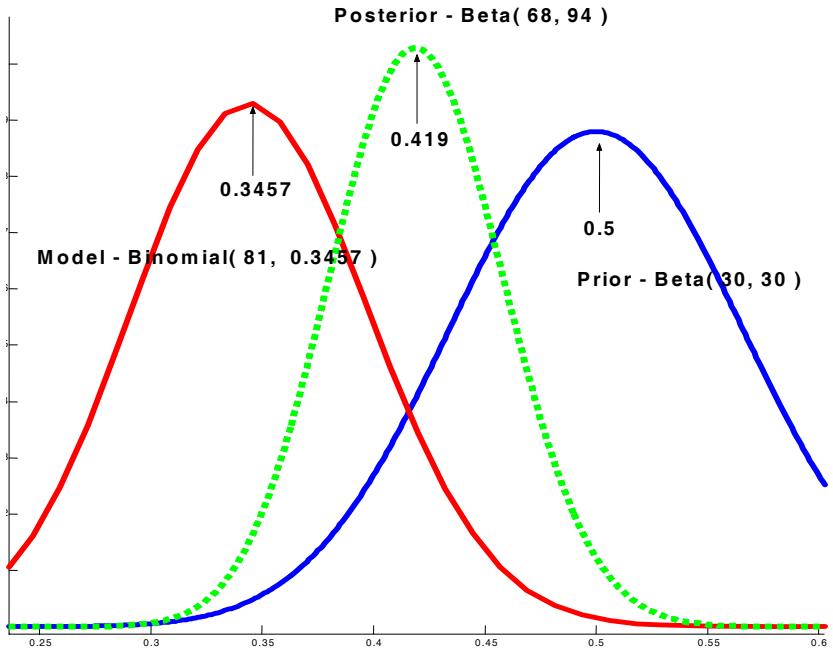

Figure 2.18 Combining of the model and prior distributions into the posterior probability.

As seen in the Figure 2.18, the *prior* and the *model* both contribute to the *posterior* (dashed) making an overall, more accurate probability distribution of θ.

2.9 Summary

In this chapter, we have discussed the conduction pathways of the heart and how, during AF, these pathways are deviated. Since the ECG is an aggregate exterior summation of the electrical activity of the heart, it can reveal characteristics of these pathways. For this reason, the ECG signals, as well as many clinical factors, have been studied in order to determine those patients who might be predisposed to AF occurrence following CABG. Many of the studies have resulted in interesting, but inconclusive results, showing a clear need for thorough study of the various ECG and clinical predictors available. In order to combine these features we discussed the use of a BN learned from the data itself using a number of structure learning techniques.

The next chapter will discuss in detail the calculation and span of the various features being implemented as well as their univariate predictive outcomes in relation to the problem.

Chapter 3

Univariate AF Prediction

In this chapter, we explore the traditional approach to discovering relationships for diagnostic medicine using a univariate predictor and present the basic methods employed in these analyses. We will also use these statistical methods to investigate the relationship of many pre- and post-surgical characteristics to the onset of AF. The univariate predictor is the most desirable predictor due to its use of a single characteristic as well as its simplicity of use and discovery. The drawback of a univariate predictor is that many problems are too complex for this type of analysis. Dealing with these situations will be addressed in later chapters.

3.1 Clinical Context

When searching for a connection between a disease and some possible cause or characteristic, these relationships can be investigated individually very simply using univariate statistics. The physician may record the disease state of the patient (either positive or negative) and the data of the possible predictor. If the possible predictor seems to indicate the outcome of diagnosis, this could lead to better prediction accuracy. However, this can be difficult to do objectively in many cases. For instance, how does one determine what quantifies statistical significance? What type of test does one use for a given type of data?

In any case, the diagnostic tool needs to be simple enough and have good enough performance to be used in a real-world clinical setting. If it is not simple, it might be prone to user error causing more confusion than benefit. If it requires too much expertise, then a hospital might resist the expense of hiring a person trained to use it. If it requires too much time to run, physicians might not use it. The different methods for measuring the performance of a system are an important consideration as well.

The performance of a diagnostic system can be quantified in terms of how well it actually performs the diagnosis. This can be calculated by observing the actual disease state and the diagnostic system's predictions on a given patient set [76]. The outcomes of this diagnostic test yield four patient classes (assuming there are two outcomes):

- True Positive (TP) – the test accurately identified the patient as having the disease
- False Positive (FP)– the test mistakenly identified the patient as having the disease
- True Negative (TN)– the test accurately identified the patient as not having the disease
- False Negative (FN) – the test mistakenly identified the patient as not having the disease

Table 3.1 Confusion Matrix

		Actual Disease State	
		Negative	Positive
Predicted Disease State	Negative	TN	FN
	Positive	FP	TP

These four outcomes can then be placed in a matrix, termed the confusion matrix, showing the number of outcomes in each of these bins. From these values, several important performance metrics can be derived which place importance on the differing qualities of a diagnostic system. Sensitivity (TP/(TP+FN)) is the measure of how well the system identifies those patients that have the disease while specificity (TN/(FP+TN)) is the measure of the systems ability to identify those without the disease. These are measured from the populations who, in reality, actually have (TP+FN) or do not have (FP+TN) the disease. Alternatively, positive predicted value (TP/(TP+FP)) tells how well the system's positive prediction actually coincides with a positive outcome and negative predictive value (TN/(TN+FN)) tells how well the system's negative prediction actually coincides with a negative outcome. These are measured from the populations derived as either positive (TP+FP) or negative (TN+FN) by the predictor itself.

Depending on the type of steps that might be taken following diagnosis, differing levels of these performance metrics are desirable. For instance, in the case of a very safe and beneficial drug being administered with very few harmful affects resulting from administration to those without the disease, a high sensitivity is very important in order to cover the entire diseased population. But, if the drug is very dangerous, a high specificity would be desirable in order to protect the patients without the disease from its harmful side effects. There are many other influencing factors associated with this decision:

- Financial costs, both direct and indirect, of treating and not treating the disease
- Side effects and benefits of the treatment
- Discomfort of the patient

- Severity of disease
- Death associated with the treatment and disease

All of these performance metrics and the associated consequences should be weighed appropriately when designing a decision support system (DSS). In the risk stratification of postoperative AF, both the failure to treat the disease and the administration of unnecessary pharmacological prophylactics has undesirable consequences [20].

3.2 Methods

In medicine, there continues to be, and always will be, the need to compare new treatments and determine which is "better." In order to prove statistical significance of improvement of one treatment over another, we usually form a hypothesis (null hypothesis, H_o) stating that there is no difference between the two treatments. Based on the data collected from both treatments and using an appropriate test, we calculate the probability of having collecting our data while H_o is true. This probability is termed the p-value. So, if the p-value is very small, the null hypothesis can be rejected. The two most widely used tests are the student t-test and the chi-squared test [76]. After finding the statistical significance of a characteristic, one should assess the characteristic's utility for diagnosis. This can be done using a receiver operating characteristic (ROC) curve [77].

3.2.1 t-test

The student t-test is a simple calculation telling if two different sample groups' means are possibly the same assuming the data are normally distributed [76]. For instance, when

comparing the age of the patient to the occurrence of post-op AF, two groups are observed: those who do develop AF and those who do not. Each of these separate groups has a range of age values from which the groups sample mean and variance can be calculated. The null hypothesis, H_o, can be considered to be that the distribution means are not sufficiently far apart to say they are different. The p-value is defined as the probability of observing the given data while the null hypothesis is true. So, if the p-value is very small, H_o can be rejected.

Unfortunately, for older patients, H_o is rejected for our example statistical test. The p-value of this test is well below 0.01 meaning it is very unlikely that both AF and normal patients have similar age distributions.

The t-test is used pervasively through medical literature to compare two groups and has identified many relationships that have been significant.

3.2.2 Chi-squared test

The chi-squared test is very similar to the t-test in that it, given data, supports or denies a given hypothesis. The chi-squared test deals in categorical data instead of a continuous data, though. An example of categorical information would be which vessel was occluded that needed to be bypassed during CABG. Each of the vessels can be thought of as a category without any clear order or hierarchy. The chi-squared test calculates the likelihood that the individual bypassed vessel had some influence on the occurrence of AF with a given p-value.

An important note is that for small samples, the chi-squared test is not statistically valid and the Fischer's Exact Test should be used [76].

3.2.3 Receiver Operating Characteristic

The receiver operating characteristic (ROC) curve is a product of 1950's research into the transmission and receiving of radio signals in a noisy environment [77]. It is basically a way of comparing the actual signal to what is reconstructed at the receiver to show how well the communication system functions. There is a parallel for this in medicine when patients have a given disease and a test is being developed in order to identify those patients. The test diagnoses should match as closely as possible to the actual patient's disease state.

The ROC curve is calculated by placing, in ascending order, the labeled feature values of the characteristic in question and determining, at each sample, what the sensitivity and specificity would be if the classification threshold was placed there. The sensitivity is then plotted against one minus the specificity making a plot that starts in the bottom left corner of the plot (sensitivity=1, specificity=0) and moves to the upper right (sensitivity=0, specificity=1). If the plotted sensitivity/specificity relationship is a straight line from corner to corner, the classification measure is equivalent to random guessing. A plot that traces up the left axis and then follows the sensitivity-equals-one asymptote has perfect classification accuracy. The quality of the classifier can be calculated by computing the area under this curve (AUC). The AUC can be thought of as a probability that the feature value of a randomly selected diseased sample is larger than the feature value of a randomly selected non-diseased sample (assuming a higher feature value

generally correlates with the disease) [78]. The closer the AUC is to one, the better the classifier [77]. In quality of a classifier based on the AUC has been broken down into several subjective quality measure where,

- 0.50 - 0.60 is Poor,
- 0.60 - 0.75 is Fair,
- 0.75 - 0.90 is Good,
- 0.90 - 0.97 is Very Good, and
- 0.97 - 1.00 is Excellent.

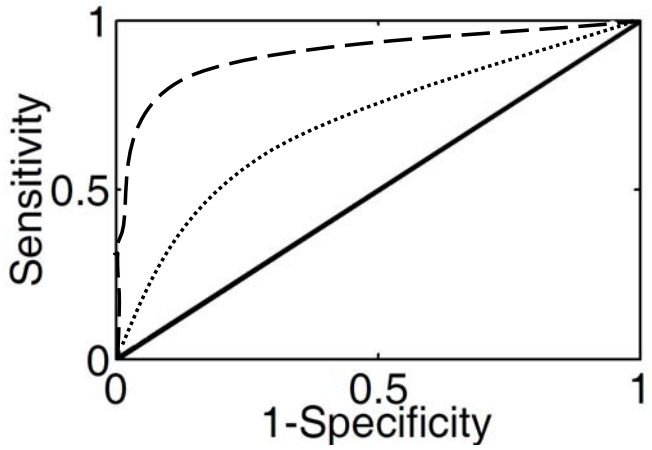

Figure 3.1 Receiver Operative Characteristic Curve. The solid line represents a classifier which would be equivalent to random guessing with an AUC of 0.5. The dotted line represents a better classifier while the dashed line is the best with the greatest AUC.

In this way, a univariate classifier can be evaluated based on the overall population distribution and classification threshold possibilities instead of at a single sensitivity and specificity value.

The ROC curve can also help to find the optimum classification boundary in a feature value to achieve the appropriate balance of sensitivity and specificity. In our application, the sensitivity and specificity are equally important (discussed further in chapter four), so we set the feature value classification boundary at the point on the ROC where the product of the sensitivity and specificity is at its peak. This can be visualized on the sensitivity/specificity product plot which shows the value of this product for all points on the ROC. Figure 3.2 shows a sample of this where the optimum classification threshold is difficult to decide just by looking at the ROC curve. By looking at the maximum of the sensitivity/specificity product plot, the optimum threshold is easily found and seems to offer good separation between the two classes represented by circles and pluses.

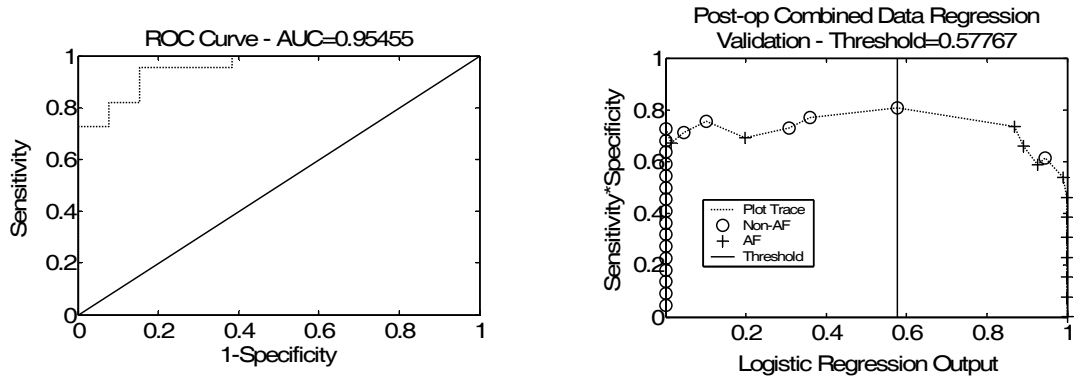

Figure 3.2 Sample ROC curve and sensitivity/specificity product plot from the output of a logistic regression classifier.

It should be noted that for instances when several patients have the same feature value, these patients' labels are spread vertically down the plot under the actual product value. This allows one to view the actual labels as well as the number of patients that fall on that

point. Examples of this phenomenon can be seen at both the far right and left of the sample plot above.

3.3 Preoperative

Table 3.2 Summary of the preoperative data showing both the total number of patient samples and features used in future analyses.

Data Type	Number of Patient Samples	Number of Features
Clinical Dataset	545	79
ECG Dataset	244	4608
Combined Clinical and ECG Dataset	545	4687

In this work, we focused on both the pre- and postoperative period for AF risk stratification. For the former, we used a dataset collected from the Atlanta Veterans Affairs (VA) Medical Center associated with Emory University. This dataset contains many demographic and clinical variables related to the surgery. Data were obtained for all patients who underwent cardiothoracic surgery between January 2000 and March 2005 under a protocol approved by the Emory University IRB. The diagnosis of post-op AF (157 of 545 subjects) was based on review of notes and ECGs. Most subjects were male (99.2%), consistent with the general VA population.

3.3.1 Clinical Dataset

Seventy-nine variables were collected including patient demographics, current medical conditions, pre- and post-op medications, echocardiogram results, ECG results, coronary angiogram, and pre-op laboratory results including the use of pre-op peroxisome proliferator activator receptor (PPAR) agonists, a patient's NYHA functional class, the European Society of Cardiology's SCORE risk measure, and the physician's estimate of

operation mortality. The total set of variables consisted of those collected by the VA Continuous Improvement in Cardiac Surgery Program (CICSP) with the addition of fields for the classes of medications prescribed at the time of surgery. A list of CICSP variables and their definitions are available at [79]. Missing data constituted roughly 20% of the total data fields.

3.3.2 ECG Feature Dataset

In addition, this dataset has standard 12-lead ECG recordings, for each patient, taken prior to surgery that are 2.5 seconds in length. This translates to roughly 2 or 3 complete cardiac cycles to be observed. The signal is sampled at 250 Hz and, in the clinical setting, was used to evaluate the patient's heart rhythm and rate in the days leading up to the surgery. The number of total recordings varies among patients: some having 10-20 while others have one. This is related to the physician's need for monitoring the patient, possibly due to pending complications or dysrhythmias.

Since these data were not originally recorded for signal processing or research purposes, many of the recordings have abnormal amplitude levels, some not large enough to span several dicretization levels. It is assumed that these particular recordings were useless to the physician for the clinical evaluation and were therefore left out of our analyses.

3.3.2.1 Pre-processing

The preprocessing of these signals included a high-pass Butterworth filter with cut-off frequency of 1 Hz to remove the DC voltage and any very low frequency baseline drift.

The signals were further Butterworth low-pass filtered at a cut-off frequency of 35 Hz to remove high frequency noise.

In order to properly extract information from the signals, important reference points in the signals such as the atrial and ventricle contractions must be observed and handled. For this reason, manual annotation was done on a single beat in each record of the offset of a T wave, the onset and offset of the P wave, and the onset of the QRS complex. These are referred to as fiducial points and are often done on several different leads. These markings indicate the important reference points of the cardiac cycle and allow for standardized comparison between patients for a given measure.

It is important to annotate the important fiducial points on several of the leads to give a complete representation of the cardiac cycle at different vantage points. For instance, the onset and offset of the P wave varies from lead to lead. For this reason, we have marked the P wave onset and offset of the standard II lead which has been compared in several studies. In addition to this channel, and overall marking was done for the I, II, and III leads together. This gives an overall impression of the entire P wave morphology from several electrode orientations. Lastly, the V_1 lead was also marked for the onset, offset, and the mid-point deflection. These points allow for computation of features such as the P wave terminal force or spatial velocity. Figure 3.3 shows the different channels and where individual fiducial points were placed.

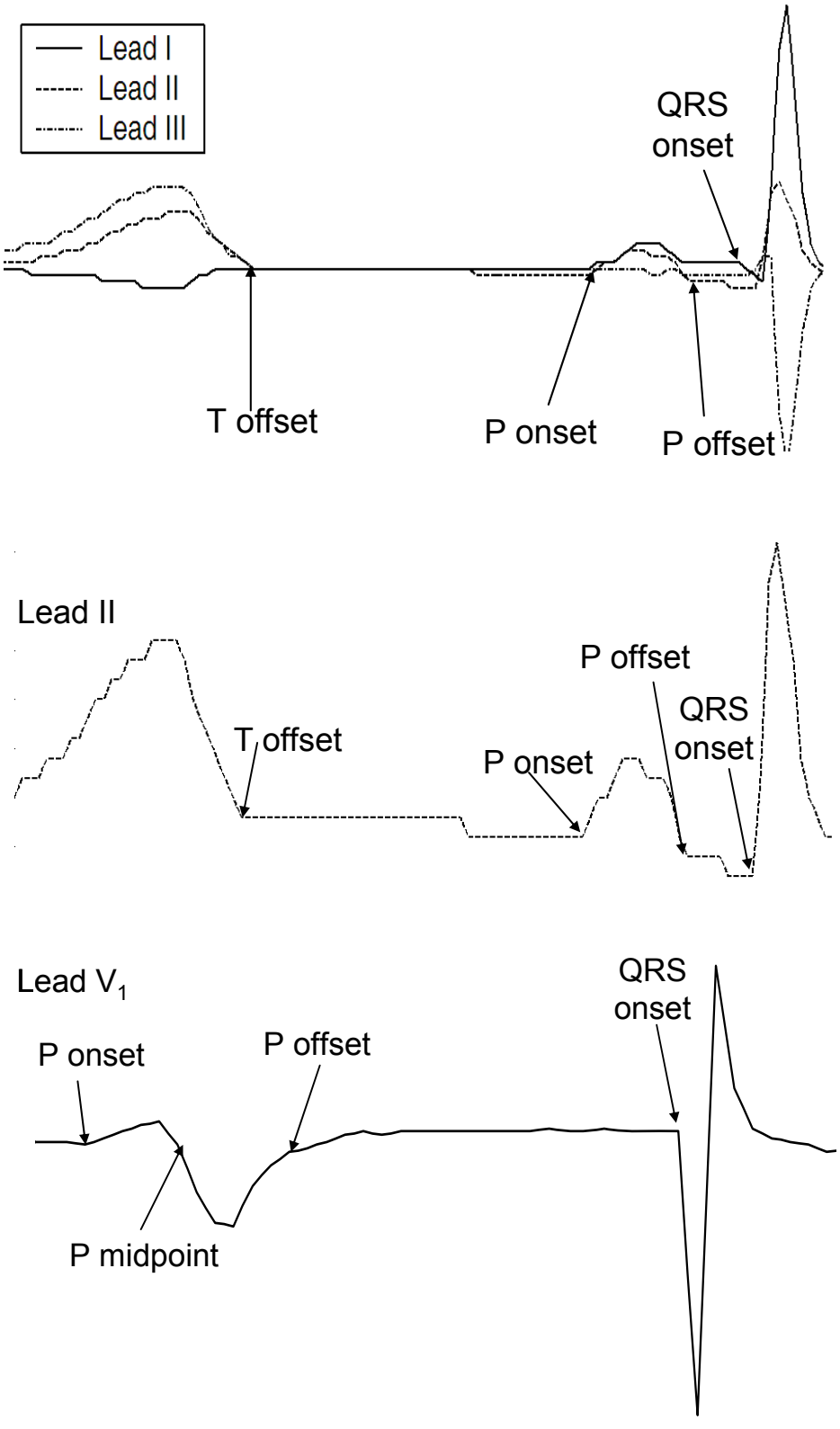

Figure 3.3 Annotations for leads II, V1, and combined I, II. and II leads.

It is important to note that the ideal ECG waveform is in no way what the physician encounters in the hospital. The inter-patient variation in waveform morphology causes great difficulty in the comparison of signals. Furthermore, the morphology of a patient's ECG waveform also changes through time. These inter-patient and intra-patient variations make fiducial point annotation difficult and frustrating [26, 28].

3.3.2.2 Feature Extraction

Following fiducial point placement, several morphological features were computed from the signals and the individual leads. For instance, the P wave duration was calculated on the V_1 lead, the II lead, and the composite I, II, and III leads. It should be noted that not all patients' leads had identifiable fiducial points preventing all features from being calculated causing missing data points in the dataset. The morphological features that were calculated include the following:

The P terminal force, calculated on the V_1 lead was a difficult feature to calculate due to its dependence on existence and voltage values of two fiducial points. For this reason, a nested set of conditional rules were used for the several permutations that arise, and the calculation of the terminal force from their locations and distances was performed. The ideal case is shown at the top of Figure 3.4 and the terminal force is defined as the time between the midpoint deflection and the P wave offset multiplied by the depth of the negative voltage curve as measured from the offset voltage [50]. The same calculation is applied to the case of the mid-point voltage being less than the offset voltage. It becomes more difficult as the offset voltage is higher than the mid-point voltage. Here, the height is measured as the average of the two voltages and the width is the time difference

between them. These differences in feature calculations are needed due to the inter-patient inconsistencies of shape and markings of the midpoint, due to its location on a slope. Additionally, alterations of the baseline that often occur between P onset and offset need to be handled in a defined and controlled way for comparison between patients. These measures can be seen in Figure 3.4.

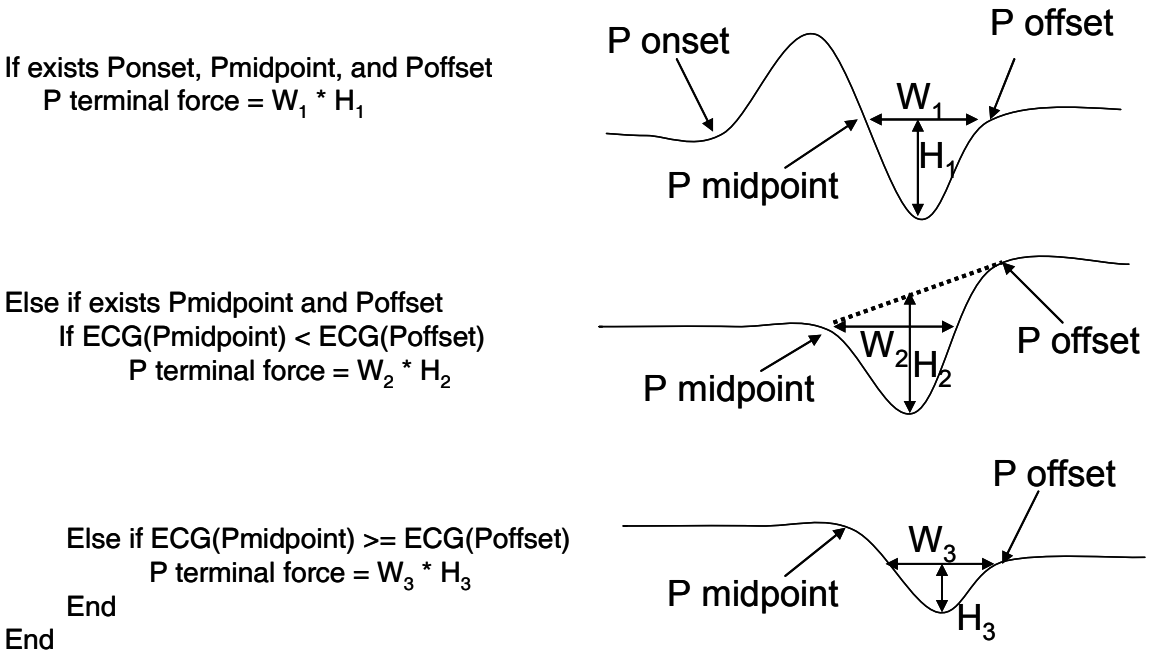

Figure 3.4 P terminal force calculation

The *P wave duration*, calculated on the V_1 lead, also becomes complicated due to its dependence on three fiducial points. If one of the points is absent, a rule must be made to calculate the overall duration. We decided that the distance between whatever points were present would be labeled the P wave duration. For instance, if there was no positive deflection (meaning there was no classic P wave onset), the distance from the midpoint to the offset would be termed the duration. Alternatively, if there was no negative

deflection, the distance from the onset to the mid point would be measured. In this manner, the P wave duration was measured with the data that could be marked and properly identified. The P wave durations were much easier to calculate on the II and composite I, II, III leads by just subtracting each lead's onset from the offset time point [20].

The *PR time interval* was measured between the composite I, II, III lead's QRS complex onset and the P wave offset [20].

The *isoelectric interval (IEI)* was measured as the P wave duration of the composite I, II, III lead minus the P wave duration of the II lead [20].

Table 3.3 Feature Set *F*

Feature	*Calculation*
Energy	$\sum x_i^2$
Nonlinear Energy (Teager Energy)	$\sum -x_i \cdot x_{i-2} + x_{i-1}^2$
Curve Length	$\sum x_i - x_{i-1}$
Hurst Coefficient	$\ln\left(\frac{range(x_i)}{std(x_i)} - \frac{i}{2}\right)$
Katz Fractal Dimension	$\sum_{i=1}^{k} \frac{\log(k-1)}{\log\left(\frac{\max(\sum_i \sqrt{(x_i - x_1)^2 + i^2})}{\sum_i \sqrt{(x_{i+1} - x_i)^2 + 1}}\right) + \log(k-1)}$
Peak Power	$\max(PSD)$
Peak Frequency	$index(\max(PSD))$
Mean Frequency	$index(mean(PSD))$
Median Frequency	$index(median(PSD))$
Spectral Entropy	$\sum PSD \cdot \log(PSD)$
Shannon Entropy	$-\sum hist(x) \cdot \log(hist(x))$

In addition to the above traditional morphological features, several time, frequency, and information domain features were calculated on the ECG. The ECG segment from the T wave offset to the Q wave onset encompasses the main region of interest in the cardiac cycle for AF, the atrial contraction period. These segments were extracted and the feature set, *F*, listed in Table 3.3, was computed. The rationale for choosing these features is based on insights and background in biological signal processing.

The energy of the signal can show the signal's tendency to stay either above or below the baseline, closely related to the signal's integral. The nonlinear energy, known as Teager's energy in [80], includes amplitude and instantaneous frequency information, along with the energy component.

Frequency domain based features can reveal other important characteristics of the signal [81]. The peak frequency and peak power identify at what frequency the signal oscillates with the most power and the magnitude of this power peak, respectively. The mean and median frequency features reveal the frequency value in the power spectrum where the mean and median frequencies appear, respectively. Spectral entropy is a measure of the regularity of the power spectrum of the signal [80]. This feature can give an indication of the overall frequency distribution, while the above frequency characteristics do not.

Shannon entropy is a measure of the randomness of the amplitude values of the signal [82]; the higher the entropy, the more disordered and closer the signal is to random Brownian motion. Both Katz fractal dimension and the Hurst parameter are measurements of the long-range dependence of the signal. These measurements can identify if a signal is becoming non-stationary, increasing in complexity, or changing its

space filling properties. Most importantly, they show the signal's self-similarity. This property can be very useful when looking for repetitions that may not be obvious to a human observer. The feature curve length tends to correlate with the two previous features closely, also showing the space-filling property without as much sensitivity to the self-similarity measure [80].

Table 3.4 Wavelet and Scales used for ECG decomposition

Wavelet Name	*Scales Calculated*
Daubechies Two	5, 10, 15, 20, 25, and 30
Daubechies Three	5, 10, 15, 20, 25, and 30
Symlets Four	5, 10, 15, 20, 25, and 30
Symlets Six	5, 10, 15, 20, 25, and 30
Coiflets One	5, 10, 15, 20, 25, and 30
Coiflets Four	5, 10, 15, 20, 25, and 30
Biorthogonal 2.2	5, 10, 15, 20, 25, and 30
Biorthogonal 4.4	5, 10, 15, 20, 25, and 30
Biorthogonal 5.5	5, 9, 13, 17, 21, and 25
Biorthogonal 6.8	5, 10, 15, 20, 25, and 30
Reverse Biorthogonal 2.2	5, 9, 13, 17, 21, and 25
Reverse Biorthogonal 4.4	5, 10, 15, 20, 25, and 30
Reverse Biorthogonal 5.5	5, 10, 15, 20, 25, and 30
Reverse Biorthogonal 6.8	5, 9, 13, 17, 21, and 25
Gaussian One	2, 4, 6, 8, 10, and 12
Gaussian Two	4, 7, 10, 13, 16, and 19
Gaussian Three	4, 7, 10, 13, 16, and 19
Gaussian Four	4, 7, 10, 13, 16, and 19
Mexican Hat	3, 5, 7, 9, 11, and 13

Following these feature computations of the actual ECG segments, wavelet decompositions of the ECGs were performed, the T offset to Q onset segments were re-extracted, and the features of feature set *F* were computed. The wavelets and their associated scales are listed in Table 3.4. These wavelets were selected based on their ability to decompose the ECG signal allowing for visually interesting dynamics around the P wave, the wave associated with the atrial contraction and AF. Additionally,

wavelets that had more lobes caused spreading of the QRS complex into the adjacent P wave at higher scales were not selected. The symlet four wavelet decomposition of an ECG sample at scales 1 through 40 can be seen in Figure 3.5. The P wave magnitude rise and fall can be seen as the scale increases.

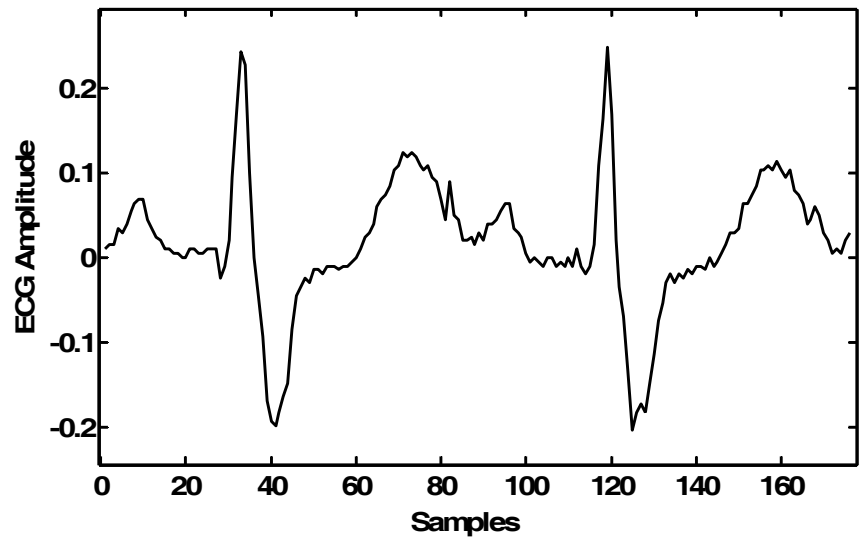

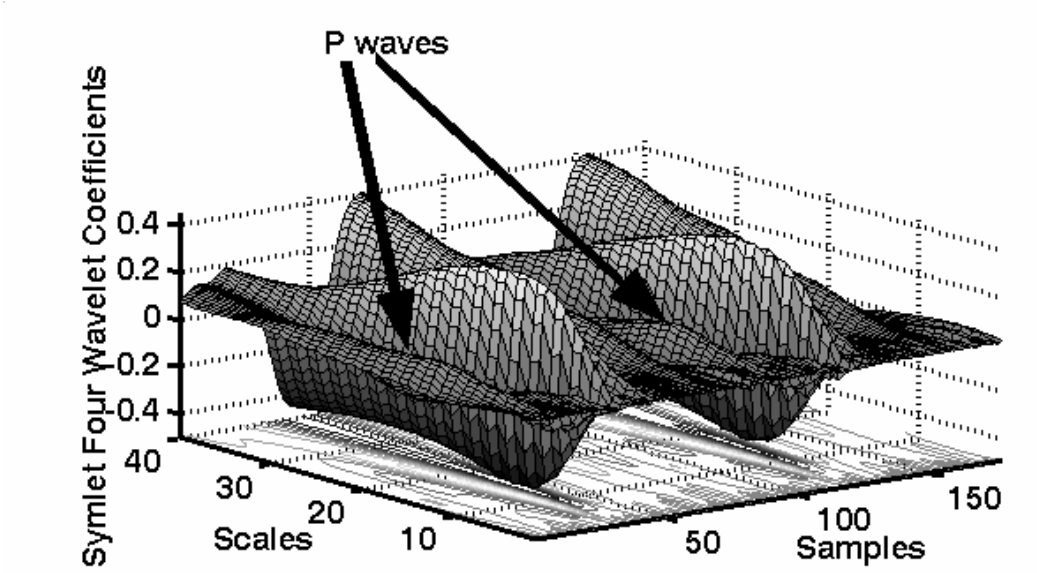

Figure 3.5 Symlet Four Wavelet Decomposition of the ECG showing the P wave changing at several scales.

In order to identify and discuss these complicated features, a naming convention has been instituted that allows for easier communication. There are several sections of the feature identifier which are separated by underscores which each have different possible values and meanings. For the preoperative data set, the first section identifies that the TQ

segment is being investigated. Next the lead is indicated as V1, I, II, or III. If a wavelet decomposition was employed, the next two sections contain the abbreviation of the wavelet employed followed by the scale that was used. The last section is the feature that was performed on the resulting signals listed above. For instance, the mean frequency of the symlet four wavelet decomposition (scale twenty) of the TQ segment on modified lead II would be abbreviated as TQ_II_sym4_sc20_Mean_Freq. This makes encoding in the algorithms and discussing the resulting features much less cumbersome.

3.4 Postoperative

Table 3.5 Summary of the postoperative data showing both the total number of patient samples and features used in future analyses.

Data Type	Number of Patient Samples	Number of Features
Clinical Dataset	80	60
ECG Dataset	46	111,672
Combined Clinical and ECG Dataset	80	111,732

Following the preoperative analysis, post surgical variables were investigated. During a postoperative atrial pacing study done several years ago, data were collected from eighty patients that were not paced. Patients were older than eighteen, in normal sinus rhythm before surgery, and on no anti-arrhythmic medications [83, 84]. Of these patients, twenty-seven develop AF in the following four days. Clinical data as well as ECG data were collected from these patients. A significant characteristic of this dataset is that some patients are missing information; for instance, the physician may have not tested the patient's cholesterol levels.

3.4.1 Clinical Dataset

The collected clinical data include the patients' demographic, preoperative, operative, and postoperative data. Some fields contain binary information, such as *History of AF* or *Beta Blocker Administered*, other fields contain continuous data, such as *Age* or *Heart Rate,* and others contained categorical data such as the *number of bypassed vessels*. Appendix A lists these data variables in their entirety.

3.4.2 ECG Feature Dataset

ECG data were also collected from patients in the form of Holter monitor tapes. Of the eighty-one patients, we have 49 with post surgical ECG recordings consisting of an intra-atrial lead and a chest lead. Most have two 48-hour tapes with between 72 and 90-hours of recorded signals. These recordings were sampled at 128 Hz with 16-bit A-to-D conversion. In some patients, the leads have been disconnected accidentally or for medical reasons. This results in only having one or no recordings at some time points for patients.

3.4.2.1 Pre-processing

Preprocessing consists of preparing the signal for feature extraction. This includes removing artifacts, filtering noise, and snipping data segments. Each ECG was filtered using both a high- and low-pass fifth-order Butterworth filter with a cutoff of one and thirty-five Hz, respectively. This removes the baseline drift DC voltage that sometimes builds on ECG electrodes (Figure 3.6) [85] as well as any high frequency noise not containing useful cardiac data.

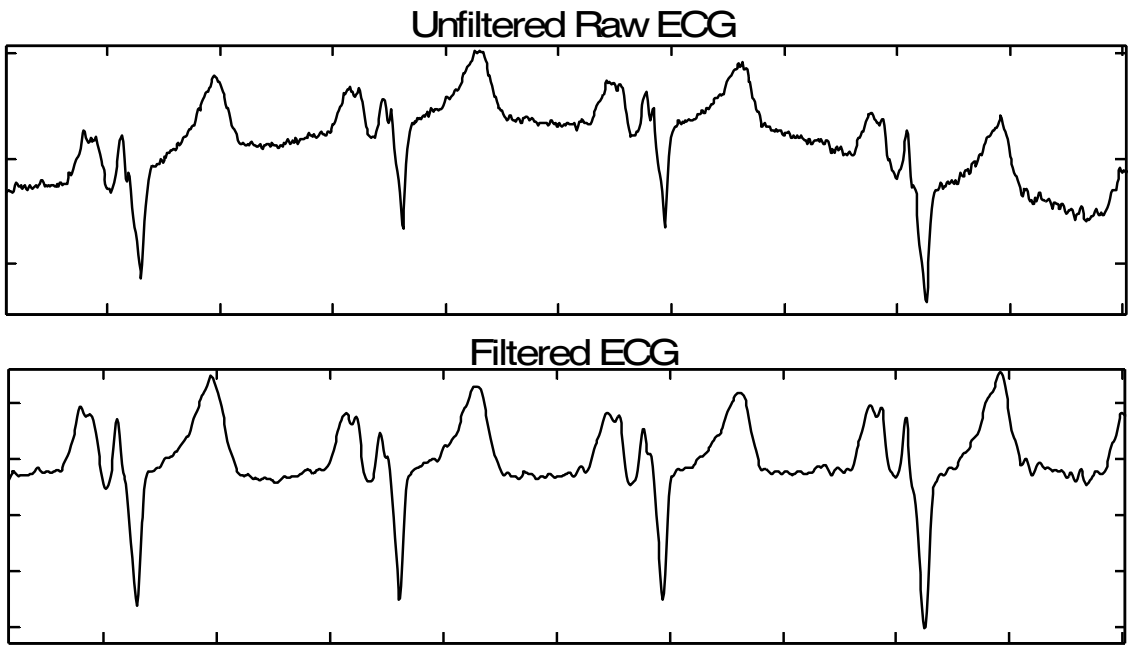

Figure 3.6 Raw Unfiltered ECG and filtered ECG

In this second dataset, we only have data directly following the surgery. We have extracted up to four, five-minute ECG segments at roughly twelve hour increments following surgery: zero, twelve, twenty-four, and thirty-six hours as shown in Figure 3.7. The locations were selected due the cardiologists' desire to identify patients early following surgery in order to administer the prophylactic when it might have the most benefit. At each of the time points, we selected a five-minute segment, trying to avoid muscle and other artifacts. This sometimes involved moving an hour away from the point of interest. These small ECG clips taken at large intervals were done to reduce the time needed for manual correction of annotations on each clip.

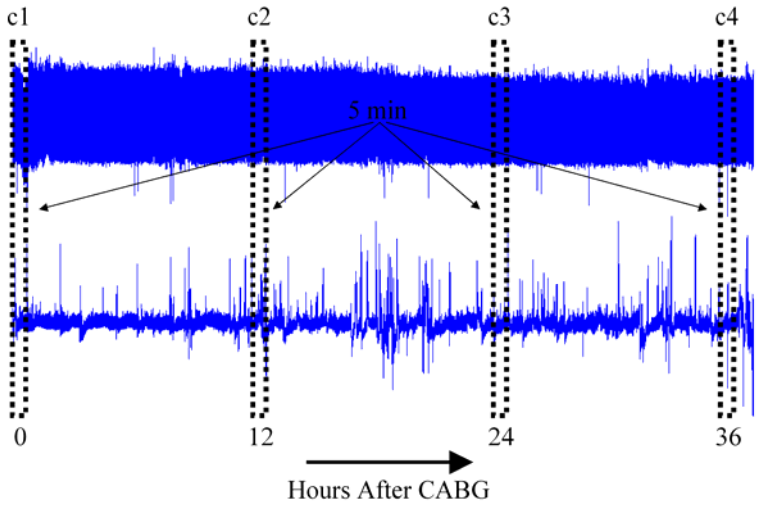

Figure 3.7. Five -minute clips of ECG are taken from both the chest and atrial leads at intervals of twelve hours following surgery.

Unlike many collected biosignals, ECGs contain "strong" reference points in the signal, from which much information can be determined. The R waves' large amplitude on the chest lead allows for identification of the ventricle contraction times, while the atrial contraction can be determined from the intra-atrial lead. Each of the five-minute segments was annotated for both ventricle contraction on the chest lead and atrial contraction on the atrial lead. With these collected time points and the signals' segments that they are associated with, many different computations can be performed.

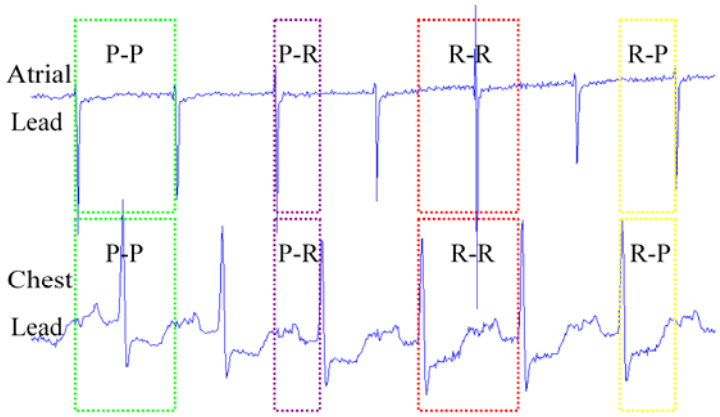

Figure 3.8. ECG segments extracted from the chest and atrial leads according to the P and R points.

With the R and P wave locations, we extracted and stored consecutive R-R, P-P, R-P, and P-R segments of the signal. This was done on both the chest and atrial lead, yielding eight different segment groups, as seen in Figure 3.8, from a single five-minute clip with each group containing all the possible peak-to-peak segments.

The durations of each of these ECG segments were also calculated as shown in Figure 3.9. The locations in time of the R positions were used to determine the heart rate (R-to-R durations). Many studies have been done investigating heart rate variability (HRV) and its association with arrhythmia occurrence, citing the importance of the sympathetic nervous system on cardiac rate control [14].

Each of the segments and their associated durations can then be analyzed for a correlation with AF by first decomposing the signal using a feature set consisting of several approaches.

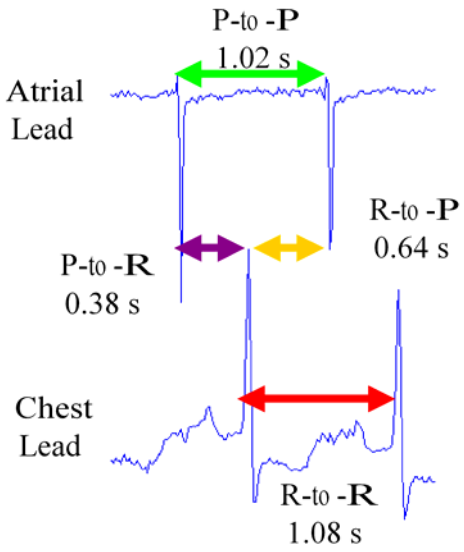

Figure 3.9. ECG segment durations observed from ECG segments.

3.4.2.2 Feature Extraction

The ECG segments were then used to calculate the feature set, *F*, comprising the eleven feature measures listed in Table 3.3. Following feature extraction on the individual ECG segments (R-R, R-P, P-P, and P-R), we run the statistics set, *S*, on each of the features calculated on each of the segments, yielding some characteristics of the data obtained from feature calculation. The statistics set, *S,* consists of the maximum, minimum, median, mean, standard deviation, skewness, and kurtosis.

The location in time of P and R positions were also used to determine the heart rate (R-to-R durations) and other time durations of importance (P-P, R-P, P-R) as referred to previously. Again, the statistics set, *S,* is then applied to all these duration measures. The durations and the locations in time are also analyzed for frequency domain information by performing a Lomb-Scargle periodogram [86]. This is needed in order to find the frequency spectrum of the non-uniformly spaced duration samples. The frequency bands

investigated were very low frequency (VLF) consisting of 0.0033 to 0.04 Hz, low frequency (LF) consisting of 0.04 to 0.15 Hz, and high frequency consisting of 0.15 to 0.4 Hz. The power in each of these bands was calculated and ratios between the bands (VLF/LF, VLF/HF, LF/HF) as well as the total power (VLF/TP, LF/TP, HF/TP) were calculated as features.

Signal averaging techniques were performed on the P wave of the signal to derive two average P waves. This was done by triggering on both the atrial contraction on the atrial lead and the ventricular contraction on the chest lead. These two P waves were subjected to the feature set *F* as well as the morphological P wave features discussed previously.

The number of ectopic beats, abnormal extra or skipped beats, was counted for each of the clips as well. These were further identified individually as premature atrial contractions (PAC) or premature ventricular contractions (PVC). These types can be identified by their timing with previous and following contractions. A PAC will generally follow the previous too closely while the next beat occurs after the usual time delay. An PVC also usually follows the previous beat too closely but the next beat has a large delay. After identifying these beats, the ratios of their occurrence were calculated as features.

Following these feature computations of the ECG segments, wavelet decompositions of the ECG clips were taken, the R-R, R-P, P-P, and P-R segments were re-extracted, and the feature set *F* and statistic set *S* were computed as previously discussed. The wavelets and their associated scales are listed in Table 3.4.

Given the inherent variability in ECG signals among patients, each of these features offers information that can be used to distinguish between patient classes. We believe

that, collectively, these features can help distinguish the two classes [87-90]. The extraction of feature values from the ECG signals reduces the dimensionality of the problem to a computationally tractable level. In this process, signal information is encoded so that it can be used for classification or prediction [91].

In order to identify and discuss these complicated features, a naming convention has been instituted that allows for easier communication. There are several sections of the feature identifier which are separated by underscores which each have different possible values and meanings. For the preoperative features, the first section is the clip identifier which starts with a "c" and follows with a number between one and four corresponding to the clips taken zero, twelve, 24, and 36 hours after surgery. The second section identifies which segment the feature is being calculated on, being either PP, PR, RP, or RR. Next identifies the feature as being taken from the chest or atrial lead. If a wavelet transform was employed, the next two identifiers will be an abbreviation of the wavelet used followed by the scale of the wavelet identified as "sc" and the number of the scale following. Next is the feature of feature set *F* that was computed and lastly comes the statistic that was computed. For instance, the curve length of the daubechies three wavelet decomposition (scale 15) of the PR segment of the Atrial lead's first clip TQ segment is abbreviated to c1_PR_Atrial_db3_sc15_Curve_length_skewness. This makes encoding in the algorithms and discussing the resulting features much less cumbersome.

3.5 Results

For both the pre- and postoperative features calculated above, univariate t-tests and Chi-squared tests were used to determine their classification potential for postoperative AF

onset. Appendix B shows the characteristics of those pre- and postoperative variables which had a p-value < 0.05 except for the postoperative continuous variable, for which only those with a p-value < 0.01 was listed due to their large amount. Table 3.6 and Table 3.7 show the univariate pre- and postoperative characteristics that have a p-value < 0.01 and 0.003, respectively. Binary and categorical variables are listed as the percentage of AF or non-AF patients in that category having the given value. Continuous variables have the mean plus or minus the standard deviation of the feature for AF or non-AF patients. For each variable, either the ratio of the patients having that characteristic in the category or the number of patients in that category is shown in these tables.

As is seen from their absence in Table 3.6, traditional ECG measures did not perform well on the preoperative cohort. The morphological P wave characteristics performed poorly as seen in Table 3.8 with the best being the P terminal force which had a p value of 0.169.

The features computed on the ECG itself, without wavelet decomposition, did not fare much better as seen in Table 3.9, with similarly low values, none having a p-value below 0.05. Two features, median frequency of the T-to-Q segment on the V_1 lead and the Shannon entropy of the T-to-Q segment on the I lead performed the best among these with p-values of 0.077 and 0.063, respectively.

Table 3.6 Preoperative features with a p-value < 0.01

Preoperative Binary Feature	Non-AF	AF	Total	p value
Preoperative AF	1.6% (6/386)	19.7% (31/157)	6.8% (37/543)	0.000
Cardiomegaly	13.7% (53/388)	29.3% (46/157)	18.2% (99/545)	0.000
Prior heart surgery	1.8% (7/388)	5.7% (9/157)	2.9% (16/545)	0.014
Current digoxin use	3.4% (13/388)	9.6% (15/157)	5.1% (28/545)	0.003
African-American	16.2% (63/388)	5.7% (9/157)	13.2% (72/545)	0.001

Preoperative Categorical Feature	Category	Non-AF	AF	Total	p value
Left Atrial Size		384	157	541	0.000
	0	58.9% (226/384)	38.2% (60/157)	52.9% (286/541)	
	1	6.8% (26/384)	7.6% (12/157)	7.0% (38/541)	
	2	23.4% (90/384)	29.9% (47/157)	25.3% (137/541)	
	3	3.9% (15/384)	12.7% (20/157)	6.5% (35/541)	
	4	1.6% (6/384)	2.5% (4/157)	1.8% (10/541)	
	5	3.9% (15/384)	7.6% (12/157)	5.0% (27/541)	
	6	1.0% (4/384)	0.6% (1/157)	0.9% (5/541)	
	7	0.5% (2/384)	0.6% (1/157)	0.6% (3/541)	
Ejection Fraction		387	157	544	0.010
	0	53.0% (205/387)	35.0% (55/157)	47.8% (260/544)	
	1	0.5% (2/387)	0.0% (0/157)	0.4% (2/544)	
	2	1.6% (6/387)	2.5% (4/157)	1.8% (10/544)	
	3	3.4% (13/387)	3.8% (6/157)	3.5% (19/544)	
	4	7.5% (29/387)	8.3% (13/157)	7.7% (42/544)	
	5	8.0% (31/387)	14.6% (23/157)	9.9% (54/544)	
	6	19.6% (76/387)	22.9% (36/157)	20.6% (112/544)	
	7	5.9% (23/387)	12.1% (19/157)	7.7% (42/544)	
	8	0.5% (2/387)	0.6% (1/157)	0.6% (3/544)	
Mitral Regurgitation		332	141	473	0.002
	1	83.1% (276/332)	68.8% (97/141)	78.9% (373/473)	
	2	11.7% (39/332)	17.7% (25/141)	13.5% (64/473)	
	3	2.1% (7/332)	6.4% (9/141)	3.4% (16/473)	
	4	3.0% (10/332)	7.1% (10/141)	4.2% (20/473)	

Table 3.6 Continued

Mammary Artery Anastamoses		388	157	545	0.003
	0	12.1% (47/388)	22.3% (35/157)	15.0% (82/545)	
	1	87.4% (339/388)	75.2% (118/157)	83.9% (457/545)	
	2	0.3% (1/388)	1.9% (3/157)	0.7% (4/545)	
	3	0.3% (1/388)	0.6% (1/157)	0.4% (2/545)	

Preoperative Continuous Feature	**Non-AF**	**AF**	**Total**	**p value**
Age	61.49+/-9.1(388)	64.98+/-8.9(157)	62.50+/-9.1(545)	0.000
Height (In)	69.70+/-2.7(388)	70.43+/-2.4(157)	69.91+/-2.6(545)	0.003
Ischemic Time (min)	61.19+/-36.5(388)	71.45+/-38.4(157)	64.14+/-37.3(545)	0.004
Cardiopulmonary bypass time (min)	98.90+/-49.7(388)	112.39+/-48.7(157)	102.78+/-49.7(545)	0.004
TQ_II_sym4_sc20_Mean_Freq	9.79+/-4.0(104)	11.67+/-4.8(54)	10.43+/-4.3(158)	0.009
TQ_II_coif1_sc15_Median_Freq	8.86+/-1.6(104)	10.06+/-3.3(54)	9.27+/-2.4(158)	0.003
TQ_V1_coif1_sc20_Peak_Freq	7.35+/-2.4(102)	6.13+/-2.9(55)	6.92+/-2.7(157)	0.006
TQ_II_bior4.4_sc5_Mean_Freq	31.97+/-5.3(104)	34.49+/-6.1(54)	32.83+/-5.7(158)	0.008
TQ_II_bior5.5_sc21_Mean_Freq	10.24+/-3.5(104)	11.91+/-4.3(54)	10.81+/-3.9(158)	0.010
TQ_II_rbio5.5_sc5_Mean_Freq	29.29+/-6.0(104)	31.92+/-6.1(54)	30.19+/-6.1(158)	0.010
TQ_II_gaus3_sc13_Peak_Freq	6.64+/-1.4(104)	5.87+/-1.9(54)	6.38+/-1.6(158)	0.004

Table 3.7 Postoperative features with a p-value < 0.003

Postoperative Continuous Feature	**Non-AF**	**AF**	**Total**	**p value**
Age	63.47+/-10.6(53)	72.59+/-6.9(27)	66.55+/-10.5(80)	0.000
c3_PP_Chest_Energy_skewness	1.93+/-1.3(26)	3.91+/-2.5(14)	2.62+/-2.0(40)	0.002
c3_PP_Chest_Energy_kurtosis	10.09+/-7.4(26)	32.10+/-31.9(14)	17.80+/-22.1(40)	0.002
c3_PP_Atrial_db2_sc5_Energy_skewness	0.43+/-0.4(29)	1.54+/-1.8(15)	0.81+/-1.2(44)	0.003
c1_PR_Atrial_db3_sc15_Curve_length_skewness	0.48+/-0.9(25)	-0.90+/-1.6(14)	-0.01+/-1.3(39)	0.001
c1_PR_Atrial_db3_sc20_Nonlinear_Energy_skewness	0.75+/-1.0(25)	-0.42+/-1.2(14)	0.33+/-1.2(39)	0.003
c1_PR_Atrial_db3_sc20_Curve_length_skewness	0.42+/-0.8(25)	-0.78+/-1.5(14)	-0.01+/-1.2(39)	0.002
c1_PR_Atrial_sym4_sc15_Curve_length_skewness	0.53+/-0.9(25)	-0.90+/-1.8(14)	0.02+/-1.5(39)	0.002
c2_PR_Atrial_sym4_sc20_Peak_Freq_skewness	0.76+/-3.7(27)	-4.30+/-5.5(14)	-0.97+/-5.0(41)	0.001
c3_PP_Atrial_sym6_sc5_Energy_skewness	0.43+/-0.3(29)	1.49+/-1.8(15)	0.79+/-1.2(44)	0.003

Table 3.7 Continued

c2_RP_Atrial_sym6_sc10_Mean_Freq_kurtosis	4.18+/-2.2(27)	11.55+/-10.7(14)	6.70+/-7.3(41)	0.001
c2_RP_Atrial_sym6_sc10_Median_Freq_kurtosis	4.07+/-3.1(27)	12.49+/-12.4(14)	6.95+/-8.5(41)	0.002
c1_PR_Atrial_sym6_sc20_Nonlinear_Energy_skewness	0.79+/-1.1(25)	-0.36+/-1.1(14)	0.38+/-1.2(39)	0.003
c2_PR_Chest_sym6_sc20_Median_Freq_min	4.80+/-1.0(27)	6.69+/-2.7(14)	5.45+/-2.0(41)	0.002
c3_PP_Atrial_coif1_sc5_Peak_Freq_std	5.34+/-2.0(29)	7.13+/-1.4(15)	5.95+/-2.0(44)	0.003
c2_RP_Atrial_coif1_sc10_Shannon_Entropy_kurtosis	5.21+/-4.8(27)	20.10+/-23.6(14)	10.30+/-15.7(41)	0.003
c1_PR_Atrial_coif1_sc15_Curve_length_skewness	0.38+/-0.7(25)	-0.97+/-1.8(14)	-0.10+/-1.4(39)	0.002
c4_PP_Atrial_coif1_sc25_Peak_Freq_mean	2.33+/-1.1(24)	1.21+/-1.0(14)	1.92+/-1.1(38)	0.002
c4_PR_Chest_coif1_sc25_Shannon_Entropy_skewness	-0.60+/-0.5(22)	-2.61+/-2.8(13)	-1.35+/-2.0(35)	0.002
c3_PP_Atrial_coif4_sc5_Energy_skewness	0.42+/-0.4(29)	1.48+/-1.7(15)	0.78+/-1.2(44)	0.003
c3_PP_Atrial_coif4_sc5_Nonlinear_Energy_skewness	0.48+/-0.4(29)	1.66+/-2.0(15)	0.88+/-1.3(44)	0.003
c2_RP_Atrial_coif4_sc10_Median_Freq_kurtosis	3.67+/-2.8(27)	8.94+/-6.6(14)	5.47+/-5.0(41)	0.001
c1_PR_Atrial_coif4_sc20_Nonlinear_Energy_skewness	0.79+/-1.0(25)	-0.33+/-1.1(14)	0.39+/-1.2(39)	0.003
c3_PP_Atrial_bior2.2_sc10_Mean_Freq_skewness	0.33+/-0.9(29)	1.66+/-1.7(15)	0.79+/-1.4(44)	0.001
c3_PP_Atrial_bior2.2_sc10_Peak_Freq_min	3.97+/-2.4(29)	1.80+/-1.6(15)	3.23+/-2.4(44)	0.003
c3_RP_Atrial_bior2.2_sc10_Mean_Freq_skewness	0.16+/-0.6(26)	1.69+/-1.8(14)	0.70+/-1.3(40)	0.000
c3_PP_Atrial_bior2.2_sc15_Katz_FD_skewness	0.60+/-0.4(29)	1.63+/-1.5(15)	0.95+/-1.1(44)	0.002
c3_PP_Atrial_bior2.2_sc15_Nonlinear_Energy_kurtosis	3.63+/-1.4(29)	12.34+/-14.7(15)	6.60+/-9.4(44)	0.003
c3_RP_Atrial_bior2.2_sc15_Katz_FD_skewness	0.68+/-0.5(26)	2.12+/-2.2(14)	1.18+/-1.5(40)	0.002
c3_PR_Atrial_bior2.2_sc15_Katz_FD_skewness	0.68+/-0.4(26)	1.87+/-1.7(14)	1.10+/-1.2(40)	0.002
c4_PP_Atrial_bior2.2_sc20_Peak_Freq_min	1.83+/-1.3(24)	0.50+/-0.8(14)	1.34+/-1.3(38)	0.002
c3_RP_Atrial_bior2.2_sc25_Katz_FD_skewness	0.66+/-0.6(26)	1.57+/-1.3(14)	0.98+/-1.0(40)	0.003
c3_RP_Atrial_bior2.2_sc25_Katz_FD_kurtosis	4.02+/-1.7(26)	9.98+/-9.2(14)	6.11+/-6.2(40)	0.002
c1_PP_Atrial_bior4.4_sc5_Peak_Freq_kurtosis	6.60+/-4.5(28)	12.82+/-7.3(15)	8.77+/-6.3(43)	0.001
c1_PR_Atrial_bior4.4_sc15_Curve_length_skewness	0.46+/-0.8(25)	-0.88+/-1.8(14)	-0.02+/-1.4(39)	0.002
c1_PR_Chest_bior4.4_sc15_Peak_Freq_std	0.57+/-0.3(25)	1.25+/-1.0(14)	0.81+/-0.7(39)	0.003
c1_PR_Atrial_bior4.4_sc20_Curve_length_skewness	0.41+/-0.8(25)	-0.81+/-1.6(14)	-0.03+/-1.3(39)	0.002
c1_PR_Atrial_bior4.4_sc25_Peak_Freq_kurtosis	20.94+/-34.0(23)	152.42+/-175.3(13)	68.42+/-124.0(36)	0.001
c2_RP_Atrial_bior4.4_sc25_Shannon_Entropy_kurtosis	4.79+/-4.4(27)	14.74+/-15.1(14)	8.19+/-10.5(41)	0.003
c3_PP_Atrial_bior5.5_sc5_Energy_skewness	0.43+/-0.4(29)	1.46+/-1.7(15)	0.78+/-1.1(44)	0.003
c4_PP_Atrial_bior5.5_sc5_Mean_Freq_max	22.30+/-3.7(24)	26.40+/-3.8(14)	23.81+/-4.2(38)	0.002
c1_PR_Atrial_bior5.5_sc17_Curve_length_skewness	0.52+/-1.0(25)	-0.88+/-1.7(14)	0.01+/-1.4(39)	0.002
c1_PR_Atrial_bior5.5_sc25_Peak_Freq_kurtosis	22.90+/-36.8(23)	149.74+/-158.7(12)	66.39+/-113.0(35)	0.001
c1_PR_Atrial_bior6.8_sc20_Curve_length_skewness	0.45+/-0.9(25)	-0.75+/-1.5(14)	0.02+/-1.3(39)	0.003
c1_PR_Atrial_rbio2.2_sc13_Curve_length_skewness	0.49+/-0.9(25)	-0.87+/-1.5(14)	0.00+/-1.3(39)	0.001

Table 3.7 Continued

c4_PP_Atrial_rbio2.2_sc17_Peak_Freq_mean	2.40+/-1.1(24)	1.20+/-0.9(14)	1.96+/-1.1(38)	0.001
c4_PP_Atrial_rbio2.2_sc21_Peak_Freq_mean	2.08+/-1.0(24)	1.06+/-0.8(14)	1.70+/-1.1(38)	0.003
c1_PR_Atrial_rbio4.4_sc15_Curve_length_skewness	0.64+/-1.2(25)	-0.84+/-1.7(14)	0.11+/-1.5(39)	0.003
c2_RP_Atrial_rbio5.5_sc10_Peak_Freq_skewness	0.36+/-1.7(27)	3.12+/-3.7(14)	1.30+/-2.8(41)	0.002
c3_RP_Atrial_rbio5.5_sc10_Shannon_Entropy_std	0.04+/-0.0(26)	0.07+/-0.0(14)	0.05+/-0.0(40)	0.002
c2_PR_Chest_rbio5.5_sc20_Median_Freq_min	4.92+/-1.1(27)	6.93+/-2.8(14)	5.61+/-2.0(41)	0.002
c1_PP_Atrial_rbio5.5_sc25_Peak_Freq_max	4.86+/-0.8(28)	3.83+/-1.1(15)	4.50+/-1.1(43)	0.002
c1_RP_Atrial_rbio5.5_sc25_Peak_Freq_max	5.08+/-1.1(25)	3.50+/-1.3(14)	4.51+/-1.4(39)	0.000
c1_PR_Atrial_rbio5.5_sc25_Peak_Freq_kurtosis	36.54+/-58.7(24)	172.79+/-176.5(11)	79.36+/-124.9(35)	0.002
c3_PP_Atrial_rbio6.8_sc5_Energy_skewness	0.40+/-0.4(29)	1.42+/-1.6(15)	0.75+/-1.1(44)	0.002
c3_PP_Atrial_rbio6.8_sc5_Nonlinear_Energy_skewness	0.45+/-0.4(29)	1.60+/-1.9(15)	0.84+/-1.2(44)	0.002
c2_RP_Atrial_rbio6.8_sc9_Mean_Freq_kurtosis	4.38+/-2.6(27)	9.74+/-7.9(14)	6.21+/-5.6(41)	0.002
c2_RP_Atrial_rbio6.8_sc9_Median_Freq_kurtosis	3.96+/-3.1(27)	10.70+/-9.0(14)	6.26+/-6.5(41)	0.001
c3_PP_Atrial_rbio6.8_sc9_Mean_Freq_min	7.20+/-0.8(29)	6.32+/-0.9(15)	6.90+/-0.9(44)	0.002
c1_PR_Atrial_rbio6.8_sc17_Curve_length_skewness	0.53+/-1.0(25)	-0.80+/-1.6(14)	0.05+/-1.4(39)	0.003
c2_PR_Atrial_rbio6.8_sc17_Peak_Freq_kurtosis	10.91+/-14.4(25)	51.14+/-53.6(14)	25.35+/-38.7(39)	0.001
c2_PR_Chest_gaus1_sc2_Mean_Freq_min	4.47+/-2.0(27)	8.72+/-4.7(14)	5.92+/-3.7(41)	0.000
c3_PP_Atrial_gaus1_sc2_Energy_skewness	0.34+/-0.6(29)	1.58+/-1.7(15)	0.76+/-1.3(44)	0.001
c3_PP_Atrial_gaus1_sc2_Energy_kurtosis	3.80+/-2.1(29)	15.92+/-19.8(15)	7.93+/-12.8(44)	0.002
c3_PR_Atrial_gaus1_sc2_Median_Freq_skewness	0.15+/-0.8(26)	2.55+/-3.4(14)	0.99+/-2.3(40)	0.001
c4_PR_Chest_gaus1_sc6_Peak_Freq_mean	5.12+/-3.1(22)	1.71+/-2.4(13)	3.85+/-3.3(35)	0.002
c3_PR_Chest_gaus1_sc8_Katz_FD_skewness	0.65+/-1.1(26)	2.17+/-1.8(14)	1.18+/-1.5(40)	0.002
c3_PR_Chest_gaus1_sc10_Energy_skewness	0.67+/-1.0(26)	2.36+/-2.2(14)	1.26+/-1.7(40)	0.002
c3_PR_Chest_gaus1_sc12_Energy_skewness	0.76+/-0.9(26)	2.58+/-2.4(14)	1.40+/-1.8(40)	0.001
c2_PR_Chest_gaus2_sc10_Median_Freq_min	4.28+/-1.1(27)	6.30+/-2.8(14)	4.97+/-2.1(41)	0.002
c4_PP_Atrial_gaus2_sc10_Peak_Freq_mean	2.44+/-1.1(24)	1.30+/-0.9(14)	2.02+/-1.2(38)	0.002
c2_PR_Atrial_gaus3_sc7_Mean_Freq_mean	7.69+/-1.6(27)	6.18+/-1.0(14)	7.17+/-1.6(41)	0.003
c2_PR_Atrial_gaus3_sc7_Peak_Freq_mean	6.90+/-1.3(27)	5.21+/-1.0(14)	6.32+/-1.5(41)	0.000
c1_PR_Atrial_gaus3_sc10_Nonlinear_Energy_skewness	0.73+/-1.0(25)	-0.39+/-1.1(14)	0.33+/-1.2(39)	0.003
c1_RP_Atrial_gaus3_sc13_Mean_Freq_min	3.29+/-1.1(25)	4.61+/-1.3(14)	3.77+/-1.3(39)	0.002
c1_RP_Atrial_gaus3_sc13_Median_Freq_min	4.25+/-1.8(25)	6.66+/-2.5(14)	5.11+/-2.3(39)	0.001
c3_PR_Chest_gaus3_sc13_Katz_FD_skewness	0.51+/-1.0(26)	2.35+/-2.4(14)	1.15+/-1.8(40)	0.001
c1_PP_Atrial_gaus3_sc19_Peak_Freq_skewness	-0.30+/-2.6(26)	-4.95+/-6.6(15)	-2.00+/-4.9(41)	0.003
c2_PR_Chest_gaus4_sc13_Median_Freq_min	4.30+/-0.6(27)	5.83+/-2.3(14)	4.82+/-1.6(41)	0.002
c2_RP_Atrial_gaus4_sc19_Shannon_Entropy_skewness	0.02+/-1.7(27)	-2.55+/-3.5(14)	-0.85+/-2.7(41)	0.003

Table 3.7 Continued

c2_RP_Atrial_mexh_sc3_Median_Freq_kurtosis	3.26+/-1.5(27)	6.24+/-3.9(14)	4.28+/-2.9(41)	0.001
c4_PP_Atrial_mexh_sc3_Peak_Freq_min	1.79+/-1.3(24)	0.43+/-0.7(14)	1.29+/-1.3(38)	0.001
c2_PR_Chest_mexh_sc7_Median_Freq_min	4.31+/-1.1(27)	6.34+/-3.0(14)	5.00+/-2.1(41)	0.003
c4_PP_Atrial_mexh_sc7_Peak_Freq_mean	2.46+/-1.1(24)	1.32+/-0.9(14)	2.04+/-1.2(38)	0.002

Table 3.8 Preoperative morphological P wave features and their univariate results.

P wave Features	**Non-AF**	**AF**	**Total**	**p value**
VAraw_Pdur_V1	24.57+/-6.6(98)	24.69+/-7.4(50)	24.61+/-6.9(148)	0.922
VAraw_Ptermfor	137.57+/-138.5(92)	105.17+/-91.8(42)	127.42+/-126.3(134)	0.169
VAraw_Pdur_II	29.38+/-5.4(101)	29.97+/-7.0(53)	29.58+/-6.0(154)	0.558
VAraw_Pdur_std	30.88+/-6.1(101)	31.06+/-5.7(54)	30.94+/-6.0(155)	0.857
VAraw_PRsegint	11.92+/-7.4(101)	11.79+/-6.2(54)	11.88+/-7.0(155)	0.909
VAraw_IEI	1.62+/-4.5(100)	0.99+/-4.8(53)	1.40+/-4.6(153)	0.420
VAraw_TP_PQlevel	-0.02+/-0.1(104)	-0.03+/-0.1(54)	-0.02+/-0.1(158)	0.425

Table 3.9 Preoperative features derived from the raw (no wavelet decomposition) ECG signal

Preoperative ECG Features	**Non-AF**	**AF**	**Total**	**p value**
TQ_V1_Energy	71.46+/-94.8(102)	87.32+/-121.4(55)	77.02+/-104.8(157)	0.367
TQ_V1_Spectral_entropy	-21876.36+/-34808.7(102)	-27716.55+/-35289.1(55)	-23922.29+/-34976.4(157)	0.320
TQ_V1_Katz_FD	1.06+/-0.1(102)	1.06+/-0.1(55)	1.06+/-0.1(157)	0.608
TQ_V1_Nonlinear_Energy	31.20+/-34.7(102)	29.04+/-29.9(55)	30.45+/-33.0(157)	0.696
TQ_V1_Mean_Freq	5.96+/-3.4(102)	5.15+/-3.9(55)	5.68+/-3.6(157)	0.176
TQ_V1_Median_Freq	4.77+/-3.1(102)	3.83+/-3.3(55)	4.44+/-3.2(157)	0.077
TQ_V1_Peak_Freq	1.73+/-3.2(102)	1.26+/-2.6(55)	1.57+/-3.0(157)	0.347
TQ_V1_Peak_Pow_Amp	2398.58+/-7257.8(102)	2877.04+/-6035.2(55)	2566.20+/-6838.4(157)	0.677
TQ_V1_Shannon_Entropy	0.23+/-0.1(102)	0.24+/-0.1(55)	0.23+/-0.1(157)	0.623
TQ_V1_Curve_length	56.74+/-52.4(102)	51.67+/-41.8(55)	54.96+/-48.9(157)	0.536
TQ_I_Energy	90.84+/-160.4(86)	84.87+/-175.4(46)	88.76+/-165.1(132)	0.844
TQ_I_Spectral_entropy -	26209.94+/-49227.1(86)	-22912.60+/-47719.5(46)	-25060.86+/-48549.9(132)	0.712

Table 3.9 Continued

TQ_I_Katz_FD	1.08+/-0.1(86)	1.07+/-0.1(46)	1.08+/-0.1(132)	0.661
TQ_I_Nonlinear_Energy	35.97+/-44.9(86)	37.64+/-86.4(46)	36.55+/-62.2(132)	0.884
TQ_I_Mean_Freq	6.04+/-2.9(86)	6.70+/-3.1(46)	6.27+/-3.0(132)	0.230
TQ_I_Median_Freq	4.56+/-2.6(86)	4.94+/-2.6(46)	4.69+/-2.6(132)	0.424
TQ_I_Peak_Freq	1.69+/-2.7(86)	1.86+/-2.7(46)	1.75+/-2.6(132)	0.738
TQ_I_Peak_Pow_Amp	1972.06+/-4787.6(86)	1210.88+/-2391.6(46)	1706.80+/-4119.5(132)	0.314
TQ_I_Shannon_Entropy	0.24+/-0.1(86)	0.27+/-0.1(46)	0.25+/-0.1(132)	0.063
TQ_I_Curve_length	60.80+/-51.8(86)	61.95+/-74.8(46)	61.20+/-60.6(132)	0.918
TQ_II_Energy	169.43+/-212.4(104)	156.41+/-198.8(54)	164.98+/-207.3(158)	0.709
TQ_II_Spectral_entropy	-61736.78+/-85461.5(104)	-64680.81+/-83390.8(54)	-62742.97+/-84504.9(158)	0.836
TQ_II_Katz_FD	1.10+/-0.1(104)	1.09+/-0.1(54)	1.10+/-0.1(158)	0.397
TQ_II_Nonlinear_Energy	50.59+/-37.9(104)	48.95+/-51.7(54)	50.03+/-43.0(158)	0.821
TQ_II_Mean_Freq	5.44+/-2.6(104)	5.42+/-2.9(54)	5.43+/-2.7(158)	0.966
TQ_II_Median_Freq	4.50+/-2.4(104)	4.37+/-2.2(54)	4.46+/-2.3(158)	0.738
TQ_II_Peak_Freq	2.37+/-2.7(104)	1.96+/-2.4(54)	2.23+/-2.6(158)	0.333
TQ_II_Peak_Pow_Amp	3659.65+/-8262.0(104)	3259.78+/-4972.8(54)	3522.99+/-7291.5(158)	0.745
TQ_II_Shannon_Entropy	0.26+/-0.1(104)	0.27+/-0.1(54)	0.26+/-0.1(158)	0.665
TQ_II_Curve_length	79.79+/-47.6(104)	72.70+/-53.4(54)	77.36+/-49.6(158)	0.396
TQ_III_Energy	131.56+/-218.7(86)	98.85+/-127.7(46)	120.17+/-192.0(132)	0.353
TQ_III_Spectral_entropy	-36906.08+/-69832.9(86)	-33597.21+/-52865.6(46)	-35752.99+/-64239.9(132)	0.779
TQ_III_Katz_FD	1.09+/-0.1(86)	1.08+/-0.1(46)	1.09+/-0.1(132)	0.907
TQ_III_Nonlinear_Energy	43.00+/-54.3(86)	48.54+/-75.9(46)	44.93+/-62.4(132)	0.629
TQ_III_Mean_Freq	5.95+/-3.3(86)	5.44+/-3.3(46)	5.77+/-3.3(132)	0.405
TQ_III_Median_Freq	4.23+/-2.4(86)	3.97+/-2.4(46)	4.14+/-2.4(132)	0.556
TQ_III_Peak_Freq	1.72+/-2.4(86)	1.37+/-2.2(46)	1.60+/-2.4(132)	0.414
TQ_III_Peak_Pow_Amp	2677.41+/-9513.2(86)	2059.31+/-3700.7(46)	2462.01+/-7969.5(132)	0.673
TQ_III_Shannon_Entropy	0.27+/-0.1(86)	0.27+/-0.1(46)	0.27+/-0.1(132)	0.863
TQ_III_Curve_length	69.30+/-56.8(86)	73.21+/-66.5(46)	70.66+/-60.1(132)	0.72

3.6 Discussion

From these univariate observations it is now important to validate how well each of the predictors might perform. In order to access this, we build the ROC curve from the individual variable and estimate the AUC. It is important to note that this uses the same training and testing set for the evaluation of the significance of a given feature just as is done in many clinical studies to date [6, 8, 9, 13, 14, 19, 46]. Even though this is not the best methodology for a predictor, this offers an opportunity for comparison to other methods and can show how an individual variable might perform with a homogeneous dataset.

We calculated the AUC for each of the pre- and postoperative continuous variables listed in Table 3.6 and Table 3.7, which are shown, along with their p-values, in Table 3.10. The postoperative values tend to be higher, though this could be due to a smaller sample size, therefore, more testing should be done to verify this hypothesis. Though they are interesting, all have an AUC having poor or fair stratification ability.

Table 3.10 AUC of the ROC for features found significant in Table 3.6 and Table 3.7

Preoperative Continuous Feature	p value	AUC of ROC
Age	0.000	0.611
Height (In)	0.003	0.584
Ischemic Time (min)	0.004	0.594
Cardiopulmonary bypass time (min)	0.004	0.589
TQ_II_sym4_sc20_Mean_Freq	0.009	0.631
TQ_II_coif1_sc15_Median_Freq	0.003	0.625
TQ_V1_coif1_sc20_Peak_Freq	0.006	0.632
TQ_II_bior4.4_sc5_Mean_Freq	0.008	0.613
TQ_II_bior5.5_sc21_Mean_Freq	0.010	0.617
TQ_II_rbio5.5_sc5_Mean_Freq	0.010	0.619
TQ_II_gaus3_sc13_Peak_Freq	0.004	0.616

Table 3.10 Continued

Postoperative Continuous Feature	p value	AUC of ROC
Age	0.000	0.757
c3_PP_Chest_Energy_skewness	0.002	0.734
c3_PP_Chest_Energy_kurtosis	0.002	0.720
c3_PP_Atrial_db2_sc5_Energy_skewness	0.003	0.768
c1_PR_Atrial_db3_sc15_Curve_length_skewness	0.001	0.791
c1_PR_Atrial_db3_sc20_Nonlinear_Energy_skewness	0.003	0.791
c1_PR_Atrial_db3_sc20_Curve_length_skewness	0.002	0.780
c1_PR_Atrial_sym4_sc15_Curve_length_skewness	0.002	0.789
c2_PR_Atrial_sym4_sc20_Peak_Freq_skewness	0.001	0.778
c3_PP_Atrial_sym6_sc5_Energy_skewness	0.003	0.754
c2_RP_Atrial_sym6_sc10_Mean_Freq_kurtosis	0.001	0.757
c2_RP_Atrial_sym6_sc10_Median_Freq_kurtosis	0.002	0.796
c1_PR_Atrial_sym6_sc20_Nonlinear_Energy_skewness	0.003	0.791
c2_PR_Chest_sym6_sc20_Median_Freq_min	0.002	0.706
c3_PP_Atrial_coif1_sc5_Peak_Freq_std	0.003	0.784
c2_RP_Atrial_coif1_sc10_Shannon_Entropy_kurtosis	0.003	0.704
c1_PR_Atrial_coif1_sc15_Curve_length_skewness	0.002	0.780
c4_PP_Atrial_coif1_sc25_Peak_Freq_mean	0.002	0.783
c4_PR_Chest_coif1_sc25_Shannon_Entropy_skewness	0.002	0.815
c3_PP_Atrial_coif4_sc5_Energy_skewness	0.003	0.740
c3_PP_Atrial_coif4_sc5_Nonlinear_Energy_skewness	0.003	0.793
c2_RP_Atrial_coif4_sc10_Median_Freq_kurtosis	0.001	0.775
c1_PR_Atrial_coif4_sc20_Nonlinear_Energy_skewness	0.003	0.794
c3_PP_Atrial_bior2.2_sc10_Mean_Freq_skewness	0.001	0.793
c3_PP_Atrial_bior2.2_sc10_Peak_Freq_min	0.003	0.794
c3_RP_Atrial_bior2.2_sc10_Mean_Freq_skewness	0.000	0.816
c3_PP_Atrial_bior2.2_sc15_Katz_FD_skewness	0.002	0.786
c3_PP_Atrial_bior2.2_sc15_Nonlinear_Energy_kurtosis	0.003	0.720
c3_RP_Atrial_bior2.2_sc15_Katz_FD_skewness	0.002	0.725
c3_PR_Atrial_bior2.2_sc15_Katz_FD_skewness	0.002	0.750
c4_PP_Atrial_bior2.2_sc20_Peak_Freq_min	0.002	0.786
c3_RP_Atrial_bior2.2_sc25_Katz_FD_skewness	0.003	0.755
c3_RP_Atrial_bior2.2_sc25_Katz_FD_kurtosis	0.002	0.709
c1_PP_Atrial_bior4.4_sc5_Peak_Freq_kurtosis	0.001	0.748
c1_PR_Atrial_bior4.4_sc15_Curve_length_skewness	0.002	0.800
c1_PR_Chest_bior4.4_sc15_Peak_Freq_std	0.003	0.766
c1_PR_Atrial_bior4.4_sc20_Curve_length_skewness	0.002	0.740
c1_PR_Atrial_bior4.4_sc25_Peak_Freq_kurtosis	0.001	0.722
c2_RP_Atrial_bior4.4_sc25_Shannon_Entropy_kurtosis	0.003	0.733
c3_PP_Atrial_bior5.5_sc5_Energy_skewness	0.003	0.729
c4_PP_Atrial_bior5.5_sc5_Mean_Freq_max	0.002	0.768
c1_PR_Atrial_bior5.5_sc17_Curve_length_skewness	0.002	0.754
c1_PR_Atrial_bior5.5_sc25_Peak_Freq_kurtosis	0.001	0.793
c1_PR_Atrial_bior6.8_sc20_Curve_length_skewness	0.003	0.757
c1_PR_Atrial_rbio2.2_sc13_Curve_length_skewness	0.001	0.780
c4_PP_Atrial_rbio2.2_sc17_Peak_Freq_mean	0.001	0.807
c4_PP_Atrial_rbio2.2_sc21_Peak_Freq_mean	0.003	0.801
c1_PR_Atrial_rbio4.4_sc15_Curve_length_skewness	0.003	0.780
c2_RP_Atrial_rbio5.5_sc10_Peak_Freq_skewness	0.002	0.733
c3_RP_Atrial_rbio5.5_sc10_Shannon_Entropy_std	0.002	0.788
c2_PR_Chest_rbio5.5_sc20_Median_Freq_min	0.002	0.717
c1_PP_Atrial_rbio5.5_sc25_Peak_Freq_max	0.002	0.756

Table 3.10 Continued

c1_RP_Atrial_rbio5.5_sc25_Peak_Freq_max	0.000	0.814
c1_PR_Atrial_rbio5.5_sc25_Peak_Freq_kurtosis	0.002	0.686
c3_PP_Atrial_rbio6.8_sc5_Energy_skewness	0.002	0.733
c3_PP_Atrial_rbio6.8_sc5_Nonlinear_Energy_skewness	0.002	0.795
c2_RP_Atrial_rbio6.8_sc9_Mean_Freq_kurtosis	0.002	0.685
c2_RP_Atrial_rbio6.8_sc9_Median_Freq_kurtosis	0.001	0.796
c3_PP_Atrial_rbio6.8_sc9_Mean_Freq_min	0.002	0.749
c1_PR_Atrial_rbio6.8_sc17_Curve_length_skewness	0.003	0.754
c2_PR_Atrial_rbio6.8_sc17_Peak_Freq_kurtosis	0.001	0.734
c2_PR_Chest_gaus1_sc2_Mean_Freq_min	0.000	0.757
c3_PP_Atrial_gaus1_sc2_Energy_skewness	0.001	0.777
c3_PP_Atrial_gaus1_sc2_Energy_kurtosis	0.002	0.731
c3_PR_Atrial_gaus1_sc2_Median_Freq_skewness	0.001	0.731
c4_PR_Chest_gaus1_sc6_Peak_Freq_mean	0.002	0.818
c3_PR_Chest_gaus1_sc8_Katz_FD_skewness	0.002	0.772
c3_PR_Chest_gaus1_sc10_Energy_skewness	0.002	0.755
c3_PR_Chest_gaus1_sc12_Energy_skewness	0.001	0.734
c2_PR_Chest_gaus2_sc10_Median_Freq_min	0.002	0.735
c4_PP_Atrial_gaus2_sc10_Peak_Freq_mean	0.002	0.798
c2_PR_Atrial_gaus3_sc7_Mean_Freq_mean	0.003	0.788
c2_PR_Atrial_gaus3_sc7_Peak_Freq_mean	0.000	0.839
c1_PR_Atrial_gaus3_sc10_Nonlinear_Energy_skewness	0.003	0.789
c1_RP_Atrial_gaus3_sc13_Mean_Freq_min	0.002	0.786
c1_RP_Atrial_gaus3_sc13_Median_Freq_min	0.001	0.783
c3_PR_Chest_gaus3_sc13_Katz_FD_skewness	0.001	0.709
c1_PP_Atrial_gaus3_sc19_Peak_Freq_skewness	0.003	0.723
c2_PR_Chest_gaus4_sc13_Median_Freq_min	0.002	0.706
c2_RP_Atrial_gaus4_sc19_Shannon_Entropy_skewness	0.003	0.780
c2_RP_Atrial_mexh_sc3_Median_Freq_kurtosis	0.001	0.788
c4_PP_Atrial_mexh_sc3_Peak_Freq_min	0.001	0.808
c2_PR_Chest_mexh_sc7_Median_Freq_min	0.003	0.728
c4_PP_Atrial_mexh_sc7_Peak_Freq_mean	0.002	0.798

Several of the traditional AF predictors show up in the superior group listed in Table 3.10 such as age and prior AF. Additionally, cardiomegaly, left atrium size, prior heart surgery, and ischemic and cardiopulmonary bypass time appear significant. Apart from these clinical features, the ECG derived features seem to perform well when calculating frequency measures on the II lead. This leads us to believe that the frequency content of the wavelet decomposed T-to-Q segment has significant risk stratification properties. The top row of Figure 3.10 shows the ECG of a non-AF and an AF patient with the offset of the T wave and the onset of the Q wave marked. The middle row of Figure 3.10 shows

this same TQ segment following wavelet decomposition with the symlet four wavelet at a scale of twenty. Notice the significantly more complex wave shape in the AF patient which then results in higher frequency components than the non-AF patient. This is illustrated in the bottom row if Figure 3.10, which shows the difference of the mean frequency of ~6.8 and ~13.7 Hz for the non-AF and AF patient, respectively. Figure 3.11 shows the averaged spectrum of the II lead's T-Q segment symlet four wavelet decomposition at scale twenty for all the patients in both AF and non-AF patients. Notice the difference of these plots particularly in the 15-40 Hz area of the spectrum which appears to show a higher magnitude for AF patients.

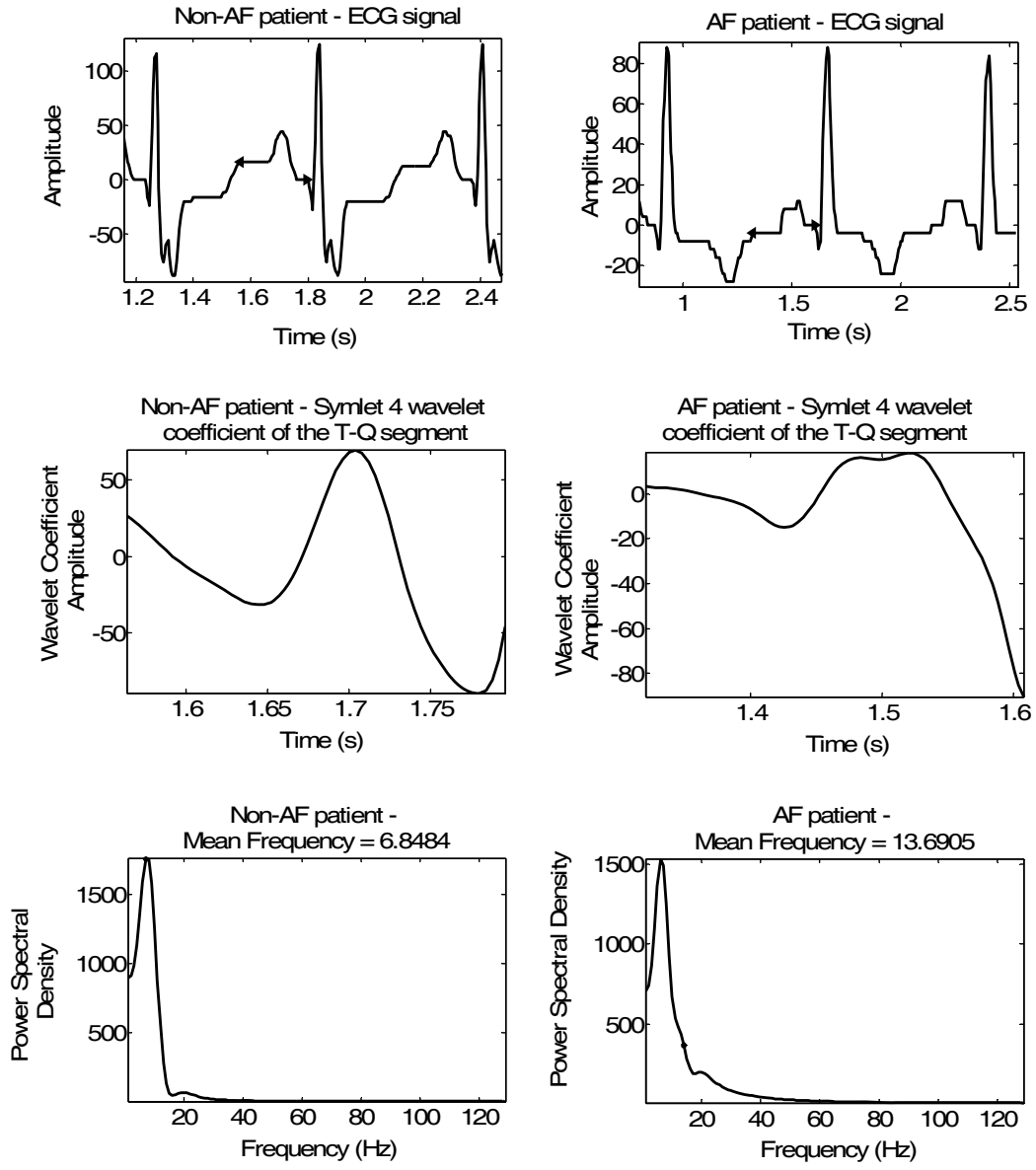

Figure 3.10 Non-AF (left column) and AF (right column) patient ECG (top row), the P wave's symlet 4 wavelet decomposition (middle row) and the spectrum of this wavelet decomposition (bottom).

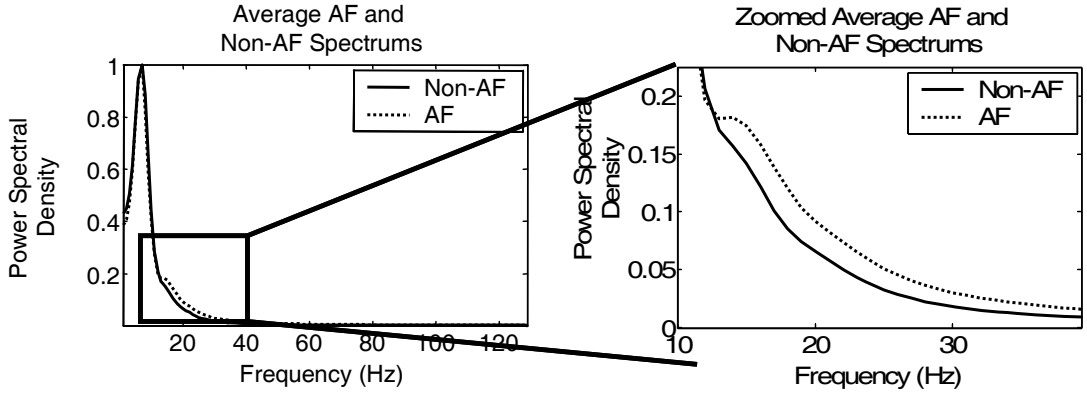

Figure 3.11 Averaged frequency spectrums of the P wave's symlet 4 wavelet decompositions (as seen in Figure 3.10) Non-AF and AF patient's (left) and a close-up of the 10-40 Hz region showing an interesting difference between the classes.

The sensitivity/specificity product plot in Figure 3.12 shows the class labeled patients and their associated feature value as well as the maximum value where an optimum classification threshold could be placed (further uses and reasoning behind this plot are discussed on chapter four). You can see a greater percentage of non-AF patients have a low feature value while those higher have a greater risk of AF. The ROC curve for this feature is shown in Figure 3.13 having an AUC of 0.6307 which does not correspond to a good classifier.

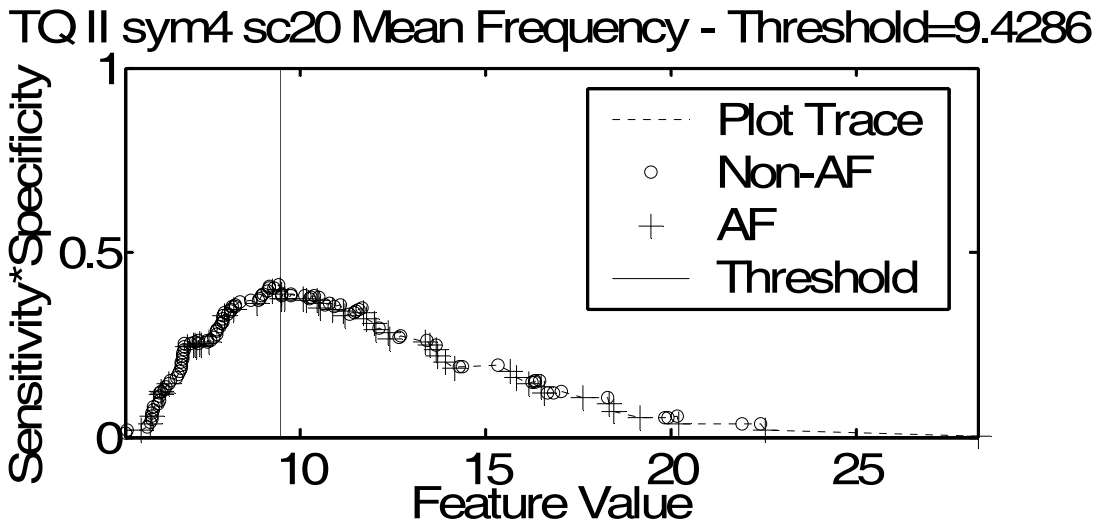

Figure 3.12 Sensitivity/specificity product plot of the symlet four (scale 20) wavelet decomposition of the TQ segment. This also marks the maximum of this plot which represents the optimum classification threshold for this feature.

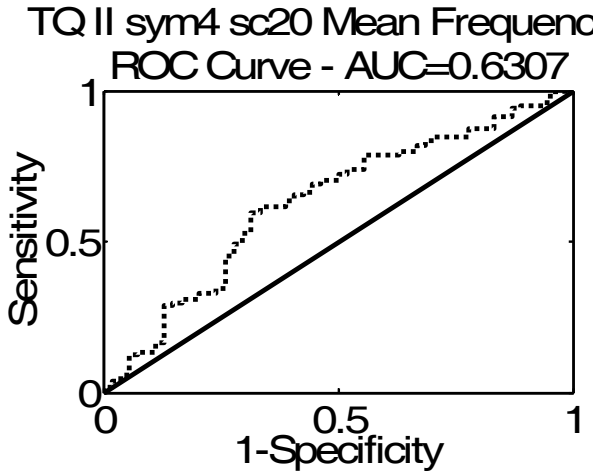

Figure 3.13 ROC of the mean frequency of the symlet four (scale 20) wavelet decomposition of the TQ segment.

In the postoperative feature set, again, age appears significant along with 2 features computed directly from the ECG on the third clips' PP segment. Additionally, many features derived from the wavelet decompositions are significant, particularly

- the atrial lead's first clips' PR segments' skewness of the curve length and
- the atrial lead's third clips' PP segments' skewness of the energy/nonlinear energy,

which occur eleven and ten times, respectively.

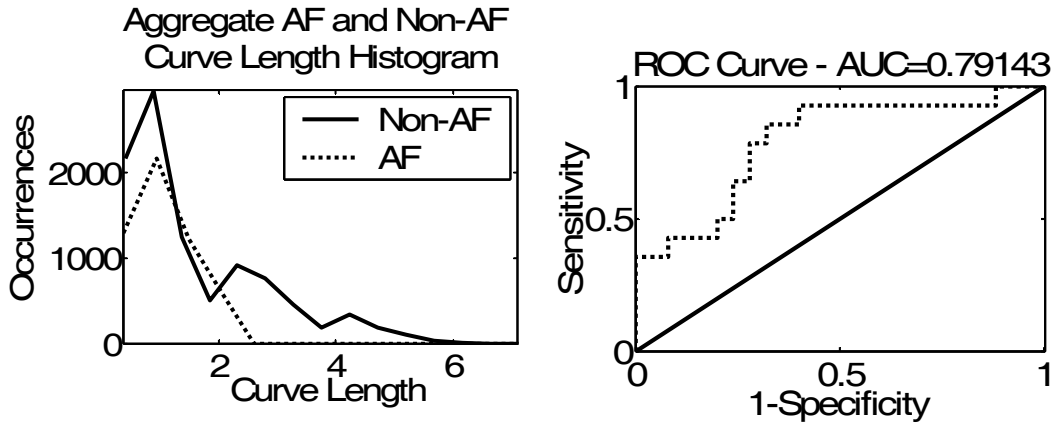

Figure 3.14 (Left) Histogram for non-AF and AF patients of the curve length of the daubechies three wavelet decomposition (scale 15) of the PR segment of the atrial lead's TQ segment. (Right) ROC for this feature.

We decided to investigate the first of these relationships more thoroughly, in particular the curve length of the daubechies three wavelet decomposition (scale 15) of the PR segment of the Atrial lead's TQ segment. The plot of occurrences of each value of this curve length is shown in Figure 3.14 for the two classes. It looks as if the right tail of the distribution is larger in the non-AF patients overall, causing a large skewness value,

while the AF patients have a small or negative skewness value. This can be thought of as AF patients have an overall smaller variation in curve length from beat to beat, while the non-AF patients' values tend to move a little higher more frequently. This is confirmed by the sensitivity/specificity product plot in Figure 3.15. The ROC curve shows an AUC of 0.791 with great potential for a three class separation system (low, medium, and high AF risk) by using the two significantly high sensitivity and specificity points which seem to hug either of the axes before the curve crosses the interior of the plot.

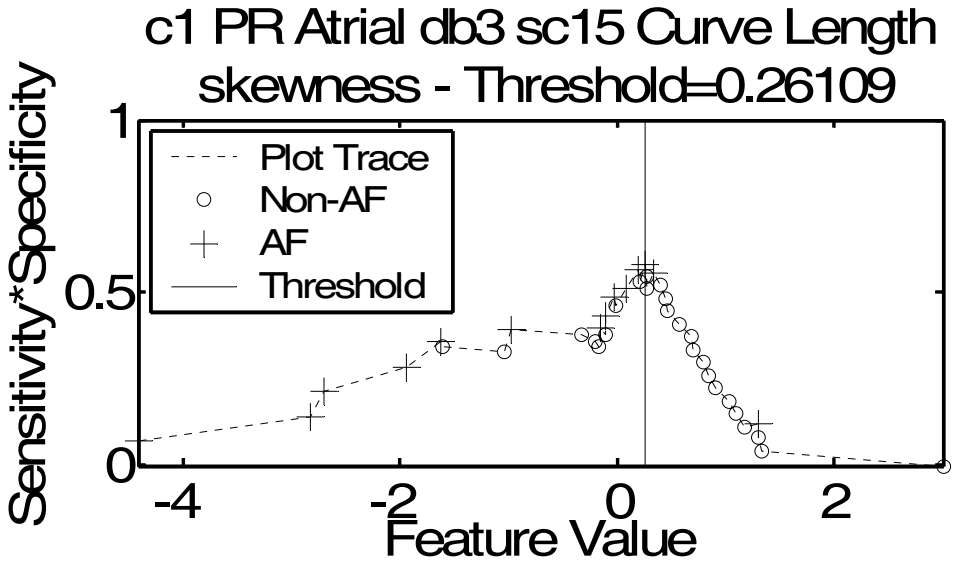

Figure 3.15 The sensitivity/specificity product plot of the curve length of the daubechies three wavelet decomposition (scale 15) of the PR segment of the atrial lead's TQ segment.

Concluding this section, though these univariate classification variables show promise, their current classification utility is too low for use in the clinical setting. Though more work should be done with better and larger data sets to determine their actual utility and robustness, we believe efforts in combining the predictive power of several variables

might yield a better classifier. We will investigate this hypothesis in the following chapters.

Chapter 4

Multivariate AF Prediction

In order to improve upon predictive accuracies found in the univariate analysis, in this chapter, we test two multivariate predictors on both the pre- and postoperative data to observe their classification ability. We perform this on the clinical data, the ECG feature data, as well as the combined dataset. When building these multivariate classifiers, we have paid particular attention to the fact that the best individual features, which we found in the preceding chapter, are not always the best feature set [92-94]. For this reason, we use a GA to select the features for these classifiers. By selecting a feature set, we reduce the dimensionality of the problem to a more generalized model with lower data collection and computation needs. The GA can sample the feature search-space effectively without becoming trapped in local maxima as would many greedy search methods.

4.1 Methods

Two typical multivariate classification techniques are being employed: the *k*-nearest neighbor algorithm (*k*-NN) and multivariate logistic regression. Both methods have a long usage history in practice and literature [91, 95] and are to be used here as a benchmark for further multivariate classifiers that will be presented in the next chapter. The features used with each of these classifiers are being selected by a GA in order to optimize the coverage of the feature search space and find the best risk stratifier's characteristics while concurrently reducing the dimensionality of the data.

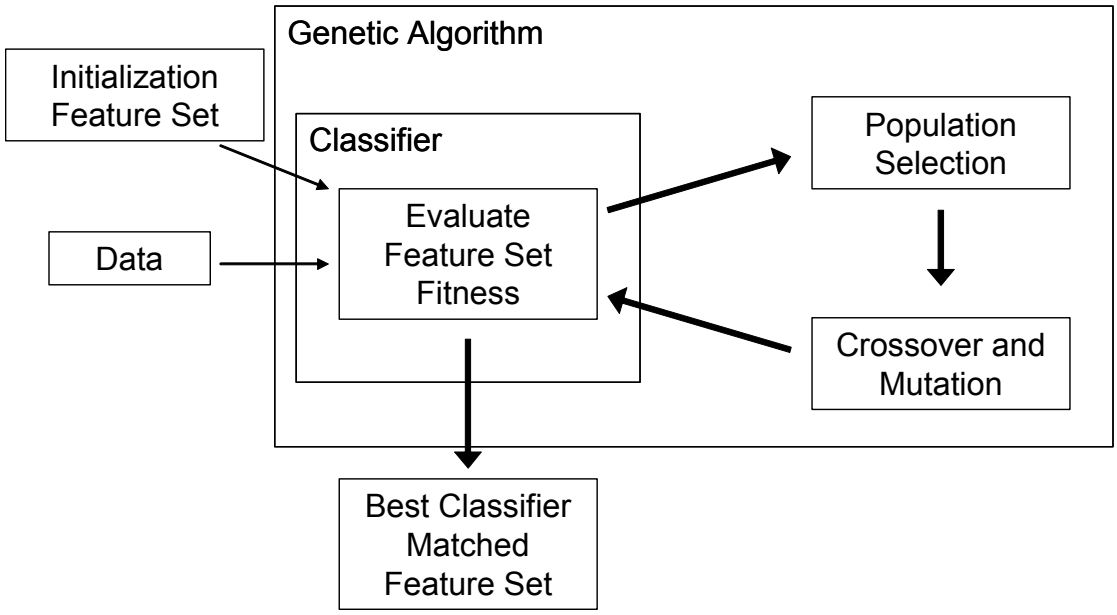

Figure 4.1 Flow Chart of GA feature selection with a classifier.

4.1.1 Logistic Regression

Logistic regression is a standard method for the modeling of binary outcomes and their dependence on predictive values, $x_{j,i}$, where i is the sample number and j is the variable number. The link between the binary outcome and the data are defined by a linear regression mapped onto the logit function of the probability of the class variable, p_i, at the i^{th} case such that:

$$\log\left(\frac{p_i}{1-p_i}\right) = \beta_0 + \beta_1 \cdot x_{1,i} + \cdots + \beta_k \cdot x_{k,i},$$

where there are k predictive variables. The $\{\beta_j\}$ are linear fit coefficients which are usually found through maximum likelihood estimation. This model allows for a smooth approximation of the predicted binary variable from predictive data. Though used often

in medical risk stratification methods, logistic regression has the unfortunate characteristic of requiring a complete dataset for training and testing, meaning no missing values.

For our application, the features are selected through evolution of the classifier performed by the GA and all samples with missing data points are removed. The regression was performed, finding the $\{\beta_j\}$ coefficients using Matlab's generalized linear model tools and the class probability, p_i is found for the entire data set. The entire set is used rather than leave-one-out (LOO) validation because when this is used with a GA, unusual results are obtained. To be more specific, while the GA searches for the best feature set with LOO, retraining of the classifier is done for every test patient, meaning a new set of $\{\beta_j\}$ parameters for every patient. The GA then looks for the feature set that allows the aligning of the different sets of $\{\beta_j\}$ parameters for perfect accuracy. The GA trained with LOO performs excellently when validated with LOO but when trained and tested on the same set, the results are poor. We have often observed this when combining LOO validation when assessing the individual's fitness in a GA if the coefficients or parameters of the classifier change with each individual tested. This is also observed in slightly different conditions by other researchers [96]. For this reason, the logistic regression's fitness will be evaluated using the entire dataset for training and testing and later validated through LOO.

The fitness of this classifier structure is evaluated by taking the probabilities and the associated class labels, constructing an ROC curve, finding the optimal classification threshold as discussed in chapter two, and calculating the sensitivity and specificity using

this threshold. Through the generations of the GA, the best feature set for risk stratification is found.

4.1.2 *k*-Nearest Neighbor

The *k*-nearest neighbor algorithm (*k*-NN) classifies samples based on the idea that its class will be that of the majority class among neighboring samples in the predictive feature space. The nearest neighbors are typically measured as those with the lowest Euclidian distance. The number of neighbors, *k*, is selected as a small fraction of the total dataset, typically odd to avoid the need for tie-breakers. Unfortunately, this classification method, like logistic regression, does not tolerate missing data points.

As in the logistic regression approach, the features were selected by the GA and all samples with missing data points were removed. Unlike logistic regression, the *k*-NN does not involve changing of any parameters during training, just the absence of the current individual from the feature space. Therefore, LOO validation is performed using all the patients but one to populate the feature space. Each test patient was labeled by finding the three nearest neighbors (k=3) and using the majority's label. We then assessed the sensitivity and specificity on the test set to find the best overall risk stratifier.

4.1.3 Genetic Algorithm

The genetic algorithm for this research was implemented in Matlab® 6.5 using the GA optimization toolbox (GAOT) [97]. The prediction of patients being either AF or non-AF patients was performed using between two and five features from the data calculated as described in chapter three. Therefore, the chromosome encoding the individual was a

vector of six integers as seen in Figure 4.2. The first integer, *p,* is a number from two to five specifying how many of the following five possible features will be used. The following five integers, f_1 through f_5, identify the actual feature to be used.

p	f_1	f_2	f_3	f_4	f_5

Figure 4.2 Chromosome integers for feature selection

We initialized the GA with a random population of 200 individuals when an initial set is not already specified and allowed the algorithm to run for up to 10,000 generations. There were two other termination conditions for the GA that allowed termination before this point. The first stopped the GA if the best individual reached the highest possible fitness of two input features (the minimum) and perfect sensitivity and specificity. The second termination condition was if the GA went for 250 iterations (over 167,000 individuals (250*(2*(50+50+50)+300+30+20+20+1))) with no improvement.

Within each generation, a specified number of crossovers and mutations were performed on the previous population:

- 50 arithmetic crossovers,
- 50 heuristic crossovers,
- 50 simple crossovers,
- 300 uniform mutations,
- 30 swap mutations
- 20 multiple point, nonuniform mutations,

- 20 single point, nonuniform mutations, and
- 1 boundary mutation.

The three crossover operators allow for good mixing of chromosomes between fit individuals. Uniform mutation is responsible for the roughly half of the new individuals allowing good coverage of the search space. Sufficient usage of this operator is important since the integers of the chromosome represent an unordered feature set and uniformly distributed mutations allow for better coverage of all possible feature combinations. If the chromosome integer coded a coefficient in a polynomial, as the value increased, the expected equation solution would move in a predetermined direction, therefore, mutations that caused small and nonuniform moves of the integer was desirable because to the adjacent value being closely related. In this implementation, as the integer identifying the feature increases, there is no clear relationship to how the classification will improve until it has been tested.

The 41 nonuniform mutations per generation are included to allow for adjacent features which may be in the same family and might be somewhat related. Please refer to [97] for further information on this toolbox and its operators. Moreover, we added the swap operator to help in rearranging the integers in the chromosome. This is not included as an option in the toolbox. This swapping of integers allows the better features to move toward the beginning of the chromosome, and as the number of selected variables decrease, a more generalized model is found and the fitness increases as we will discuss later. The list of operators above allows for excellent mixing through the generations and

creates a minimum of 167,000 individuals to be tested through the minimum 250 generations.

We used both elitist and normalized geometric distribution selection [97] to keep the best individuals as well as a fair mix of more diverse individuals. The fitness function for the GA was chosen to be a mix of both the sensitivity and the specificity of the classifier. We chose to use the product of these two measures because it sets both cases of high sensitivity/low specificity and vice versa to zero as seen in Figure 4.3 [98], something the sum does not provide. It puts more emphasis on a classifier being both sensitive and specific in imbalanced training sets as is needed in postoperative risk stratification.

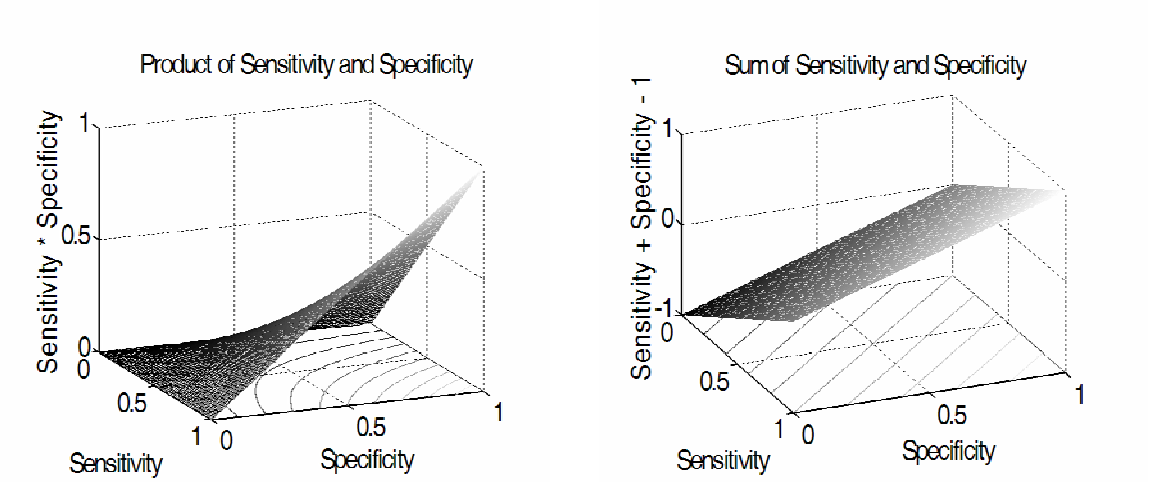

Figure 4.3 Fitness surfaces for product (left) and sum (right) of sensitivity and specificity.

In addition to the product of the sensitivity and the specificity, we also wanted to punish a classifier based on its complexity, *i.e.* the number of variables required. For instance, a classifier requiring a doctor to perform five tests is not as desirable as a classifier with

only two data inputs. For this reason, the fitness was penalized for every feature needed for classification, making the fitness function

$$fitness = sensitivity \cdot specificity \cdot 0.99^{f_T}$$

where f_T is the total number of features.

4.2 Evaluation

We ran four different GAs for feature selection with both the *k*-NN and the logistic regression: on the clinical data alone, the ECG data alone, and two initializations of the combined data types. The classifiers that used clinical or ECG data alone were initialized with a random population of individuals. The classifiers which used both the clinical and ECG data together were tested using both the best individuals from the previous clinical and ECG data only experiments, as well as by random population initialization. These different initializations will allow both the possibility of building on previously discovered maxima as well as starting at random.

Since none of the ECG features overlap between the pre- and post-surgical datasets and very few of the clinical features are comparable (different collection or recording methods), we did not perform a combined run of pre- and postoperative data.

4.3 Results

For each of the classifiers, we list the variables that were found to be of importance as well as the fitness of the classifier, the total dataset's sensitivity/specificity, the number of generations required to reach this solution, and the number of patients the classification

system used, both non-AF (NAF) and AF. We have also plotted the fitness of the classifiers in relation to the generation number of the GA. For the *k*-NN classifiers, when the number of variables is three or less, we have plotted the feature space and where the patients fall in this space actually as well as their predicted location. For the logistic regression classifiers, we have plotted the ROC curve of the classifier and its associated sensitivity/specificity product plot and the associated maximum which defines our identified optimum classification threshold. Additionally, we have plotted each patient's value on the regression curve as well as the associated threshold found in the previous plot. The summary of all of these results are seen here in Table 4.1 with their specifics in the sections following. Since the combined data classifier results that initialized with previous best individuals used repeated feature sets from the clinical or ECG data only runs, they are not presented in this table.

Table 4.1 Logistic regression and *k*-NN classifier results

			Features	Sen/Spec	Fitness	NAF/AF	Generations
Preoperative	Clinical	Reg.	5	0.64/0.81	0.4932	116/75	202
		k-NN	5	0.67/0.80	0.5082	158/97	98
	ECG	Reg.	5	0.72/0.86	0.5848	84/46	773
		k-NN	4	0.63/0.82	0.4975	84/46	65
	Combined	Reg.	5	0.76/0.83	0.6030	84/46	53
		k-NN	2	0.63/0.80	0.4908	84/46	24
Postoperative	Clinical	Reg.	4	1/1	0.9606	14/6	29
		k-NN	3	0.83/0.93	0.7508	14/6	150
	ECG	Reg.	2	1/1	0.9801	17/6	214
		k-NN	4	1/1	0.9606	20/13	160
	Combined	Reg.	3	1/1	0.9703	22/13	35
		k-NN	4	0.92/1	0.8867	22/13	72

4.3.1 Preoperative Risk Stratifiers

4.3.1.1 Clinical Dataset

4.3.1.1.1 Logistic Regression

The logistic regression model of the preoperative clinical data took 202 generations to find a classifier with a fitness of 0.4932, a sensitivity of 0.64, and a specificity of 0.81 using the following five variables.

- Ejection Fraction (3 level categorical: normal, moderate, severe LV function)
- Preoperative AF occurrence
- Cardiomegaly
- Left ventricle end-diastolic pressure – preoperative
- CABG distal anastomoses (number with vein)

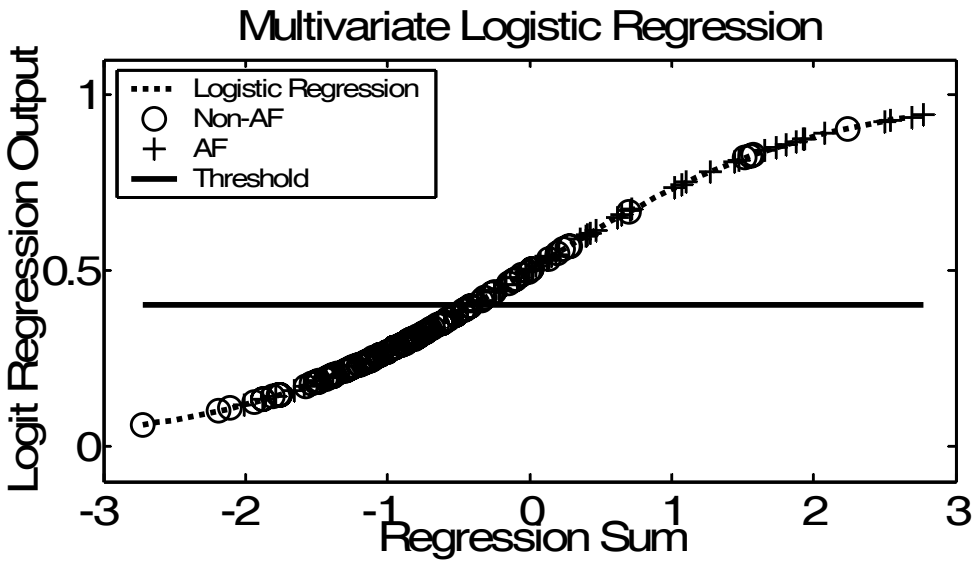

Figure 4.4 Preoperative clinical dataset's logistic regression plot

For this feature set, missing data points limited the dataset to 116 non-AF patients and 75 AF patients. The $\{\beta_j\}$ regression coefficients for this model were [-0.4630, 0.4449, 0.6368, 0.5296, 0.2454, 0.3805] and the regression as well as the patient positions on this regression are shown in Figure 4.4. All the values seem to have a positive relation to AF with preoperative AF occurrence and cardiomegaly being the strongest characteristics. Both of these variables as well as ejection fraction and the number of anastamoses (though of the mammery artery, not a vein) were found to be univariately significant in chapter three. Poor ejection fraction and high diastolic blood pressure are signs of a possibly ailing heart and a large number of anastamoses (loops in the circular system sometimes formed in response to a need for more blood flow) possibly show previous ischemic conditions. Figure 4.5 shows the evolution of the classifier with the fitness of the best individual as well as the average fitness of the population. There seems to be good mixing showing that the evolving population was not too closely tied to the fittest individual yet yielded improvements to these individuals.

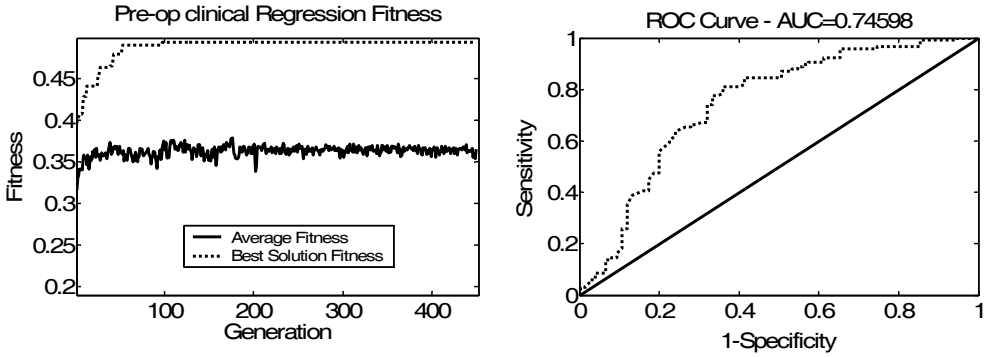

Figure 4.5 Evolutionary fitness plot and the ROC curve of the preoperative clinical dataset's logistic regression

Figure 4.5 also shows the ROC of this classifier, making it a fair to good risk stratifier (AUC = 0.75). The sensitivity/specificity product plot, shown in Figure 4.6, shows the threshold value of the logistic regression found to best separate the classes, 0.40361.

This threshold is set immediately above the maximum of this curve for optimal separation given our need for equally high sensitivity and specificity. We set it immediately above this value to prevent the patient that defines the maximum from having an indeterminate predicted class. This optimum threshold selection method is used for all threshold determination in this work. The figure shows that the AF patients tend to have values over this threshold while non-AF patients tend to be under this value.

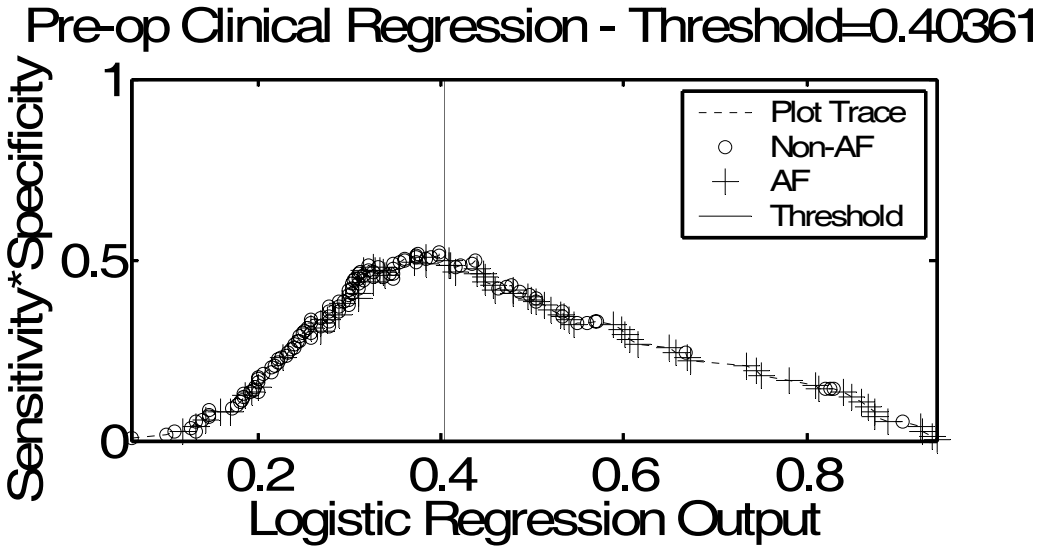

Figure 4.6 Product of the sensitivity and specificity of the logistic regression output of the preoperative clinical dataset including the maximum point indicating the optimum threshold.

4.3.1.1.2 k-Nearest Neighbor

The *k*-NN classifier of the preoperative clinical data took 98 generations to find a classifier with a fitness of 0.5082, a sensitivity of 0.67, and a specificity of 0.80 using the following five variables:

- CABG distal anastomoses (total number)
- Preoperative AF occurrence
- Left atrial hypertrophy
- Low density lipoprotein
- Emergency Surgical Priority

For this feature set, missing data points limited the dataset to 158 non-AF patients and 97 AF patients. Again, anastamoses appear as a predictor as well as the preoperative occurrence of AF. Anastamoses, preoperative AF occurrence, as well as left atrial size were also seen as independent predictors in chapter three and the first two were also in the logistic regression system above. Large left atrial size also tends to be a sign of increased load on the heart which could be a possible indicator of increased AF risk. Figure 4.7 shows the evolution of the classifier implying good mixing and a steady increase in fitness.

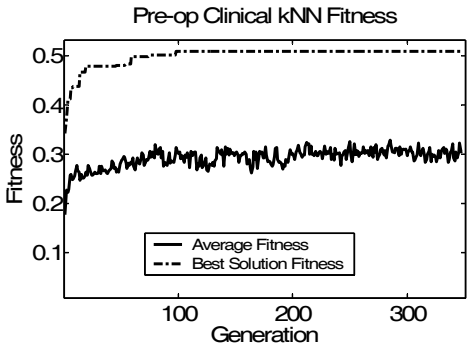

Figure 4.7 Evolutionary fitness plot of the preoperative clinical dataset's *k*-NN classifier

4.3.1.2 ECG Feature Dataset

4.3.1.2.1 Logistic Regression

The logistic regression model of the preoperative ECG data took 773 generations to find a feature set with a fitness of 0.5848, a sensitivity of 0.72, and a specificity of 0.86 using the following five variables.

- TQ_V1_coif1_sc20_Peak_Freq
- TQ_III_rbio2.2_sc9_Mean_Freq
- TQ_III_db2_sc15_Nonlinear Energy
- TQ_I_mexh_sc13_Mean_Freq
- TQ_II_gaus1_sc2_Median_Freq

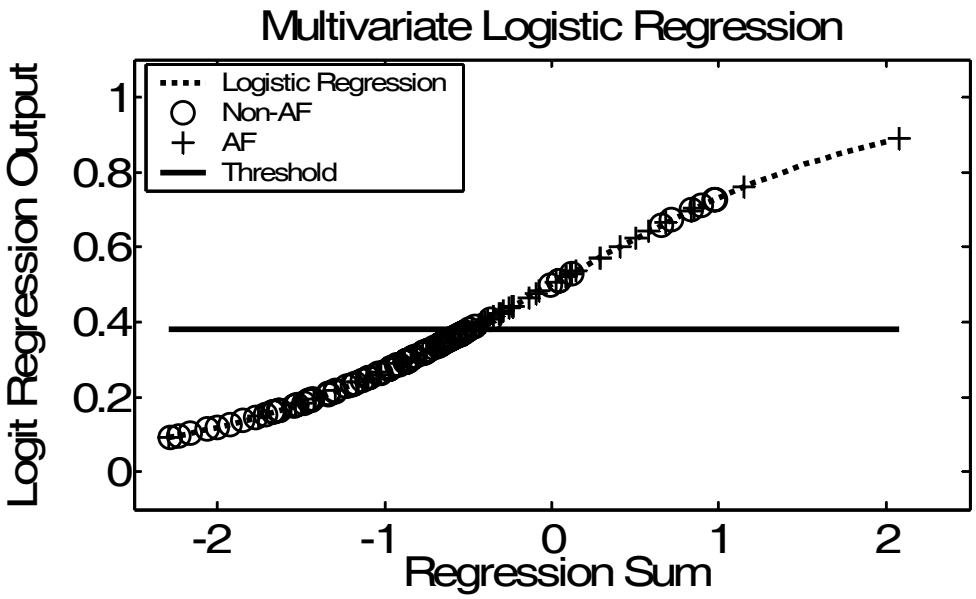

Figure 4.8 Preoperative ECG dataset logistic regression plot

For this feature set, missing data points limited the dataset to 84 non-AF patients and 46 AF patients. The $\{\beta_j\}$ regression coefficients for this model were [-0.6702, -0.6157, 0.4388, 0.3990, -0.2805, -0.2183] and the regression as well as the patient positions on this regression is shown in Figure 4.8. The first, fourth, and fifth features have a negative relation to AF occurrence. The first feature, TQ_V1_coif1_sc20_Peak_Freq, was also identified as a significant independent univariate predictor in chapter three where it again had an inverse relationship to AF occurrence. It is also the most heavily weighted variable in the regression model. Figure 4.9 shows the evolution of the classifier implying good mixing and a steady increase in fitness.

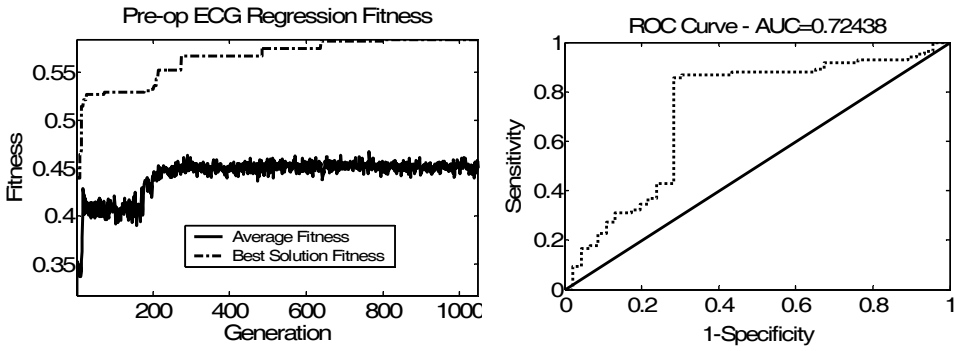

Figure 4.9 Evolutionary fitness plot and the ROC curve of the preoperative ECG dataset's logistic regression

Figure 4.9 shows the ROC of this classifier, making it a fair risk stratifier (AUC = 0.72). The sensitivity/specificity product plot, shown in Figure 4.10, shows the threshold value of the logistic regression found to best separate the classes, 0.38157. The figure shows that the AF patients tend to have values over this threshold while non-AF patients tend to be under this value.

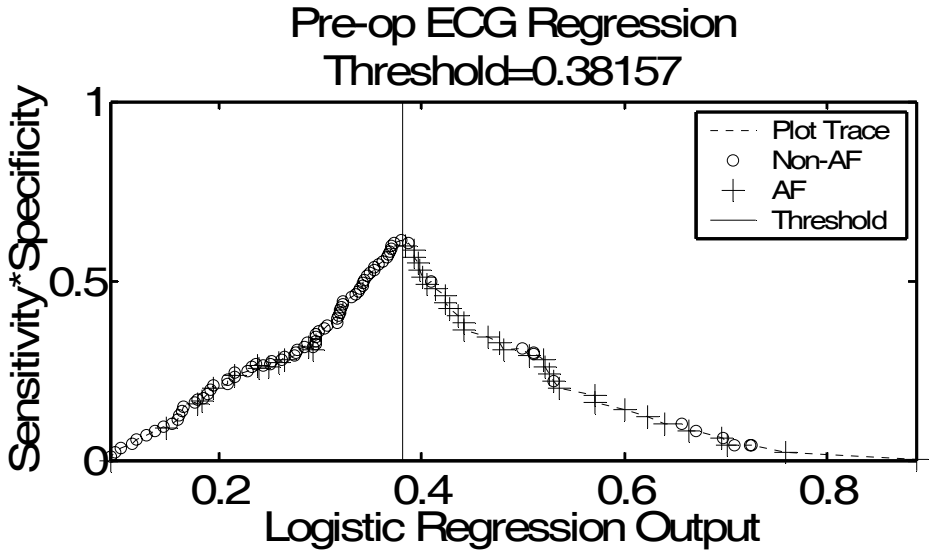

Figure 4.10 Product of the sensitivity and specificity of the logistic regression output of the preoperative ECG dataset including the maximum point indicating the optimum threshold.

4.3.1.2.2 k-Nearest Neighbor

The *k*-NN classifier of the preoperative ECG data took 65 generations to find a classifier with a fitness of 0.4975, a sensitivity of 0.63, and a specificity of 0.82 using the following four variables:

- TQ_III_db3_sc30_Katz_FD
- TQ_II_rbio2.2_sc5_Median_Freq
- TQ_I_sym6_sc10_sc10_Peak_Freq
- TQ_V1_gaus3_sc19_Nonlinear_Energy

For this feature set, missing data points limited the dataset to 84 non-AF patients and 46 AF patients. Notice that these features were not independently significant predictors in chapter three or found in the previous regression approach, yet are the best ECG data

based *k*-NN feature combination found. Figure 4.11 shows the evolution of the classifier, again implying good mixing and a steady increase in fitness.

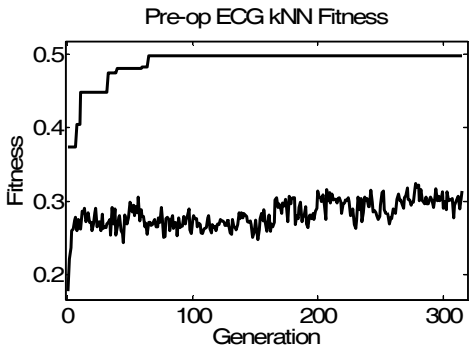

Figure 4.11 Evolutionary fitness plot of the preoperative ECG dataset's *k*-NN classifier

4.3.1.3 Clinical and ECG Combined Dataset

4.3.1.3.1 Logistic Regression

When initialized with the best individuals of the previous clinical or ECG data experiments, the combined dataset results matched one of these previous individuals. The best logistic regression individual used the same variables found in the ECG only feature set, while the best *k*-NN individual used the same variables as in the clinical only feature set.

When randomly initialized, new and different solutions were found. The logistic regression model of the preoperative combined data took 53 generations to find a

classifier with a fitness of 0.6030, a sensitivity of 0.76, and a specificity of 0.83 using the following five variables:

- TQ_III_gaus4_sc10_Mean_Freq
- Smoking Currently
- TQ_V1_gaus2_sc7_Shannon_Entropy
- TQ_II_bior4.4_sc25_Spectral_Entropy
- TQ_I_sym4_sc15_Mean_Freq

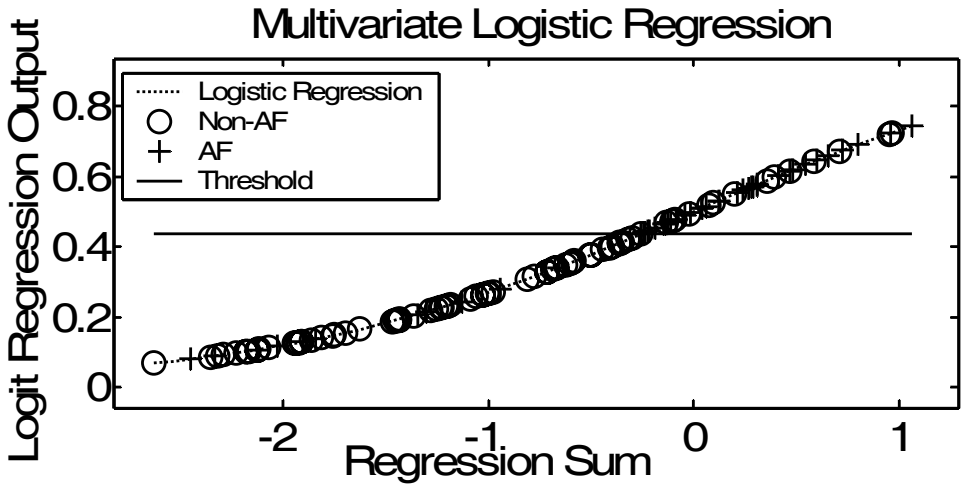

Figure 4.12 Preoperative combined clinical and ECG dataset logistic regression plot.

For this feature set, missing data points limited the dataset to 84 non-AF patients and 46 AF patients. The $\{\beta_j\}$ regression coefficients for this model were [-0.76087, 0.5533, 0.6082, -0.2858, 0.0815, 0.1732] and the regression as well as the patient positions on this regression is shown in Figure 4.12. Notice that a single clinical feature is being used in conjunction with several ECG features for our final classifier. Figure 4.13 shows the evolution of the classifier implying good mixing and a steady increase in fitness.

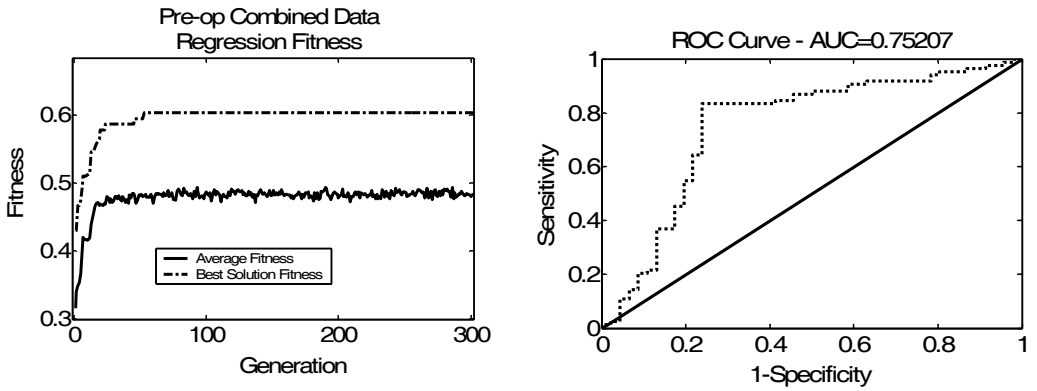

Figure 4.13 Evolutionary fitness plot of the preoperative combined clinical and ECG dataset's logistic regression

Figure 4.13 shows the ROC curve of this classifier making it a good risk stratifier (AUC=0.75). The sensitivity/specificity product plot, shown in Figure 4.14, shows the threshold value of the logistic regression found to best separate the classes, 0.43616. The figure shows that the AF patients tend to have values over this threshold while non-AF patients tend to be under this value.

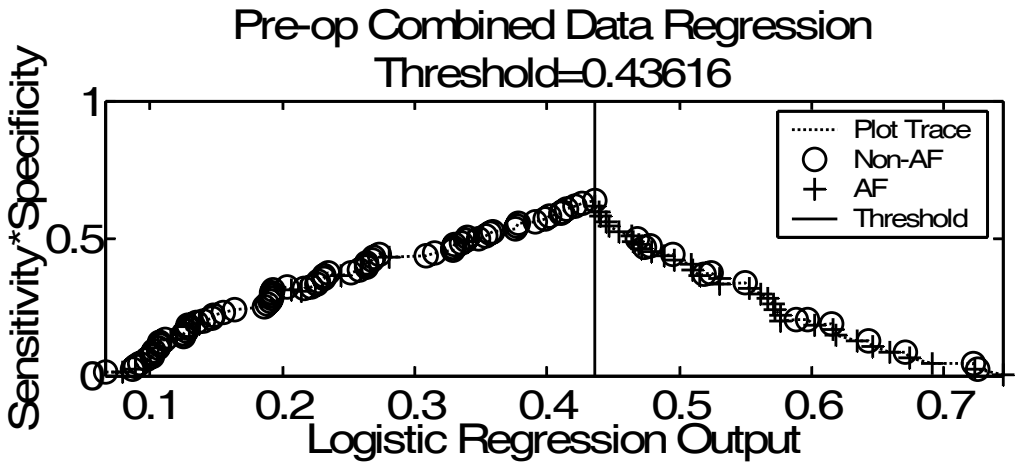

Figure 4.14 Product of the sensitivity and specificity of the logistic regression output of the preoperative combined clinical and ECG dataset including the maximum point indicating the optimum threshold.

4.3.1.3.2 k-Nearest Neighbor

The *k*-NN classifier of the preoperative combined clinical and ECG data took 24 generations to find a classifier with a fitness of 0.4908, a sensitivity of 0.63, and a specificity of 0.80 using the following two variables:

- TQ_I_coif1_sc20_Peak_Freq
- TQ_III_rbio2.2_sc9_Median_Freq

The second of these features is very similar to the TQ_III_rbio2.2_sc9_Mean_Freq used in the ECG data regression analysis found previously. For this feature set, missing data points limited the dataset to 84 non-AF patients and 46 AF patients. Figure 4.15 shows the evolution of the classifier, again implying good mixing and a steady increase in fitness.

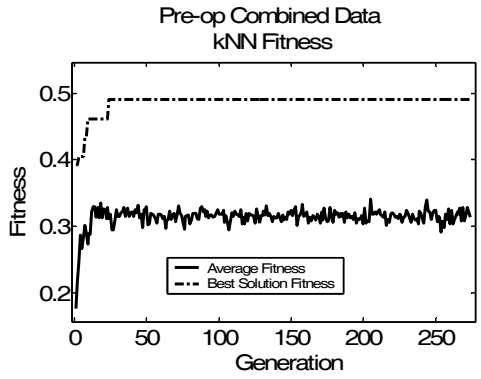

Figure 4.15 Evolutionary fitness plot of the preoperative combined clinical and ECG dataset's *k*-NN classifier

With there being two predictive variables, we were able to plot these and show both the actual classes and predicted classes of all the patients in Figure 4.16.

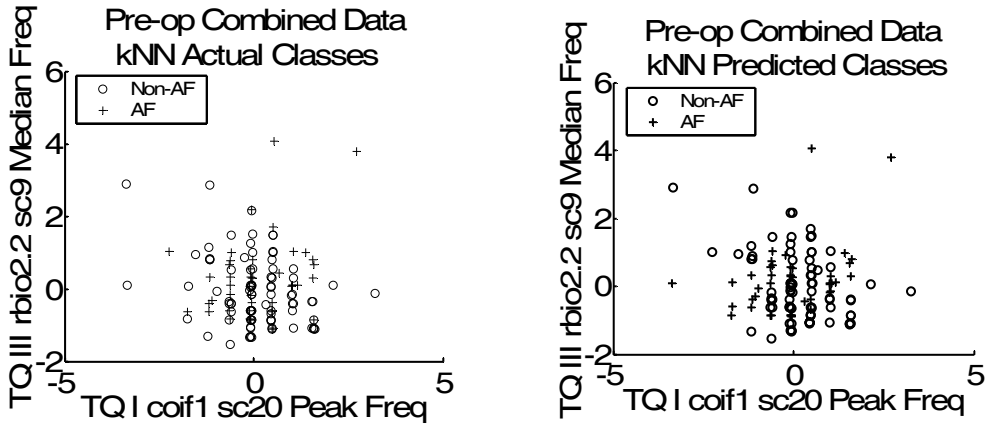

Figure 4.16 Non-AF and AF patient samples plotted in the optimum feature space found by the *k*-NN. The actual class labels are in the left plot while the right shows the predicted class labels.

Though there seems to be a slight AF clustering in the left and right areas of the plots, the overlap between the classes are very large without any apparent separation. We believe

that this classifier was found to be the best, not because of actual class separation but by chance.

4.3.2 Postoperative Risk Stratifiers

4.3.2.1 Clinical Dataset

4.3.2.1.1 Logistic Regression

The logistic regression model of the postoperative clinical data took 29 generations to find a classifier with a fitness of 0.9606 and a perfect sensitivity and specificity using the following four variables:

- Performed vessel bypasses (number)
- Age
- High temperature during surgery (C^o)
- Left main coronary artery disease

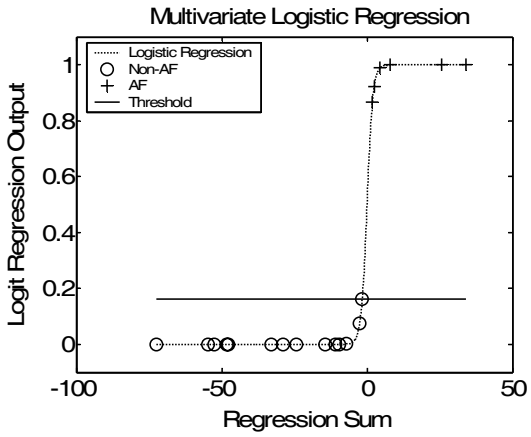

Figure 4.17 Postoperative clinical dataset logistic regression plot

For this feature set, missing data points limited the dataset to 14 non-AF patients and 6 AF patients. The $\{\beta_j\}$ regression coefficients for this model were [-16.5715, -10.9853, 25.6700, -7.7289, -16.1106] and the regression as well as the patient positions on this regression is shown in Figure 4.17. The extreme step seen in this regression is a result of the large separation between the classes in this regression and the large range of the regression sum. Age is certainly a predictor of AF that has been discussed in chapter two and was significant in chapter three's univariate analysis. Additionally, the number of vessels bypassed increases the time of the surgery and the stress put on the patients heart, which could possibly make it more susceptible to AF. Figure 4.18 shows the evolution of the classifier implying good mixing and a steady increase in fitness.

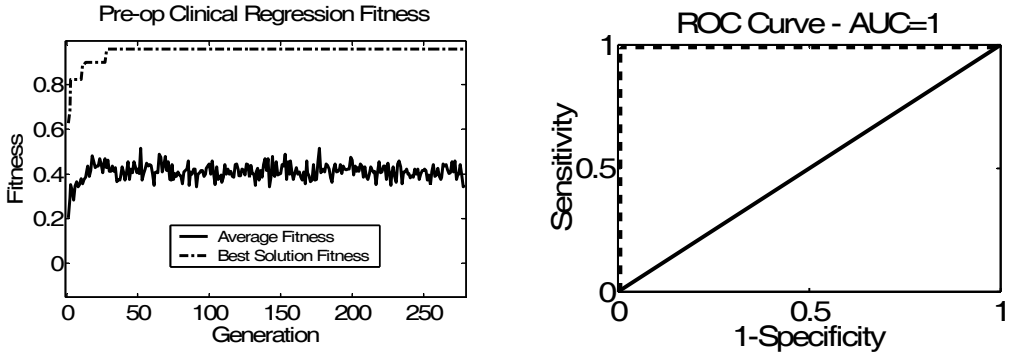

Figure 4.18 Evolutionary fitness plot and ROC curve of the postoperative clinical dataset's logistic regression

Figure 4.18 also shows the perfect 1.00 AUC of this classifier making it an excellent risk stratifier. The sensitivity/specificity product plot, depicted in Figure 4.19, shows the threshold value of the logistic regression found to best separate the classes, 0.16131. The

figure shows that the AF patients tend to have values over this threshold while non-AF patients tend to be under this value.

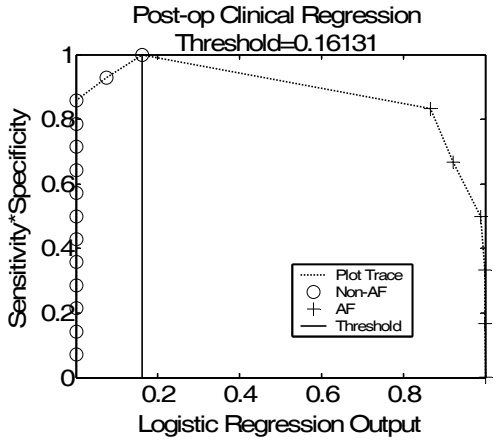

Figure 4.19 Product of the sensitivity and specificity of the logistic regression output of the postoperative clinical dataset including the maximum point indicating the optimum threshold.

4.3.2.1.2 k-Nearest Neighbor

The *k*-NN classifier of the postoperative clinical data took 150 generations to find a classifier with a fitness of 0.7508, a sensitivity of 0.83, and a specificity of 0.93 using the following three variables:

- Age
- Left anterior descending coronary artery disease
- Calcium blocker administration

For this feature set, missing data points limited the dataset to 14 non-AF patients and 6 AF patients. Again, age is found to be an important predictor along with another vessel

having coronary artery disease as we saw in the previous regression predictor. Figure 4.20 shows the evolution of the classifier having good mixing and a steady increase in fitness.

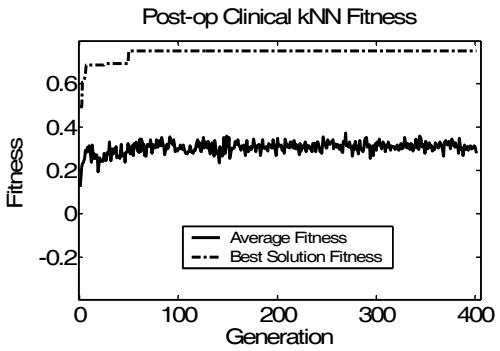

Figure 4.20 Evolutionary fitness plot of the postoperative clinical dataset's *k*-NN classifier

With there being three predictive variables, we were able to plot these in three dimensions and show both the actual classes and predicted classes of all the patients in Figure 4.21. You can see the continuous age variable being an important predictor and both the calcium blocker and coronary artery disease of the left anterior descending separating the non-AF patients from the cluster of AF patients that remain.

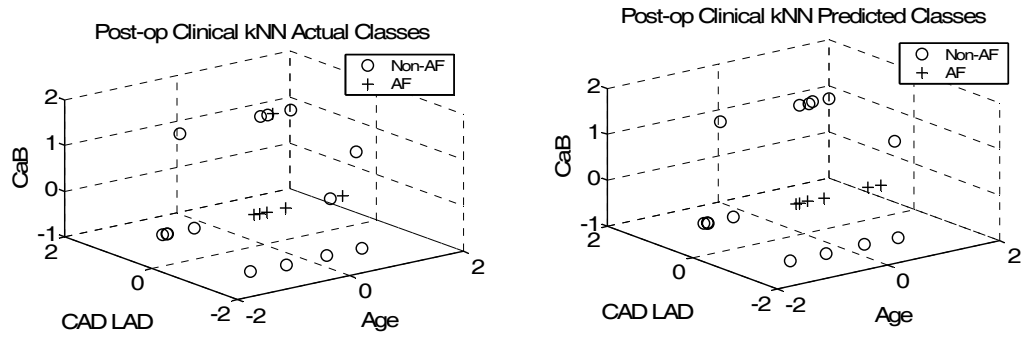

Figure 4.21 Non-AF and AF patient samples plotted in the optimum feature space found by the *k*-NN. The actual class labels are in the left plot while the right shows the predicted class labels.

4.3.2.2 ECG Feature Dataset

4.3.2.2.1 Logistic Regression

The logistic regression model of the postoperative ECG data took 214 generations to find a classifier with a fitness of 0.9801 and a perfect sensitivity and specificity using two variables.

- C3_PR_Atrial_mexh_sc11_Peak_Freq_kurtosis
- C4_PR_Chest_rbio5.5_sc20_Median_Freq_max

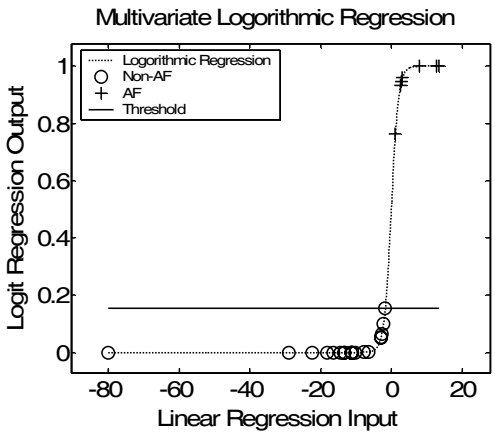

Figure 4.22 Postoperative ECG dataset logistic regression plot

For this feature set, missing data points limited the dataset to 17 non-AF patients and 6 AF patients. The $\{\beta_j\}$ regression coefficients for this model were [-11.0210, 1.1592, 22.9708] and the regression as well as the patient positions on this regression is shown in Figure 4.22. As the weight of the second variable is much larger than that of the first, this is a very significant feature though it did not appear to be independently significant in chapter three. Figure 4.23 shows the evolution of the classifier, again with good mixing and a steady increase in fitness.

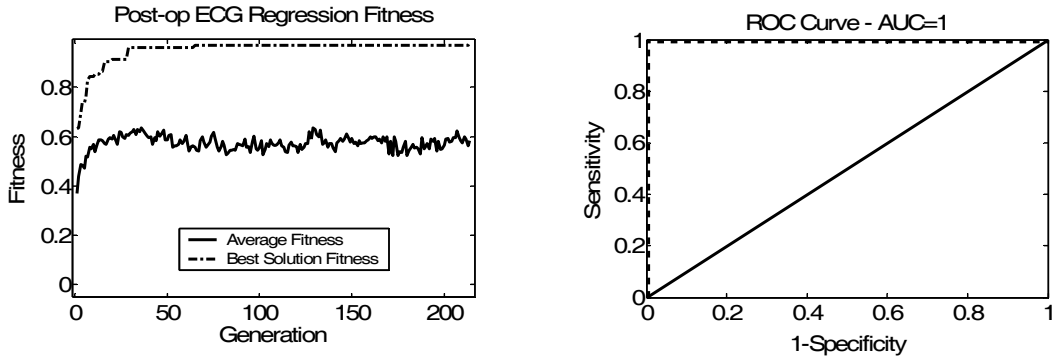

Figure 4.23 Evolutionary fitness plot of the postoperative ECG dataset's logistic regression

Figure 4.23 shows the "perfect" ROC curve of this classifier making it an excellent risk stratifier (AUC = 1.00). The sensitivity/specificity product plot, shown in Figure 4.24, shows the threshold value of the logistic regression found to best separate the classes, 0.15375. The figure shows that, again, the AF patients tend to have values over this threshold while non-AF patients tend to be under this value.

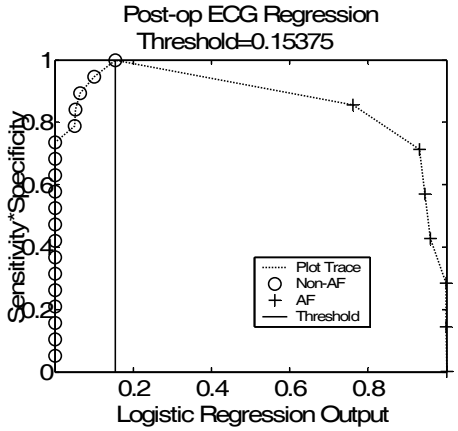

Figure 4.24 Product of the sensitivity and specificity of the logistic regression output of the postoperative ECG dataset including the maximum point indicating the optimum threshold.

4.3.2.2.2 k-Nearest Neighbor

The *k*-NN classifier of the postoperative ECG data took 160 generations to find a classifier with a fitness of 0.9606 and a perfect sensitivity and specificity using the following four variables:

- C4_PP_ Atrial _sym6_sc10_Curve_Length_max
- C4_RP_Atrial_rbio5.5_sc5_Curve_Length_mean
- C3_PP_Atrial_bio4.4_sc5_Energy_skewness
- C1_PR_Chest_bior4.4_sc25_Shannon_Entropy_max

For this feature set, missing data points limited the dataset to 20 non-AF patients and 13 AF patients. Most of the features selected for this classifier as well as for the last are from the later two clips, 24 and 36 hours after surgery (C3 and C4). This could be a reflection of the patient's susceptibility to AF as the patient heals. Remember that AF tends to occur most on the second or third day following surgery. Figure 4.25 shows the evolution of the

classifier with good mixing in the population and a sudden jump in the best individual's fitness after roughly 100 generations. These significant evolutionary leaps are the reason we chose to perform 250 iterations with no improvement before halting the GA.

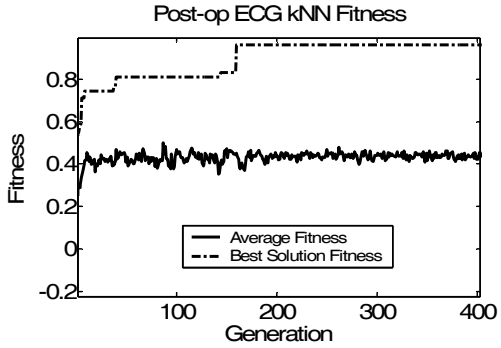

Figure 4.25 Evolutionary fitness plot of the postoperative ECG dataset's *k*-NN classifier

4.3.2.3 Clinical and ECG Combined Datasets

Again, when initialized with the best individuals of the previous clinical or ECG data only experiments, the combined dataset results matched one of these previous individuals. This time the best individual for both classifiers used the same variables found in the ECG only feature set that was found previously. When randomly initialized, new and different solutions were found.

4.3.2.3.1 Logistic Regression

The logistic regression model of the preoperative combined data took 35 generations to find a classifier with a fitness of 0.9703 and a perfect sensitivity and specificity 1.00 using the following three variables:

- C2_PR_Chest_Curve_Length_max
- C4_RP_Atrial_db2_sc30_Shannon_Entropy_skewness
- C4_PP_Atrial_rbio5.5_sc25_Peak_Pow_Amp_max

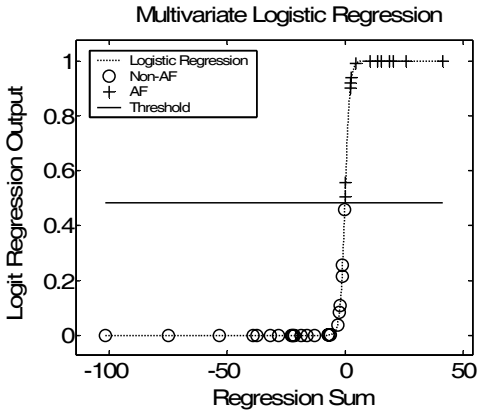

Figure 4.26 Postoperative combined clinical and ECG dataset logistic regression plot

Again, several c4 clips are found important pointing to the later features' importance. For this feature set, missing data points limited the dataset to 22 non-AF patients and 13 AF patients. The $\{\beta_j\}$ regression coefficients for this model were [-10.0613, -23.7183, 20.0191, -7.9062] and the regression as well as the patient positions on this regression is shown in Figure 4.26. Figure 4.27 shows the evolution of the classifier implying good mixing and a steady increase in fitness.

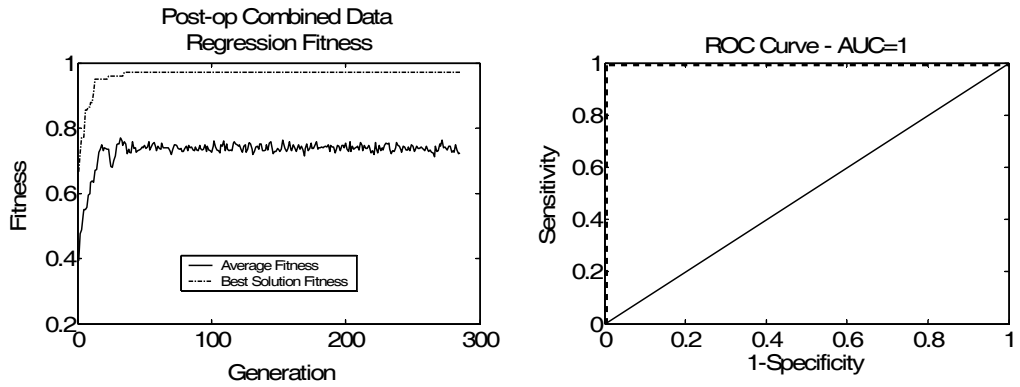

Figure 4.27 Evolutionary fitness plot of the postoperative combined clinical and ECG dataset's logistic regression

Figure 4.27 shows the perfect ROC curve of this classifier making it a good risk stratifier (AUC=1.00). The sensitivity/specificity product plot, shown in Figure 4.28, shows the threshold value of the logistic regression found to best separate the classes, 0.48232. The figure shows that the AF patients tend to have values over this threshold while non-AF patients tend to be under this value.

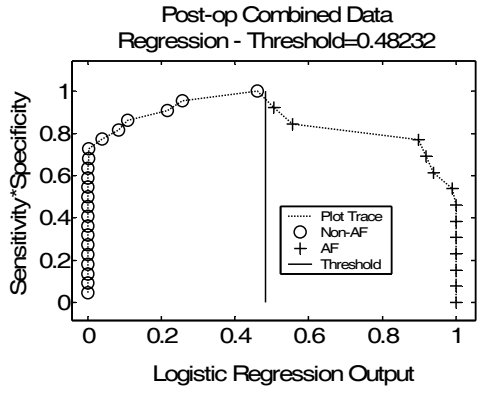

Figure 4.28 Product of the sensitivity and specificity of the logistic regression output of the postoperative combined clinical and ECG dataset including the maximum point indicating the optimum threshold.

4.3.2.3.2 k-Nearest Neighbor

The *k*-NN classifier of the preoperative combined clinical and ECG data took 72 generations to find a classifier with a fitness of 0.8867, a sensitivity of 0.92, and a specificity of 1.00 using the following four variables:

- C4_PP_Atrial_rbio2.2_sc5_Energy_max
- C3_PR_Chest_coif4_sc10_Mean_Freq_std
- C4_PR_Chest_rbio5.5_sc15_Spectral_Entropy_kurtosis
- C3_RP_Atrial_rbio5.5_sc15_Curve_Length_max

For this feature set, missing data points limited the dataset to 22 non-AF patients and 13 AF patients. Figure 4.29 shows the evolution of the classifier, again implying good mixing and a steady increase in fitness.

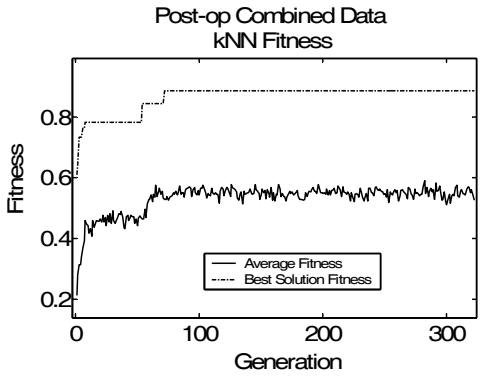

Figure 4.29 Evolutionary fitness plot of the postoperative combined clinical and ECG dataset's *k*-NN classifier

4.4 Validation

Since none of the above multivariate logistic regression classifiers could use leave-one-out (LOO) validation, we performed LOO validation on these classifiers after the best individual was found. This is not needed for the *k*-NN classifier since it was performed in the GA yet its results are presented again. The LOO validation results are shown in Table 4.2. Again, only the random initialized GA classifier results are listed in this table since the best individual initialization results are repeated from the clinical or ECG data cases.

Table 4.2 Validation Results of logistic regression and *k*-NN classifier

			Sen/Spec	Fitness
Preoperative	Clinical	Reg.	0.64/0.76	0.4617
		k-NN	0.67/0.80	0.5082
	ECG	Reg.	0.65/0.74	0.4578
		k-NN	0.63/0.82	0.4975
	Combined	Reg.	0.72/0.71	0.4873
		k-NN	0.63/0.80	0.4908
Postoperative	Clinical	Reg.	1/0.79	0.7548
		k-NN	0.83/0.93	0.7508
	ECG	Reg.	1/0.95	0.9192
		k-NN	1/1	0.9606
	Combined	Reg.	0.85/0.95	0.7837
		k-NN	0.92/1	0.8867

4.4.1 Preoperative Risk Stratifiers

4.4.1.1 Clinical Dataset – Logistic Regression

Figure 4.30 shows the ROC curve for the preoperative clinical dataset logistic regression classifier with an AUC of 0.71, considered a fair classifier. This is slightly less than the 0.75 AUC that was reported when trained and tested on the same set. This similar result

with both LOO and full-set training/testing could indicate that this is a fairly strong risk stratification system.

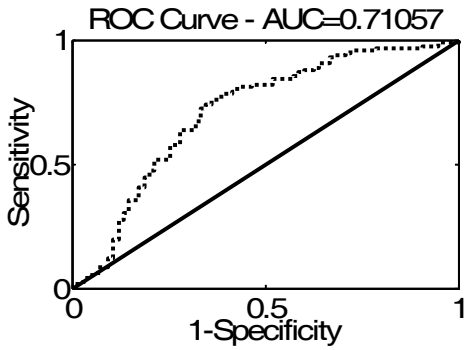

Figure 4.30 ROC curve of the validation of the preoperative clinical dataset's logistic regression

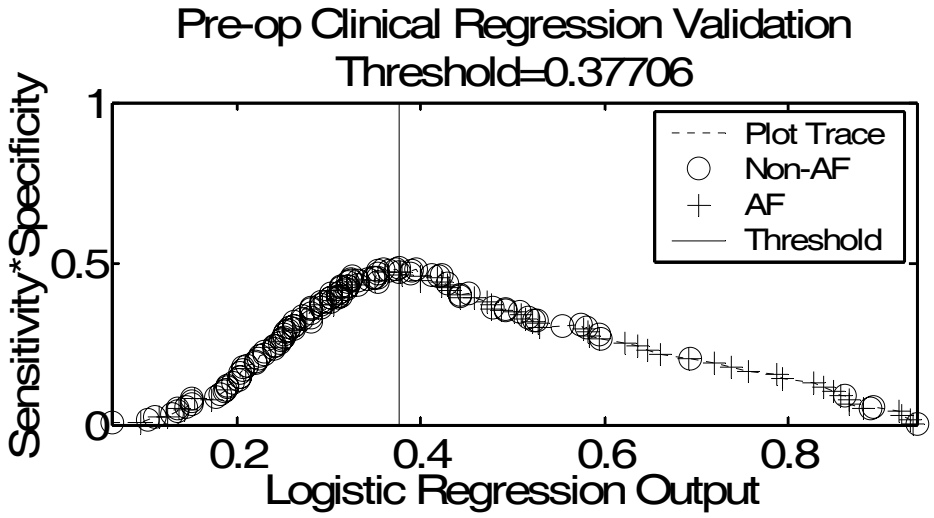

Figure 4.31 Product of the sensitivity and specificity of the validation of the logistic regression output of the preoperative clinical dataset including the maximum point indicating the optimum threshold.

Figure 4.31 shows the sensitivity/specificity product plot as well as the new classification threshold of 0.37706. This is slightly less than the 0.40361 that was set in the previous testing of this classifier but the plots look very similar with similar patient placement even though every patient had a different $\{\beta_j\}$ regression coefficient set.

4.4.1.2 ECG Feature Dataset – Logistic Regression

Figure 4.32 shows the ROC curve for the preoperative ECG dataset logistic regression classifier with an AUC of 0.6633, considered a fair classifier. This is less than the 0.72 AUC that was reported when trained and tested on the same set. This slightly larger change could indicate that this is not quite as strong as the previous risk stratification system.

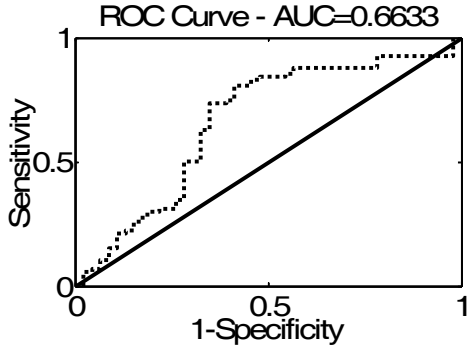

Figure 4.32 ROC curve of the validation of the preoperative ECG dataset's logistic regression

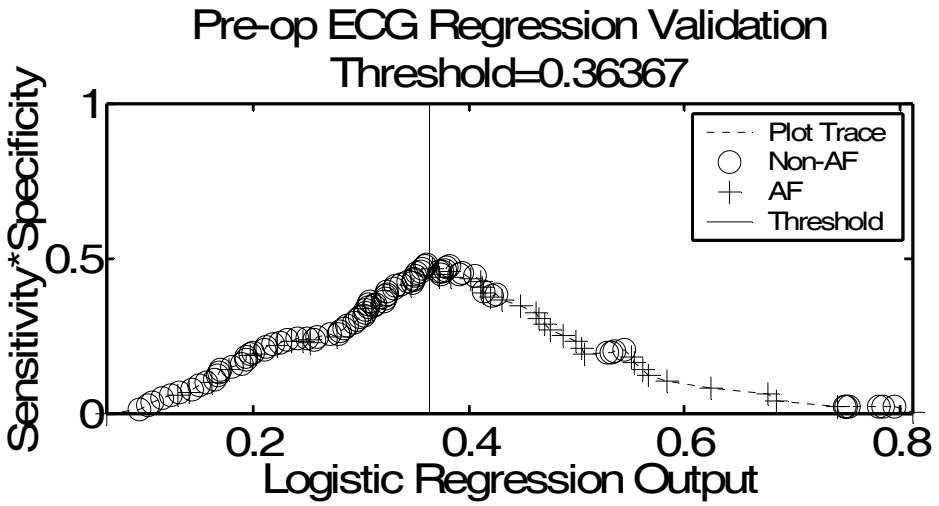

Figure 4.33 Product of the sensitivity and specificity of the validation of the logistic regression output of the preoperative ECG dataset including the maximum point indicating the optimum threshold.

Figure 4.33 shows the sensitivity/specificity product plot as well as the new classification threshold of 0.36367. This is slightly less than the 0.38157 that was set in the previous testing of this classifier and the non-AF points around the threshold have shifted significantly but there is still a fair separation between the classes in spite of this.

4.4.1.3 Clinical and ECG Combined Dataset – Logistic Regression

Figure 4.34 shows the ROC curve for the preoperative combined clinical and ECG dataset logistic regression classifier with an AUC of 0.6915, considered a fair classifier. This is less than the 0.75 AUC that was reported when trained and tested on the same set. This slightly larger change could indicate that this is not as informative as the previous risk stratification system.

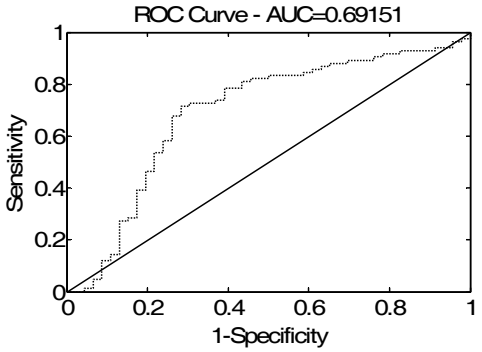

Figure 4.34 ROC curve of the validation of the preoperative combined clinical and ECG dataset's logistic regression

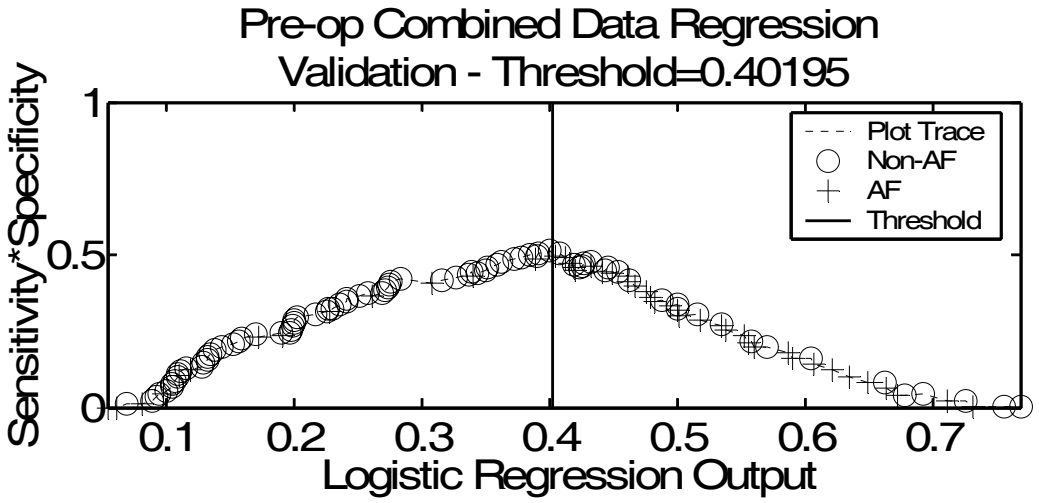

Figure 4.35 Product of the sensitivity and specificity of the validation of the logistic regression output of the preoperative combined clinical and ECG dataset including the maximum point indicating the optimum threshold.

Figure 4.35 shows the sensitivity/specificity product plot as well as the new classification threshold of 0.40195. This is slightly less than the 0.43616 that was set in the previous testing of this classifier and the plots look slightly different with less of a sensitivity/specificity product peak, which defined a strong boundary between classes.

This could be indicative of over-fitting, but the classification performance is still much better than random.

4.4.2 Postoperative Risk Stratifiers

4.4.2.1 Clinical Dataset – Logistic Regression

Figure 4.36 shows the ROC curve for the postoperative clinical dataset logistic regression classifier with an AUC of 0.86, considered a good classifier. This is significantly less than the perfect 1.00 AUC that was reported when trained and tested on the same set. Additionally, Figure 4.36 shows the sensitivity/specificity product plot. This shape has changed significantly and the patient position is different from the plot seen previously. Though not statistically convincing, this predictor still has promise following further experimentation with a larger dataset.

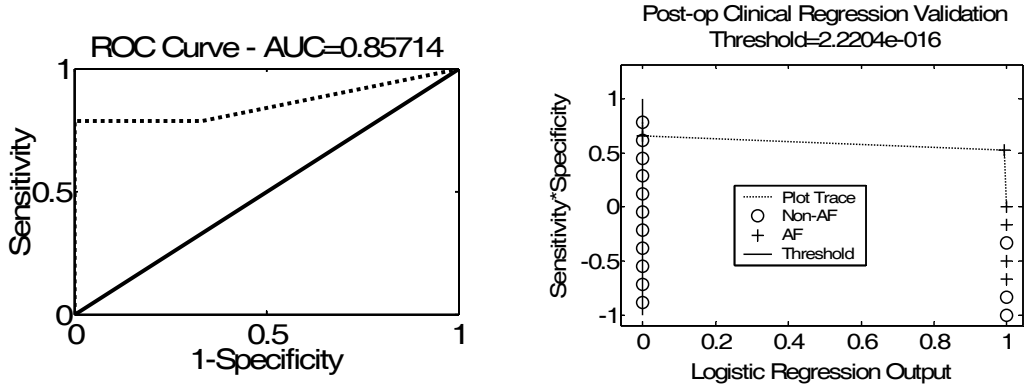

Figure 4.36 ROC curve and the product of the sensitivity and specificity of the validation of the logistic regression output of the postoperative clinical dataset including the maximum point indicating the optimum threshold.

4.4.2.2 ECG Feature Dataset – Logistic Regression

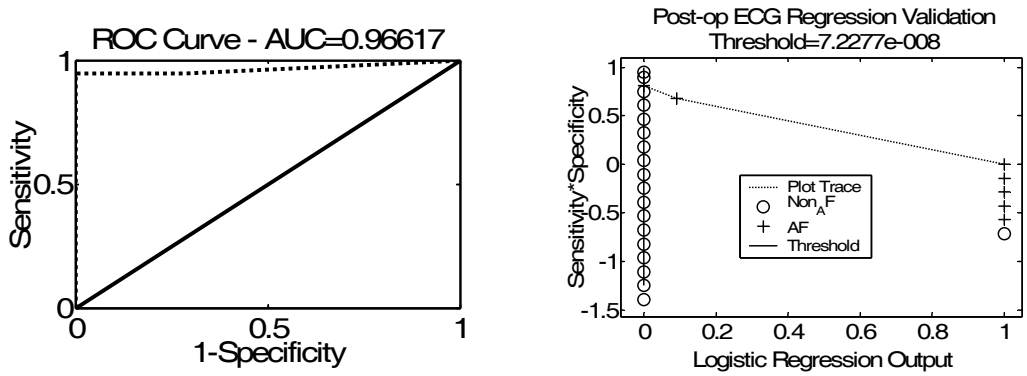

Figure 4.37 ROC curve and the product of the sensitivity and specificity of the validation of the logistic regression output of the postoperative ECG dataset including the maximum point indicating the optimum threshold

Figure 4.37 shows the ROC curve for the postoperative ECG dataset logistic regression classifier with an AUC of 0.96617, considered a very good classifier. This is similar to the perfect 1.00 AUC that was reported when trained and tested on the same set. Figure 4.37 shows the sensitivity/specificity product plot. Patient position has changed somewhat yet good classification is still reached, though this variable set should be tested with a larger sample size.

4.4.2.3 Clinical and ECG Combined Dataset – Logistic Regression

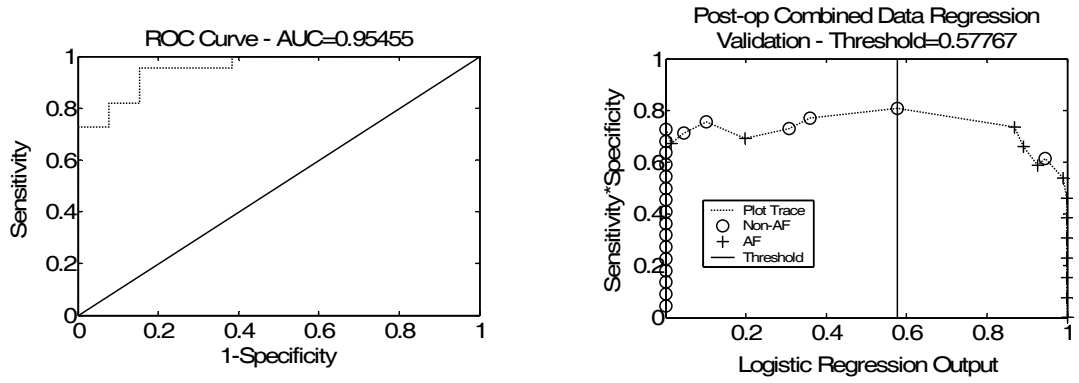

Figure 4.38 ROC curve and the product of the sensitivity and specificity of the validation of the logistic regression output of the postoperative combined clinical and ECG dataset including the maximum point indicating the optimum threshold.

Figure 4.38 shows the ROC curve for the postoperative combined clinical and ECG dataset logistic regression classifier with an AUC of 0.9546, considered a very good classifier. This is similar to the perfect 1.00 AUC that was reported when trained and tested on the same set. The patient position in the sensitivity/specificity product plot (Figure 4.39) has changed somewhat from the plot seen previously, yet there is still good separation though this should be further tested with a larger sample size.

4.5 Discussion

We should be careful comparing the results above to determine the best *method* for finding a classifier as the regression method's GA fitness was trained and tested on the same set while the *k*-NN used LOO. However, we can compare the *results* using a given classifier with a given set of features on this cohort. In fact, the postoperative data were

separated better by both classifiers and on both clinical and ECG data. We believe that with such a large feature set and such a small dataset, there exists a good probability of finding a pair of feature by pure random chance that would yield these results making these classifiers strongly overfitted. To test this for certain, a larger sample size is needed. Since we do not have this sample set and we desire a preoperative classification system (better treatment options for the patient), we will focus on the preoperative classifiers. Furthermore, since regression performed equally or better than the *k*-NN in the preoperative data and that physicians are well acquainted with this type of scoring risk stratification methods, we chose this to be the benchmark method for comparison in the next chapter. Since, the ECG dataset's logistic regression has some signs of overfitting and the combined dataset's classifer uses less than a quarter of the supplied dataset, we select the preoperative clinical logistic regression classifier as the best classifier of this chapter.

Also notice that the final combined clinical and ECG classifiers, when initialized with the previous best individuals, always seemed to be the same feature set that was discovered in one of the individual clinical or ECG classifier discoveries. This seems to show that these individuals overpower the rest of the population's individuals, possibly preventing effective search of the rest of the search space. As for performance of these initializations, the fixed and the random initializations return solutions with insignificant fitness differences.

Analysis of the features used in the multivariate classifiers shows that many of the features found in the univariate analysis done in chapter three are certainly helpful for

multivariate predictors. We also find that these cannot make up all of a classifier. We reap significant gains by trying many feature combinations that may resolve class subsets which might not be separated by use of only independently significant variables. Additionally, we see age, preoperative AF occurrence, number of anastamoses, coronary artery disease, and heart chamber size (atrial or left ventricular) appear prominently in the risk stratifiers. In the preoperative ECG feature set, we see a strong showing of frequency domain features performed on low to mid scale wavelet decompositions. This could be a further realization of the frequency differences described in the ECG wavelet decomposition discussed in chapter three. In the preoperative ECG feature set, we don't see this frequency domain dominance but there certainly are a significant numbers of c3 and c4 clips (clips taken at 24 and 36 hours following surgery). These clips occur near to when the majority of the patients go into AF, possibly showing a physiological precursor to AF onset. Though this would be of significant research interest, the applicability of current prophylactic measures would be ineffective this close to AF onset.

A major limitation of these methods of classification is their need for complete datasets. Otherwise, patients with missing data points must be left out of the analysis and we have no predictive means. This has greatly reduced this dataset as is seen in Table 4.3. Some patient groups are reduced more than 50%, greatly decreasing the value of our classifier and contributing to the over fitting problem.

Table 4.3 Summary of Sample usage and reduction when patients with missing data points were excluded from analysis in logistic regression or *k*-NN classification.

		Total Patients (NAF/AF)		Features	Patients Analyzed NAF/AF
Preoperative	Clinical	388/157	Reg.	5	116/75
			k-NN	5	158/97
	ECG	104/54	Reg.	5	84/46
			k-NN	4	84/46
	Combined	388/157	Reg.	5	84/46
			k-NN	2	84/46
Postoperative	Clinical	53/27	Reg.	4	14/6
			k-NN	3	14/6
	ECG	29/15	Reg.	2	17/6
			k-NN	4	20/13
	Combined	53/27	Reg.	3	22/13
			k-NN	4	22/13

It is evident that we need a classifier that can handle the missing data that will be encountered in a clinical setting where there might not be time to get results back from a test. The patient may need emergency surgery immediately, and a classification system that can still perform satisfactorily with missing data points is a high priority. For this reason, we will investigate a BN in the next chapter which can handle missing variables by relying on the data points which are provided. In this way, as the physician gets data, it can be entered in the model for a better risk stratification estimate. Additionally, as the system is fed more data, it continues to be further trained and improves future predictions.

Chapter 5

Bayesian network based AF Prediction

In this chapter, we present several methods for building Bayesian networks from data and assess each based on performance of risk stratification of pre- and postoperative AF. One should take note of the ability of the BN to incorporate the entire dataset into their analysis including cases with missing data points. This greatly reduces the influence of overfitting the previous chapters' classifiers were effected by. Additionally, the BN can infer information probabilistically, much as a doctor would when weighing and combining previous information, making its usage and acceptance more likely in a clinical setting.

5.1 Methods

Three different BN classifiers are developed in this chapter, all previously described in chapter two:

- Naïve BNs evolved with a GA,
- Traditional BNs built with the greedy K2 algorithm, and
- Traditional BNs evolved with a GA.

5.1.1 GA Built Naïve Bayesian Classifier

To ease the computational burden and the exponentially increasing need for data samples as the number of nodes increase in a BN structure, a naïve BN assumes conditional

independence between the adjacent parents in a network. The child node's joint probability is the product of each of the child's probabilities conditioned on that parent only, as explained in chapter two. To determine the actual prediction, we calculate the likelihood ratio between the prediction of AF and non-AF, allowing the denominator of Bayes' rule to cancel, dismissing any complications in calculating the predictive variable's joint probability.

We use the same GA method and chromosome structure as shown in Figure 4.2 to select the feature sets of a naïve BN in this chapter. We allow the AF node to have two to five predictive parent variables and no secondary parents.

5.1.2 K2-built Bayesian Network

By adding nodes greedily, a reasonable traditional Bayesian network can be found relatively quickly, though the chance of finding the best network is very slim. To counter this disadvantage, when building the network using K2, we allowed the network to have five first-level parents and five second-level parent nodes. We also performed a second structure construction using three first- and second-level parents. These second-level parents allow for prediction of their child in the case of a missing value. We allow this network a greater number of predictive variables, in order to compensate for the lack of a global optimization routine the other BNs will have the benefit of evolving under.

Traditionally, this network building method requires a causal list of the variables, meaning that causes must precede effects. Since the cause and effect relationship is not clear for almost all of these relationships, we have removed this requirement to allow the

greedy addition of any node on the list. Additionally, for the evaluation of the network's fitness, the dataset is allowed no missing data points. For this reason, patients with missing data points in the variables of interest during a particular networks' training were removed. All patients that had at least one filled data point that the classifier used were included in testing.

5.1.3 GA Built Traditional Bayesian Network

We chose to allow two to three first-level parents and zero to two second-level parents in this network. This puts this network at a slight disadvantage to the naïve network and the K2-built network which has a possible five first-level nodes. However, the optimization training performed by the GA roughly accounts for this difference as we will see in the results.

5.1.4 Genetic Algorithm

The chromosome for the GA built traditional BN was constructed in a manner to reflect the tree structure of the network. The first integer in the chromosome, *p,* is the number of parents the node of interest has, the occurrence of AF. Following this, there are *p* vectors of integers, which code for each of the branches that the first-level nodes begin. Within each of these vectors, the first integer encodes the feature number of this first-level node branch. The next integer, *p',* encodes the number of second-level parents this first-level parent has, while following this are the integers that encode those features. The chromosome construction is seen in Figure 5.1.

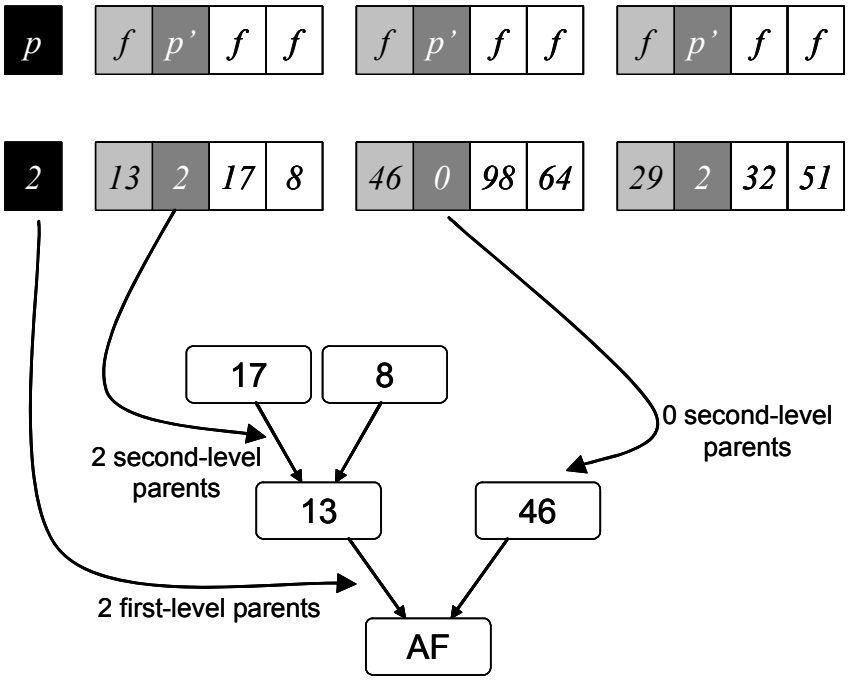

Figure 5.1 Encoded chromosome for the BN structure and feature nodes. An example is shown of how these value are made into the structure.

The chromosome always contains the maximum number of possible node combinations, while the *p* and *p'* integers limit which of those feature nodes will be used. This allows for point-to-point crossovers and mutations to occur in identical places in the graph. The unused values in the chromosome add significantly to the size and complexity of the chromosome and slightly degrades the utility of the GA crossovers and mutations, due to some of the alleles being unused for a given structure. However, as seen in nature, many genes of an organism stay inactive through their lifetime and are passed down to future generations for later mutations or crossovers to activate [99], so this is seen as safeguarding diversity and consistent gene transmission, not a complexity drawback.

The genetic algorithm parameters, including generations, initializations, crossover and mutation rates, etc., are the same as those listed in chapter four. There are far greater

numbers of possibilities for the structure in these networks though, due to the larger chromosome. However, the global maximum is still approached due to the termination condition of stopping only after the GA has run 250 generations with no improvement.

5.2 Evaluation

For the creation of probability tables, the number of values a parameter may take, must be limited. Therefore, after extraction, feature values are discretized into binary form, based on their value being above or below a certain threshold. This threshold was set using a receiver operating characteristic (ROC) curve, where a feature value is predictive of the variable of interest—in this case, the occurrence of AF. We used the same method for finding the optimum threshold, as seen in chapter four: the maximum of the sensitivity/specificity product plot. This discretization of the data allows for the computation of well-populated conditional probability tables needed to build a BN classifier.

For each of these networks created, both pre- and postoperative data were evaluated for clinical and ECG data, as well as their combined data sets, just as was done for the logistic regression and *k*-NN classifiers in the previous chapter, making a total of eighteen networks. Since the GA evolved classifiers in chapter four identified only previously created solutions, the combined data set classifiers in this chapter were all initialized randomly.

5.3 Results

For each BN classifier, we show the network structure that was found to have the best fitness, given this dataset and structural limitations. The average population fitness, as well as the best individual's fitness, are also plotted to show the evolutionary process that was performed through the GA to find this individual. We additionally plot the sensitivity/specificity product for all patient values, which also shows the optimum threshold point for separation of the non-AF and AF classes. The ROC plot of the classifier is shown along with the AUC, showing the quality of the classifier or its ability to order and separate the classes. For each classifier we also list the number of first-level parents/features used by that classifier, the sensitivity and specificity, the fitness, the number of patients the classification system used, both non-AF (NAF) and (AF), and the number of generations required to reach this solution. The summary of all of these results are seen here in Table 5.1 with their specifics in the sections following.

Table 5.1 For each classifier, the number of first-level parents/features used, the sensitivity and specificity, the fitness, the number non-AF(NAF) and AF patients used, and the number of GA generations were run before finding this optimum solution.

			First-level Features	*Sen/Spec*	*Fitness*	*NAF/AF*	*Generations*
Preoperative	*Clinical*	*Naïve BN*	*5*	*0.63/0.73*	*0.70029*	*388/157*	*13*
		K2 BN 3 prnts	*3*	*0.59/0.31*	*0.46658*		*N/A*
		K2 BN 5- prnts	*5*	*0.45/0.75*	*0.53568*		
		Traditional BN	*3*	*0.61/0.71*	*0.68139*		*19*
	ECG	*Naïve BN*	*5*	*0.70/0.62*	*0.60962*	*162/82*	*263*
		K2 BN 3- prnts	*3*	*0.65/0.44*	*0.52609*		*N/A*
		K2 BN 5- prnts	*5*	*0.46/0.78*	*0.61047*		
		Traditional BN	*3*	*0.51/0.86*	*0.73032*		*452*
	Combined	*Naïve BN*	*5*	*0.68/0.68*	*0.69438*	*388/157*	*382*
		K2 BN 3- prnts	*3*	*0.38/0.46*	*0.52558*		*N/A*
		K2 BN 5- prnts	*5*	*0.36/0.71*	*0.45477*		
		Traditional BN	*3*	*0.61/0.58*	*0.6056*		*52*
Postoperative	*Clinical*	*Naïve BN*	*5*	*0.89/0.91*	*0.91976*	*53/27*	*24*
		K2 BN 3- prnts	*2*	*0/1*	*0.4803*		*N/A*
		K2 BN 5- prnts					
		Traditional BN	*3*	*0.85/0.92*	*0.8955*		*23*
	ECG	*Naïve BN*	*4*	*1/0.90*	*0.94359*	*30/16*	*42*
		K2 BN 3- prnts	*3*	*0.19/0.83*	*0.46532*		*N/A*
		K2 BN 5- prnts	*5*	*0/1*	*0.41726*		
		Traditional BN	*3*	*0.94/0.93*	*0.9496*		*203*
	Combined	*Naïve BN*	*3*	*0.96/0.83*	*0.93063*	*53/27*	*297*
		K2 BN 3- prnts	*2*	*0/1*	*0.4803*		*N/A*
		K2 BN 5- prnts					
		Traditional BN	*3*	*0.41/0.89*	*0.7092*		*13*

5.3.1 Preoperative Risk Stratifiers

5.3.1.1 Clinical Dataset

5.3.1.1.1 Naïve Bayesian Network

The naïve BN of the preoperative clinical data took 13 generations to find a classifier with a fitness of 0.70029, a sensitivity of 0.63, and a specificity of 0.73 using the five variables in the structure seen in Figure 5.2. We see preoperative AF or atrial flutter as a predictor, which we also saw to be statistically significant in chapter three, as well as being significant in previous authors' work in chapter two. In chapter three, we also saw that race (specifically black) and having cardiomegaly were statistically significant. Chapter four's multivariate predictors also used preoperative AF, smoking, and cardiomegaly in their best individuals.

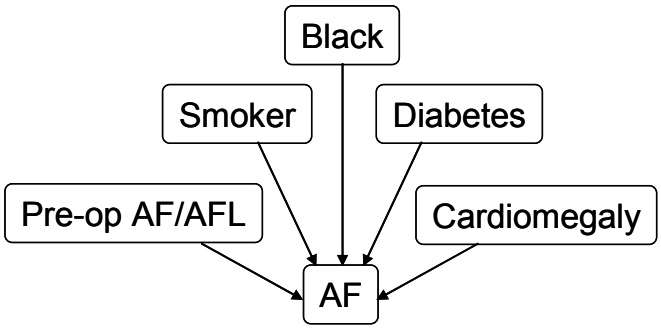

Figure 5.2 Naïve BN with the best fitness for the preoperative clinical dataset.

Figure 5.3 shows the evolution of the classifier with the fitness of the best individual as well as the average fitness of the population. There seems to be good mixing, showing that the evolving population was not too closely tied to the fittest individual. Notice that

the best individual was found in the thirteenth generation, but the plot continues to show 250 generations following this, as this is one of the terminating conditions of the GA.

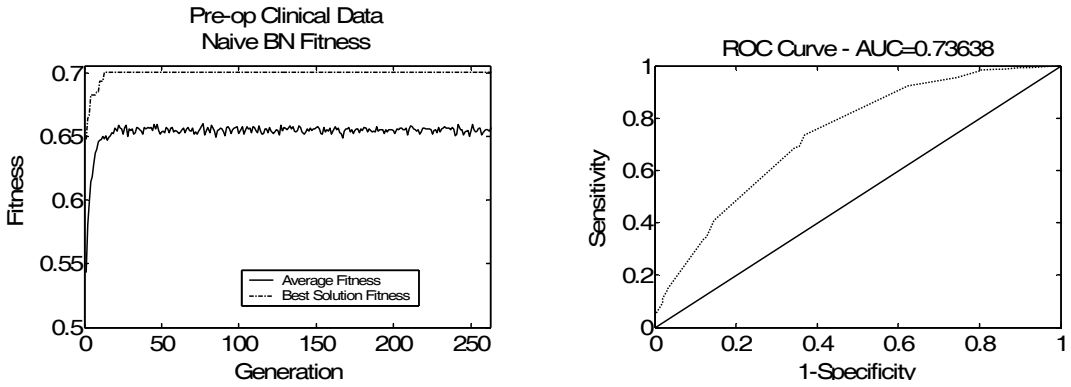

Figure 5.3 Evolutionary fitness plot and ROC curve of the preoperative clinical dataset's naive BN.

Figure 5.3 shows the ROC of this classifier, with an AUC of 0.74, making it a fair to good risk stratifier. The sensitivity/specificity product plot, shown in Figure 5.4, shows the threshold value of the likelihood of AF occurrence output from the naïve BN found to best separate the classes, 0.0046709. This threshold is set immediately above the maximum of this curve for optimal separation, given our need for equally high sensitivity and specificity as discussed in chapter four. Again, the threshold was set immediately above this value to prevent the patient that defines the maximum from having an indeterminate predicted class. This optimum threshold selection method is used for all threshold determination in this work.

While it is difficult to discern the individuals in the plot, one can see that the AF patients tend to have values above this threshold while non-AF patients tend to be under this value.

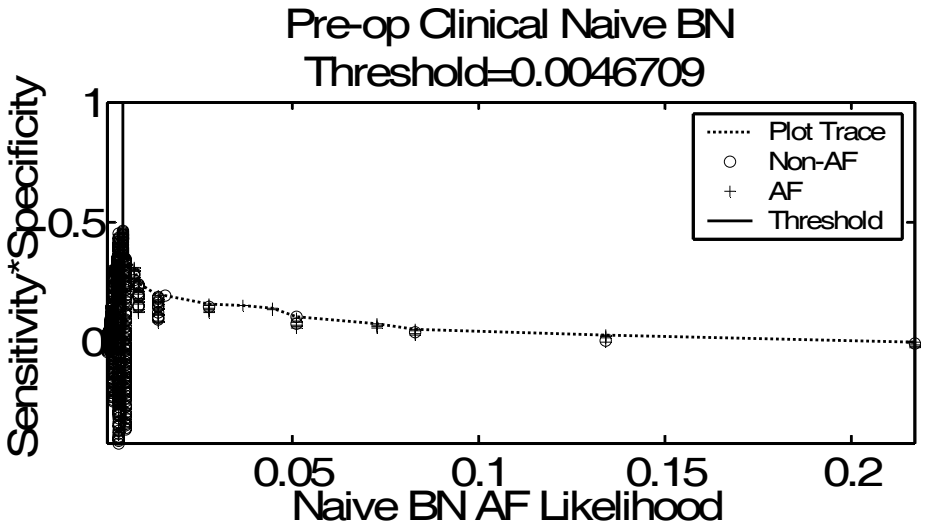

Figure 5.4 Product of the sensitivity and specificity of the naïve BN output of the preoperative clinical dataset, including the maximum point indicating the optimum threshold.

5.3.1.1.2 K2-built Traditional Bayesian Network

The 3-parent restricted K2-built traditional BN of the preoperative clinical data has a fitness of 0.46658, a sensitivity of 0.59, and a specificity of 0.31, using the three first-level and the five second-level variables in the structure seen in Figure 5.5. Notice that smoking appears as a second-level node in this graph, while it was a first-level node in the previous BN. Additionally, left atrial size and mitral valve regurgitation appeared in chapter three as a statistically significant univariate predictor. Chapter four's multivariate

predictors also used left ventricle diastolic pressure, left atrial hypertrophy, low density lipoprotein, ejection fraction, and smoking.

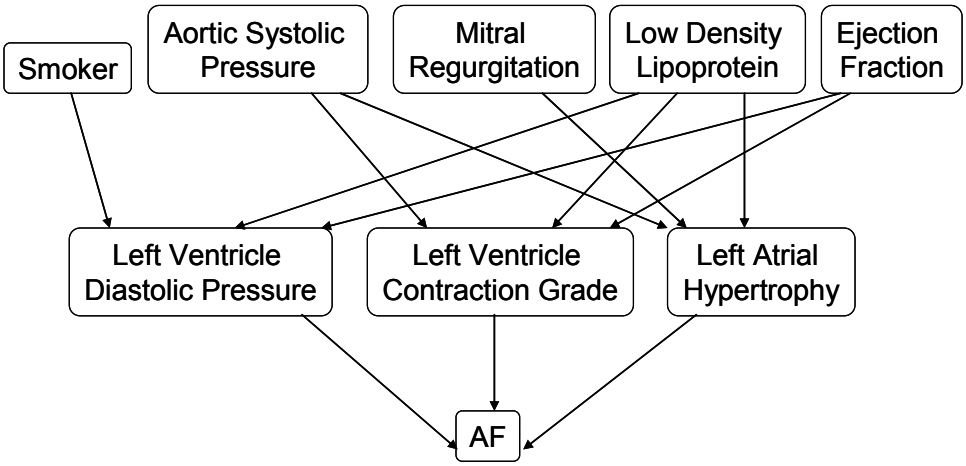

Figure 5.5 K2-built 3-parent BN with the best fitness for the preoperative clinical dataset.

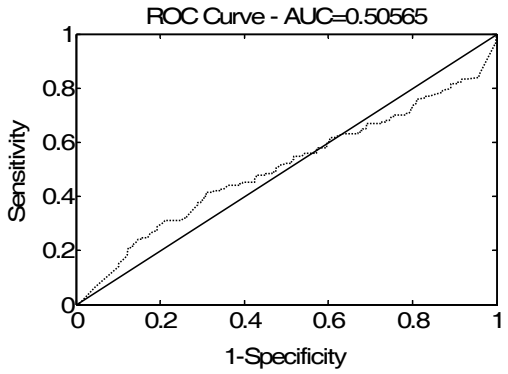

Figure 5.6 ROC curve of the preoperative clinical dataset's K2-built 3-parent BN.

Figure 5.6 shows the ROC of this classifier, making it a poor risk stratifier (AUC = 0.51). The sensitivity/specificity product plot, shown in Figure 5.7, shows the threshold value of the likelihood of AF occurrence tat was output from the traditional K2-built BN found to

best separate the classes, 0.47608. There does not appear to be a good separation of the two classes of data and the sensitivity/specificity product maximum is a fairly low value. These observations, combined with the low AUC, make this a poor classifier.

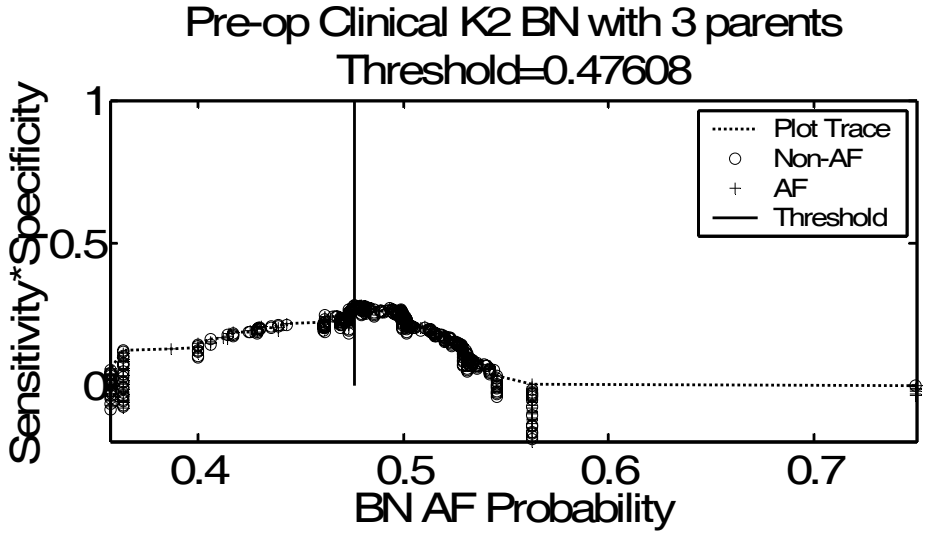

Figure 5.7 Product of the sensitivity and specificity of the K2-built 3-parent BN output of the preoperative clinical dataset including the maximum point indicating the optimum threshold.

The 5-parent restricted K2-built traditional BN of the preoperative clinical data has a fitness of 0.53568, a sensitivity of 0.45, and a specificity of 0.75, using the five first-level and the six second-level variables in the structure seen in Figure 5.8. Since this structure is built by adding nodes one-by-one in a greedy manner, it has the same nodes seen in the previous graph with several added. You can see that two second-level nodes in the previous network, mitral valve regurgitation and low density lipoprotein, were shifted to first-level nodes. This shows that a strong correlation exists between the second-level nodes and the node of interest, which in this work is the occurrence of postoperative AF.

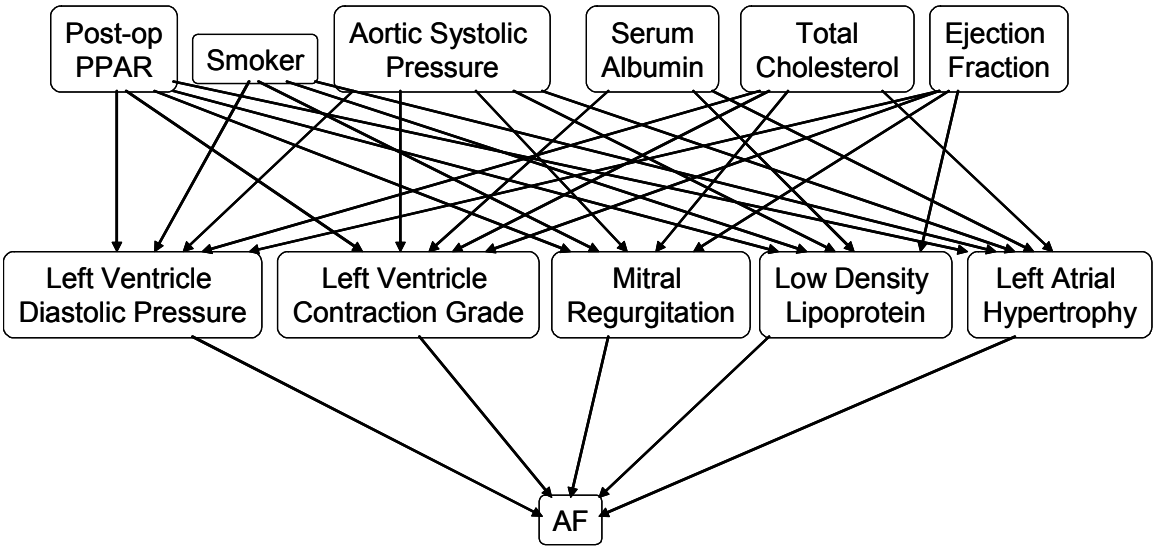

Figure 5.8 K2-built 5-parent BN with the best fitness for the preoperative clinical dataset.

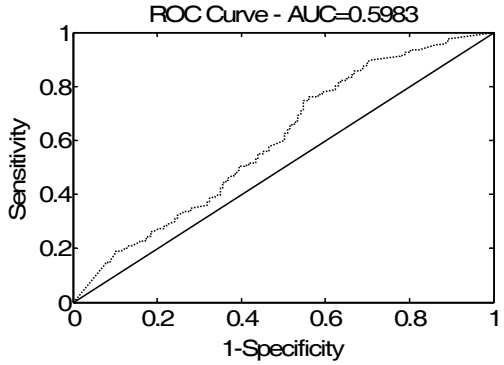

Figure 5.9 ROC curve of the preoperative clinical dataset's K2-built 5-parent BN.

Figure 5.9 shows the ROC of this classifier, with an AUC equal to 0.60, making it a poor to fair risk stratifier. The sensitivity/specificity product plot, shown in Figure 5.10, shows the threshold value of the likelihood of AF occurrence output from the traditional K2-built BN found to best separate the classes, 0.53929. There does not appear to be a good separation of the two classes of data and the sensitivity/specificity product maximum is a fairly low value. This reinforces the fact that this is only a poor to fair classifier.

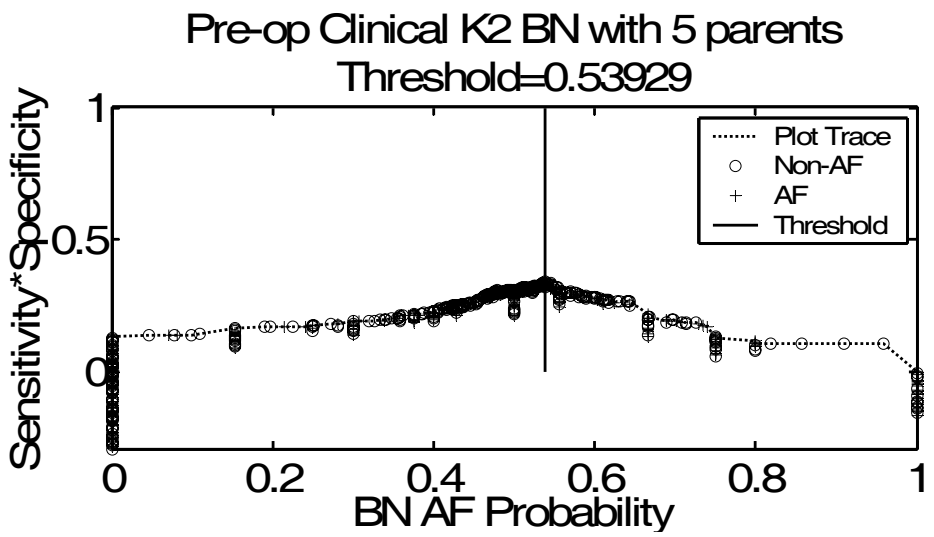

Figure 5.10 Product of the sensitivity and specificity of the K2-built 5-parent BN output of the preoperative clinical dataset including the maximum point indicating the optimum threshold.

5.3.1.1.3 GA Built Traditional Bayesian Network

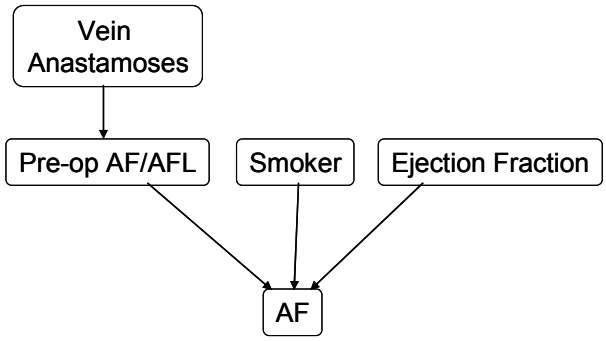

Figure 5.11 Traditional BN with the best fitness for the preoperative clinical dataset.

The GA built traditional BN of the preoperative clinical data took 19 generations to find a classifier with a fitness of 0.68139, a sensitivity of 0.61, and a specificity of 0.71, using the three first-level and one second-level variables in the structure seen in Figure 5.11.

We see that the preoperative occurrence of AF, smoking, and ejection fraction are once again predictors as found in this chapter, as well as in chapters three and four. The number of anastamoses is once again a predictor, as seen previously in chapter four, but we find it interesting that this node was included. Second-level nodes only contribute to a patient's risk stratification for AF if the first-level node it is connected to has a missing value. In this dataset, preoperative AF had only two missing values of 545 patients. We can only assume that predicting these two patients made it better than a competing network or that the GA never created an individual which did not have this node.

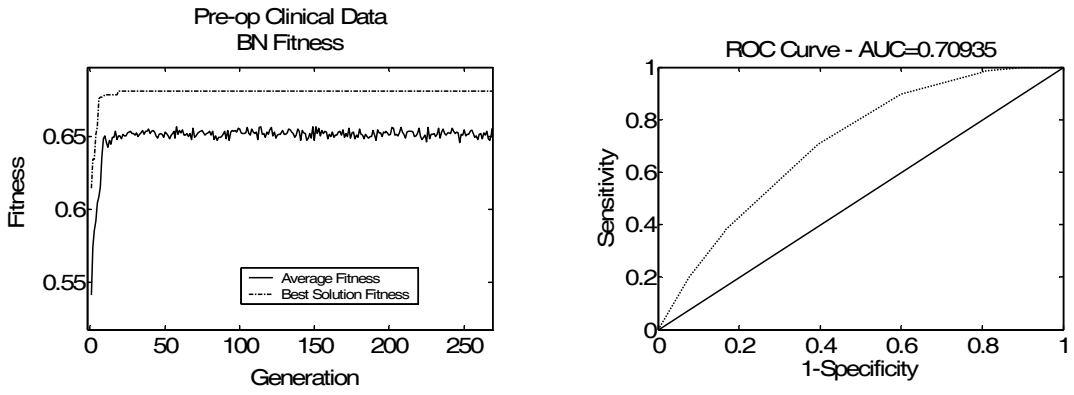

Figure 5.12 Evolutionary fitness plot and ROC curve of the preoperative clinical dataset's traditional BN.

Figure 5.12 shows the evolution of the classifier with the fitness of the best individual as well as the average fitness of the population. There seems to continue to be good mixing after finding the best solution relatively early in the number of generations.

Figure 5.12 also shows the ROC of this classifier, making it a fair risk stratifier (AUC = 0.71). The sensitivity/specificity product plot, shown in Figure 5.13, shows the threshold

value of the likelihood of AF occurrence output from the GA built traditional BN found to best separate the classes, 0.22086. There do appear to be relatively more AF patients with probability values above the threshold, yet a great number of non-AF patients have these values as well.

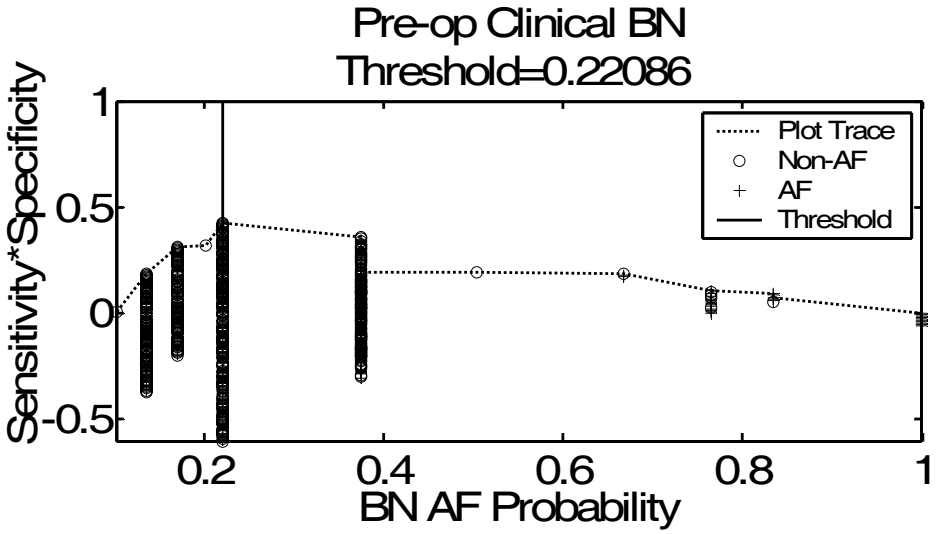

Figure 5.13 Product of the sensitivity and specificity of the traditional BN output of the preoperative clinical dataset including the maximum point indicating the optimum threshold.

5.3.1.2 ECG Feature Dataset

5.3.1.2.1 Naïve Bayesian Network

The naïve BN of the preoperative ECG data took 263 generations to find a classifier with a fitness of 0.60962, a sensitivity of 0.70, and a specificity of 0.62, using the five variables in the structure seen in Figure 5.14. The feature TQ_II_sym4_sc20_Median_Freq is very similar to TQ_II_sym4_sc20_Mean_Freq that

was statistically significant in chapter three, which we investigated further by plotting an ROC and a sensitivity/specificity product graph. None of the other features appear to be significant in chapters three or four. Additionally, notice the exclusive usage of the II lead in this classifier, which is similar to this lead's domination of statistically significant features in chapter three.

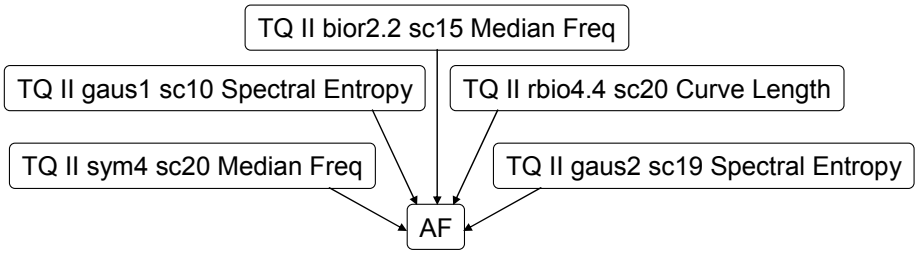

Figure 5.14 Naïve BN with the best fitness for the preoperative ECG dataset.

Figure 5.15 shows the evolution of the classifier with the fitness of the best individual as well as the average fitness of the population. There seems to be good mixing, showing that the evolving population was not too closely tied to the fittest individual. Additionally, you see more fit individuals being found after more than one hundred generations of no improvements. This is why one of the termination conditions is that it must run for 250 generations with no improvements without stopping, making it more likely that we found the most fit individual.

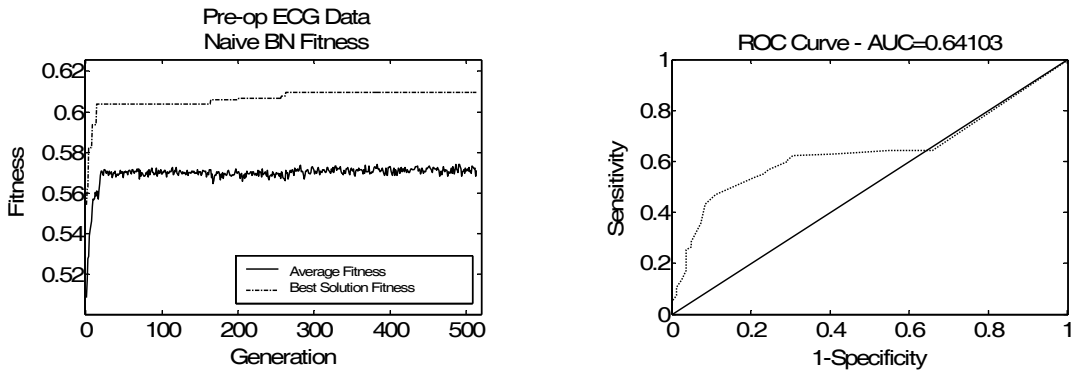

Figure 5.15 Evolutionary fitness plot and ROC curve of the preoperative ECG dataset's naive BN.

Figure 5.15 also shows the ROC of this classifier with an AUC of 0.64, making it a fair risk stratifier. The sensitivity/specificity product plot, shown in Figure 5.16, shows the threshold value of the likelihood of AF occurrence output from the naïve BN found to best separate the classes, 0.030448. While it is difficult to discern the individuals in the plot, one can see that the AF patients tend to have values above this threshold while non-AF patients tend to be under this value. Notice that many patients fall near the zero or on the 0.5 likelihood value, an interesting result given it is the result of the product of five probabilities.

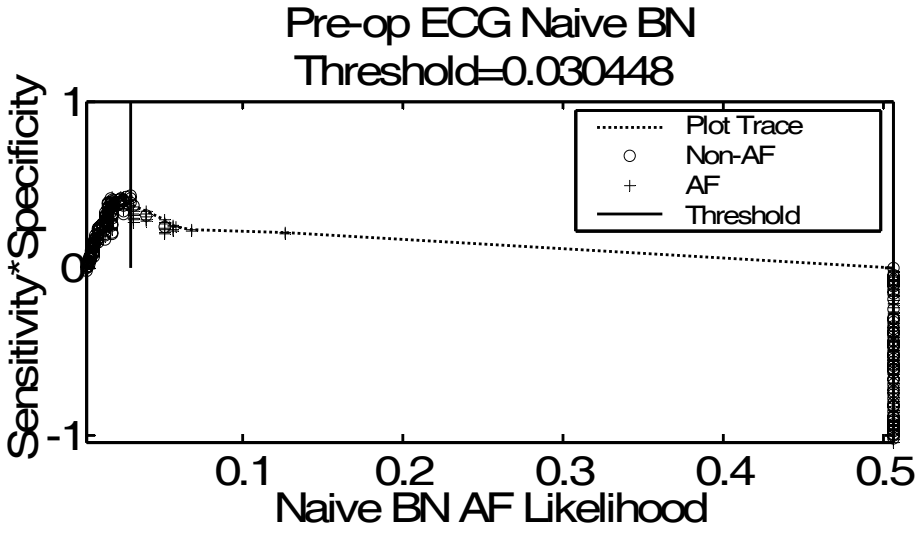

Figure 5.16 Product of the sensitivity and specificity of the naïve BN output of the preoperative ECG dataset including the maximum point indicating the optimum threshold.

5.3.1.2.2 K2-built Traditional Bayesian Network

The 3-parent restricted K2-built traditional BN of the preoperative ECG data has a classifier with a fitness of 0.52609, a sensitivity of 0.65, and a specificity of 0.44 using the three first-level and the four second-level variables in the structure seen in Figure 5.17. Notice that the greedy K2 algorithm added P wave morphological features almost exclusively. The V_1 lead's P wave duration had a p value of 0.922 when investigated in chapter three, yet in this chapter, after binary discretization it is chosen as a first-level node. The other P wave morphological features chosen have similarly poor univariate predictive results. The only explanations of this could be that the binary discretization improved these features' utility or that when paired with other features with full conditional probability tables, it matches more of the dataset's samples.

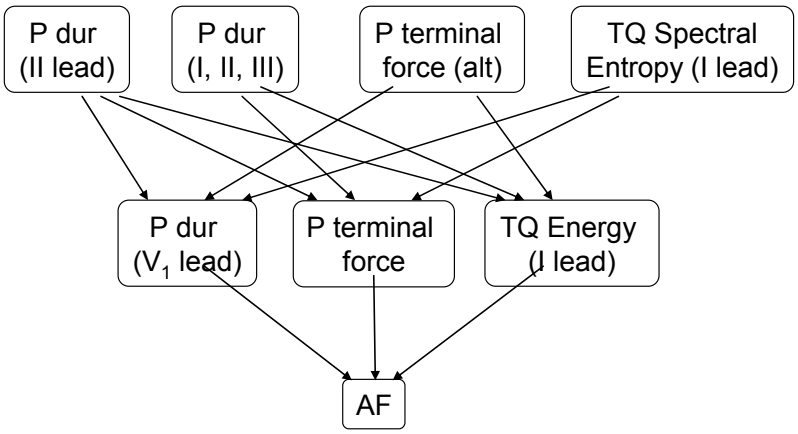

Figure 5.17 K2-built 3-parent BN with the best fitness for the preoperative ECG dataset.

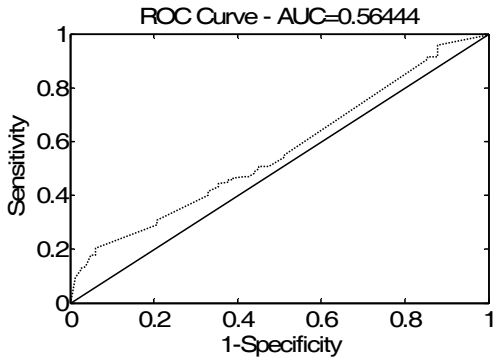

Figure 5.18 ROC curve of the preoperative ECG dataset's K2-built 3-parent BN.

Figure 5.18 shows the ROC of this classifier, making it a poor risk stratifier (AUC = 0.56). The sensitivity/specificity product plot, Figure 5.19, shows the threshold value of the likelihood of AF occurrence output from the traditional K2-built BN found to best separate the classes, 0.42528. There does not appear to be a good separation of the two classes of data and the sensitivity/specificity product maximum is a fairly low value. This reinforces that fact that this is a poor classifier.

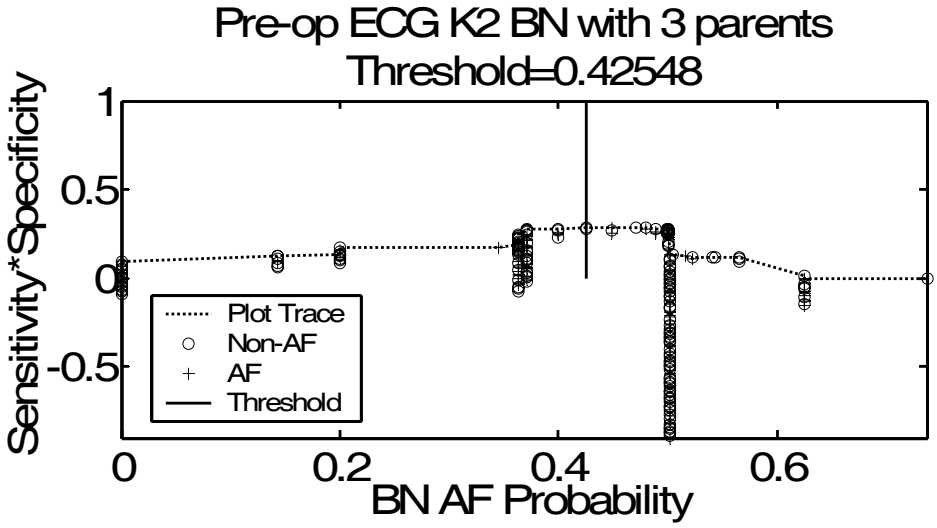

Figure 5.19 Product of the sensitivity and specificity of the K2-built 3-parent BN output of the preoperative ECG dataset including the maximum point indicating the optimum threshold.

The 5-parent restricted K2-built traditional BN of the preoperative ECG data has a fitness of 0.61047, a sensitivity of 0.46, and a specificity of 0.78 using the five first-level and the six second-level variables in the structure seen in Figure 5.20. Since this structure is built by adding nodes one-by-one in a greedy manner, it has the same nodes seen in the previous graph with several added. You can see that, again, two second-level nodes in the previous network, the P durations of the II lead and the combined I, II, and II lead, were shifted to first-level nodes. This reinforces that a strong correlation exists between the second-level nodes and the node of interest. Additionally, several additional morphological features were added as second-level nodes.

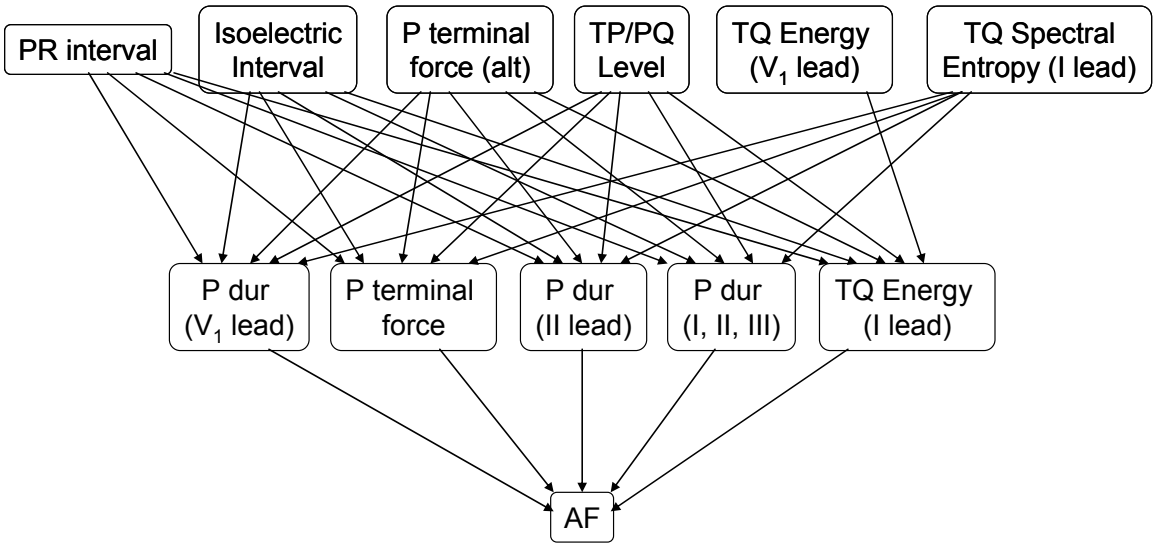

Figure 5.20 K2-built 5-parent BN with the best fitness for the preoperative ECG dataset.

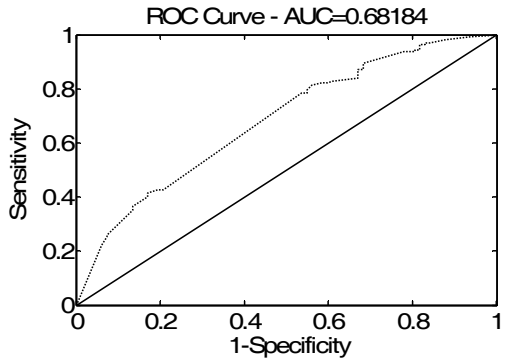

Figure 5.21 ROC curve of the preoperative ECG dataset's K2-built 5-parent BN.

Figure 5.21 shows the ROC of this classifier, making it a fair risk stratifier (AUC = 0.68). The sensitivity/specificity product plot, shown in Figure 5.22, shows the threshold value of the likelihood of AF occurrence output from the traditional K2-built BN found to best separate the classes, 0.40936. There does not appear to be a good separation of the two classes of data and the sensitivity/specificity product maximum is a fairly low value.

Additionally, many of the probability values fall immediately on the threshold line indicating possible over fitting, which could possibly cause difficulty during validation.

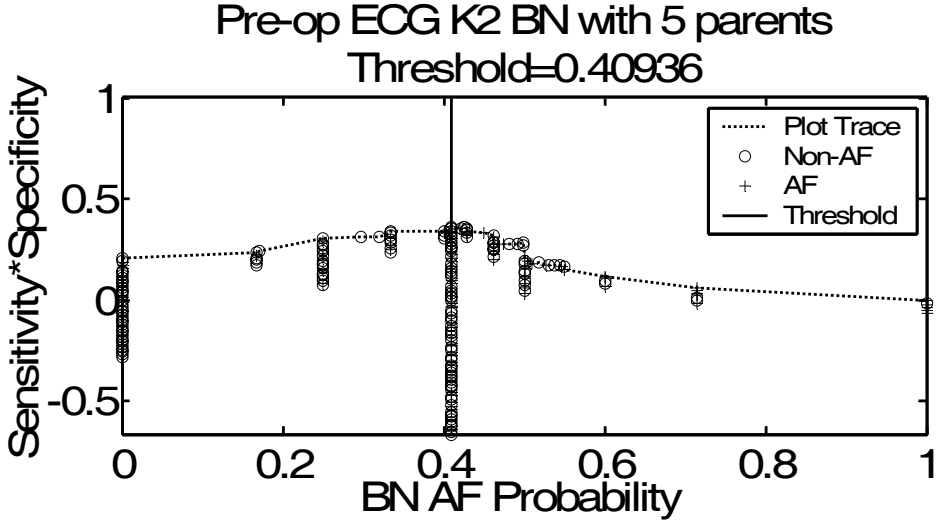

Figure 5.22 Product of the sensitivity and specificity of the K2-built 5-parent BN output of the preoperative ECG dataset including the maximum point indicating the optimum threshold.

5.3.1.2.3 GA Built Traditional Bayesian Network

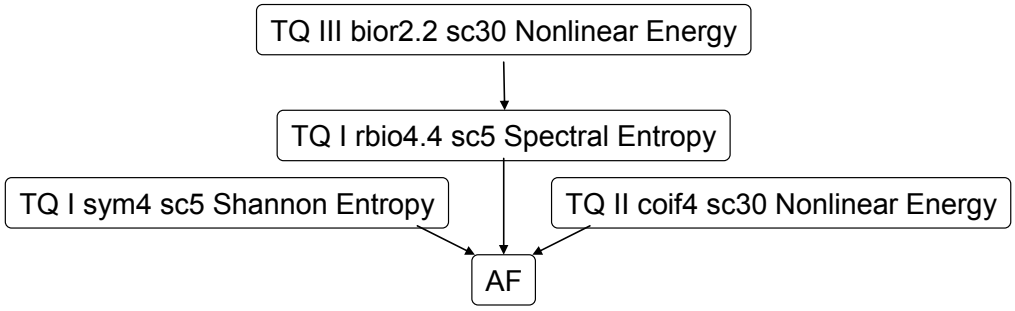

Figure 5.23 Traditional BN with the best fitness for the preoperative ECG dataset.

The GA built traditional BN of the preoperative ECG data took 452 generations to find a classifier with a fitness of 0.73032, a sensitivity of 0.51, and a specificity of 0.86 using the three first-level and one second-level variables in the structure seen in Figure 5.23. This is an interesting combination of features as none of these have been identified in the previous univariate or multivariate analyses as being significant yet together they give the highest overall separation of all the preoperative risk stratification classifiers. This could just be a case of overfitting because of the sheer number of features that were tried to separate these 244 patients into their classes. Though, if this were the case, it would seem that the naïve BN training would have also found a better network than the 0.61 fitness that it achieved with this dataset.

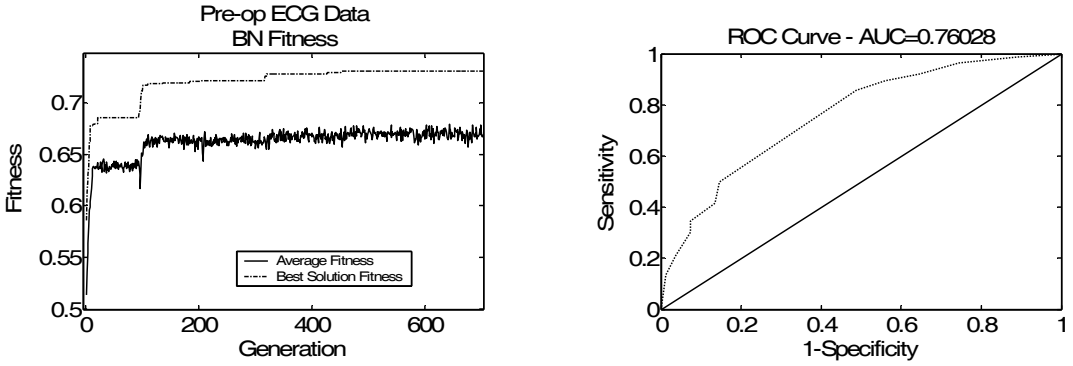

Figure 5.24 Evolutionary fitness plot of the preoperative ECG dataset's traditional BN.

Figure 5.24 shows the evolution of the classifier with the fitness of the best individual as well as the average fitness of the population. There seems to be good mixing showing that the evolving population was not too closely tied to the fittest individual. Additionally, we see a significant improvement in both the populations average fitness as

well as the best individual at around generation number 100. Changes in the average population fitness curve which coincide with the best individual's fitness can indicate that the GA has found a new significantly better point in the feature space which not only improves that individual but imparts this improvement to its children and it improves their fitness as well. Typically, if the new global fitness maximum is an extremely narrow peak in the feature space, it only helps a single individual and not its children. If this were the case, the average population fitness would not improve significantly enough for a large noticeable change in its value.

Figure 5.24 shows the ROC of this classifier, making it a good risk stratifier (AUC = 0.76). The sensitivity/specificity product plot, shown in Figure 5.25, shows the threshold value of the likelihood of AF occurrence output from the GA built traditional BN found to best separate the classes, 0.49854. There appear to be relatively more AF patients with probability values above the threshold yet a great number of non-AF patients have these values as well. We also see a great number of patients that fall immediately before this boundary which, when validated with leave-one-out, could make this a poor risk stratifier.

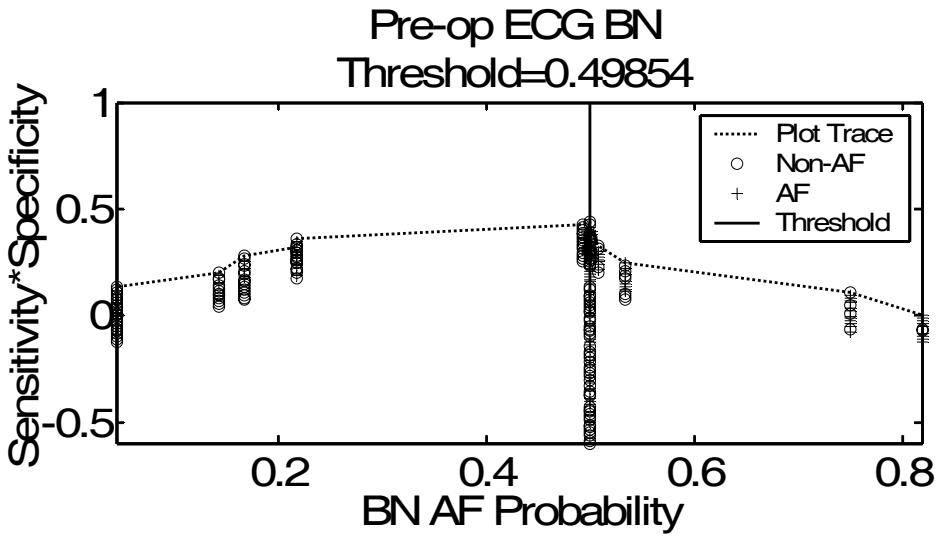

Figure 5.25 Product of the sensitivity and specificity of the traditional BN output of the preoperative ECG dataset including the maximum point indicating the optimum threshold.

5.3.1.3 Clinical and ECG Combined Dataset

5.3.1.3.1 Naïve Bayesian Network

The naïve BN of the preoperative combined clinical and ECG data took 382 generations to find a classifier with a fitness of 0.69438, a sensitivity of 0.68, and a specificity of 0.68 using the five variables in the structure seen in Figure 5.26. Notice the similarity of this network to that found by the naïve BN found in the clinical dataset. The only variable difference is an exchange of diabetes and left ventricle ejection fraction. Though this graph is slightly less fit than the BN with diabetes, these variables have been found to be correlated possibly explaining their interchangeability [100].

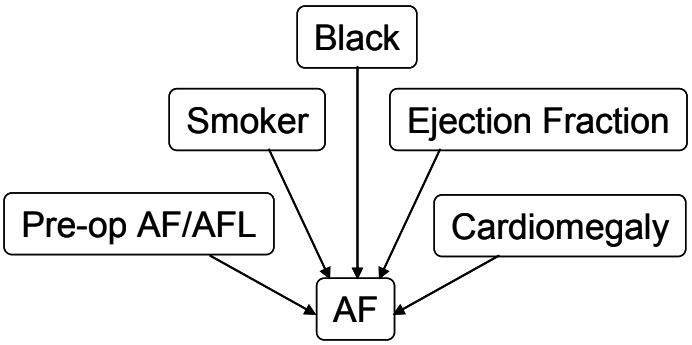

Figure 5.26 Naïve BN with the best fitness for the preoperative combined clinical and ECG dataset.

Figure 5.27 shows the evolution of the classifier with the fitness of the best individual as well as the average fitness of the population. There seems to be good mixing showing that the evolving population was not too closely tied to the fittest individual. Additionally, we again see significant improvements in both the populations average fitness as well as the best individual after seemingly long periods of no improvement.

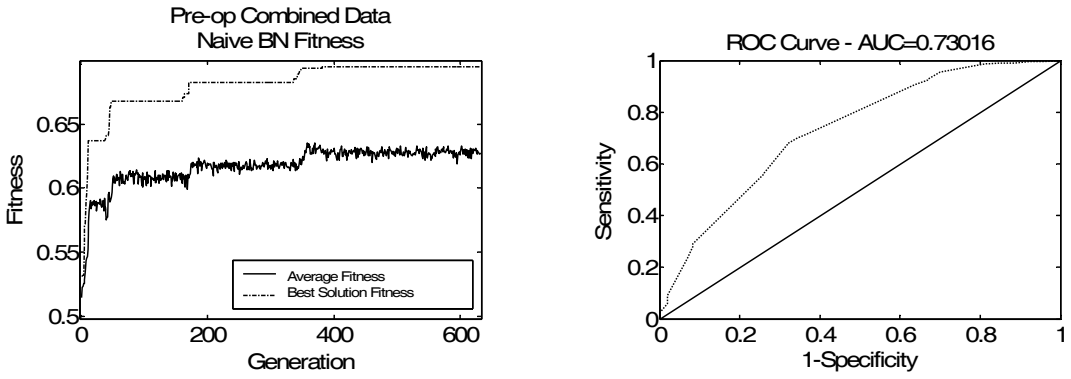

Figure 5.27 Evolutionary fitness plot and ROC curve of the preoperative combined clinical and ECG dataset's naive BN.

Figure 5.27 shows the ROC of this classifier, making it a fair risk stratifier (AUC = 0.73). The sensitivity/specificity product plot, shown in Figure 5.28, shows the threshold value of the likelihood of AF occurrence output from the naïve BN found to best separate the classes, 0.0034239. While it is difficult to discern the individuals in the plot, one can see that the AF patients tend to have values above this threshold while non-AF patients tend to be under this value.

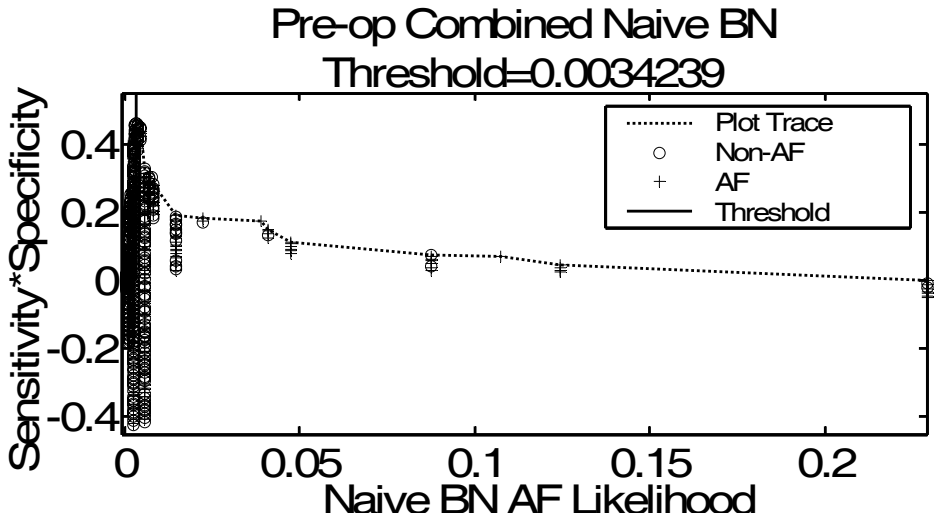

Figure 5.28 Product of the sensitivity and specificity of the naïve BN output of the preoperative combined clinical and ECG dataset including the maximum point indicating the optimum threshold.

5.3.1.3.2 K2-built Traditional Bayesian Network

The 3-parent restricted K2-built traditional BN of the preoperative combined clinical and ECG data had a fitness of 0.52558, a sensitivity of 0.38, and a specificity of 0.46 using the three first-level and the five second-level variables in the structure seen in Figure

5.29. This BN shows a definite mixing of both clinical and ECG features with several nodes we have seen in both univariate and multivariate use previously.

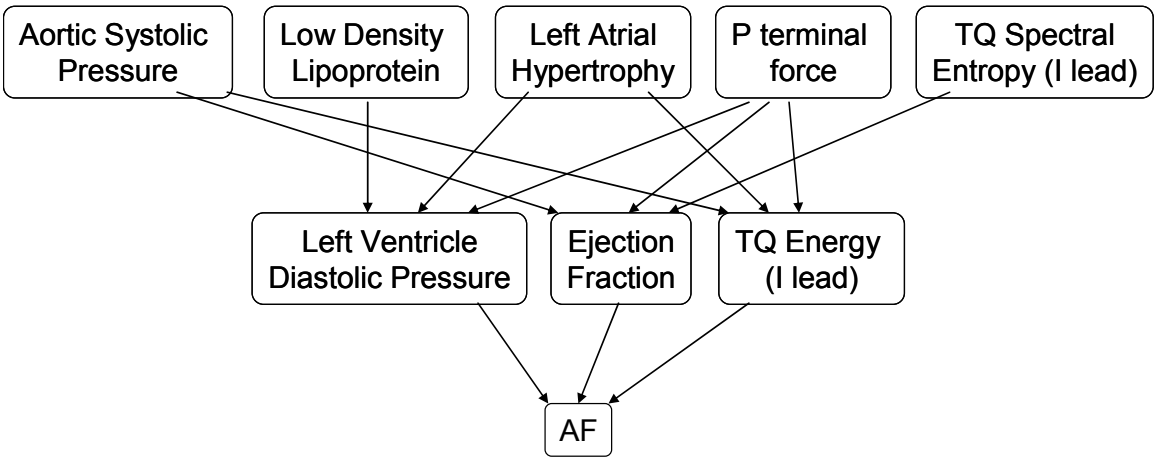

Figure 5.29 K2-built 3-parent BN with the best fitness for the preoperative combined clinical and ECG dataset.

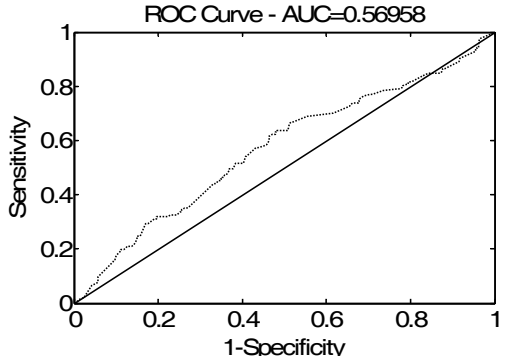

Figure 5.30 ROC curve of the preoperative combined clinical and ECG dataset's K2-built 3-parent BN.

Figure 5.30 shows the ROC of this classifier, making it a poor risk stratifier (AUC = 0.57). The sensitivity/specificity product plot, shown in Figure 5.31, shows the threshold value of the likelihood of AF occurrence output from the traditional K2-built BN found to

best separate the classes, 0.52219. There does not appear to be a good separation of the two classes of data and the sensitivity/specificity product maximum is a fairly low value. This reinforces that fact that this is a poor classifier.

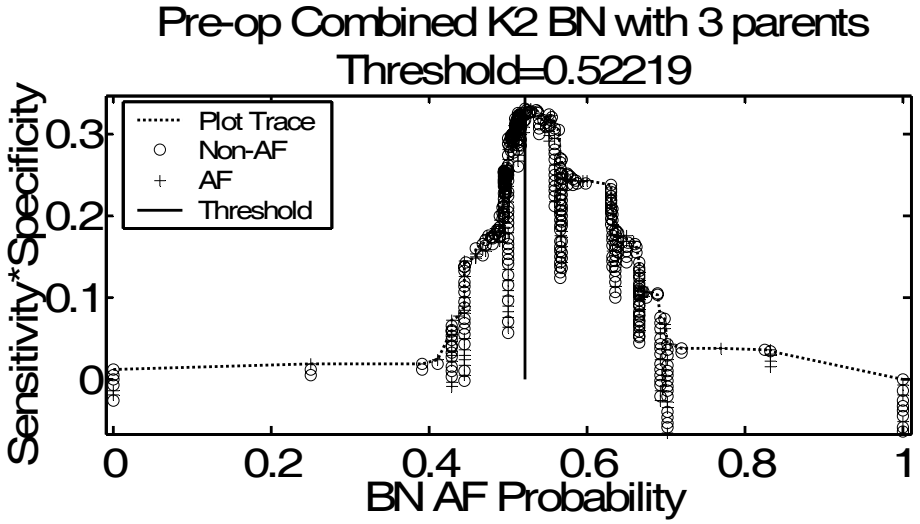

Figure 5.31 Product of the sensitivity and specificity of the K2-built 3-parent BN output of the preoperative combined clinical and ECG dataset including the maximum point indicating the optimum threshold.

The 5-parent restricted K2-built traditional BN of the preoperative combined clinical and ECG data had a fitness of 0.45477, a sensitivity of 0.36, and a specificity of 0.71 using the five first-level and the seven second-level variables in the structure seen in Figure 5.32. Since this structure is built by adding nodes one-by-one in a greedy manner, it has the same nodes seen in the previous graph with several added. You can see that, again, two second-level nodes in the previous network were shifted to first-level nodes. Additionally, we continue to the see many of the same features that we have seen in the

clinical and ECG dataset's K2-built networks which is expected since if they were superior in their individual datasets, they are likely to be superior in the combined set.

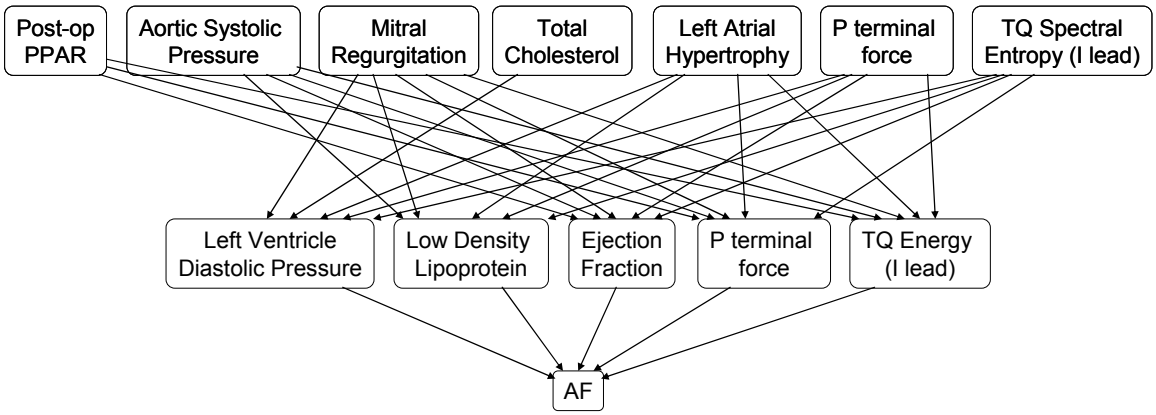

Figure 5.32 K2-built 5-parent BN with the best fitness for the preoperative combined clinical and ECG dataset.

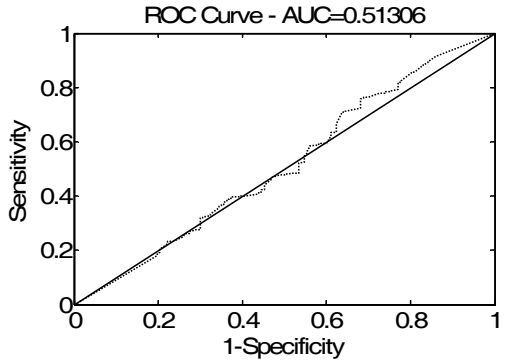

Figure 5.33 ROC curve of the preoperative combined clinical and ECG dataset's K2-built 5-parent BN.

Figure 5.33 shows the ROC of this classifier, making it a poor risk stratifier (AUC = 0.51). The sensitivity/specificity product plot, shown in Figure 5.34, shows the threshold value of the likelihood of AF occurrence output from the traditional K2-built BN found to

best separate the classes, 0.59545. There does not appear to be a good separation of the two classes of data and the sensitivity/specificity product maximum is a fairly low value. This reinforces that fact that this is a poor classifier.

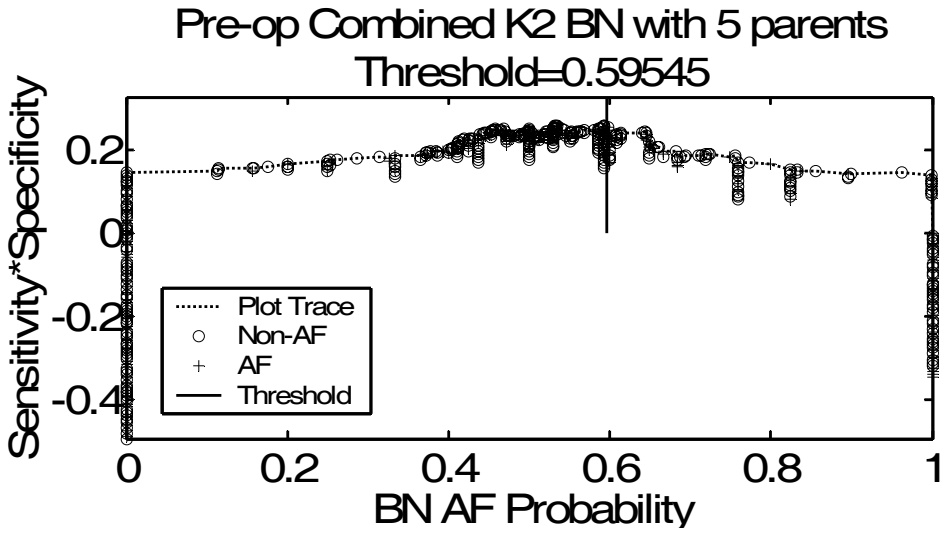

Figure 5.34 Product of the sensitivity and specificity of the K2-built 5-parent BN output of the preoperative combined clinical and ECG dataset including the maximum point indicating the optimum threshold.

5.3.1.3.3 GA Built Traditional Bayesian Network

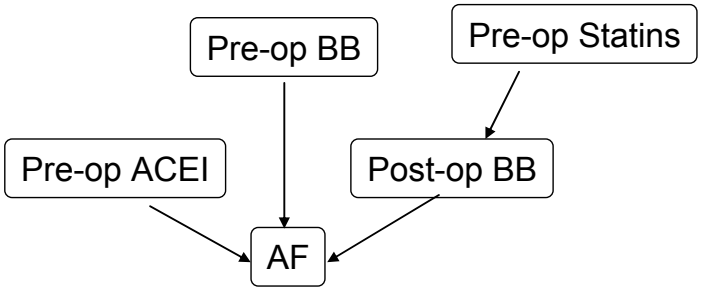

Figure 5.35 Traditional BN with the best fitness for the preoperative combined clinical and ECG dataset.

The GA built traditional BN of the preoperative combined clinical and ECG data took 52 generations to find a classifier with a fitness of 0.6056, a sensitivity of 0.61, and a specificity of 0.58 using the three first-level and one second-level variables in the structure seen in Figure 5.35. This is an interesting combination of features as none of these have been identified in the previous univariate or multivariate analyses. It is also interesting that all of these nodes are based on the administration of medication.

It may be surprising to see postoperative β-blocker (BB) as a predictor in a "preoperative" risk stratification system, but keep in mind that the label of pre- or postoperative classifiers identifies what the data collection was most focused on. In both of these datasets, important predictors were including without regard to pre- or postoperative status (*i.e.* pre- and post-op BB, etc.).

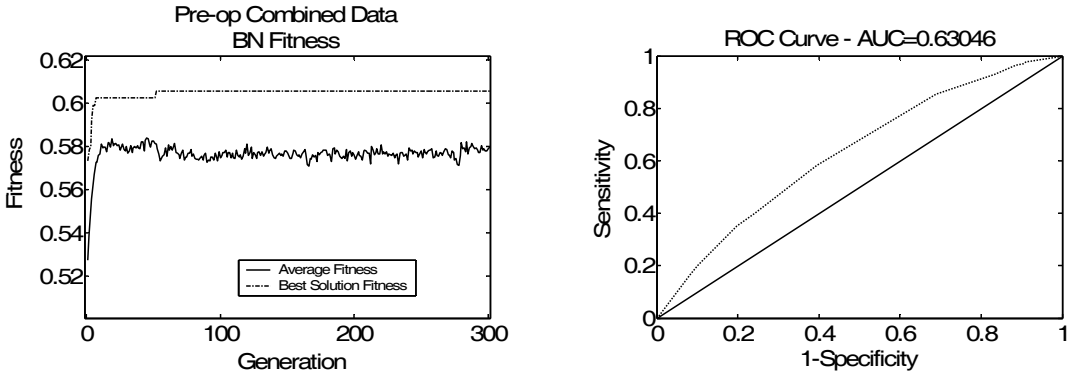

Figure 5.36 Evolutionary fitness plot and ROC curve of the preoperative combined clinical and ECG dataset's traditional BN.

Figure 5.36 shows the evolution of the classifier with the fitness of the best individual as well as the average fitness of the population. There seems to be good mixing showing that the evolving population was not too closely tied to the fittest individual.

Figure 5.36 shows the ROC of this classifier, making it a poor risk stratifier (AUC = 0.63). The sensitivity/specificity product plot, shown in Figure 5.37, shows the threshold value of the likelihood of AF occurrence output from the GA built traditional BN found to best separate the classes, 0.25263. There does not appear to be a good separation of the two classes of data and the sensitivity/specificity product maximum is a fairly low value. This reinforces that fact that this is a poor classifier.

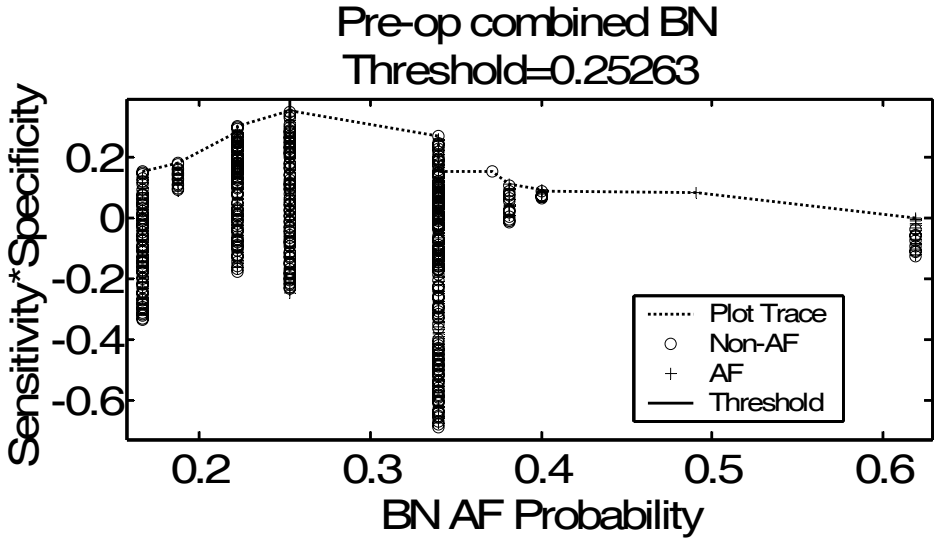

Figure 5.37 Product of the sensitivity and specificity of the traditional BN output of the preoperative combined clinical and ECG dataset including the maximum point indicating the optimum threshold.

5.3.2 Postoperative Risk Stratifiers

5.3.2.1 Clinical Dataset

5.3.2.1.1 Naïve BN

The naïve BN of the postoperative clinical data took 24 generations to find a classifier with a fitness of 0.91976, a sensitivity of 0.89, and a specificity of 0.91 using the five variables in the structure seen in Figure 5.38. Notice that mitral regurgitation was also seen as a significant variable in chapter three preoperative univariate analysis. Additionally, preoperative P wave duration on lead II and β-blocker administration were found to be important variables as we have seen other researchers did in chapter two.

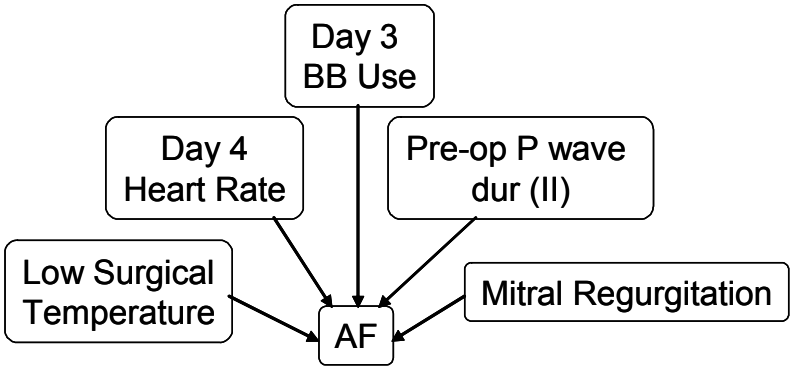

Figure 5.38 Naïve BN with the best fitness for the postoperative clinical dataset.

Figure 5.39 shows the evolution of the classifier with the fitness of the best individual as well as the average fitness of the population. There seems to be good mixing showing that the evolving population was not too closely tied to the fittest individual.

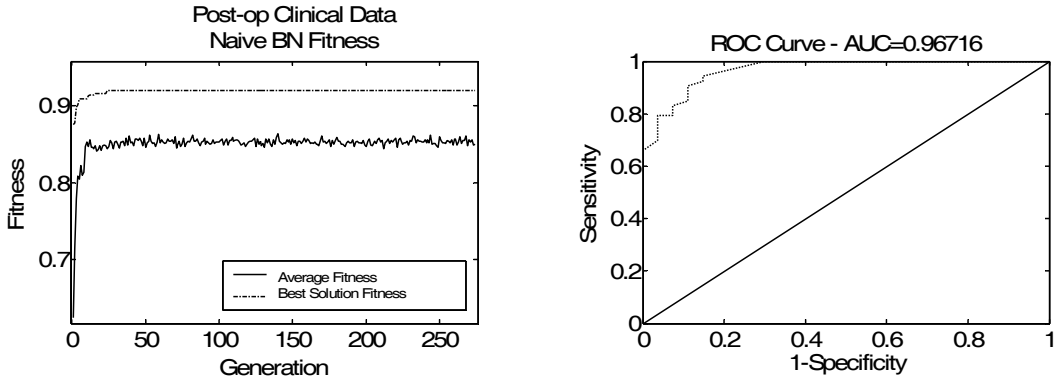

Figure 5.39 Evolutionary fitness plot and ROC curve of the postoperative clinical dataset's naive BN.

Figure 5.39 shows the ROC of this classifier, making it an excellent risk stratifier (AUC = 0.97). The sensitivity/specificity product plot, shown in Figure 5.40, shows the threshold value of the likelihood of AF occurrence output from the naïve BN found to best separate the classes, 0.042453. One can see that the AF patients tend to have values above this threshold while non-AF patients tend to be under this value. The very tall and relatively narrow peak of the sensitivity/specificity product curve shows how well this classifier separates as well as orders the output predictions.

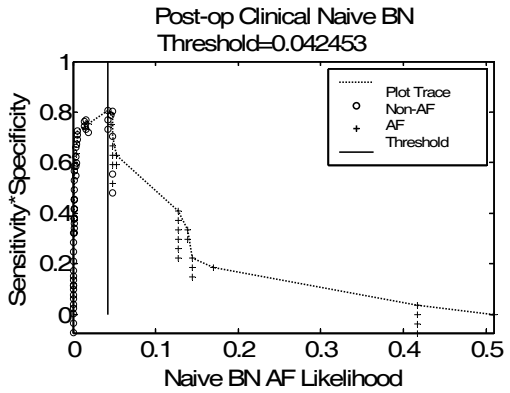

Figure 5.40 Product of the sensitivity and specificity of the naïve BN output of the postoperative clinical dataset including the maximum point indicating the optimum threshold.

5.3.2.1.2 K2-built Traditional Bayesian Network

The 3-parent restricted K2-built traditional BN of the postoperative clinical data had a fitness of 0.4803, a sensitivity of zero, and a specificity of one using the two first-level and the two second-level variables in the structure seen in Figure 5.41.

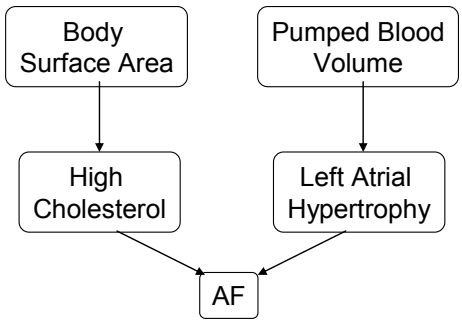

Figure 5.41 K2-built 3-parent BN with the best fitness for the postoperative clinical dataset.

Figure 5.42 shows the ROC of this classifier, making it an extremely poor risk stratifier (AUC = 0.50). The sensitivity/specificity product plot depicted in Figure 5.42 shows that all of the patients have a zero probability of AF. Obviously this is not a suitable classifier to stratify risk of these patients.

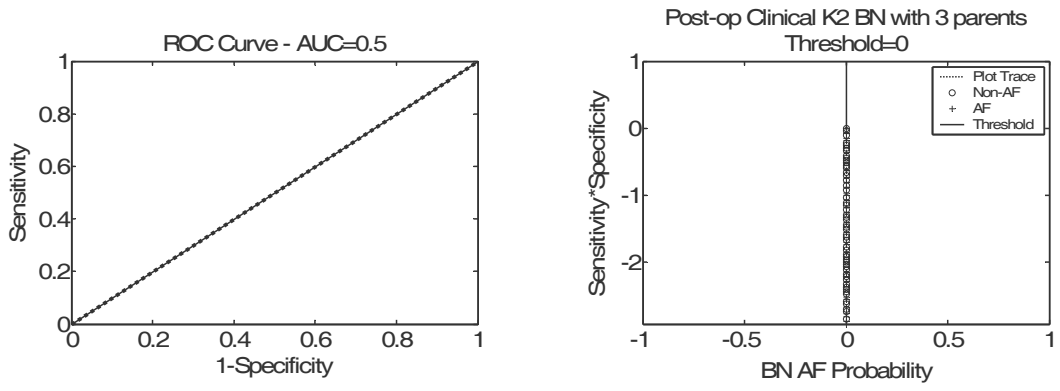

Figure 5.42 ROC curve and the product of the sensitivity and specificity of the K2-built 3-parent BN output of the postoperative clinical dataset including the maximum point indicating the optimum threshold.

The 5-parent restricted K2-built traditional BN has the same results as the previous 3-parent K2-built network. Figure 5.43 shows the ROC of this classifier and the sensitivity/specificity product plot.

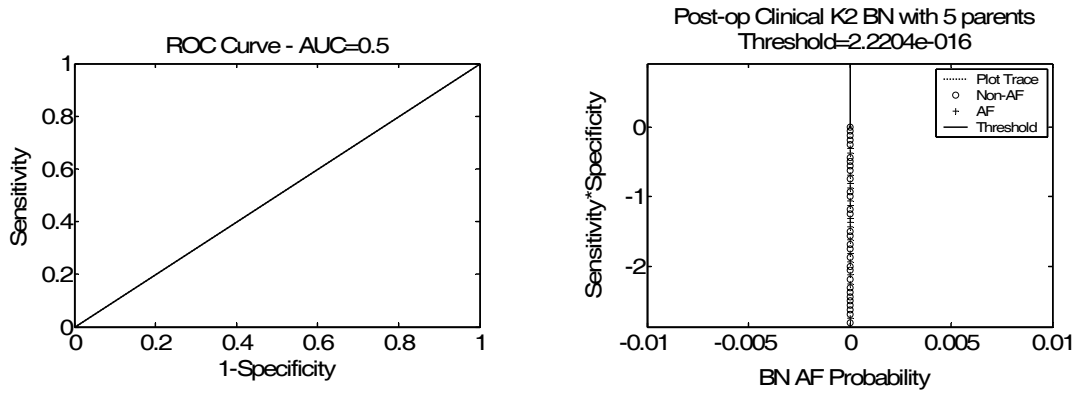

Figure 5.43 ROC curve and product of the sensitivity and specificity of the K2-built 5-parent BN output of the postoperative clinical dataset including the maximum point indicating the optimum threshold.

5.3.2.1.3 GA Built Traditional Bayesian Network

The GA built traditional BN of the postoperative clinical data took 23 generations to find a classifier with a fitness of 0.8955, a sensitivity of 0.85, and a specificity of 0.92 using the three first-level and one second-level variables in the structure seen in Figure 5.44. We see that the number of bypassed vessels was selected as a predictive variable which is directly related to the length and complexity of the surgery. Also, the patient's heart rate as the come into the ICU as well as the heart rate on the third post-surgical day is important. This variable seems to be less desirable though since some patients would develop AF before day three.

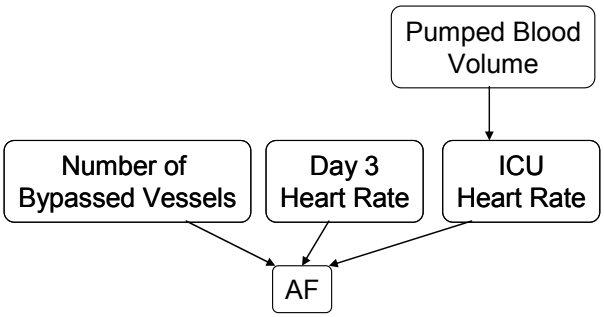

Figure 5.44 Traditional BN with the best fitness for the postoperative clinical dataset.

Figure 5.45 shows the evolution of the classifier with the fitness of the best individual as well as the average fitness of the population. There seems to be good mixing after finding the best solution not long after initialization.

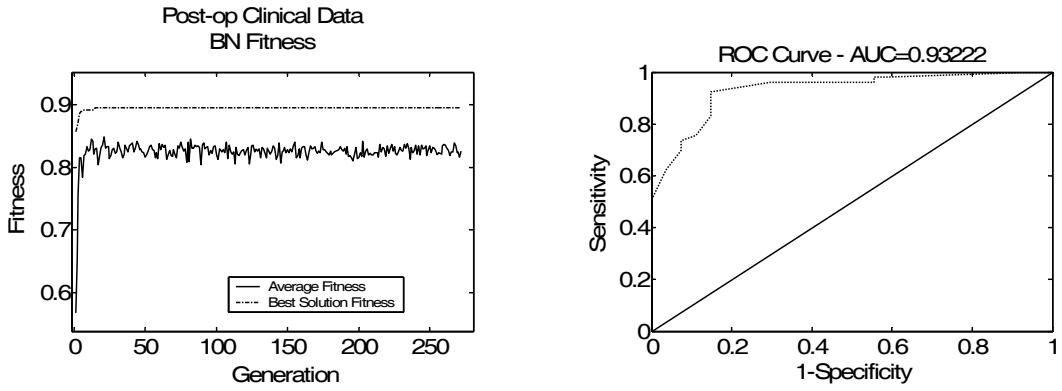

Figure 5.45 Evolutionary fitness plot ad ROC curve of the postoperative clinical dataset's traditional BN.

Figure 5.45 shows the ROC of this classifier, making it a very good risk stratifier (AUC = 0.93). The sensitivity/specificity product plot, shown in Figure 5.46, shows the threshold value of the likelihood of AF occurrence output from the GA built traditional BN found

to best separate the classes, 0.4444. One can see that the AF patients tend to have values above this threshold while non-AF patients tend to be under this value. The very tall peak of the sensitivity/specificity product curve shows how well this classifier separates as well as orders the output predictions.

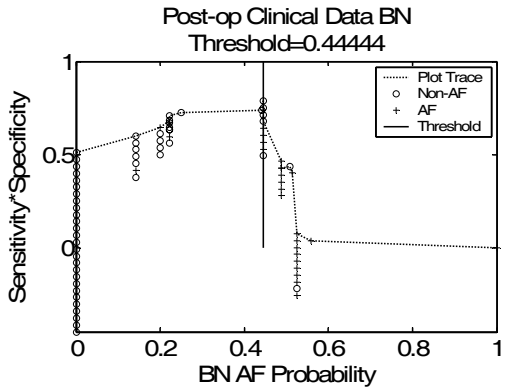

Figure 5.46 Product of the sensitivity and specificity of the traditional BN output of the postoperative clinical dataset including the maximum point indicating the optimum threshold.

5.3.2.2 ECG Feature Dataset

5.3.2.2.1 Naïve Bayesian Network

The naïve BN of the postoperative ECG data took 42 generations to find a classifier with a fitness of 0.94359, a sensitivity of 1, and a specificity of 0.90 using the four variables in the structure seen in Figure 5.47. These features are evenly distributed throughout the 36 hours following surgery as well as using the PR and RP segments of the ECG equally.

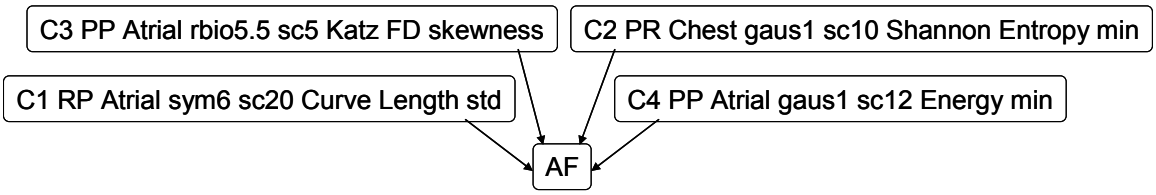

Figure 5.47 Naïve BN with the best fitness for the postoperative ECG dataset.

Figure 5.48 shows the evolution of the classifier with the fitness of the best individual as well as the average fitness of the population. There seems to be good mixing and a steady increase in average and the best individual's fitness

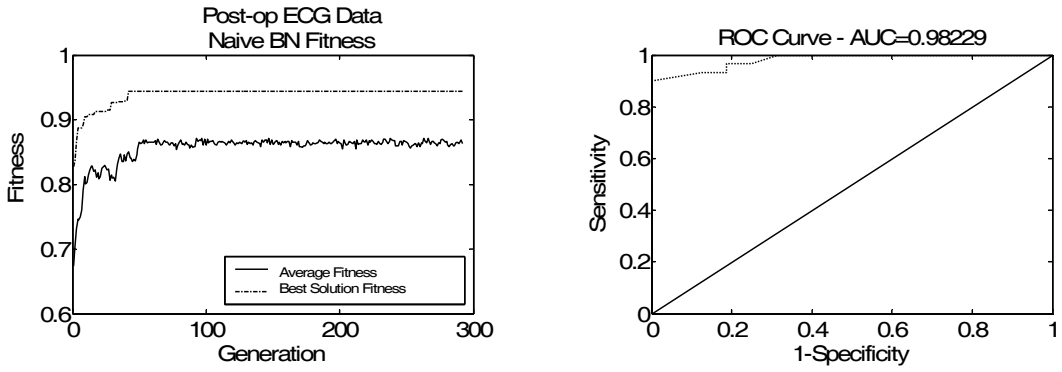

Figure 5.48 Evolutionary fitness plot and ROC curve of the postoperative ECG dataset's naive BN.

Figure 5.48 shows the ROC of this classifier, making it an excellent risk stratifier (AUC = 0.98). The sensitivity/specificity product plot, shown in Figure 5.49, shows the threshold value of the likelihood of AF occurrence output from the naïve BN found to best separate the classes, 0.07098. While it is difficult to discern the individuals in the plot, one can see that the AF patients tend to have values above this threshold while non-

AF patients tend to be under this value. Again, the peak is tall and narrow showing excellent classification and ordering.

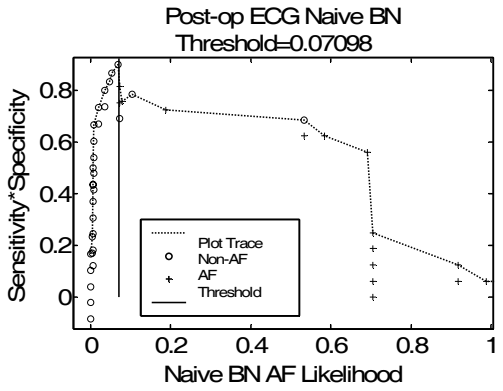

Figure 5.49 Product of the sensitivity and specificity of the naïve BN output of the postoperative ECG dataset including the maximum point indicating the optimum threshold.

5.3.2.2.2 K2-built Traditional Bayesian Network

The 3-parent restricted K2-built traditional BN of the postoperative ECG data had a fitness of 0.46532, a sensitivity of 0.19, and a specificity of 0.83 using the three first-level and the five second-level variables in the structure seen in Figure 5.50. None of these features appear as significant in chapter three or four. An interesting similarity between them all is that they are all derived from the PR segment of the electrogram signals. This is the segment that contains the P wave which corresponds to the atrial contraction.

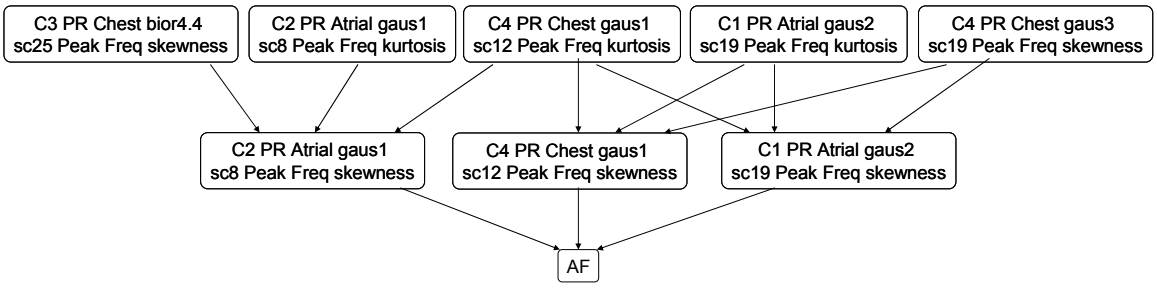

Figure 5.50 K2-built 3-parent BN with the best fitness for the postoperative ECG dataset.

Figure 5.51 shows the ROC of this classifier, making it an extremely poor risk stratifier (AUC = 0.51). The sensitivity/specificity product plot, shown in Figure 5.52, shows that almost all of the patients have a zero probability of AF. Obviously this is not a suitable classifier to stratify risk of these patients

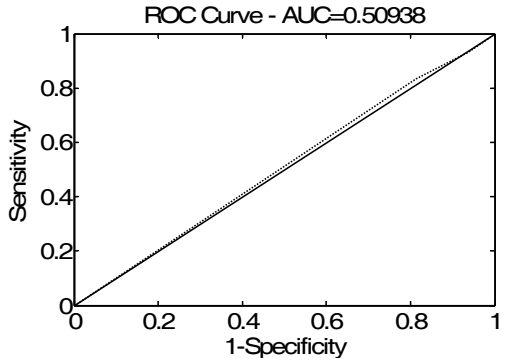

Figure 5.51 ROC curve of the postoperative ECG dataset's K2-built 3-parent BN.

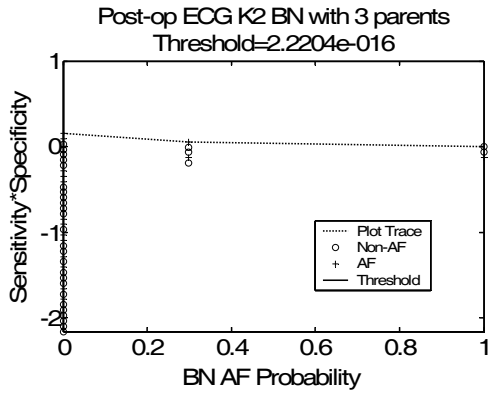

Figure 5.52 Product of the sensitivity and specificity of the K2-built 3-parent BN output of the postoperative ECG dataset including the maximum point indicating the optimum threshold.

5.3.2.2.3 GA Built Traditional Bayesian Network

The GA built traditional BN of the postoperative ECG data took 203 generations to find a classifier with a fitness of 0.9496, a sensitivity of 0.94, and a specificity of 0.93 using the three first-level and one second-level variables in the structure seen in Figure 5.53. Again, none of these variables are in the univariate or the multivariate classifiers found in chapters three and four. It is interesting that all of the features are calculated from the atrial electrogram lead.

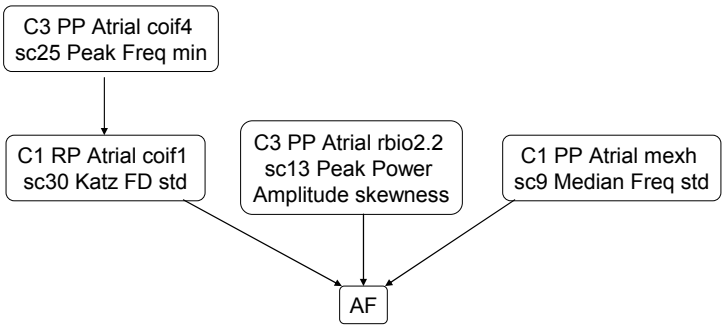

Figure 5.53 Traditional BN with the best fitness for the postoperative ECG dataset.

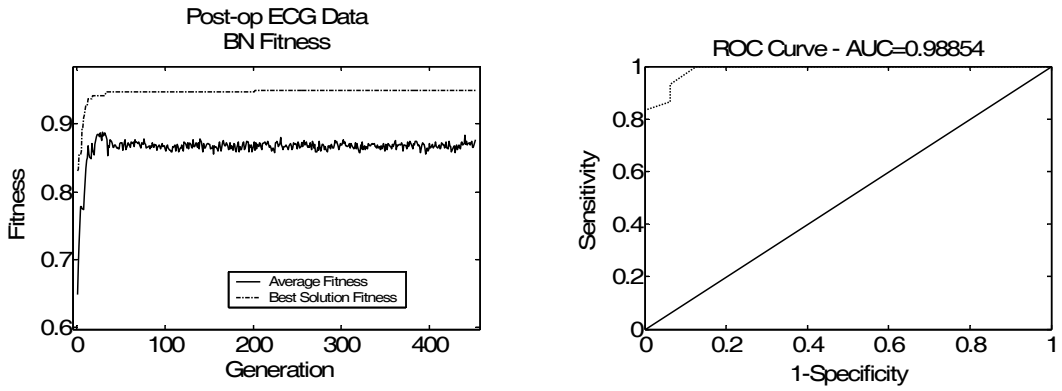

Figure 5.54 Evolutionary fitness plot and ROC curve of the postoperative ECG dataset's traditional BN.

Figure 5.54 shows the evolution of the classifier with the fitness of the best individual as well as the average fitness of the population. There seems to be good mixing showing that the evolving population was not too closely tied to the fittest individual.

Figure 5.54 shows the ROC of this classifier, making it an excellent risk stratifier (AUC = 0.99). The sensitivity/specificity product plot, shown in Figure 5.55, shows the threshold value of the likelihood of AF occurrence output from the GA built traditional BN found to best separate the classes, 0.5. One can see that the AF patients tend to have values above this threshold while non-AF patients tend to be under this value. The very

tall peak of the sensitivity/specificity product curve shows how well this classifier separates as well as orders the output predictions.

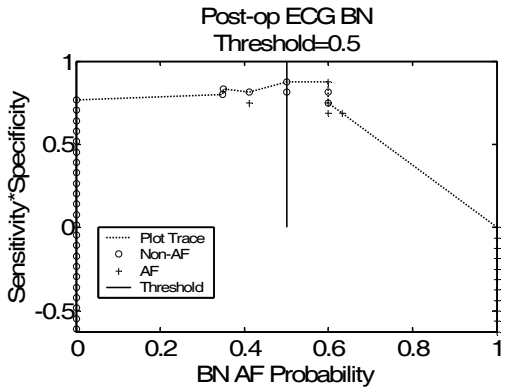

Figure 5.55 Product of the sensitivity and specificity of the traditional BN output of the postoperative ECG dataset including the maximum point indicating the optimum threshold.

5.3.2.3 Clinical and ECG Combined Dataset

5.3.2.3.1 Naïve Bayesian Network

The naïve BN of the postoperative combined clinical and ECG data took 297 generations to find a classifier with a fitness of 0.93063, a sensitivity of 0.96, and a specificity of 0.83 using the three variables in the structure seen in Figure 5.56. Again, the heart rate on day four seems to be a good feature for risk stratification as it was used in the clinical dataset. This is a poor feature to use for early risk stratification though. The other features do not appear significant in earlier analyses.

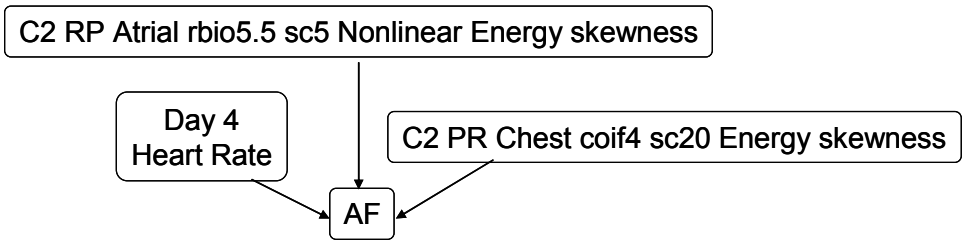

Figure 5.56 Naïve BN with the best fitness for the postoperative combined clinical and ECG dataset.

Figure 5.57 shows the evolution of the classifier with the fitness of the best individual as well as the average fitness of the population. There seems to be good mixing showing that the evolving population was not too closely tied to the fittest individual. Notice the large jump in the average population fitness that occurred around generation number 110. This indicates the possible addition of a feature with a surrounding feature space of greatly increased fitness. As the individual spun off new individuals, many of the new individuals were significantly more fit in this new feature space compared to those that were spun off the previous best individual.

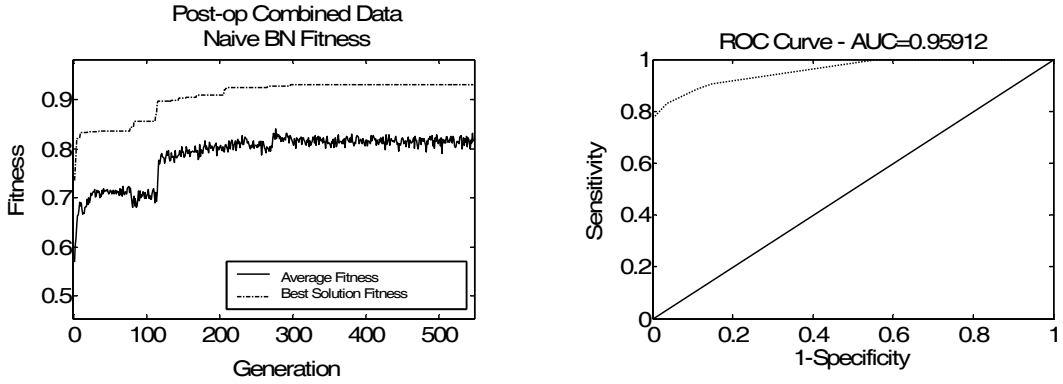

Figure 5.57 Evolutionary fitness plot and ROC curve of the postoperative combined clinical and ECG dataset's naive BN.

Figure 5.57 shows the ROC of this classifier, making it an excellent risk stratifier (AUC = 0.96). The sensitivity/specificity product plot, Figure 5.58, shows the threshold value of the likelihood of AF occurrence output from the naïve BN found to best separate the classes, 0.018825. One can see that the AF patients tend to have values above this threshold while non-AF patients tend to be under this value. As you can see, the peak is not as narrow as other sensitivity/specificity product plots relating to the fact that the classification ordering is not as good as in more narrow classifiers' plots.

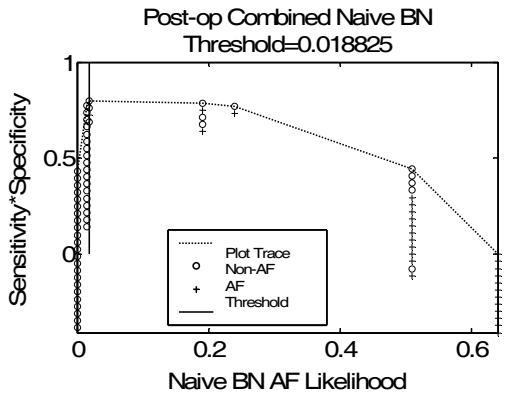

Figure 5.58 Product of the sensitivity and specificity of the naïve BN output of the postoperative combined clinical and ECG dataset including the maximum point indicating the optimum threshold.

5.3.2.3.2 K2-built Traditional Bayesian Network

The 3-parent restricted K2-built traditional BN of the postoperative combined clinical and ECG data had a fitness of 0.4803, a sensitivity of zero, and a specificity of one using the two first-level and the two second-level variables in the structure seen in Figure 5.59.

This network is almost exactly the same network built for clinical dataset with the exchange of one ECG feature for a clinical feature.

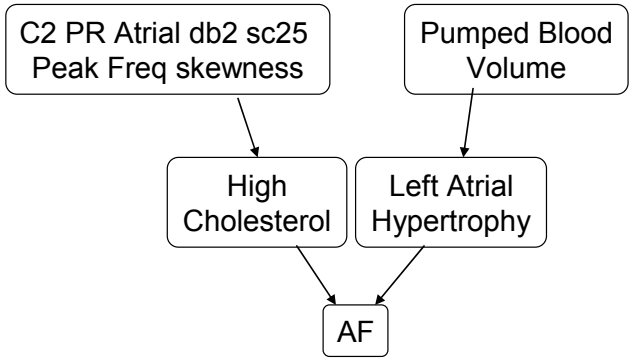

Figure 5.59 K2-built 3-parent BN with the best fitness for the postoperative combined clinical and ECG dataset.

Unfortunately, the result of this classifier is very similar to the clinical dataset's result. Figure 5.60 shows the ROC of this classifier, making it an extremely poor risk stratifier (AUC = 0.50). The sensitivity/specificity product plot, shown in Figure 5.60, shows that all of the patients have a zero probability of AF. Obviously this is not a suitable classifier to stratify risk of these patients. Since the 3-parent network reached the maximum score before reaching the three allowed parents, there is no reason to test a 5-parent K2-built network because it will stop with the same network.

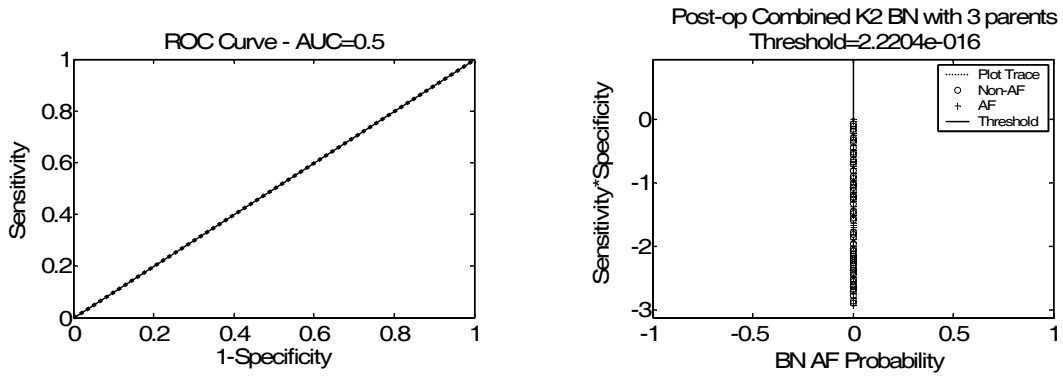

Figure 5.60 ROC curve and the product of the sensitivity and specificity of the K2-built 3-parent BN output of the postoperative combined clinical and ECG dataset including the maximum point indicating the optimum threshold.

5.3.2.3.3 GA Built Traditional Bayesian Network

The GA built traditional BN of the postoperative combined clinical and ECG data took 13 generations to find a classifier with a fitness of 0.7092, a sensitivity of 0.41, and a specificity of 0.89 using the three first-level and one second-level variables in the structure seen in Figure 5.61. We see that the time between the R peaks immediately as the patient is coming out of surgery seems to be of significant importance in this classifier.

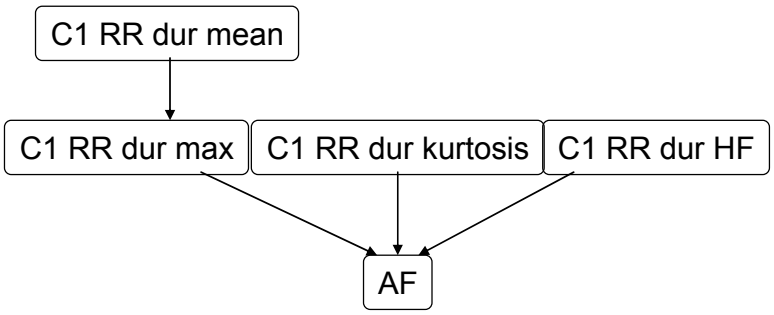

Figure 5.61 Traditional BN with the best fitness for the postoperative combined clinical and ECG dataset.

Figure 5.62 shows the evolution of the classifier with the fitness of the best individual as well as the average fitness of the population. There seems to be good mixing showing that the evolving population was not too closely tied to the fittest individual.

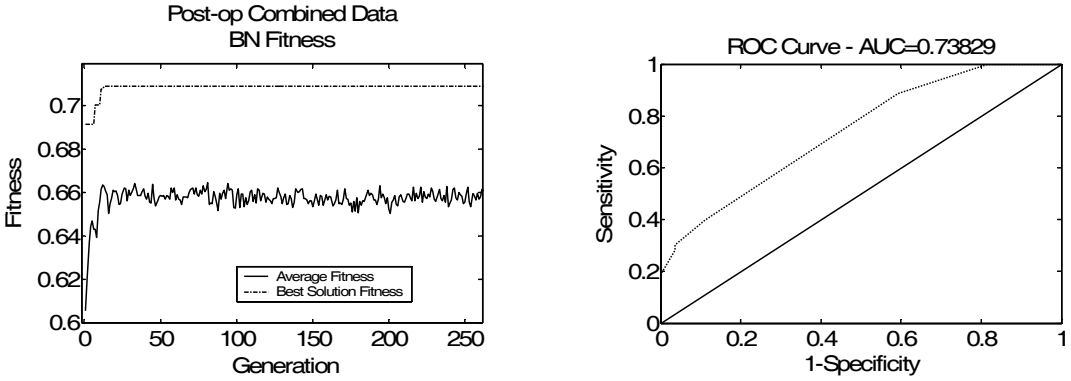

Figure 5.62 Evolutionary fitness plot of the postoperative combined clinical and ECG dataset's traditional BN.

Figure 5.62 shows the ROC of this classifier, making it a fair to good risk stratifier (AUC = 0.74). The sensitivity/specificity product plot, shown in Figure 5.63, shows the threshold value of the likelihood of AF occurrence output from the GA built traditional

BN found to best separate the classes, 0.49797. One can see that the AF patients tend to have values above this threshold while non-AF patients tend to be under this value.

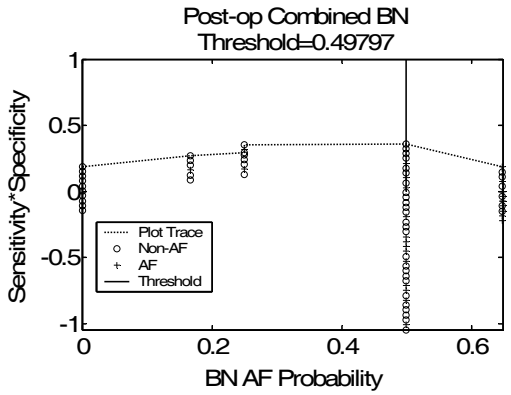

Figure 5.63 Product of the sensitivity and specificity of the traditional BN output of the postoperative combined clinical and ECG dataset including the maximum point indicating the optimum threshold.

5.4 Validation

In order to see how well these systems continue to perform when not trained and tested on the same points, we again performed leave-one-out (LOO) validation as performed in chapter four. This was limited to the GA built naïve and tradition BNs due to the generally poor performance of the K2-built networks. A summary of these validation results is shown here in Table 5.2.

Table 5.2 Summary of validation performance of the GA built naive and traditional BNs

			Sen/Spec	*Fitness*
Preoperative	Clinical	Naïve BN	0.63/0.73	0.63609
		Traditional BN	0.61/0.71	0.56503
	ECG	Naïve BN	0.76/0.54	0.50263
		Traditional BN	0.61/0.59	0.53099
	Combined	Naïve BN	0.68/0.68	0.63389
		Traditional BN	0.13/0.59	0.48694
Postoperative	Clinical	Naïve BN	0.81/0.85	0.80213
		Traditional BN	0.37/0.89	0.55951
	ECG	Naïve BN	0.81/0.87	0.87654
		Traditional BN	1/0.93	0.94859
	Combined	Naïve BN	0.96/0.83	0.88656
		Traditional BN	0.75/0.80	0.6454

5.4.1 Preoperative Risk Stratifiers

5.4.1.1 Clinical Dataset

5.4.1.1.1 Naïve Bayesian Network

Referring back to Figure 5.3, we see that compared to Figure 5.64, the AUC has dropped from 0.74 to 0.67 but many of the significant points along the curve continue to remain in the same location while the overall curve has become more of a stair-step pattern. This tells us that the new training data actually spread the points out in the prediction-output probability space so that all the points are no longer landing at many of the same AF prediction probability. This is seen to be true in the sensitivity/specificity product plots by comparing Figure 5.65 to Figure 5.4.

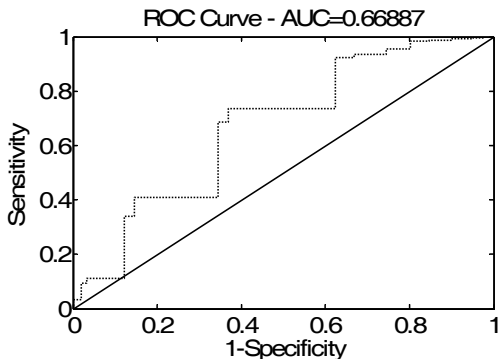

Figure 5.64 ROC curve of the preoperative clinical dataset's validation of the naive BN.

Figure 5.65 has quite a few new probability values which the patients posses, though many still fall in the zero probability region.

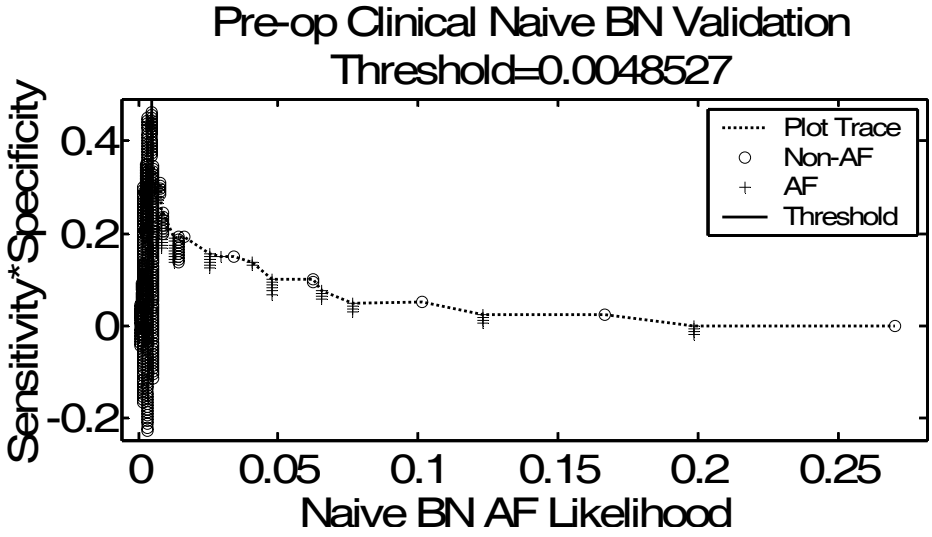

Figure 5.65 Product of the sensitivity and specificity of the validation of the naive BN output of the preoperative clinical dataset including the maximum point indicating the optimum threshold.

5.4.1.1.2 GA Built Traditional Bayesian Network

Referring back to Figure 5.12, we see that compared to Figure 5.66, the AUC of the validation of this network has dropped from 0.71 to 0.59 but again, many of the significant points along the curve remain in the same location. When retraining the BN's probability tables for every patient tested using different training points, the probability values in this table change slightly in every cell. These slight changes result in a slightly more diverse set of probability outcomes as we see in comparing Figure 5.67 to Figure 5.13. You can see that there are now thirteen different outcome probabilities where there were previously eleven.

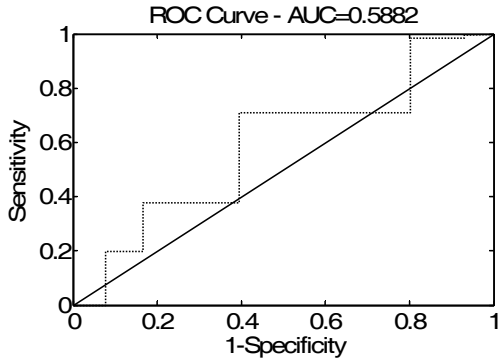

Figure 5.66 ROC curve of the preoperative clinical dataset's validation of the traditional BN.

We also observe another interesting trait of these new possible predictive probability outcomes: the AF and the non-AF patients actually separate into their own classes on either side of the probability value that they previously held together in Figure 5.13. This results from the removal of the single patient from the training of the probability tables.

Here we see that the removal of a single AF patient caused the other values to move slightly left while the removal of a non-AF patient caused the non-AF patient's probability values to move slightly right. This is an example to an issue with leave-one-out validation we discussed in chapter four [96]. This phenomenon will be a common trait in many of our LOO validation results but these results still show the classifier's ability to separate the classes based on a single threshold by using sensitivity and specificity.

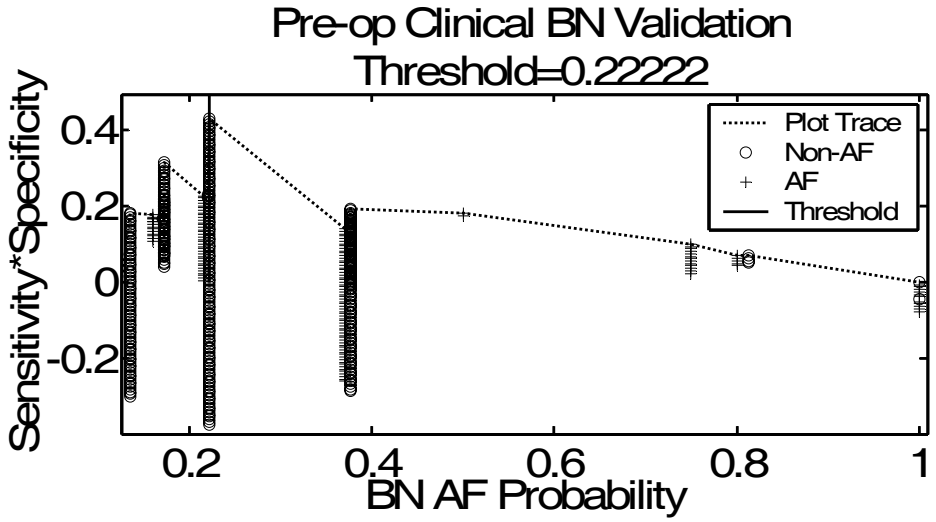

Figure 5.67 Product of the sensitivity and specificity of the validation of the traditional BN output of the preoperative clinical dataset including the maximum point indicating the optimum threshold.

5.4.1.2 ECG Feature Dataset

5.4.1.2.1 Naïve Bayesian Network

Referring back to Figure 5.15, we see that compared to Figure 5.68, the AUC has dropped from 0.64 to 0.53 but, again, the significant points along the curve remain in the same location and the stair-step pattern appears. The separation of the classes from individual probability values are seen again in the sensitivity/specificity product plot, Figure 5.69. Much of the change in AUC can be attributed to all the patients of both classes that previously had a probability of 0.5 causing a diagonal line on the right side of AUC curve to the top right corner. When LOO validation was performed, it moved the probability values as we discussed previously causing the diagonal line of the sensitivity/specificity product plot to turn into a stair step that dropped the area under the curve significantly.

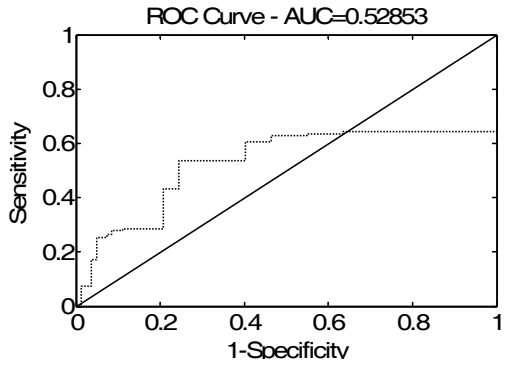

Figure 5.68 ROC curve of the preoperative ECG dataset's validation of the naive BN.

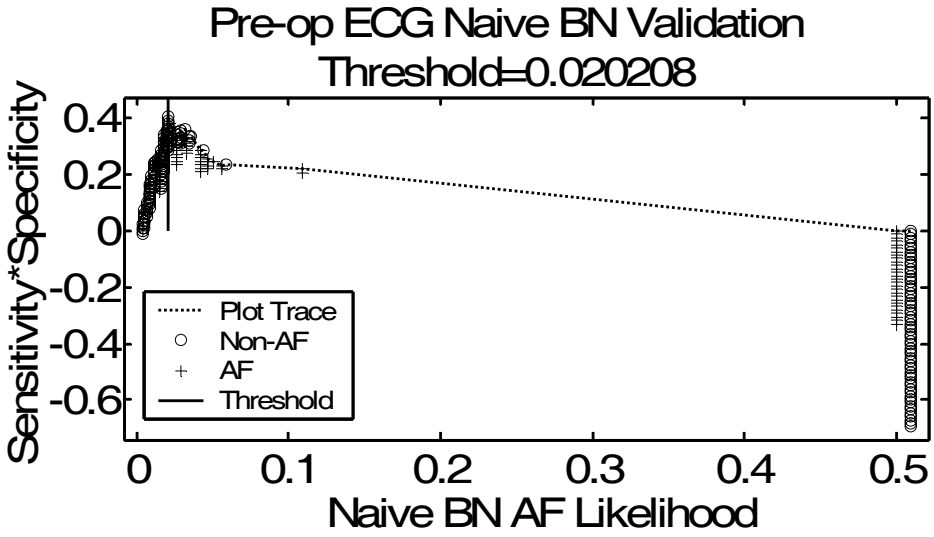

Figure 5.69 Product of the sensitivity and specificity of the validation of the naive BN output of the preoperative ECG dataset including the maximum point indicating the optimum threshold.

5.4.1.2.2 GA Built Traditional Bayesian Network

Referring back to Figure 5.24, we see that compared to Figure 5.70, the AUC of the validation of this network has dropped from 0.76 to 0.55 but this time, we don't see that most of the boundary point of the curve stay in the same place. In fact, all of them have dropped reducing the AUC significantly. Looking at the two sensitivity/specificity product plots in Figure 5.25 and Figure 5.71, we see that many of the patient probability values went from clustered on 0.5 to spread across the probability axis. This drastically changed the ordering and resulted in large swing in the AUC as well as an entirely new optimum threshold. This appears to be a case of over fitting.

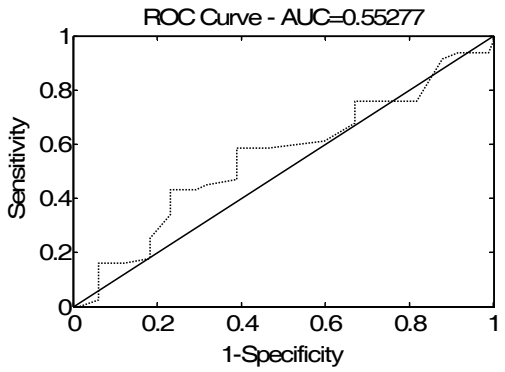

Figure 5.70 ROC curve of the preoperative ECG dataset's validation of the traditional BN.

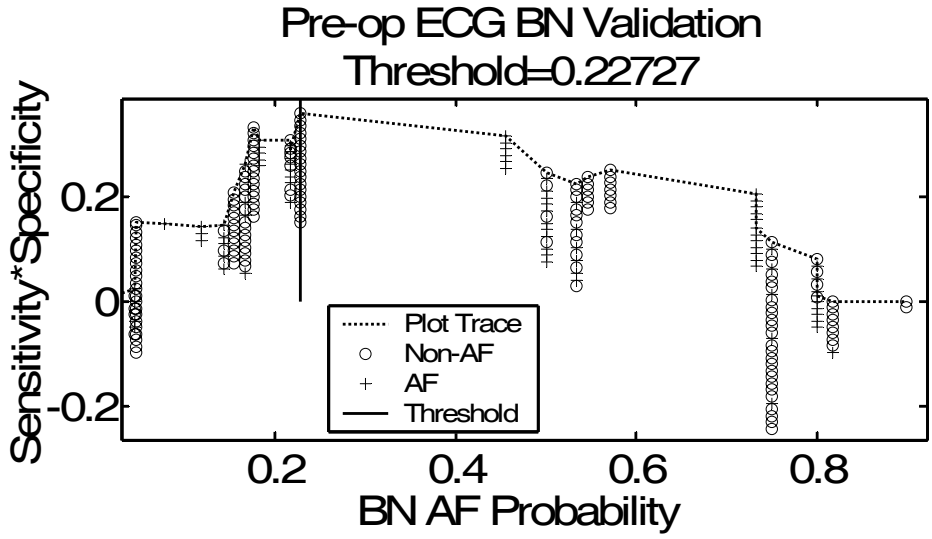

Figure 5.71 Product of the sensitivity and specificity of the validation of the traditional BN output of the preoperative ECG dataset including the maximum point indicating the optimum threshold.

5.4.1.3 Clinical and ECG Combined Dataset

5.4.1.3.1 Naïve Bayesian Network

Looking back to Figure 5.27, we see that compared to Figure 5.72, the AUC has dropped from 0.73 to 0.67 but, again, the significant points along the curve remain in the same location and the stair-step pattern appears. The separation of the classes from individual probability values are seen again in the sensitivity/specificity product plot as seen in Figure 5.73. Much of the change in AUC can be attributed to this stair step pattern, but overall this does not appear to be a case of over fitting.

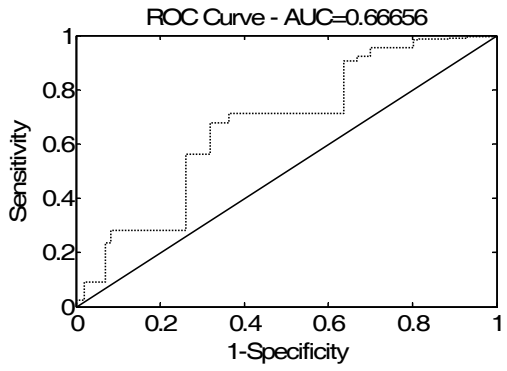

Figure 5.72 ROC curve of the preoperative combined clinical and ECG dataset's validation of the naive BN.

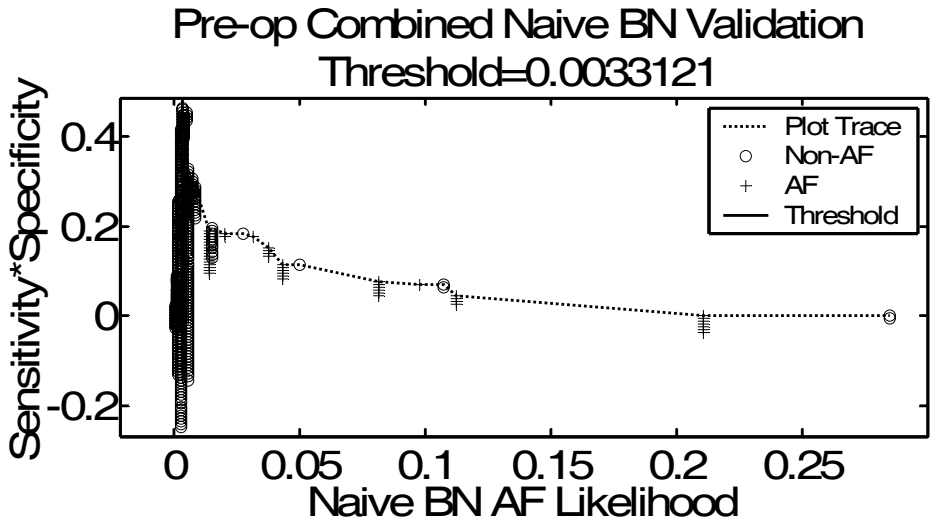

Figure 5.73 Product of the sensitivity and specificity of the validation of the naive BN output of the preoperative combined clinical and ECG dataset including the maximum point indicating the optimum threshold.

5.4.1.3.2 GA Built Traditional Bayesian Network

Observing Figure 5.36, we see that compared to Figure 5.74, the AUC of the validation of this network has dropped from 0.63 to 0.51. Again, we see similar changes in the ROC, Figure 5.74, and the sensitivity/specificity product plot, Figure 5.75, that we saw in the previously GA built traditional BN. An entirely new optimal threshold is selected and a large number of patient probabilities are now clustered around that new threshold. This, again, looks like a case of over fitting.

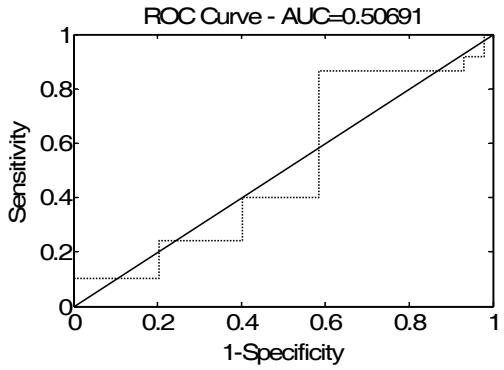

Figure 5.74 ROC curve of the preoperative combined clinical and ECG dataset's validation of the traditional BN.

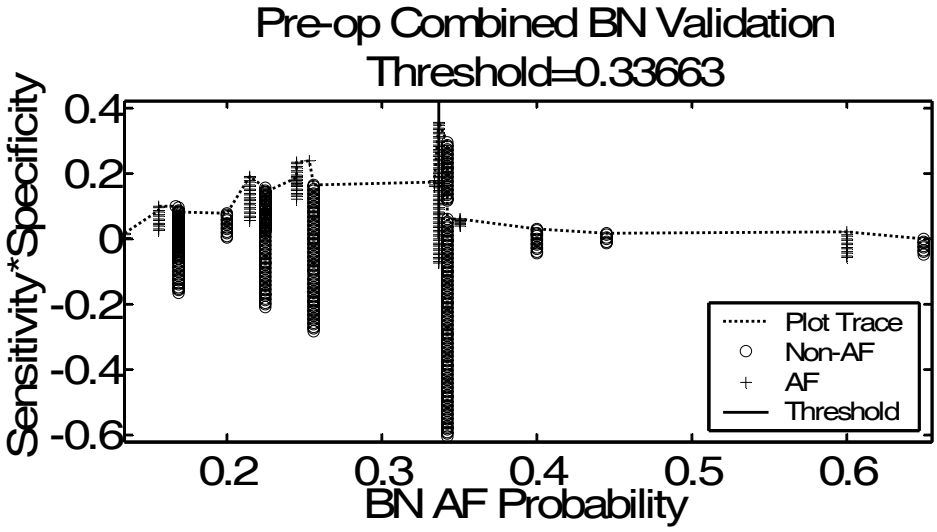

Figure 5.75 Product of the sensitivity and specificity of the validation of the traditional BN output of the preoperative combined clinical and ECG dataset including the maximum point indicating the optimum threshold.

5.4.2 Postoperative Risk Stratifiers

5.4.2.1 Clinical Dataset

5.4.2.1.1 Naïve Bayesian Network

Looking back to Figure 5.39, we see that compared to Figure 5.76, the AUC has dropped from 0.97 to 0.84 and the shape of the ROC has changed somewhat significantly. Although this may lead one to the thought of over fitting, the optimum threshold is not far from the original threshold and there continues to be good separation between the classes on the sensitivity/specificity product plot as seen in Figure 5.77. Our one worry for this entire family of postoperative classifiers is the small sample size that can be trained and tested with. This seems to give the classifiers a better chance, given a fairly large feature set, of finding better solutions. Though this can not be ignored, it should not invalidate the possibility of one of these classifiers being the solution cardiologists need.

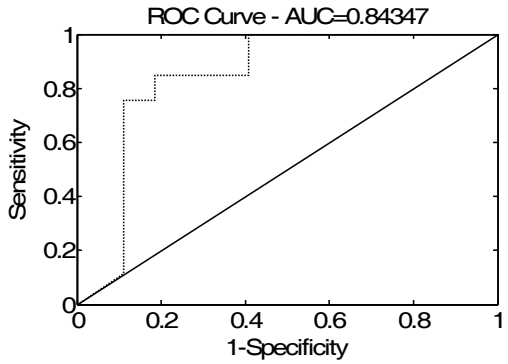

Figure 5.76 ROC curve of the postoperative clinical dataset's validation of the naive BN.

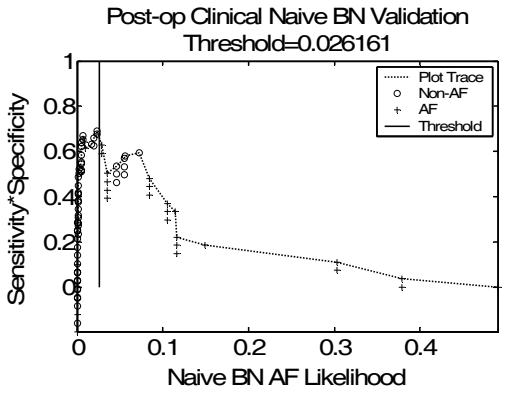

Figure 5.77 Product of the sensitivity and specificity of the validation of the naive BN output of the postoperative clinical dataset including the maximum point indicating the optimum threshold.

5.4.2.1.2 GA Built Traditional Bayesian Network

Referring back to Figure 5.45, we see that compared to Figure 5.78, the AUC of the validation of this network has dropped from 0.93 to 0.58. Again, we see similar changes in the ROC, Figure 5.78, and the sensitivity/specificity product plot, Figure 5.79, that we saw in some of the previously GA built traditional BN. Previously, there were no AF patients with probabilities of zero and now there are quite a few. This has completely changed the shape of the ROC and sensitivity/specificity product plot, all leading us to conclude that this is a case of over fitting.

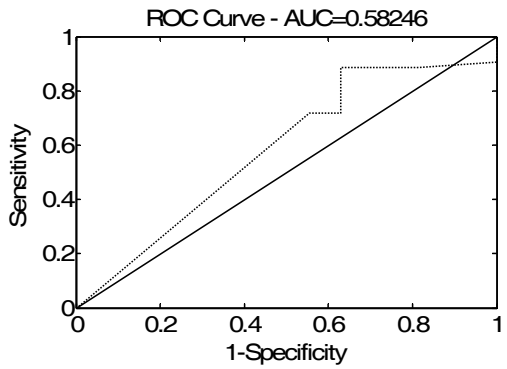

Figure 5.78 ROC curve of the postoperative clinical dataset's validation of the traditional BN.

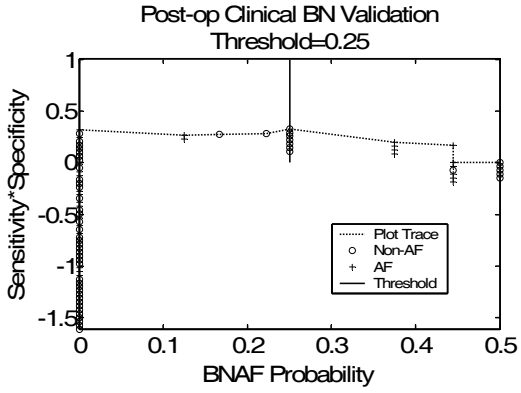

Figure 5.79 Product of the sensitivity and specificity of the validation of the traditional BN output of the postoperative clinical dataset including the maximum point indicating the optimum threshold.

5.4.2.2 ECG Feature Dataset

5.4.2.2.1 Naïve Bayesian Network

Observing Figure 5.48, we see that compared to Figure 5.80, the AUC has dropped from 0.98 to 0.91 following validation. The AUC value seems to still indicate a good classifier

and this holds true when looking at the sensitivity /specificity plot in Figure 5.81 which still shows excellent separation.

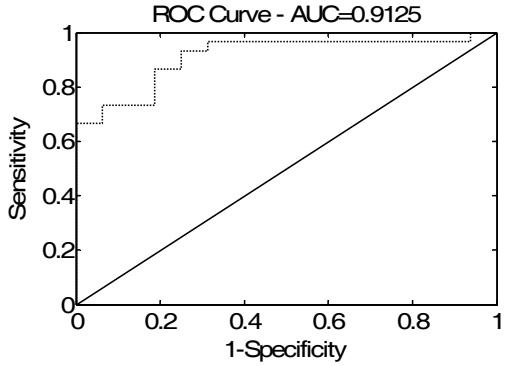

Figure 5.80 ROC curve of the postoperative ECG dataset's validation of the naive BN.

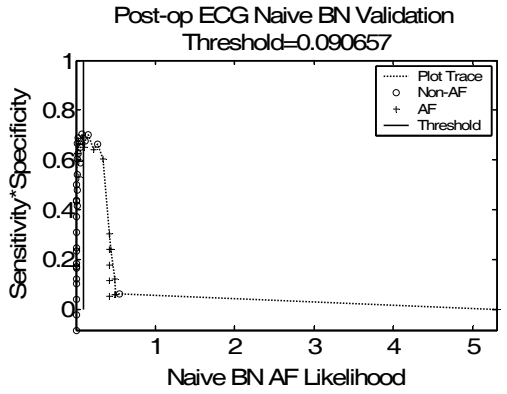

Figure 5.81 Product of the sensitivity and specificity of the validation of the naive BN output of the postoperative ECG dataset including the maximum point indicating the optimum threshold.

5.4.2.2.2 GA Built Traditional Bayesian Network

Referring back to Figure 5.54, we see that compared to Figure 5.82, the AUC of the validation of this network held constant at an almost perfect 0.99. We see small changes

in the ROC, Figure 5.82, and the sensitivity/specificity product plot, Figure 5.83, which are to be expected in any validation. There seems to be excellent separation among the classes following validation with good potential for a low/medium/high risk scale for stratification purposes. We must keep in mind though that this network was found using only 46 patients and over 111,000 features. Chances were very high that a combination of features could be found to stratify these few patients with excellent accuracy.

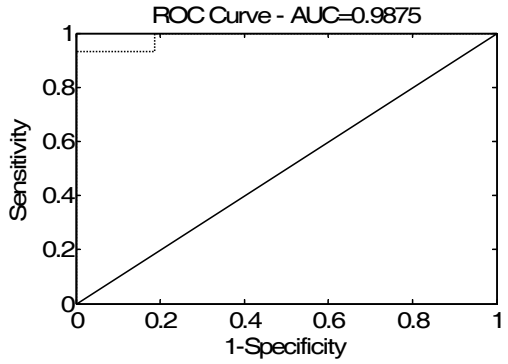

Figure 5.82 ROC curve of the postoperative ECG dataset's validation of the traditional BN.

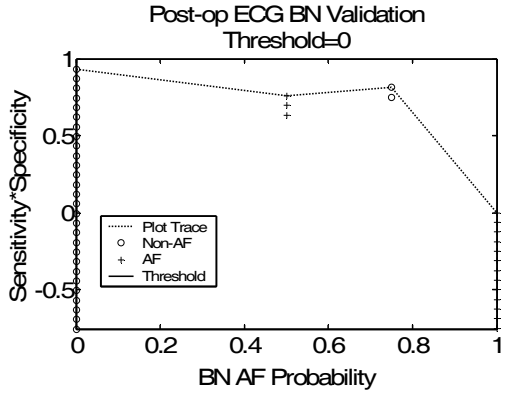

Figure 5.83 Product of the sensitivity and specificity of the validation of the traditional BN output of the postoperative ECG dataset including the maximum point indicating the optimum threshold.

5.4.2.3 Clinical and ECG Combined Dataset

5.4.2.3.1 Naïve Bayesian Network

Comparing Figure 5.57 and Figure 5.84, we see that compared to Figure 5.84, the AUC has dropped from 0.96 to 0.91 following validation. The AUC value seems to still indicate a good classifier and this holds true when looking at the sensitivity /specificity plot in Figure 5.85 which still shows excellent separation.

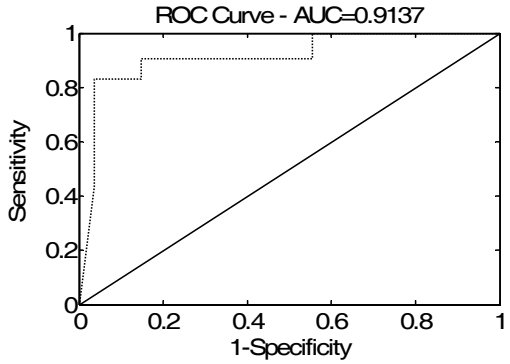

Figure 5.84 ROC curve of the postoperative combined clinical and ECG dataset's validation of the naive BN.

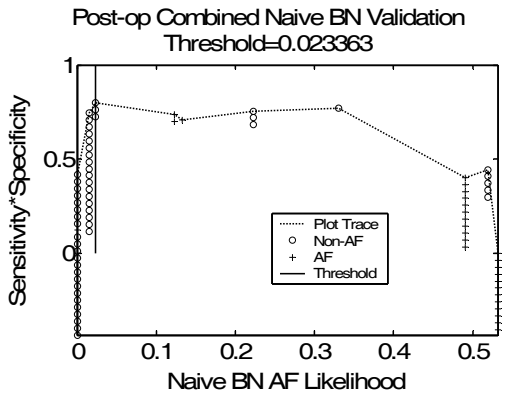

Figure 5.85 Product of the sensitivity and specificity of the validation of the naive BN output of the postoperative combined clinical and ECG dataset including the maximum point indicating the optimum threshold.

5.4.2.3.2 GA Built Traditional Bayesian Network

When comparing Figure 5.62 to Figure 5.86, we see that the AUC has dropped from 0.74 to 0.67 following validation. We see significant changes in the ROC and the sensitivity/specificity product plot, Figure 5.87. There seems to be fair separation among the classes following validation but the large changes in the curves and positions of the patients on the probability axis makes it possibly over fit causing generalization issues. Only a larger dataset could allow investigation of this.

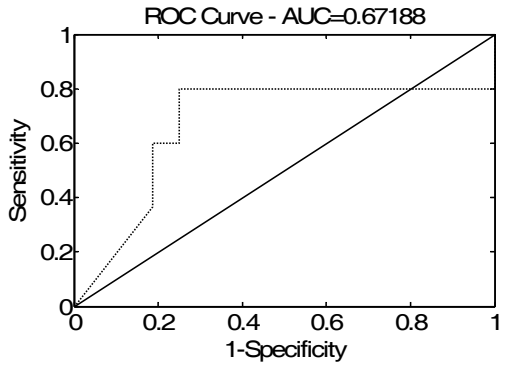

Figure 5.86 ROC curve of the postoperative combined clinical and ECG dataset's validation of the traditional BN.

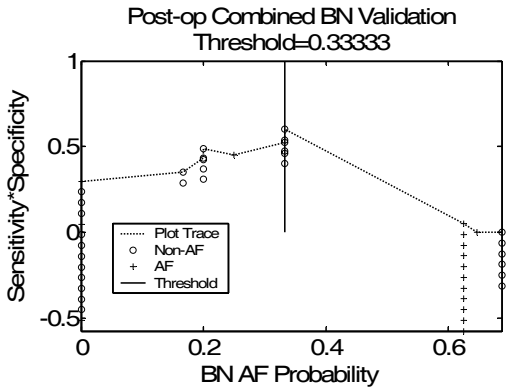

Figure 5.87 Product of the sensitivity and specificity of the validation of the traditional BN output of the postoperative combined clinical and ECG dataset including the maximum point indicating the optimum threshold.

5.5 Discussion

We can see by the results summarized in Table 5.1 that the greedy K2-built traditional BNs do not perform well when compared to genetically evolved BNs. In all cases except one, the preoperative ECG dataset, the K2-built BNs were the worst tested. This is an interesting finding, since both the 3-parent K2 BNs and the traditional BN use the same

probability table computations and the same number of first-level nodes, yet they have drastically different fitness values. This shows the importance of finding the global maximum, versus greedily adding nodes in building a BN, given medical data with missing data points. Additionally, the 5-parent K2 BNs and the naïve BNs have the same number of first-level parents and it still performs worse. This shows the importance of using the independent conditional probability assumption associated with the naïve networks when using a relatively small dataset.

In finding that the K2-built BNs performed so poorly, we investigated the cause, finding that when the K2 method looked greedily for the best nodes to add, it chose nodes with mostly missing data points. Previously, we described that the K2 method required a full dataset with no missing values to build the network. When we modified it to ignore missing data points and calculate the score on the data it had, it found that by adding nodes with very little data, it maximized, possibly by chance, the Bayesian scoring criterion. For this reason, structures were built with nodes having significant missing data and poorly populated joint probability tables. Though a compensation factor could be added to the K2 scoring criterion to account for the amount of data missing, possibly a probability of missingness term, optimization of greedy BN structure building is not the focus of this work and could be investigated in future works.

Table 5.3 The winning classifiers for each of the different pre- and postoperative datasets for training and testing as well as their individual fitness.

	Preoperative		*Postoperative*	
	Training	*Testing*	*Training*	*Testing*
Clinical Dataset	Naïve BN (Fitness=0.70029)	Naïve BN (Fitness=0.63609)	Naïve BN (Fitness=0.91976)	Naïve BN (Fitness=0.80213)
ECG	Traditional BN	Traditional BN	Traditional BN	Traditional BN

Dataset	(Fitness=0.73032)	(Fitness=0.53099)	(Fitness=0.9496)	(Fitness=0.94859)
Combined Clinical and ECG Dataset	Naïve BN (Fitness=0.69438)	Naïve BN (Fitness=0.63389)	Naïve BN (Fitness=0.93063)	Naïve BN (Fitness=0.88656)

We see again that the preoperative data were not as easily handled by our classifiers as the postoperative data. Besides the fact that the operation itself would affect the patient's characteristics, this is most likely due to two characteristics of the postoperative dataset:

- the small number of patients that were collected and
- the large number of ECG features calculated.

For instance, the best performing classifier of those investigated was the GA built traditional BN performed on the postoperative ECG dataset. Though this was the best classifier by fitness value alone, the three first-level features were selected out of over 111,000 features, and it was performed on only 46 patients. This can be compared to the corresponding preoperative dataset which had 4,608 features with 244 patients. This is the most extreme case but it does illustrate that the likelihood of an excellent solution being found for the postoperative data is much higher.

Analyzing the training results in Table 5.1 and the testing/validation results in Table 5.2, which were combined into Table 5.3, seems to show that the naïve BN performs better than the GA built traditional BN for the clinical dataset and the combined clinical and ECG dataset. Meanwhile, the GA built traditional network is superior on the ECG dataset. We believe these results are largely determined by two factors:

- the BN building structure restrictions we imposed and
- missing data in the datasets.

The naïve BN was allowed up to five first-level parents, since the naïve conditional independence assumption relaxed the amount of data needed to populate probability tables. Remember, the amount of data required to populate the probability tables rises exponentially as the number of parents in a traditional BN increases. Therefore, for the traditional BN, the maximum number of first-level parents allowed was three versus five, due to the dataset size. With an extra two possible variables, this gives the naïve BN two extra dimensions to separate the classes. Although the altered definition of the joint probability in the naïve BN somewhat degrades its exact representation of the data, the independence assumption uses more data to determine the value of each cell of these probability tables, making them generally more accurate in relation to the prediction. Though this seems to be the case for these naïve BNs, for an infinitely large and varied dataset, we believe the traditional BN would beat the naïve BN. For instance, the preoperative clinical dataset's naïve and traditional BNs were similar, having several overlapping feature selections. If the traditional BN were allowed to pick more than three first-level nodes and it had enough data to fill the probability tables of these nodes, it probably would have equaled or beat the naïve network.

Not only did the structural limitations contribute to the differences between these BN's fitness, but the composition of the dataset did as well. Notice that for the ECG only dataset, the traditional BN held the highest fitness, while the naïve network is much less fit. Yet, for the combined clinical and ECG dataset, the naïve is far better than the traditional BN. This is a difference in the dataset composition of these two classifiers. The combined clinical and ECG dataset has 244 out of 545 patients that have no ECG features at all. That is a huge chunk of data with no values. Since clinical values were

available for all of the patients, and we saw before that the naïve network was better suited for this data, it was chosen over the traditional BN.

Additionally, the naïve BN seemed slightly more robust than the traditional networks, seeing that they generally decreased less in fitness during validation than the traditional BN did. The one exception seems to be the postoperative ECG dataset analysis, but this dataset is very small, making its validation prone to bias.

In order to determine the better classifier between chapters four and five, we compare the best of each chapter: the preoperative clinical logistic regression and naïve BN. Though their fitness values are not directly comparable since they were computed by different methods, we can compare their sensitivity, specificity, use of data, and robustness. The sensitivity and specificity of the logistic regression are slightly better than the naïve BN for training as well as testing. However, the regression classifier used significantly fewer patient samples to derive this classifier, roughly one third of the patients needing classification. This was due to the missing data points in the dataset, which this classifier cannot tolerate. The naïve BN, on the other hand risk stratified all presented patients, handling any missing data points. This coupled with the intuitive use of a probabilistic system that a cardiologist would more likely accept, caused the preoperative clinical naïve BN, shown with probability table values in Figure 5.88, to be the clear superior.

When comparing the features that were used in our favorite classifiers of chapter four and five (preoperative clinical multivariate logistic regression and naïve BN, respectively), we see that the two have several common clinical features. Preoperative AF occurrence and cardiomegaly appear in both of these classifiers, as well as a number of others.

Ejection fraction, which replaces diabetes in the clinical dataset naïve classifier to arrive at the combined clinical and ECG dataset classifier, is also prominent through these analyses, much like smoking. Notice that many of these prominent features have appeared very little in the prior art, possibly due to our cohort or to the previous studies' greedy feature selection methods.

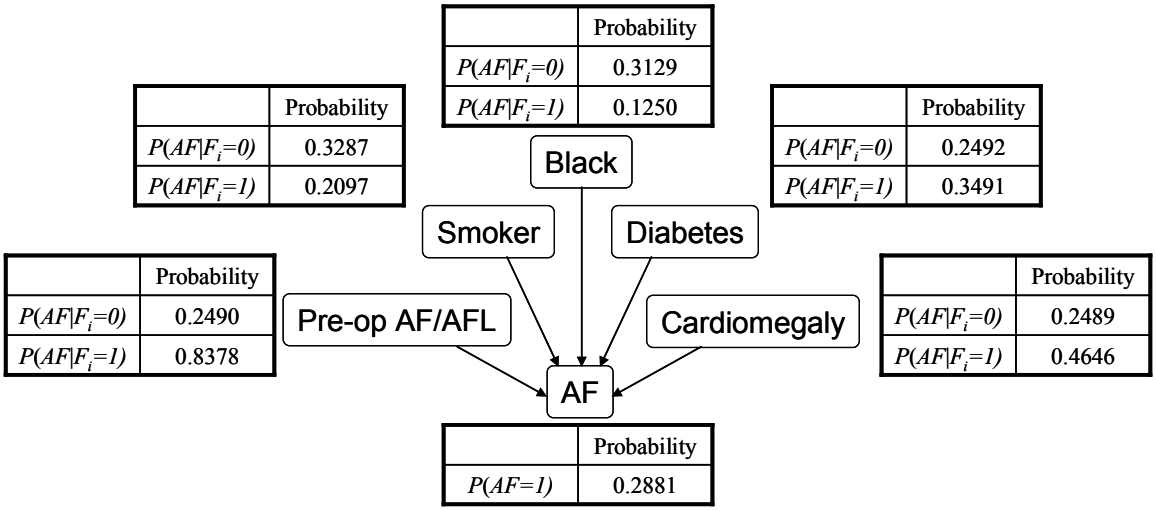

Figure 5.88 The naive BN that was selected for the best postoperative AF risk stratification system.

When observing the probabilities of the best risk stratifier, pictured in Figure 5.88, we notice that in this cohort, current smokers and African-Americans have a decreased occurrence of AF. It is very surprising that smoking, a variable long associated with pathological conditions, appears less frequently in smokers ($p = 0.004$). The other three variables in the classifier contribute to the occurrence of AF with preoperative AF being the most significant.

In summary, we believe that the best BN classifier is the naïve network found using the preoperative clinical dataset. It has an AUC of 0.67 and a sensitivity and specificity of 0.63 and 0.73, respectively, for training and testing on the same data. This, is almost identical to the combined clinical and ECG dataset preoperative naïve BN except for the exchange of diabetes and ejection fraction. These classifiers seem to generalize well to new data, are simple, and their probability tables are easily populated with smaller datasets.

5.6 Classifier Context

Table 5.4 Point system for risk stratification system of postoperative AF. Borrowed from [17].

Predictor	***Points***
Age	
<30	6
30-39	12
40-49	18
50-59	24
60-69	30
70-79	36
≥80	42
Medical History	
Atrial Fibrillation	7
Chronic Obstructive Pulmonary Disease	4
Concurrent Valve Surgery	6
Withdrawal of Postoperative Treatment	
β-blocker	6
ACE Inhibitor	5
β-Blocker Treatment	
Preoperative and Postoperative	-7
Postoperative	-11
Preoperative and Postoperative ACE Inhibitor Treatment	-5

Postoperative Treatment	
Potassium Supplementation	-5
NSAIDs	-7

In order to put our final classifier in the context of the current state of the art for risk stratification of postoperative AF, we present our results alongside a current risk stratification standard. For this we chose a recently published risk stratification method [17] that was also used by another author in a retrospective study of amiodarone prophalaxis in 2006 [7]. This risk stratification method uses a point scoring method related to multivariate regression. The point values for each of the characteristics seen in Table 5.4 are summed and placed on a scale that translates to the patient's risk of postoperative AF (low risk: <14, medium risk: 14 to 31, high risk: >31).

When performing this risk stratification method on our dataset, we did not have any information on postoperative potassium supplementation. This was only five possible points, so we do not believe that it invalidates the comparison. Additionally since our dataset has some missing points, we decided that any missing values would be counted as a negative for that characteristic, meaning no points are awarded. This again does not have a large bearing on the comparison, since in total there were only twelve missing data points for all ten variables and 545 patients. Instead of using the high, medium, and low risk classes they assigned in their paper, we found the optimum threshold for high and low risk stratification, sixteen (16) points, using the maximum of the sensitivity/specificity product plot, Figure 5.90, as we have on all of the classifiers in this work. This makes a more fair comparison of the outputs of the systems.

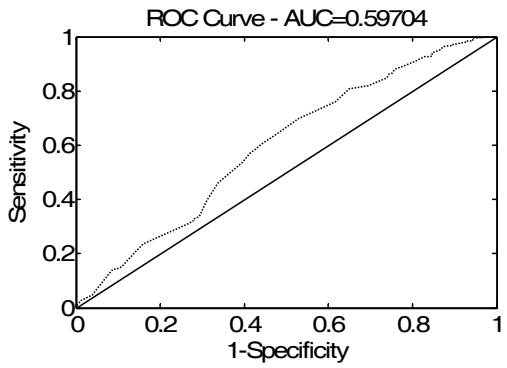

Figure 5.89 ROC of postoperative AF risk stratification method presented in [17].

One can see the ROC curve of the clinical state of the art postoperative AF risk stratification method performed on our data in Figure 5.89 as well as the sensitivity/specificity product plot in Figure 5.90. In comparing these to the corresponding validation plots from the naïve BN performed on the clinical dataset seen in Figure 5.64 and Figure 5.65, our classifier has an AUC of 0.67 versus the other method's 0.60. This is the difference between a fair classifier and a borderline fair/poor classifier.

We should keep in mind that our classifier was tailored using this data while the state of the art classifier was built using their own, and it is difficult to compare the two. We have tried to address this concern by using our LOO validation results in the above comparison. However, these results remain inconclusive as to which is the better classifier. Regardless of this, we can point out that the state of the art system uses eleven features while ours uses only five. If developed with more features, the difference would surely tip even more in the BN's favor. Additionally, the BN tolerates missing data points which this method would have difficulties with.

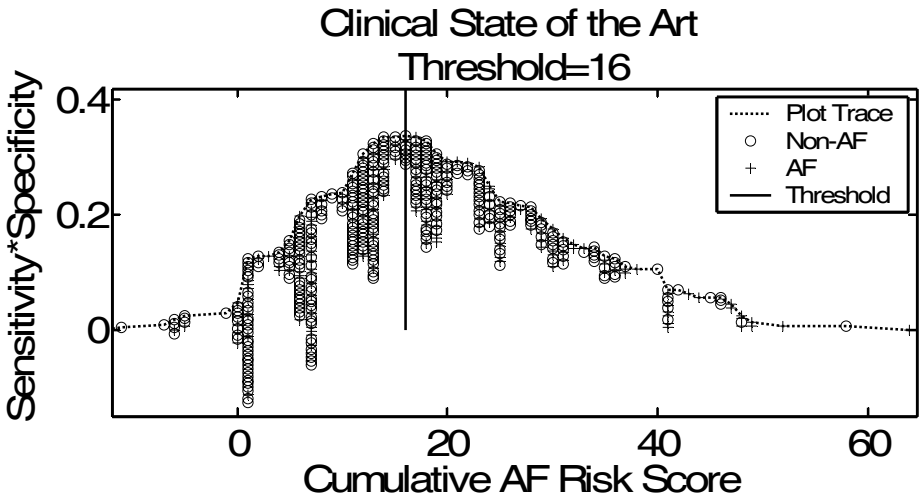

Figure 5.90 Sensitivity/Specificity Product plot of the postoperative AF risk stratification method presented in [17].

5.7 Classifier Usage

The first usage of the BN classifiers is that which we have presented throughout this chapter; the BN is trained using the frequentist probabilities calculated directly from the data and then future patients' risk is computed by inputting their known predictive variables. This is a well respected way of performing and using Bayesian classifiers for inference.

However, we could also approach this from the perspective that the probabilities that the BN encodes are merely one possible probability combination and the actual probability values are unknown. Therefore, by quantifying other degrees of belief such as a doctor's prior experience or data provided in a clinical study, we might additionally include these types of data in our prediction. Bayesian statistics, as we discussed in chapter two, accounts for this by providing a means of combining prior information with the already

built BN. This gives the cardiologist the opportunity to perform an online sensitivity analysis by providing their own prior or posterior probability for any of the nodes in the network, as pointed out in Figure 5.91, and change these to observe the outcome's corresponding reaction. Then, the likelihood ratio can be calculated for the AF and non-AF prediction probabilities.

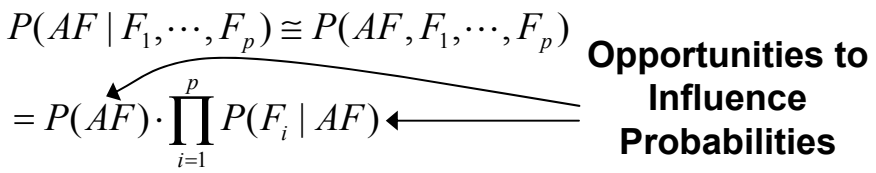

Figure 5.91 Naive BN AF prediction calculation given features F_1 through F_p where p is the number of first-level parents. The possible locations for adjusting the prediction probabilities are also labeled. Following this, the likelihood ratio would be calculated prior to prediction.

In practice, these probabilities and their current values might be presented to the physician on a computer monitor with adjustable sliders allowing their alteration while showing the predictive outcome change. This allows the physician to test the hypotheses that the recommendation was made on and see under what conditions this recommendation would be reversed. Though this trial-and-error balancing act could be a little more art than science, this tool is based on solid quantification of data mixed with educated clinician estimations in a structured statistical framework.

Chapter 6

Conclusion

In this concluding chapter, we discuss the predictive techniques we developed in the previous chapters and their benefits and drawbacks. Additionally, we reiterate our reasoning for the selection of the naïve BN classifier and offer suggestions for future work.

6.1 Classifier Summary

This work has presented univariate and multivariate risk stratification routines in the form of:

- A single variable,
- GA feature-selected multivariate logistic regression,
- GA feature-selected *k*-Nearest Neighbor,
- GA feature-selected naïve BN,
- Greedily-built (K2 method) traditional BN, and
- GA learned structure and feature-selected traditional BN.

Of the univariate predictors, it seems that the patient's age is the most reliable, as well as the best recognized. Unfortunately, this does not offer the sensitivity or specificity needed for making clinical decisions. The multivariate logistic regression seems to be prominent in the literature and has worked well in our experiments when the features are selected by GA. The *k*-NN actually performed slightly better than regression in terms of fitness,

though this method requires the loading of all training points into memory to perform tests, a significant problem when dealing with high dimensional, large dataset problems. Additionally, the cluster theory that the *k*-NN is based on has not gained acceptance with clinicians who seem to prefer regression or probability models. The traditional BNs were particularly useful in the ECG datasets when it was offered a large number of features. Overall, the GA feature-selected naïve BNs performed the best while offering other superior qualities that allow easy of use and robustness to clinical situations. Specifically, the naïve BN built using preoperative clinical data had the best combination of performance and usability. For instance, BNs are based on probabilities of previous AF patients' data. This is similar to how a cardiologist might use their past experience to make decisions. Additionally, naïve BNs require less data to populate their probability tables due to their independent conditional probability assumptions. Since BNs perform inference probabilistically, physicians can use this classifier when some of the inputs have missing values. This is not possible with classifiers such as multivariate regression or *k*-NN. As we saw in chapter four, these classifiers discarded sometimes more than half of the patient population when finding the optimum feature subset. The BNs, on the other hand, always used all the patient data it was presented with and returned a comparable fitness.

6.2 Suggested Work

One of the main obstacles to the ECG analysis of the datasets is the lack of automated ECG annotation. Though there are certainly systems which do this in the hospital, these were not available for this work. A greater volume of quality ECG recordings and

annotations would allow much more advanced feature extraction routines to be performed, including various machine learning techniques.

Though we have investigated many types of BNs in this study, there are a number of questions that need to be better understood to advance the use of these systems in a decision support role in medicine. We urge the use of these systems with larger sets of data, especially datasets that were collected in the hospital. In this way, missing data would appear as it naturally would instead of in a simulated manner. This would allow the BN to "learn" what missing values happen in what circumstances, allowing it to tailor itself to the best possible predictions in realistic cases.

Larger datasets would also allow a number of other interesting investigations. In this work, we were limited by the number of levels we could discretize the data because if we allowed more than binary, this increases the size of the joint probability tables, thereby requiring more data points to create accurate probability estimates. We think a more varied discretization scheme for some interesting variables (*i.e.* age, left atrial volume, ejection fraction, etc.) could yield additional predictive information.

Traditional BNs also perform best with large amounts of data and we think with a larger dataset, the traditional BNs might have been the best classifier, but this cannot be verified until a larger dataset is analyzed.

An interesting topic would be the resolution of the probability shifting that occurs when using LOO validation as we saw in chapter five. This might be resolved through a probability correction term in the fitness function indicating the number of patients used

and discarded. This same type of approach might also be applied to the K2 greedy BN building method to cure its selection of variables with few patient samples.

Lastly, we suggest the use of these methods of GA feature selection in naïve BNs and GA structure learning and feature selection for traditional BNs to be used in other medical fields. Their flexibility, robustness, and accuracy make them ideal for use in real world applications and we feel this methodology lends itself well to a wide range of risk stratification needs present in the medical community.

Appendix A

Pre- and Postoperative Variable List

Preoperative Variables

Pre-operative AF
Pre-operative use of ACEI
Post-operative use of ACEI
Pre-operative use of statins
Post-op use of statins
Pre-op use of BB
Post-op use of BB
Pre-op PPAR
Post-op PPAR
ARB
NSAIDS
Pre-operative use of IABP
history of smoking (>3 months smoking vs. less than 3 months)
current smoking
hypertension
active endocarditis
age
serum albumin
ASA classification
Aortic valve replacement
Mitral valve replacement
Body Mass Index
Body surface area
Number of total anastomoses
Number of major coronaries with >50% stenosis
Percent circ stenosis
Cardiomegaly
COPD
Total CPB time in minutes
Creatinine level
Current diuretic
Current digoxin use
Cerebral vascular disease
Diabetes (oral or insulin vs. none)
Angina, CCS functional class
NHYA class

Functional status
Hemoglobin
IV NTG within 48 hours before surgery
Valve repair
Mitral regurgitation
Percent left main stenosis
Physician's pre-operative estimate of mortality
Prior heart surgery (
Prior MI
Resting ST depression
Percent rca stenosis
Percent lad stenosis
Peripheral vascular disease
Pulmonary rales
Total cholesterol
Low density lipoprotein
LV contraction grade
Priority level
Great vessel repair
Left Atrial Size
Race

Postoperative Variables

Age
Sex
Body Surface Area
Weight (kg)
Ethanol (+1 qd)
Current Smoker
Past Smoker
Hypertension
Cholesterol
History of Coronary Artery Disease (CAD)
History of Supraventricular Tachycardia
History of Nonsustained Ventricle Tachycardia (nsusVT)
Family History of Coronary Artery Disease
History of VT or Sudden Cardiac Death
Left Ventricle end-diastolic pressure (LVEDP)
Diabetes
Chronic Obstructive Pulmonary Disease
Hyperthyroidism
Rheumatic Fever
Chronic Renal Failure
Prior Myocardial Infarction

Cardiomyopathy
Valve Disease
Prior Percutaneous transluminal coronary angioplasty
Prior CABG
History of AF
Ejection Fraction Percentage
Mitral Regurgitation
CAD Left Main Artery Obstruction
CAD Left Anterior Descending Artery Obstruction
CAD Circumflex Artery Obstruction
Right Coronary Artery Obstruction
Patent Ductus Arteriosus
Aortic Valve Surgery
Left Atrium Thickness
P-wave duration (II lead)
Number of Vessels Bypassed
Use of Mammary Artery
Aortic Cross Clamp Time
Cardiopulmonary Bypass Time
Artificially Pumped Blood Volume
Body Temperature Low
Body Temperature High
Second Operation Performed
Myocardial Infarction
Atrioventricular Block
Death
Intra-aortic Balloon Pump
Time in Intensive Care Unit
Time in SpDU
Time in Hospital
β Blocker Administration Post-op Days 1-5
CK Enzyme Level
Potassium Level
Heart Rate for Hospital Stay
Pre-ventricular Beat Count

Appendix B

Extended Univariate Results

Preoperative Univariate Results

Preoperative Binary Features	Non-AF	AF	Total	p value
Pre_Bb_Key	58.0% (225/388)	68.8% (108/157)	61.1% (333/545)	0.019
Post_BB_Key	89.7% (347/387)	82.2% (129/157)	87.5% (476/544)	0.017
AF_fl_preop	1.6% (6/386)	19.7% (31/157)	6.8% (37/543)	0.000
diabetes	35.6% (138/388)	47.1% (74/157)	38.9% (212/545)	0.012
cm	13.7% (53/388)	29.3% (46/157)	18.2% (99/545)	0.000
currsmok	37.9% (147/388)	24.8% (39/157)	34.1% (186/545)	0.004
reststd	9.5% (37/388)	4.5% (7/157)	8.1% (44/545)	0.049
priorhs	1.8% (7/388)	5.7% (9/157)	2.9% (16/545)	0.014
curdig	3.4% (13/388)	9.6% (15/157)	5.1% (28/545)	0.003
Htn	82.5% (320/388)	91.1% (143/157)	85.0% (463/545)	0.011
mvr	1.8% (7/388)	6.4% (10/157)	3.1% (17/545)	0.005
la	26.6% (42/158)	39.2% (38/97)	31.4% (80/255)	0.035
black	16.2% (63/388)	5.7% (9/157)	13.2% (72/545)	0.001
prevsmok	26.0% (101/388)	37.6% (59/157)	29.4% (160/545)	0.007

Preoperative Categorical Feature	Category	Non-AF	AF	Total	p value
LA_Key		384	157	541	0.000
	0	58.9% (226/384)	38.2% (60/157)	52.9% (286/541)	
	1	6.8% (26/384)	7.6% (12/157)	7.0% (38/541)	
	2	23.4% (90/384)	29.9% (47/157)	25.3% (137/541)	
	3	3.9% (15/384)	12.7% (20/157)	6.5% (35/541)	
	4	1.6% (6/384)	2.5% (4/157)	1.8% (10/541)	
	5	3.9% (15/384)	7.6% (12/157)	5.0% (27/541)	
	6	1.0% (4/384)	0.6% (1/157)	0.9% (5/541)	
	7	0.5% (2/384)	0.6% (1/157)	0.6% (3/541)	
EF_Key		387	157	544	0.010
	0	53.0% (205/387)	35.0% (55/157)	47.8% (260/544)	
	1	0.5% (2/387)	0.0% (0/157)	0.4% (2/544)	
	2	1.6% (6/387)	2.5% (4/157)	1.8% (10/544)	
	3	3.4% (13/387)	3.8% (6/157)	3.5% (19/544)	
	4	7.5% (29/387)	8.3% (13/157)	7.7% (42/544)	
	5	8.0% (31/387)	14.6% (23/157)	9.9% (54/544)	
	6	19.6% (76/387)	22.9% (36/157)	20.6% (112/544)	
	7	5.9% (23/387)	12.1% (19/157)	7.7% (42/544)	
	8	0.5% (2/387)	0.6% (1/157)	0.6% (3/544)	
Surgery_Key		387	157	544	0.005
	1	4.7% (18/387)	1.9% (3/157)	3.9% (21/544)	
	2	15.8% (61/387)	8.9% (14/157)	13.8% (75/544)	
	3	30.5% (118/387)	27.4% (43/157)	29.6% (161/544)	
	4	30.0% (116/387)	32.5% (51/157)	30.7% (167/544)	
	5	3.4% (13/387)	6.4% (10/157)	4.2% (23/544)	
	6	0.8% (3/387)	0.0% (0/157)	0.6% (3/544)	
	7	2.3% (9/387)	3.8% (6/157)	2.8% (15/544)	
	8	4.9% (19/387)	8.9% (14/157)	6.1% (33/544)	
	9	0.5% (2/387)	1.3% (2/157)	0.7% (4/544)	
	10	0.3% (1/387)	3.8% (6/157)	1.3% (7/544)	
	11	5.2% (20/387)	3.8% (6/157)	4.8% (26/544)	
	12	1.8% (7/387)	1.3% (2/157)	1.7% (9/544)	
race		387	157	544	0.005
	0	30.2% (117/387)	34.4% (54/157)	31.4% (171/544)	
	4	16.3% (63/387)	5.7% (9/157)	13.2% (72/544)	
	5	0.3% (1/387)	1.3% (2/157)	0.6% (3/544)	

	6	53.2% (206/387)	58.6% (92/157)	54.8% (298/544)	
Csmok		317	135	452	0.026
	1	22.4% (71/317)	25.2% (34/135)	23.2% (105/452)	
	2	39.7% (126/317)	25.9% (35/135)	35.6% (161/452)	
	3	6.0% (19/317)	5.2% (7/135)	5.8% (26/452)	
	4	31.9% (101/317)	43.7% (59/135)	35.4% (160/452)	
fcc		388	157	545	0.009
	1	76.8% (298/388)	66.2% (104/157)	73.8% (402/545)	
	2	15.5% (60/388)	21.7% (34/157)	17.2% (94/545)	
	3	6.2% (24/388)	12.1% (19/157)	7.9% (43/545)	
	4	1.5% (6/388)	0.0% (0/157)	1.1% (6/545)	
cad		376	156	532	0.010
	0	5.9% (22/376)	12.8% (20/156)	7.9% (42/532)	
	1	6.6% (25/376)	5.8% (9/156)	6.4% (34/532)	
	2	27.7% (104/376)	17.9% (28/156)	24.8% (132/532)	
	3	59.8% (225/376)	63.5% (99/156)	60.9% (324/532)	
mitreg		332	141	473	0.002
	1	83.1% (276/332)	68.8% (97/141)	78.9% (373/473)	
	2	11.7% (39/332)	17.7% (25/141)	13.5% (64/473)	
	3	2.1% (7/332)	6.4% (9/141)	3.4% (16/473)	
	4	3.0% (10/332)	7.1% (10/141)	4.2% (20/473)	
cabgda_		388	157	545	0.028
	0	8.5% (33/388)	13.4% (21/157)	9.9% (54/545)	
	1	5.2% (20/388)	7.0% (11/157)	5.7% (31/545)	
	2	19.1% (74/388)	8.9% (14/157)	16.1% (88/545)	
	3	30.4% (118/388)	30.6% (48/157)	30.5% (166/545)	
	4	33.5% (130/388)	33.1% (52/157)	33.4% (182/545)	
	5	2.8% (11/388)	6.4% (10/157)	3.9% (21/545)	
	6	0.5% (2/388)	0.6% (1/157)	0.6% (3/545)	
cabgdai		388	157	545	0.003
	0	12.1% (47/388)	22.3% (35/157)	15.0% (82/545)	
	1	87.4% (339/388)	75.2% (118/157)	83.9% (457/545)	
	2	0.3% (1/388)	1.9% (3/157)	0.7% (4/545)	
	3	0.3% (1/388)	0.6% (1/157)	0.4% (2/545)	

Preoperative Continuous Feature	**Non-AF**	**AF**	**Total**	**p value**
age	61.49+/-9.1(388)	64.98+/-8.9(157)	62.50+/-9.1(545)	0.000
htin	69.70+/-2.7(388)	70.43+/-2.4(157)	69.91+/-2.6(545)	0.003
bsa	2.04+/-0.2(388)	2.08+/-0.2(157)	2.05+/-0.2(545)	0.017
lvedp	15.96+/-7.4(249)	18.11+/-10.5(113)	16.63+/-8.5(362)	0.025
lad	72.01+/-29.8(381)	65.37+/-31.8(157)	70.07+/-30.5(538)	0.022
isct	61.19+/-36.5(388)	71.45+/-38.4(157)	64.14+/-37.3(545)	0.004
cpbt	98.90+/-49.7(388)	112.39+/-48.7(157)	102.78+/-49.7(545)	0.004
totalchol	175.68+/-48.8(346)	165.67+/-46.6(137)	172.84+/-48.4(483)	0.040
TQ_V1_db2_sc5_Mean_Freq	25.80+/-4.8(102)	28.34+/-8.0(55)	26.69+/-6.2(157)	0.014
TQ_V1_db2_sc5_Median_Freq	23.94+/-5.6(102)	26.47+/-8.5(55)	24.83+/-6.8(157)	0.026
TQ_II_db2_sc5_Mean_Freq	25.45+/-6.1(104)	28.06+/-7.3(54)	26.34+/-6.6(158)	0.019
TQ_II_db2_sc5_Median_Freq	23.58+/-6.9(104)	26.34+/-7.6(54)	24.52+/-7.3(158)	0.022
TQ_II_db2_sc15_Peak_Freq	8.05+/-2.6(104)	7.10+/-2.8(54)	7.72+/-2.7(158)	0.039
TQ_II_db2_sc20_Curve_length	313.30+/-107.7(104)	276.96+/-102.6(54)	300.88+/-107.0(158)	0.043
TQ_III_db2_sc25_Mean_Freq	13.52+/-5.8(86)	15.59+/-5.0(46)	14.24+/-5.6(132)	0.041
TQ_II_db2_sc30_Peak_Freq	6.22+/-1.4(104)	5.63+/-1.7(54)	6.02+/-1.5(158)	0.022
TQ_V1_db3_sc5_Mean_Freq	29.53+/-4.5(102)	31.53+/-7.0(55)	30.23+/-5.6(157)	0.031
TQ_I_db3_sc5_Shannon_Entropy	0.21+/-0.1(86)	0.18+/-0.1(46)	0.20+/-0.1(132)	0.045
TQ_II_db3_sc5_Mean_Freq	29.91+/-5.5(104)	32.26+/-6.6(54)	30.72+/-6.0(158)	0.018
TQ_II_db3_sc20_Median_Freq	10.32+/-3.2(104)	11.61+/-3.6(54)	10.76+/-3.4(158)	0.023
TQ_III_db3_sc20_Mean_Freq	15.10+/-5.5(86)	17.60+/-5.6(46)	15.97+/-5.7(132)	0.015
TQ_II_db3_sc25_Mean_Freq	10.15+/-3.8(104)	11.82+/-4.8(54)	10.72+/-4.2(158)	0.018
TQ_V1_db3_sc30_Shannon_Entropy	0.29+/-0.1(102)	0.26+/-0.1(55)	0.28+/-0.1(157)	0.011
TQ_II_db3_sc30_Nonlinear_Energy	660.75+/-624.7(104)	480.05+/-325.8(54)	598.99+/-547.0(158)	0.049
TQ_II_db3_sc30_Mean_Freq	8.49+/-3.0(104)	9.62+/-3.7(54)	8.87+/-3.3(158)	0.040
TQ_II_sym4_sc5_Shannon_Entropy	0.21+/-0.1(104)	0.18+/-0.1(54)	0.20+/-0.1(158)	0.049
TQ_V1_sym4_sc10_Peak_Freq	13.05+/-3.0(102)	11.85+/-3.5(55)	12.63+/-3.2(157)	0.028
TQ_II_sym4_sc15_Median_Freq	9.65+/-2.8(104)	10.66+/-3.1(54)	9.99+/-3.0(158)	0.042
TQ_II_sym4_sc20_Mean_Freq	9.79+/-4.0(104)	11.67+/-4.8(54)	10.43+/-4.3(158)	0.009
TQ_II_sym4_sc20_Median_Freq	7.45+/-1.8(104)	8.26+/-2.6(54)	7.73+/-2.1(158)	0.021
TQ_II_sym6_sc5_Mean_Freq	30.07+/-5.3(104)	32.01+/-6.2(54)	30.73+/-5.7(158)	0.042
TQ_V1_sym6_sc15_Median_Freq	12.96+/-3.8(102)	11.68+/-3.2(55)	12.51+/-3.6(157)	0.036
TQ_III_sym6_sc15_Mean_Freq	15.89+/-6.1(86)	18.28+/-5.9(46)	16.72+/-6.1(132)	0.032
TQ_III_sym6_sc15_Median_Freq	11.57+/-3.7(86)	12.99+/-3.8(46)	12.07+/-3.8(132)	0.040

TQ_II_sym6_sc20_Mean_Freq	11.26+/-4.3(104)	13.20+/-5.2(54)	11.93+/-4.7(158)	0.013
TQ_II_sym6_sc20_Median_Freq	8.47+/-2.2(104)	9.38+/-3.0(54)	8.78+/-2.6(158)	0.035
TQ_II_sym6_sc25_Mean_Freq	8.55+/-3.3(104)	9.85+/-3.9(54)	9.00+/-3.6(158)	0.029
TQ_II_coif1_sc15_Mean_Freq	13.77+/-3.6(104)	15.20+/-4.9(54)	14.26+/-4.1(158)	0.038
TQ_II_coif1_sc15_Median_Freq	8.86+/-1.6(104)	10.06+/-3.3(54)	9.27+/-2.4(158)	0.003
TQ_V1_coif1_sc20_Peak_Freq	7.35+/-2.4(102)	6.13+/-2.9(55)	6.92+/-2.7(157)	0.006
TQ_II_coif4_sc20_Nonlinear_Energy	343.50+/-338.0(104)	245.04+/-169.2(54)	309.85+/-294.6(158)	0.046
TQ_II_coif4_sc25_Mean_Freq	8.90+/-3.4(104)	10.37+/-4.1(54)	9.40+/-3.7(158)	0.017
TQ_V1_bior2.2_sc5_Mean_Freq	34.10+/-4.8(102)	35.90+/-6.4(55)	34.73+/-5.5(157)	0.049
TQ_II_bior2.2_sc5_Mean_Freq	33.73+/-5.9(104)	36.22+/-6.6(54)	34.58+/-6.2(158)	0.017
TQ_II_bior2.2_sc5_Median_Freq	32.72+/-7.0(104)	35.56+/-7.3(54)	33.70+/-7.2(158)	0.019
TQ_V1_bior2.2_sc10_Peak_Freq	15.16+/-3.9(102)	16.68+/-4.4(55)	15.69+/-4.1(157)	0.027
TQ_II_bior2.2_sc20_Median_Freq	11.00+/-3.3(104)	12.45+/-4.2(54)	11.50+/-3.7(158)	0.018
TQ_III_bior2.2_sc20_Mean_Freq	16.65+/-6.1(86)	19.42+/-6.0(46)	17.62+/-6.2(132)	0.013
TQ_III_bior2.2_sc20_Median_Freq	12.74+/-3.7(86)	14.42+/-3.8(46)	13.33+/-3.8(132)	0.015
TQ_II_bior2.2_sc25_Mean_Freq	11.63+/-4.7(104)	13.38+/-5.2(54)	12.23+/-4.9(158)	0.034
TQ_II_bior2.2_sc25_Median_Freq	8.90+/-2.4(104)	9.97+/-3.0(54)	9.27+/-2.7(158)	0.017
TQ_II_bior4.4_sc5_Mean_Freq	31.97+/-5.3(104)	34.49+/-6.1(54)	32.83+/-5.7(158)	0.008
TQ_II_bior4.4_sc5_Median_Freq	30.17+/-6.0(104)	32.13+/-5.4(54)	30.84+/-5.8(158)	0.045
TQ_II_bior4.4_sc20_Mean_Freq	12.48+/-4.8(104)	14.24+/-5.3(54)	13.08+/-5.1(158)	0.038
TQ_II_bior4.4_sc20_Median_Freq	9.04+/-2.8(104)	10.13+/-3.0(54)	9.41+/-2.9(158)	0.028
TQ_II_bior4.4_sc25_Mean_Freq	9.72+/-3.9(104)	11.33+/-4.5(54)	10.27+/-4.2(158)	0.021
TQ_V1_bior5.5_sc9_Mean_Freq	18.96+/-5.2(102)	20.84+/-5.6(55)	19.62+/-5.4(157)	0.037
TQ_III_bior5.5_sc9_Peak_Freq	16.08+/-4.0(86)	14.54+/-3.9(46)	15.55+/-4.0(132)	0.036
TQ_III_bior5.5_sc17_Mean_Freq	13.57+/-4.6(86)	15.45+/-4.1(46)	14.23+/-4.5(132)	0.021
TQ_II_bior5.5_sc21_Nonlinear_Energy	277.84+/-263.7(104)	197.69+/-152.7(54)	250.45+/-234.4(158)	0.041
TQ_II_bior5.5_sc21_Mean_Freq	10.24+/-3.5(104)	11.91+/-4.3(54)	10.81+/-3.9(158)	0.010
TQ_II_bior5.5_sc21_Median_Freq	7.88+/-1.3(104)	8.55+/-2.3(54)	8.11+/-1.8(158)	0.021
TQ_II_bior5.5_sc25_Mean_Freq	8.72+/-3.5(104)	10.05+/-4.1(54)	9.17+/-3.8(158)	0.036
TQ_II_bior6.8_sc20_Nonlinear_Energy	357.34+/-373.0(104)	246.18+/-176.7(54)	319.35+/-323.5(158)	0.040
TQ_II_bior6.8_sc20_Mean_Freq	12.15+/-4.6(104)	13.80+/-5.1(54)	12.71+/-4.8(158)	0.042
TQ_II_bior6.8_sc20_Median_Freq	9.15+/-2.7(104)	10.20+/-3.0(54)	9.51+/-2.8(158)	0.026
TQ_II_bior6.8_sc25_Mean_Freq	9.36+/-3.6(104)	10.96+/-4.4(54)	9.91+/-3.9(158)	0.015
TQ_II_bior6.8_sc25_Median_Freq	7.78+/-1.6(104)	8.46+/-2.4(54)	8.01+/-2.0(158)	0.037
TQ_III_rbio2.2_sc13_Shannon_Entropy	0.22+/-0.1(86)	0.19+/-0.1(46)	0.21+/-0.1(132)	0.046
TQ_II_rbio4.4_sc5_Mean_Freq	27.58+/-6.0(104)	29.86+/-5.6(54)	28.36+/-6.0(158)	0.023
TQ_III_rbio4.4_sc15_Mean_Freq	14.51+/-5.6(86)	16.81+/-5.0(46)	15.31+/-5.5(132)	0.021
TQ_II_rbio4.4_sc20_Mean_Freq	9.86+/-3.9(104)	11.58+/-4.7(54)	10.45+/-4.2(158)	0.015
TQ_II_rbio5.5_sc5_Mean_Freq	29.29+/-6.0(104)	31.92+/-6.1(54)	30.19+/-6.1(158)	0.010
TQ_II_rbio5.5_sc5_Median_Freq	26.93+/-6.3(104)	29.25+/-6.4(54)	27.72+/-6.4(158)	0.030
TQ_II_rbio5.5_sc15_Median_Freq	11.88+/-3.2(104)	13.37+/-4.4(54)	12.39+/-3.7(158)	0.017
TQ_II_rbio5.5_sc20_Mean_Freq	11.68+/-4.6(104)	13.66+/-5.6(54)	12.36+/-5.0(158)	0.018
TQ_II_rbio5.5_sc20_Median_Freq	8.85+/-2.7(104)	10.04+/-3.5(54)	9.26+/-3.1(158)	0.020
TQ_V1_rbio5.5_sc25_Peak_Freq	7.29+/-2.3(102)	6.41+/-2.6(55)	6.98+/-2.4(157)	0.030
TQ_II_rbio5.5_sc25_Mean_Freq	9.14+/-3.6(104)	10.54+/-4.2(54)	9.62+/-3.8(158)	0.028
TQ_II_rbio6.8_sc17_Nonlinear_Energy	279.02+/-286.2(104)	190.19+/-141.4(54)	248.66+/-249.6(158)	0.033
TQ_III_rbio6.8_sc17_Mean_Freq	13.71+/-4.6(86)	15.70+/-4.5(46)	14.41+/-4.6(132)	0.018
TQ_II_rbio6.8_sc21_Mean_Freq	9.97+/-3.6(104)	11.66+/-4.6(54)	10.55+/-4.1(158)	0.012
TQ_II_rbio6.8_sc21_Median_Freq	7.79+/-1.5(104)	8.47+/-2.4(54)	8.02+/-1.9(158)	0.034
TQ_II_rbio6.8_sc25_Mean_Freq	8.36+/-3.3(104)	9.60+/-3.8(54)	8.78+/-3.5(158)	0.037
TQ_V1_gaus1_sc2_Mean_Freq	14.82+/-3.3(102)	16.66+/-7.2(55)	15.47+/-5.1(157)	0.030
TQ_II_gaus1_sc6_Peak_Freq	5.97+/-1.6(104)	5.37+/-2.0(54)	5.77+/-1.8(158)	0.040
TQ_II_gaus1_sc6_Curve_length	254.82+/-90.8(104)	219.70+/-76.5(54)	242.82+/-87.6(158)	0.016
TQ_II_gaus1_sc8_Curve_length	331.11+/-119.8(104)	288.94+/-104.2(54)	316.70+/-116.1(158)	0.030
TQ_III_gaus1_sc12_Peak_Freq	3.12+/-2.1(86)	4.15+/-2.6(46)	3.48+/-2.3(132)	0.014
TQ_II_gaus2_sc7_Energy	673.71+/-852.6(104)	429.42+/-420.0(54)	590.22+/-741.6(158)	0.049
TQ_III_gaus2_sc7_Mean_Freq	14.92+/-6.1(86)	17.20+/-5.5(46)	15.72+/-6.0(132)	0.037
TQ_II_gaus3_sc7_Mean_Freq	14.23+/-5.7(104)	16.36+/-6.5(54)	14.96+/-6.0(158)	0.035
TQ_II_gaus3_sc7_Median_Freq	11.10+/-3.8(104)	12.54+/-4.6(54)	11.59+/-4.2(158)	0.039
TQ_II_gaus3_sc10_Katz_FD	1.24+/-0.1(104)	1.21+/-0.1(54)	1.23+/-0.1(158)	0.045
TQ_II_gaus3_sc10_Peak_Freq	6.74+/-2.1(104)	5.91+/-2.4(54)	6.45+/-2.2(158)	0.028
TQ_III_gaus3_sc10_Peak_Pow_Amp	2640.15+/-2803.0(86)	4384.08+/-6049.1(46)	3247.89+/-4285.3(132)	0.025
TQ_V1_gaus3_sc13_Peak_Freq	6.65+/-2.3(102)	5.78+/-2.6(55)	6.34+/-2.4(157)	0.032
TQ_II_gaus3_sc13_Peak_Freq	6.64+/-1.4(104)	5.87+/-1.9(54)	6.38+/-1.6(158)	0.004
TQ_II_gaus3_sc13_Curve_length	448.88+/-177.8(104)	391.25+/-158.6(54)	429.18+/-173.1(158)	0.047
TQ_V1_gaus3_sc16_Median_Freq	9.09+/-2.1(102)	8.18+/-2.3(55)	8.77+/-2.2(157)	0.013
TQ_V1_gaus3_sc16_Peak_Freq	6.55+/-2.4(102)	5.66+/-2.6(55)	6.24+/-2.5(157)	0.033
TQ_II_gaus3_sc16_Peak_Freq	6.29+/-1.3(104)	5.81+/-1.6(54)	6.13+/-1.4(158)	0.046
TQ_III_gaus3_sc16_Mean_Freq	10.07+/-4.2(86)	11.79+/-3.6(46)	10.67+/-4.0(132)	0.020
TQ_III_gaus3_sc19_Shannon_Entropy	0.25+/-0.1(86)	0.21+/-0.1(46)	0.24+/-0.1(132)	0.021

TQ_II_gaus4_sc4_Mean_Freq	25.33+/-5.6(104)	27.58+/-6.1(54)	26.10+/-5.8(158)	0.021
TQ_III_gaus4_sc7_Shannon_Entropy	0.15+/-0.1(86)	0.19+/-0.1(46)	0.17+/-0.1(132)	0.026
TQ_III_gaus4_sc10_Mean_Freq	15.26+/-5.5(86)	17.80+/-5.4(46)	16.14+/-5.6(132)	0.012
TQ_III_gaus4_sc10_Median_Freq	11.69+/-3.1(86)	13.14+/-3.1(46)	12.19+/-3.2(132)	0.011
TQ_II_gaus4_sc13_Nonlinear_Energy	363.74+/-377.8(104)	255.49+/-181.6(54)	326.74+/-327.8(158)	0.049
TQ_II_gaus4_sc13_Mean_Freq	10.85+/-4.0(104)	12.53+/-4.7(54)	11.42+/-4.3(158)	0.019
TQ_II_gaus4_sc13_Median_Freq	8.56+/-1.9(104)	9.45+/-2.5(54)	8.86+/-2.2(158)	0.015
TQ_II_gaus4_sc16_Mean_Freq	8.46+/-3.1(104)	9.69+/-3.8(54)	8.88+/-3.4(158)	0.030
TQ_II_mexh_sc5_Energy	697.83+/-878.1(104)	446.13+/-435.6(54)	611.80+/-764.4(158)	0.049
TQ_III_mexh_sc5_Mean_Freq	14.88+/-6.1(86)	17.15+/-5.5(46)	15.67+/-6.0(132)	0.037

Postoperative Univariate Results

Preoperative Continuous Feature	Non-AF	AF	Total	p value
age	63.47+/-10.6(53)	72.59+/-6.9(27)	66.55+/-10.5(80)	0.000
c4_ectopicRatio	0.06+/-0.2(26)	0.31+/-0.4(14)	0.15+/-0.3(40)	0.006
c4_PVCRatio	0.05+/-0.2(26)	0.27+/-0.3(14)	0.13+/-0.3(40)	0.007
c2_RR_Chest_Peak_Freq_mean	0.98+/-0.7(28)	0.35+/-0.2(13)	0.78+/-0.7(41)	0.005
c3_PP_Atrial_Curve_length_kurtosis	2.99+/-0.9(29)	4.55+/-2.7(15)	3.52+/-1.8(44)	0.006
c3_PP_Chest_Energy_skewness	1.93+/-1.3(26)	3.91+/-2.5(14)	2.62+/-2.0(40)	0.002
c3_PP_Chest_Energy_kurtosis	10.09+/-7.4(26)	32.10+/-31.9(14)	17.80+/-22.1(40)	0.002
c1_PR_Chest_db2_sc5_Shannon_Entropy_max	0.37+/-0.0(25)	0.32+/-0.1(14)	0.35+/-0.1(39)	0.005
c2_PR_Chest_db2_sc5_Nonlinear_Energy_skewness	6.15+/-5.9(27)	1.48+/-2.1(14)	4.55+/-5.4(41)	0.006
c2_PR_Chest_db2_sc5_Shannon_Entropy_max	0.36+/-0.0(27)	0.30+/-0.1(14)	0.34+/-0.1(41)	0.004
c3_PP_Atrial_db2_sc5_Energy_skewness	0.43+/-0.4(29)	1.54+/-1.8(15)	0.81+/-1.2(44)	0.003
c3_PP_Atrial_db2_sc5_Katz_FD_skewness	0.53+/-0.4(29)	1.60+/-2.1(15)	0.89+/-1.3(44)	0.009
c3_PP_Atrial_db2_sc5_Nonlinear_Energy_skewness	0.49+/-0.4(29)	1.64+/-2.1(15)	0.88+/-1.4(44)	0.007
c3_PP_Atrial_db2_sc5_Peak_Freq_mean	18.54+/-4.3(29)	22.50+/-3.8(15)	19.89+/-4.5(44)	0.004
c3_PP_Atrial_db2_sc5_Curve_length_skewness	0.15+/-0.3(29)	0.61+/-0.8(15)	0.31+/-0.5(44)	0.007
c3_RP_Atrial_db2_sc5_Peak_Freq_skewness	-0.09+/-0.9(26)	-0.87+/-0.8(14)	-0.36+/-0.9(40)	0.008
c3_PR_Atrial_db2_sc5_Energy_skewness	0.61+/-0.6(26)	1.74+/-1.8(14)	1.01+/-1.3(40)	0.005
c3_PP_Atrial_db2_sc10_Katz_FD_kurtosis	3.98+/-2.6(29)	10.13+/-11.0(15)	6.08+/-7.2(44)	0.006
c4_RP_Atrial_db2_sc10_Peak_Freq_min	1.66+/-1.6(22)	0.35+/-0.7(13)	1.17+/-1.5(35)	0.009
c1_PR_Atrial_db2_sc15_Nonlinear_Energy_skewness	0.53+/-0.9(25)	-0.55+/-1.4(14)	0.14+/-1.2(39)	0.006
c3_PP_Atrial_db2_sc15_Katz_FD_kurtosis	4.08+/-2.5(29)	14.99+/-21.2(15)	7.80+/-13.4(44)	0.009
c1_PR_Atrial_db2_sc20_Nonlinear_Energy_skewness	0.47+/-0.8(25)	-0.44+/-1.2(14)	0.14+/-1.1(39)	0.008
c1_PR_Atrial_db2_sc20_Mean_Freq_kurtosis	8.02+/-9.1(25)	82.01+/-126.0(14)	34.58+/-82.3(39)	0.005
c1_PR_Atrial_db2_sc20_Peak_Pow_Amp_skewness	1.51+/-1.4(25)	0.27+/-0.9(14)	1.06+/-1.4(39)	0.007
c2_PR_Atrial_db2_sc20_Median_Freq_mean	7.10+/-3.0(27)	4.81+/-1.3(14)	6.32+/-2.7(41)	0.009
c2_PR_Atrial_db2_sc25_Median_Freq_mean	6.99+/-3.1(27)	4.58+/-1.2(14)	6.17+/-2.8(41)	0.008
c2_PR_Chest_db2_sc25_Peak_Freq_kurtosis	14.58+/-17.1(21)	127.87+/-188.7(10)	51.13+/-117.4(31)	0.009
c4_RP_Atrial_db2_sc25_Shannon_Entropy_skewness	-1.26+/-1.6(22)	0.18+/-1.3(13)	-0.72+/-1.6(35)	0.009
c2_PR_Atrial_db2_sc30_Peak_Freq_kurtosis	23.04+/-49.2(23)	153.31+/-186.5(12)	67.70+/-129.5(35)	0.003
c4_RP_Atrial_db2_sc30_Shannon_Entropy_skewness	-1.38+/-2.0(22)	0.48+/-1.3(13)	-0.69+/-1.9(35)	0.004
c4_PR_Atrial_db2_sc30_Shannon_Entropy_kurtosis	4.15+/-2.1(22)	12.34+/-13.3(13)	7.19+/-9.0(35)	0.007
c1_PR_Atrial_db3_sc5_Mean_Freq_min	12.07+/-2.3(25)	9.96+/-2.0(14)	11.31+/-2.4(39)	0.006
c1_PR_Atrial_db3_sc5_Peak_Freq_min	9.92+/-3.0(25)	7.21+/-2.7(14)	8.95+/-3.1(39)	0.008
c2_PR_Chest_db3_sc5_Nonlinear_Energy_skewness	6.12+/-5.8(27)	1.45+/-2.0(14)	4.53+/-5.3(41)	0.006
c3_PP_Atrial_db3_sc5_Energy_skewness	0.44+/-0.4(29)	1.51+/-1.8(15)	0.81+/-1.2(44)	0.003
c3_PP_Atrial_db3_sc5_Katz_FD_skewness	0.50+/-0.4(29)	1.63+/-2.1(15)	0.89+/-1.3(44)	0.006
c3_PP_Atrial_db3_sc5_Nonlinear_Energy_skewness	0.49+/-0.4(29)	1.66+/-2.1(15)	0.89+/-1.3(44)	0.005
c3_PP_Atrial_db3_sc5_Peak_Freq_mean	18.94+/-3.7(29)	22.28+/-3.5(15)	20.08+/-3.9(44)	0.006
c3_PR_Atrial_db3_sc5_Energy_skewness	0.63+/-0.6(26)	1.75+/-1.8(14)	1.02+/-1.2(40)	0.005
c1_PR_Atrial_db3_sc15_Curve_length_skewness	0.48+/-0.9(25)	-0.90+/-1.6(14)	-0.01+/-1.3(39)	0.001
c1_PR_Chest_db3_sc15_Peak_Freq_skewness	0.17+/-1.8(25)	-1.98+/-2.6(14)	-0.60+/-2.3(39)	0.004
c3_PP_Atrial_db3_sc15_Katz_FD_kurtosis	4.12+/-2.6(29)	17.78+/-27.2(15)	8.78+/-17.0(44)	0.010
c3_PP_Atrial_db3_sc15_Curve_length_kurtosis	4.18+/-2.2(29)	11.29+/-14.0(15)	6.60+/-8.9(44)	0.010
c1_PR_Atrial_db3_sc20_Nonlinear_Energy_skewness	0.75+/-1.0(25)	-0.42+/-1.2(14)	0.33+/-1.2(39)	0.003
c1_PR_Atrial_db3_sc20_Peak_Freq_kurtosis	25.99+/-34.8(24)	110.60+/-134.4(13)	55.72+/-92.0(37)	0.006
c1_PR_Atrial_db3_sc20_Curve_length_skewness	0.42+/-0.8(25)	-0.78+/-1.5(14)	-0.01+/-1.2(39)	0.002
c1_PR_Atrial_db3_sc25_Nonlinear_Energy_skewness	0.79+/-1.0(25)	-0.28+/-1.0(14)	0.40+/-1.1(39)	0.003
c1_PR_Atrial_db3_sc25_Peak_Freq_max	5.02+/-3.0(25)	2.50+/-2.1(14)	4.12+/-3.0(39)	0.009
c1_PR_Atrial_db3_sc25_Curve_length_skewness	0.30+/-0.8(25)	-0.55+/-1.1(14)	-0.00+/-1.0(39)	0.008
c2_PR_Chest_db3_sc25_Median_Freq_min	4.43+/-1.3(27)	6.19+/-2.7(14)	5.03+/-2.1(41)	0.007
c1_PR_Atrial_db3_sc30_Nonlinear_Energy_skewness	0.77+/-1.0(25)	-0.20+/-1.0(14)	0.42+/-1.1(39)	0.007
c4_PR_Chest_db3_sc30_Shannon_Entropy_skewness	-1.04+/-1.2(22)	-2.51+/-1.6(13)	-1.59+/-1.5(35)	0.003
c2_PR_Chest_sym4_sc5_Nonlinear_Energy_skewness	6.03+/-5.9(27)	1.47+/-2.1(14)	4.47+/-5.3(41)	0.008
c3_PP_Atrial_sym4_sc5_Energy_skewness	0.44+/-0.4(29)	1.50+/-1.8(15)	0.80+/-1.2(44)	0.003
c3_PP_Atrial_sym4_sc5_Katz_FD_skewness	0.48+/-0.3(29)	1.63+/-2.1(15)	0.87+/-1.3(44)	0.006
c3_PP_Atrial_sym4_sc5_Nonlinear_Energy_skewness	0.48+/-0.4(29)	1.65+/-2.1(15)	0.88+/-1.3(44)	0.005
c3_PP_Atrial_sym4_sc5_Curve_length_skewness	0.12+/-0.4(29)	0.62+/-0.8(15)	0.29+/-0.6(44)	0.009
c3_PR_Atrial_sym4_sc5_Energy_skewness	0.61+/-0.5(26)	1.73+/-1.8(14)	1.01+/-1.2(40)	0.005
c2_PR_Chest_sym4_sc10_Nonlinear_Energy_mean	0.00+/-0.0(26)	0.00+/-0.0(14)	0.00+/-0.0(40)	0.006
c1_PR_Atrial_sym4_sc15_Curve_length_skewness	0.53+/-0.9(25)	-0.90+/-1.8(14)	0.02+/-1.5(39)	0.002
c2_PR_Chest_sym4_sc15_Mean_Freq_min	4.92+/-1.0(27)	6.59+/-2.8(14)	5.49+/-2.0(41)	0.008
c2_PR_Chest_sym4_sc15_Median_Freq_min	5.83+/-1.7(27)	8.37+/-4.0(14)	6.70+/-2.9(41)	0.007
c1_PR_Atrial_sym4_sc20_Nonlinear_Energy_skewness	0.75+/-1.1(25)	-0.40+/-1.1(14)	0.34+/-1.2(39)	0.003
c1_PR_Atrial_sym4_sc20_Curve_length_skewness	0.40+/-0.8(25)	-0.77+/-1.5(14)	-0.02+/-1.2(39)	0.003
c2_PR_Atrial_sym4_sc20_Peak_Freq_skewness	0.76+/-3.7(27)	-4.30+/-5.5(14)	-0.97+/-5.0(41)	0.001
c2_PR_Chest_sym4_sc20_Mean_Freq_min	4.59+/-1.3(27)	6.13+/-2.3(14)	5.12+/-1.8(41)	0.009
c2_PR_Chest_sym4_sc20_Median_Freq_min	5.39+/-1.8(27)	7.98+/-3.5(14)	6.28+/-2.8(41)	0.004
c4_RP_Atrial_sym4_sc20_Peak_Freq_mean	3.52+/-1.1(22)	2.50+/-0.8(13)	3.14+/-1.1(35)	0.006
c1_RP_Atrial_sym4_sc25_Mean_Freq_max	5.97+/-1.6(25)	4.39+/-1.6(14)	5.41+/-1.8(39)	0.005
c1_RP_Atrial_sym4_sc25_Peak_Freq_max	4.62+/-1.3(25)	3.32+/-1.5(14)	4.15+/-1.5(39)	0.007
c1_PR_Atrial_sym4_sc25_Nonlinear_Energy_skewness	0.73+/-1.1(25)	-0.30+/-1.0(14)	0.36+/-1.2(39)	0.008

c2_PR_Atrial_sym4_sc25_Peak_Freq_skewness	1.24+/-5.4(24)	-3.50+/-4.4(14)	-0.50+/-5.5(38)	0.008
c3_RP_Atrial_sym4_sc30_Shannon_Entropy_std	0.04+/-0.0(26)	0.02+/-0.0(14)	0.03+/-0.0(40)	0.005
c4_RP_Atrial_sym4_sc30_Peak_Freq_mean	2.41+/-0.8(22)	1.45+/-1.2(13)	2.05+/-1.1(35)	0.007
c1_RP_Atrial_sym6_sc5_Shannon_Entropy_max	0.30+/-0.1(25)	0.21+/-0.1(14)	0.26+/-0.1(39)	0.009
c2_PR_Chest_sym6_sc5_Nonlinear_Energy_skewness	6.02+/-5.9(27)	1.45+/-2.0(14)	4.46+/-5.4(41)	0.008
c2_PR_Chest_sym6_sc5_Mean_Freq_std	2.59+/-1.2(27)	1.62+/-0.7(14)	2.26+/-1.1(41)	0.007
c2_PR_Chest_sym6_sc5_Peak_Freq_max	23.94+/-6.2(27)	18.14+/-5.0(14)	21.96+/-6.4(41)	0.004
c3_PP_Atrial_sym6_sc5_Energy_skewness	0.43+/-0.3(29)	1.49+/-1.8(15)	0.79+/-1.2(44)	0.003
c3_PP_Atrial_sym6_sc5_Katz_FD_skewness	0.47+/-0.4(29)	1.62+/-2.0(15)	0.86+/-1.3(44)	0.005
c3_PP_Atrial_sym6_sc5_Nonlinear_Energy_skewness	0.48+/-0.4(29)	1.65+/-2.0(15)	0.88+/-1.3(44)	0.004
c3_PP_Atrial_sym6_sc5_Curve_length_skewness	0.14+/-0.4(29)	0.65+/-0.8(15)	0.31+/-0.6(44)	0.005
c3_PR_Atrial_sym6_sc5_Energy_skewness	0.61+/-0.6(26)	1.76+/-1.8(14)	1.01+/-1.3(40)	0.004
c2_RP_Atrial_sym6_sc10_Mean_Freq_kurtosis	4.18+/-2.2(27)	11.55+/-10.7(14)	6.70+/-7.3(41)	0.001
c2_RP_Atrial_sym6_sc10_Median_Freq_kurtosis	4.07+/-3.1(27)	12.49+/-12.4(14)	6.95+/-8.5(41)	0.002
c3_RP_Atrial_sym6_sc10_Mean_Freq_min	7.00+/-1.3(26)	5.81+/-1.2(14)	6.59+/-1.3(40)	0.006
c1_PP_Atrial_sym6_sc15_Mean_Freq_min	4.41+/-0.9(28)	5.33+/-1.0(15)	4.73+/-1.0(43)	0.004
c1_RP_Atrial_sym6_sc15_Mean_Freq_min	4.50+/-1.1(25)	5.71+/-1.2(14)	4.94+/-1.3(39)	0.004
c1_RP_Atrial_sym6_sc15_Median_Freq_min	5.40+/-1.7(25)	7.18+/-2.3(14)	6.04+/-2.1(39)	0.010
c1_PR_Atrial_sym6_sc15_Spectral_entropy_skewness	0.98+/-1.2(25)	-0.13+/-1.0(14)	0.58+/-1.2(39)	0.005
c1_PR_Atrial_sym6_sc15_Curve_length_skewness	0.71+/-1.3(25)	-0.90+/-1.8(14)	0.13+/-1.7(39)	0.003
c4_PR_Chest_sym6_sc15_Peak_Freq_min	1.82+/-1.9(22)	0.15+/-0.6(13)	1.20+/-1.7(35)	0.004
c1_PR_Atrial_sym6_sc20_Nonlinear_Energy_skewness	0.79+/-1.1(25)	-0.36+/-1.1(14)	0.38+/-1.2(39)	0.003
c1_PR_Atrial_sym6_sc20_Curve_length_skewness	0.42+/-0.9(25)	-0.75+/-1.4(14)	-0.00+/-1.2(39)	0.003
c2_PR_Atrial_sym6_sc20_Peak_Freq_skewness	1.42+/-4.8(27)	-3.21+/-4.6(14)	-0.16+/-5.2(41)	0.005
c2_PR_Chest_sym6_sc20_Median_Freq_min	4.80+/-1.0(27)	6.69+/-2.7(14)	5.45+/-2.0(41)	0.002
c1_RP_Atrial_sym6_sc25_Mean_Freq_max	5.85+/-1.3(25)	4.57+/-1.6(14)	5.39+/-1.5(39)	0.009
c1_RP_Atrial_sym6_sc25_Median_Freq_max	8.30+/-2.2(25)	6.10+/-2.5(14)	7.51+/-2.5(39)	0.007
c1_PR_Atrial_sym6_sc25_Nonlinear_Energy_skewness	0.74+/-1.1(25)	-0.26+/-1.0(14)	0.38+/-1.1(39)	0.006
c3_RP_Atrial_sym6_sc25_Peak_Freq_min	1.23+/-1.1(26)	2.21+/-0.9(14)	1.58+/-1.1(40)	0.008
c1_RP_Atrial_sym6_sc30_Mean_Freq_max	5.22+/-1.1(25)	4.08+/-1.4(14)	4.81+/-1.3(39)	0.007
c1_RP_Atrial_sym6_sc30_Median_Freq_max	7.38+/-1.9(25)	5.40+/-2.6(14)	6.67+/-2.3(39)	0.010
c2_RP_Atrial_sym6_sc30_Shannon_Entropy_skewness	0.15+/-1.8(27)	-1.88+/-2.3(14)	-0.54+/-2.2(41)	0.003
c2_PP_Atrial_coif1_sc5_Peak_Freq_std	5.01+/-1.7(29)	6.44+/-1.5(15)	5.50+/-1.7(44)	0.007
c2_PR_Chest_coif1_sc5_Nonlinear_Energy_skewness	6.11+/-5.9(27)	1.48+/-2.1(14)	4.53+/-5.4(41)	0.007
c3_PP_Atrial_coif1_sc5_Energy_skewness	0.45+/-0.4(29)	1.50+/-1.8(15)	0.81+/-1.2(44)	0.004
c3_PP_Atrial_coif1_sc5_Katz_FD_skewness	0.53+/-0.4(29)	1.65+/-2.1(15)	0.91+/-1.4(44)	0.008
c3_PP_Atrial_coif1_sc5_Nonlinear_Energy_skewness	0.49+/-0.4(29)	1.64+/-2.1(15)	0.88+/-1.4(44)	0.007
c3_PP_Atrial_coif1_sc5_Peak_Freq_std	5.34+/-2.0(29)	7.13+/-1.4(15)	5.95+/-2.0(44)	0.003
c3_PR_Atrial_coif1_sc5_Energy_skewness	0.62+/-0.6(26)	1.73+/-1.7(14)	1.01+/-1.2(40)	0.005
c3_PR_Atrial_coif1_sc5_Spectral_entropy_skewness	1.30+/-1.8(26)	3.96+/-3.9(14)	2.23+/-2.9(40)	0.005
c2_RP_Atrial_coif1_sc10_Shannon_Entropy_kurtosis	5.21+/-4.8(27)	20.10+/-23.6(14)	10.30+/-15.7(41)	0.003
c2_PR_Chest_coif1_sc10_Nonlinear_Energy_mean	0.00+/-0.0(26)	0.00+/-0.0(14)	0.00+/-0.0(40)	0.007
c4_PP_Atrial_coif1_sc10_Peak_Freq_min	1.94+/-1.9(24)	0.43+/-0.7(14)	1.38+/-1.7(38)	0.007
c1_PR_Atrial_coif1_sc15_Nonlinear_Energy_skewness	0.48+/-0.8(25)	-0.55+/-1.4(14)	0.11+/-1.2(39)	0.007
c1_PR_Atrial_coif1_sc15_Curve_length_skewness	0.38+/-0.7(25)	-0.97+/-1.8(14)	-0.10+/-1.4(39)	0.002
c3_PP_Atrial_coif1_sc15_Katz_FD_kurtosis	3.92+/-2.2(29)	15.51+/-20.7(15)	7.87+/-13.2(44)	0.004
c3_PP_Atrial_coif1_sc15_Nonlinear_Energy_kurtosis	4.49+/-3.2(29)	17.75+/-26.0(15)	9.01+/-16.3(44)	0.009
c3_PP_Atrial_coif1_sc15_Peak_Freq_min	1.10+/-1.2(29)	0.23+/-0.5(15)	0.81+/-1.1(44)	0.008
c1_PR_Atrial_coif1_sc20_Nonlinear_Energy_skewness	0.48+/-0.8(25)	-0.43+/-1.2(14)	0.16+/-1.1(39)	0.008
c1_PR_Atrial_coif1_sc20_Curve_length_skewness	0.29+/-0.7(25)	-0.82+/-1.5(14)	-0.11+/-1.2(39)	0.004
c2_PR_Chest_coif1_sc20_Median_Freq_min	4.85+/-1.0(27)	6.72+/-2.9(14)	5.49+/-2.0(41)	0.004
c3_PP_Atrial_coif1_sc20_Katz_FD_kurtosis	4.49+/-3.0(29)	13.32+/-16.9(15)	7.50+/-10.8(44)	0.008
c3_PP_Atrial_coif1_sc20_Peak_Freq_min	1.16+/-1.2(29)	0.27+/-0.5(15)	0.85+/-1.1(44)	0.010
c4_PP_Atrial_coif1_sc20_Peak_Freq_mean	2.79+/-1.1(24)	1.64+/-1.1(14)	2.36+/-1.2(38)	0.004
c4_RP_Atrial_coif1_sc20_Peak_Freq_mean	2.87+/-2.2(22)	1.02+/-1.3(13)	2.19+/-2.1(35)	0.009
c1_RP_Atrial_coif1_sc25_Median_Freq_max	9.13+/-2.7(25)	6.55+/-2.8(14)	8.20+/-3.0(39)	0.007
c1_PR_Chest_coif1_sc25_Mean_Freq_skewness	1.36+/-2.3(25)	-0.72+/-2.1(14)	0.61+/-2.4(39)	0.009
c2_PR_Chest_coif1_sc25_Median_Freq_min	4.58+/-1.7(27)	6.85+/-3.2(14)	5.36+/-2.5(41)	0.005
c4_PP_Atrial_coif1_sc25_Peak_Freq_mean	2.33+/-1.1(24)	1.21+/-1.0(14)	1.92+/-1.1(38)	0.002
c4_RP_Atrial_coif1_sc25_Peak_Freq_mean	2.35+/-1.7(22)	0.89+/-1.3(13)	1.81+/-1.7(35)	0.010
c4_PR_Chest_coif1_sc25_Shannon_Entropy_skewness	-0.60+/-0.5(22)	-2.61+/-2.8(13)	-1.35+/-2.0(35)	0.002
c4_PP_Atrial_coif1_sc30_Peak_Freq_mean	2.06+/-1.0(24)	1.14+/-0.9(14)	1.72+/-1.1(38)	0.008
c2_PR_Chest_coif4_sc5_Nonlinear_Energy_skewness	6.00+/-5.9(27)	1.45+/-1.9(14)	4.45+/-5.4(41)	0.008
c3_PP_Atrial_coif4_sc5_Energy_skewness	0.42+/-0.4(29)	1.48+/-1.7(15)	0.78+/-1.2(44)	0.003
c3_PP_Atrial_coif4_sc5_Katz_FD_skewness	0.47+/-0.4(29)	1.61+/-2.0(15)	0.86+/-1.3(44)	0.004
c3_PP_Atrial_coif4_sc5_Nonlinear_Energy_skewness	0.48+/-0.4(29)	1.66+/-2.0(15)	0.88+/-1.3(44)	0.003
c3_PP_Atrial_coif4_sc5_Median_Freq_max	26.56+/-4.8(29)	30.52+/-3.6(15)	27.91+/-4.8(44)	0.008
c3_PP_Atrial_coif4_sc5_Curve_length_skewness	0.10+/-0.4(29)	0.59+/-0.7(15)	0.27+/-0.6(44)	0.006
c3_PR_Atrial_coif4_sc5_Energy_skewness	0.61+/-0.6(26)	1.77+/-1.8(14)	1.01+/-1.3(40)	0.004
c1_PP_Atrial_coif4_sc10_Mean_Freq_kurtosis	3.73+/-2.3(28)	6.83+/-4.4(15)	4.81+/-3.5(43)	0.004
c2_RP_Atrial_coif4_sc10_Mean_Freq_kurtosis	3.99+/-2.4(27)	8.61+/-8.1(14)	5.57+/-5.5(41)	0.008
c2_RP_Atrial_coif4_sc10_Median_Freq_kurtosis	3.67+/-2.8(27)	8.94+/-6.6(14)	5.47+/-5.0(41)	0.001
c2_PR_Chest_coif4_sc10_Mean_Freq_std	1.32+/-0.8(27)	0.68+/-0.4(14)	1.10+/-0.7(41)	0.007
c2_PR_Chest_coif4_sc10_Median_Freq_std	1.72+/-1.0(27)	0.97+/-0.3(14)	1.47+/-0.9(41)	0.010
c3_PP_Atrial_coif4_sc10_Peak_Freq_skewness	1.31+/-1.6(29)	-0.32+/-2.4(15)	0.76+/-2.0(44)	0.009
c3_RP_Atrial_coif4_sc10_Mean_Freq_min	7.40+/-1.4(26)	6.20+/-1.2(14)	6.98+/-1.4(40)	0.009
c1_PP_Atrial_coif4_sc15_Peak_Freq_min	3.39+/-0.6(28)	4.03+/-0.8(15)	3.62+/-0.7(43)	0.004
c1_PR_Atrial_coif4_sc15_Curve_length_skewness	0.71+/-1.4(25)	-0.82+/-1.7(14)	0.16+/-1.6(39)	0.004
c2_PR_Chest_coif4_sc15_Peak_Freq_skewness	0.01+/-1.8(27)	-1.68+/-1.9(14)	-0.56+/-2.0(41)	0.008
c1_PR_Atrial_coif4_sc20_Nonlinear_Energy_skewness	0.79+/-1.0(25)	-0.33+/-1.1(14)	0.39+/-1.2(39)	0.003
c1_PR_Atrial_coif4_sc20_Curve_length_skewness	0.41+/-0.9(25)	-0.75+/-1.4(14)	-0.01+/-1.2(39)	0.003
c1_RP_Atrial_coif4_sc25_Peak_Freq_std	0.47+/-0.4(25)	0.19+/-0.1(14)	0.37+/-0.3(39)	0.009
c1_PR_Atrial_coif4_sc25_Nonlinear_Energy_skewness	0.75+/-1.0(25)	-0.23+/-0.9(14)	0.40+/-1.1(39)	0.006
c1_PR_Atrial_coif4_sc25_Peak_Freq_kurtosis	24.22+/-35.5(23)	116.11+/-146.5(13)	57.41+/-100.8(36)	0.007
c1_PP_Atrial_coif4_sc30_Mean_Freq_skewness	-0.22+/-2.2(28)	2.75+/-5.0(15)	0.82+/-3.7(43)	0.010
c2_RP_Atrial_coif4_sc30_Shannon_Entropy_skewness	0.05+/-2.0(27)	-2.07+/-2.7(14)	-0.67+/-2.4(41)	0.007
c2_PR_Chest_coif4_sc30_Peak_Freq_std	0.93+/-0.6(27)	0.44+/-0.4(14)	0.76+/-0.6(41)	0.005
c3_PR_Chest_coif4_sc30_Spectral_entropy_kurtosis	4.49+/-2.6(26)	9.31+/-8.4(14)	6.18+/-5.8(40)	0.010
c2_PR_Chest_bior2.2_sc5_Nonlinear_Energy_skewness	6.20+/-5.3(27)	1.64+/-2.2(14)	4.64+/-4.9(41)	0.004
c2_PR_Chest_bior2.2_sc5_Median_Freq_std	3.47+/-0.8(27)	2.79+/-0.7(14)	3.24+/-0.8(41)	0.008
c3_PP_Atrial_bior2.2_sc5_Energy_skewness	0.55+/-0.3(29)	1.71+/-2.2(15)	0.95+/-1.4(44)	0.008
c3_PR_Atrial_bior2.2_sc5_Energy_skewness	0.68+/-0.4(26)	1.79+/-2.0(14)	1.07+/-1.3(40)	0.008
c2_PR_Atrial_bior2.2_sc10_Peak_Freq_std	1.22+/-0.9(27)	2.41+/-1.8(14)	1.63+/-1.4(41)	0.007

c3_PP_Atrial_bior2.2_sc10_Mean_Freq_skewness	0.33+/-0.9(29)	1.66+/-1.7(15)	0.79+/-1.4(44)	0.001
c3_PP_Atrial_bior2.2_sc10_Peak_Freq_min	3.97+/-2.4(29)	1.80+/-1.6(15)	3.23+/-2.4(44)	0.003
c3_RP_Atrial_bior2.2_sc10_Mean_Freq_skewness	0.16+/-0.6(26)	1.69+/-1.8(14)	0.70+/-1.3(40)	0.000
c3_RP_Atrial_bior2.2_sc10_Peak_Freq_skewness	0.19+/-1.1(26)	1.86+/-2.8(14)	0.77+/-2.0(40)	0.009
c3_PR_Atrial_bior2.2_sc10_Katz_FD_skewness	0.71+/-0.8(26)	1.97+/-1.9(14)	1.15+/-1.4(40)	0.005
c1_PR_Chest_bior2.2_sc15_Peak_Freq_skewness	0.08+/-1.9(25)	-2.28+/-3.4(14)	-0.77+/-2.8(39)	0.009
c3_PP_Atrial_bior2.2_sc15_Katz_FD_skewness	0.60+/-0.4(29)	1.63+/-1.5(15)	0.95+/-1.1(44)	0.002
c3_PP_Atrial_bior2.2_sc15_Nonlinear_Energy_skewness	0.48+/-0.5(29)	1.43+/-1.5(15)	0.80+/-1.0(44)	0.003
c3_PP_Atrial_bior2.2_sc15_Nonlinear_Energy_kurtosis	3.63+/-1.4(29)	12.34+/-14.7(15)	6.60+/-9.4(44)	0.003
c3_RP_Atrial_bior2.2_sc15_Katz_FD_skewness	0.68+/-0.5(26)	2.12+/-2.2(14)	1.18+/-1.5(40)	0.002
c3_PR_Atrial_bior2.2_sc15_Katz_FD_skewness	0.68+/-0.4(26)	1.87+/-1.7(14)	1.10+/-1.2(40)	0.002
c3_PR_Atrial_bior2.2_sc15_Katz_FD_kurtosis	3.64+/-1.0(26)	12.97+/-16.5(14)	6.91+/-10.6(40)	0.006
c4_PP_Atrial_bior2.2_sc15_Peak_Freq_min	2.75+/-1.9(24)	1.14+/-1.4(14)	2.16+/-1.9(38)	0.010
c3_PP_Atrial_bior2.2_sc20_Katz_FD_skewness	0.45+/-0.5(29)	1.65+/-2.1(15)	0.86+/-1.4(44)	0.005
c3_PP_Atrial_bior2.2_sc20_Nonlinear_Energy_skewness	0.43+/-0.6(29)	1.74+/-2.4(15)	0.88+/-1.6(44)	0.007
c3_PP_Atrial_bior2.2_sc20_Nonlinear_Energy_kurtosis	3.68+/-1.4(29)	17.86+/-28.1(15)	8.52+/-17.5(44)	0.009
c3_RP_Atrial_bior2.2_sc20_Katz_FD_skewness	0.63+/-0.6(26)	1.75+/-1.8(14)	1.02+/-1.3(40)	0.005
c3_PR_Atrial_bior2.2_sc20_Katz_FD_kurtosis	3.86+/-1.5(26)	12.32+/-15.9(14)	6.82+/-10.1(40)	0.010
c4_PP_Atrial_bior2.2_sc20_Peak_Freq_min	1.83+/-1.3(24)	0.50+/-0.8(14)	1.34+/-1.3(38)	0.002
c1_PR_Atrial_bior2.2_sc25_Peak_Freq_kurtosis	23.01+/-31.8(24)	129.61+/-173.3(12)	58.54+/-112.7(36)	0.006
c3_PP_Atrial_bior2.2_sc25_Katz_FD_skewness	0.53+/-0.4(29)	1.32+/-1.3(15)	0.80+/-0.9(44)	0.004
c3_PP_Atrial_bior2.2_sc25_Katz_FD_kurtosis	3.41+/-1.1(29)	10.52+/-14.2(15)	5.84+/-8.8(44)	0.010
c3_PP_Atrial_bior2.2_sc25_Nonlinear_Energy_kurtosis	3.74+/-1.5(29)	11.39+/-13.4(15)	6.35+/-8.5(44)	0.004
c3_PP_Atrial_bior2.2_sc25_Peak_Freq_min	1.53+/-1.2(29)	0.53+/-0.8(15)	1.19+/-1.2(44)	0.006
c3_RP_Atrial_bior2.2_sc25_Katz_FD_skewness	0.66+/-0.6(26)	1.57+/-1.3(14)	0.98+/-1.0(40)	0.003
c3_RP_Atrial_bior2.2_sc25_Katz_FD_kurtosis	4.02+/-1.7(26)	9.98+/-9.2(14)	6.11+/-6.2(40)	0.002
c1_RP_Atrial_bior2.2_sc30_Peak_Freq_kurtosis	20.27+/-42.2(25)	113.56+/-161.5(14)	53.76+/-110.0(39)	0.009
c2_PR_Chest_bior2.2_sc30_Mean_Freq_min	3.64+/-0.9(27)	4.61+/-1.4(14)	3.97+/-1.2(41)	0.010
c4_RP_Atrial_bior2.2_sc30_Median_Freq_min	4.40+/-1.8(22)	2.96+/-0.6(13)	3.86+/-1.6(35)	0.008
c4_RP_Atrial_bior2.2_sc30_Median_Freq_mean	6.61+/-2.5(22)	4.41+/-1.3(13)	5.79+/-2.4(35)	0.006
c4_RP_Atrial_bior2.2_sc30_Peak_Freq_mean	2.84+/-1.5(22)	1.37+/-1.4(13)	2.29+/-1.6(35)	0.008
c1_PP_Atrial_bior4.4_sc5_Peak_Freq_kurtosis	6.60+/-4.5(28)	12.82+/-7.3(15)	8.77+/-6.3(43)	0.001
c2_PR_Atrial_bior4.4_sc5_Peak_Freq_skewness	0.32+/-1.3(27)	1.33+/-0.5(14)	0.66+/-1.2(41)	0.009
c2_PR_Chest_bior4.4_sc5_Nonlinear_Energy_skewness	6.09+/-5.7(27)	1.48+/-2.1(14)	4.52+/-5.2(41)	0.006
c3_PP_Atrial_bior4.4_sc5_Energy_skewness	0.46+/-0.3(29)	1.57+/-2.0(15)	0.84+/-1.3(44)	0.005
c3_PP_Atrial_bior4.4_sc5_Katz_FD_skewness	0.53+/-0.4(29)	1.68+/-2.2(15)	0.92+/-1.4(44)	0.008
c3_PP_Atrial_bior4.4_sc5_Nonlinear_Energy_skewness	0.51+/-0.4(29)	1.71+/-2.2(15)	0.92+/-1.4(44)	0.006
c3_PP_Atrial_bior4.4_sc5_Mean_Freq_max	29.08+/-5.7(29)	33.70+/-3.8(15)	30.66+/-5.6(44)	0.008
c3_PP_Atrial_bior4.4_sc5_Mean_Freq_mean	19.77+/-3.9(29)	23.11+/-3.1(15)	20.91+/-3.9(44)	0.006
c3_PR_Atrial_bior4.4_sc5_Energy_skewness	0.62+/-0.5(26)	1.75+/-1.9(14)	1.02+/-1.3(40)	0.007
c4_PP_Atrial_bior4.4_sc10_Peak_Freq_min	5.08+/-1.3(24)	3.71+/-1.3(14)	4.58+/-1.4(38)	0.004
c1_PR_Atrial_bior4.4_sc15_Nonlinear_Energy_skewness	0.80+/-1.4(25)	-0.57+/-1.5(14)	0.31+/-1.6(39)	0.007
c1_PR_Atrial_bior4.4_sc15_Curve_length_skewness	0.46+/-0.8(25)	-0.88+/-1.8(14)	-0.02+/-1.4(39)	0.002
c1_PR_Chest_bior4.4_sc15_Peak_Freq_std	0.57+/-0.3(25)	1.25+/-1.0(14)	0.81+/-0.7(39)	0.003
c3_PP_Atrial_bior4.4_sc15_Katz_FD_kurtosis	4.10+/-2.7(29)	17.69+/-26.4(15)	8.74+/-16.6(44)	0.008
c3_PP_Atrial_bior4.4_sc15_Curve_length_kurtosis	4.26+/-2.2(29)	13.18+/-17.7(15)	7.30+/-11.1(44)	0.010
c4_PR_Chest_bior4.4_sc15_Shannon_Entropy_skewness	-0.43+/-1.1(22)	-1.89+/-1.9(13)	-0.97+/-1.6(35)	0.008
c1_PR_Atrial_bior4.4_sc20_Nonlinear_Energy_skewness	0.72+/-1.0(25)	-0.40+/-1.1(14)	0.31+/-1.2(39)	0.003
c1_PR_Atrial_bior4.4_sc20_Curve_length_skewness	0.41+/-0.8(25)	-0.81+/-1.6(14)	-0.03+/-1.3(39)	0.002
c2_PR_Chest_bior4.4_sc20_Median_Freq_min	4.97+/-0.9(27)	6.68+/-2.7(14)	5.55+/-1.9(41)	0.004
c1_PR_Atrial_bior4.4_sc25_Nonlinear_Energy_skewness	0.72+/-1.1(25)	-0.29+/-1.0(14)	0.36+/-1.1(39)	0.006
c1_PR_Atrial_bior4.4_sc25_Peak_Freq_kurtosis	20.94+/-34.0(23)	152.42+/-175.3(13)	68.42+/-124.0(36)	0.001
c1_PR_Atrial_bior4.4_sc25_Curve_length_skewness	0.30+/-0.8(25)	-0.68+/-1.2(14)	-0.05+/-1.1(39)	0.006
c2_RP_Atrial_bior4.4_sc25_Shannon_Entropy_kurtosis	4.79+/-4.4(27)	14.74+/-15.1(14)	8.19+/-10.5(41)	0.003
c2_PR_Chest_bior4.4_sc25_Median_Freq_min	4.34+/-1.1(27)	6.04+/-2.4(14)	4.92+/-1.8(41)	0.004
c1_RP_Atrial_bior4.4_sc30_Mean_Freq_std	0.45+/-0.3(25)	0.22+/-0.2(14)	0.37+/-0.3(39)	0.008
c1_RP_Atrial_bior4.4_sc30_Median_Freq_max	7.99+/-2.4(25)	5.62+/-2.7(14)	7.14+/-2.7(39)	0.008
c1_RP_Atrial_bior4.4_sc30_Peak_Freq_max	4.38+/-1.0(25)	3.39+/-1.2(14)	4.03+/-1.1(39)	0.008
c2_PP_Atrial_bior4.4_sc30_Shannon_Entropy_kurtosis	4.29+/-3.0(29)	8.80+/-8.0(15)	5.83+/-5.6(44)	0.009
c2_PR_Chest_bior4.4_sc30_Median_Freq_std	1.06+/-0.5(27)	0.62+/-0.5(14)	0.91+/-0.5(41)	0.008
c3_PP_Atrial_bior5.5_sc5_Energy_skewness	0.43+/-0.4(29)	1.46+/-1.7(15)	0.78+/-1.1(44)	0.003
c3_PP_Atrial_bior5.5_sc5_Katz_FD_skewness	0.49+/-0.3(29)	1.62+/-2.1(15)	0.87+/-1.3(44)	0.005
c3_PP_Atrial_bior5.5_sc5_Nonlinear_Energy_skewness	0.48+/-0.4(29)	1.61+/-2.0(15)	0.86+/-1.3(44)	0.004
c3_PP_Atrial_bior5.5_sc5_Mean_Freq_max	23.49+/-4.6(29)	27.78+/-5.5(15)	24.95+/-5.3(44)	0.009
c3_PP_Atrial_bior5.5_sc5_Mean_Freq_mean	16.21+/-2.7(29)	18.69+/-2.6(15)	17.06+/-2.9(44)	0.005
c3_PP_Atrial_bior5.5_sc5_Median_Freq_max	24.98+/-4.1(29)	28.83+/-4.2(15)	26.29+/-4.5(44)	0.005
c3_PP_Atrial_bior5.5_sc5_Median_Freq_mean	18.37+/-3.3(29)	21.37+/-2.8(15)	19.39+/-3.4(44)	0.004
c3_PR_Atrial_bior5.5_sc5_Energy_skewness	0.61+/-0.6(26)	1.73+/-1.8(14)	1.00+/-1.2(40)	0.005
c4_PP_Atrial_bior5.5_sc5_Mean_Freq_max	22.30+/-3.7(24)	26.40+/-3.8(14)	23.81+/-4.2(38)	0.002
c1_PP_Atrial_bior5.5_sc9_Mean_Freq_kurtosis	3.88+/-2.5(28)	7.42+/-6.0(15)	5.12+/-4.3(43)	0.009
c1_PP_Atrial_bior5.5_sc9_Median_Freq_kurtosis	3.53+/-2.3(28)	7.18+/-5.9(15)	4.81+/-4.2(43)	0.006
c1_RP_Atrial_bior5.5_sc9_Median_Freq_kurtosis	3.31+/-1.5(25)	7.36+/-7.2(14)	4.77+/-4.8(39)	0.010
c1_PR_Atrial_bior5.5_sc9_Shannon_Entropy_kurtosis	3.16+/-1.7(25)	5.55+/-3.6(14)	4.02+/-2.8(39)	0.009
c2_PR_Chest_bior5.5_sc9_Mean_Freq_std	1.32+/-1.0(27)	0.58+/-0.2(14)	1.07+/-0.9(41)	0.007
c2_PR_Chest_bior5.5_sc9_Median_Freq_max	19.77+/-4.9(27)	15.18+/-4.6(14)	18.20+/-5.2(41)	0.006
c3_PP_Atrial_bior5.5_sc9_Mean_Freq_min	7.58+/-1.0(29)	6.65+/-1.0(15)	7.26+/-1.1(44)	0.004
c4_RP_Atrial_bior5.5_sc9_Curve_length_kurtosis	3.75+/-1.8(22)	7.36+/-5.8(13)	5.09+/-4.1(35)	0.010
c1_PR_Atrial_bior5.5_sc13_Curve_length_skewness	0.62+/-1.2(25)	-0.87+/-2.0(14)	0.08+/-1.7(39)	0.006
c1_PP_Atrial_bior5.5_sc17_Mean_Freq_min	3.97+/-0.8(28)	4.63+/-0.7(15)	4.20+/-0.8(43)	0.010
c1_PP_Atrial_bior5.5_sc17_Peak_Freq_mean	3.97+/-0.6(28)	4.55+/-0.6(15)	4.17+/-0.6(43)	0.004
c1_RP_Atrial_bior5.5_sc17_Mean_Freq_min	4.03+/-0.9(25)	4.85+/-0.9(14)	4.33+/-0.9(39)	0.007
c1_PR_Atrial_bior5.5_sc17_Nonlinear_Energy_skewness	0.78+/-1.3(25)	-0.46+/-1.2(14)	0.33+/-1.4(39)	0.005
c1_PR_Atrial_bior5.5_sc17_Curve_length_skewness	0.52+/-1.0(25)	-0.88+/-1.7(14)	0.01+/-1.4(39)	0.002
c2_PR_Atrial_bior5.5_sc17_Peak_Freq_kurtosis	15.75+/-20.0(26)	72.73+/-95.1(14)	35.69+/-63.5(40)	0.005
c1_PR_Atrial_bior5.5_sc21_Nonlinear_Energy_skewness	0.68+/-1.0(25)	-0.37+/-1.1(14)	0.30+/-1.1(39)	0.005
c1_PR_Atrial_bior5.5_sc21_Curve_length_skewness	0.36+/-0.8(25)	-0.77+/-1.4(14)	-0.05+/-1.2(39)	0.004
c2_PR_Chest_bior5.5_sc21_Median_Freq_min	4.51+/-0.8(27)	6.01+/-2.4(14)	5.02+/-1.7(41)	0.005
c1_PR_Atrial_bior5.5_sc25_Nonlinear_Energy_skewness	0.71+/-1.1(25)	-0.29+/-1.0(14)	0.35+/-1.2(39)	0.009
c1_PR_Atrial_bior5.5_sc25_Peak_Freq_kurtosis	22.90+/-36.8(23)	149.74+/-158.7(12)	66.39+/-113.0(35)	0.001
c2_PP_Atrial_bior6.8_sc5_Peak_Freq_max	27.55+/-5.6(29)	32.30+/-2.2(15)	29.17+/-5.2(44)	0.003
c2_PR_Chest_bior6.8_sc5_Nonlinear_Energy_skewness	6.01+/-5.7(27)	1.48+/-2.1(14)	4.46+/-5.2(41)	0.007
c3_PP_Atrial_bior6.8_sc5_Energy_skewness	0.45+/-0.3(29)	1.54+/-1.9(15)	0.82+/-1.2(44)	0.004
c3_PP_Atrial_bior6.8_sc5_Katz_FD_skewness	0.49+/-0.4(29)	1.64+/-2.1(15)	0.89+/-1.4(44)	0.006

c3_PP_Atrial_bior6.8_sc5_Nonlinear_Energy_skewness	0.51+/-0.4(29)	1.70+/-2.1(15)	0.91+/-1.4(44)	0.004
c3_PP_Atrial_bior6.8_sc5_Mean_Freq_max	26.93+/-5.2(29)	31.49+/-3.7(15)	28.48+/-5.2(44)	0.005
c3_PP_Atrial_bior6.8_sc5_Median_Freq_max	27.70+/-4.6(29)	31.55+/-3.7(15)	29.01+/-4.7(44)	0.008
c3_PP_Atrial_bior6.8_sc5_Peak_Freq_std	4.01+/-1.7(29)	5.30+/-1.0(15)	4.45+/-1.6(44)	0.009
c3_PP_Atrial_bior6.8_sc5_Curve_length_skewness	0.13+/-0.4(29)	0.61+/-0.8(15)	0.29+/-0.6(44)	0.008
c3_RP_Atrial_bior6.8_sc5_Peak_Freq_std	4.55+/-1.5(26)	5.86+/-1.3(14)	5.01+/-1.5(40)	0.008
c3_PR_Atrial_bior6.8_sc5_Energy_skewness	0.62+/-0.5(26)	1.77+/-1.9(14)	1.02+/-1.3(40)	0.006
c3_PR_Atrial_bior6.8_sc10_Mean_Freq_kurtosis	4.53+/-2.6(26)	8.26+/-5.6(14)	5.84+/-4.3(40)	0.007
c1_PP_Atrial_bior6.8_sc15_Peak_Freq_min	3.29+/-0.7(28)	4.00+/-0.8(15)	3.53+/-0.8(43)	0.005
c1_PR_Atrial_bior6.8_sc15_Curve_length_skewness	0.73+/-1.4(25)	-0.81+/-1.7(14)	0.18+/-1.7(39)	0.004
c1_PR_Atrial_bior6.8_sc20_Nonlinear_Energy_skewness	0.85+/-1.2(25)	-0.34+/-1.1(14)	0.43+/-1.3(39)	0.004
c1_PR_Atrial_bior6.8_sc20_Curve_length_skewness	0.45+/-0.9(25)	-0.75+/-1.5(14)	0.02+/-1.3(39)	0.003
c2_PR_Chest_bior6.8_sc20_Median_Freq_min	4.87+/-0.9(27)	6.60+/-2.6(14)	5.46+/-1.9(41)	0.003
c1_PR_Atrial_bior6.8_sc25_Nonlinear_Energy_skewness	0.74+/-1.0(25)	-0.25+/-1.0(14)	0.39+/-1.1(39)	0.005
c2_PR_Chest_bior6.8_sc25_Median_Freq_min	4.29+/-1.3(27)	6.07+/-2.6(14)	4.90+/-2.0(41)	0.006
c1_PP_Atrial_bior6.8_sc30_Mean_Freq_std	0.35+/-0.2(28)	0.18+/-0.1(15)	0.29+/-0.2(43)	0.007
c1_RP_Atrial_bior6.8_sc30_Peak_Freq_max	4.26+/-0.9(25)	3.36+/-1.1(14)	3.94+/-1.1(39)	0.009
c1_PR_Atrial_bior6.8_sc30_Peak_Freq_max	4.96+/-2.5(25)	2.82+/-2.0(14)	4.19+/-2.5(39)	0.009
c2_RP_Atrial_bior6.8_sc30_Shannon_Entropy_skewness	0.01+/-1.5(27)	-2.37+/-3.5(14)	-0.80+/-2.6(41)	0.004
c2_RP_Atrial_bior6.8_sc30_Shannon_Entropy_kurtosis	5.15+/-7.3(27)	26.44+/-38.0(14)	12.42+/-24.6(41)	0.007
c2_PR_Chest_bior6.8_sc30_Median_Freq_std	1.14+/-0.5(27)	0.62+/-0.5(14)	0.96+/-0.6(41)	0.005
c3_PP_Atrial_rbio2.2_sc5_Energy_skewness	0.38+/-0.6(29)	1.40+/-1.7(15)	0.73+/-1.2(44)	0.006
c3_PP_Atrial_rbio2.2_sc5_Katz_FD_skewness	0.44+/-0.4(29)	1.44+/-1.7(15)	0.78+/-1.2(44)	0.005
c3_PP_Atrial_rbio2.2_sc5_Nonlinear_Energy_skewness	0.42+/-0.5(29)	1.42+/-1.8(15)	0.76+/-1.2(44)	0.006
c3_PP_Atrial_rbio2.2_sc5_Curve_length_skewness	0.07+/-0.4(29)	0.59+/-0.8(15)	0.25+/-0.6(44)	0.008
c3_RP_Atrial_rbio2.2_sc5_Peak_Freq_kurtosis	4.66+/-2.7(26)	11.46+/-11.9(14)	7.04+/-7.9(40)	0.008
c1_PR_Chest_rbio2.2_sc9_Peak_Freq_std	0.73+/-0.6(25)	1.51+/-1.0(14)	1.01+/-0.8(39)	0.003
c2_PR_Chest_rbio2.2_sc9_Nonlinear_Energy_mean	0.00+/-0.0(26)	0.00+/-0.0(14)	0.00+/-0.0(40)	0.010
c3_PP_Atrial_rbio2.2_sc9_Peak_Freq_min	1.24+/-1.3(29)	0.17+/-0.4(15)	0.88+/-1.2(44)	0.004
c1_PR_Atrial_rbio2.2_sc13_Nonlinear_Energy_skewness	0.76+/-1.4(25)	-0.50+/-1.3(14)	0.30+/-1.5(39)	0.009
c1_PR_Atrial_rbio2.2_sc13_Curve_length_skewness	0.49+/-0.9(25)	-0.87+/-1.5(14)	0.00+/-1.3(39)	0.001
c3_PP_Atrial_rbio2.2_sc13_Katz_FD_kurtosis	4.34+/-2.9(29)	18.63+/-26.9(15)	9.21+/-17.0(44)	0.007
c3_PP_Atrial_rbio2.2_sc13_Peak_Freq_mean	2.95+/-1.7(29)	1.70+/-0.9(15)	2.53+/-1.6(44)	0.010
c4_PP_Atrial_rbio2.2_sc13_Peak_Freq_mean	2.97+/-1.2(24)	1.75+/-1.1(14)	2.52+/-1.3(38)	0.004
c4_RP_Atrial_rbio2.2_sc13_Peak_Freq_mean	2.69+/-1.8(22)	1.11+/-1.3(13)	2.11+/-1.8(35)	0.010
c4_PR_Atrial_rbio2.2_sc13_Peak_Freq_max	7.59+/-4.5(22)	3.42+/-3.6(13)	6.04+/-4.6(35)	0.008
c1_PR_Atrial_rbio2.2_sc17_Nonlinear_Energy_skewness	0.64+/-1.1(25)	-0.42+/-1.1(14)	0.26+/-1.2(39)	0.006
c1_PR_Atrial_rbio2.2_sc17_Curve_length_skewness	0.36+/-0.8(25)	-0.72+/-1.3(14)	-0.03+/-1.2(39)	0.004
c2_PR_Chest_rbio2.2_sc17_Median_Freq_min	4.69+/-1.3(27)	6.84+/-3.2(14)	5.42+/-2.3(41)	0.004
c3_PR_Chest_rbio2.2_sc17_Shannon_Entropy_std	0.01+/-0.0(26)	0.03+/-0.0(14)	0.02+/-0.0(40)	0.003
c4_PP_Atrial_rbio2.2_sc17_Peak_Freq_mean	2.40+/-1.1(24)	1.20+/-0.9(14)	1.96+/-1.1(38)	0.001
c4_RP_Atrial_rbio2.2_sc17_Peak_Freq_mean	2.28+/-1.6(22)	0.84+/-1.1(13)	1.75+/-1.6(35)	0.007
c2_PR_Chest_rbio2.2_sc21_Median_Freq_min	4.56+/-1.9(27)	6.90+/-3.4(14)	5.36+/-2.7(41)	0.007
c2_PR_Chest_rbio2.2_sc21_Shannon_Entropy_mean	0.34+/-0.0(27)	0.30+/-0.1(14)	0.32+/-0.0(41)	0.008
c3_PR_Atrial_rbio2.2_sc21_Median_Freq_kurtosis	5.72+/-8.3(26)	22.47+/-27.1(14)	11.58+/-18.8(40)	0.006
c4_PP_Atrial_rbio2.2_sc21_Peak_Freq_mean	2.08+/-1.0(24)	1.06+/-0.8(14)	1.70+/-1.1(38)	0.003
c4_RP_Atrial_rbio2.2_sc21_Peak_Freq_mean	1.98+/-1.4(22)	0.77+/-1.0(13)	1.53+/-1.4(35)	0.009
c2_PR_Chest_rbio2.2_sc25_Shannon_Entropy_max	0.37+/-0.0(27)	0.34+/-0.0(14)	0.36+/-0.0(41)	0.007
c3_PR_Atrial_rbio2.2_sc25_Mean_Freq_skewness	0.65+/-1.8(26)	3.77+/-5.1(14)	1.74+/-3.6(40)	0.007
c1_PP_Atrial_rbio4.4_sc5_Peak_Freq_min	8.05+/-1.9(28)	6.00+/-3.1(15)	7.34+/-2.5(43)	0.010
c3_PP_Atrial_rbio4.4_sc5_Energy_skewness	0.42+/-0.4(29)	1.42+/-1.6(15)	0.76+/-1.1(44)	0.004
c3_PP_Atrial_rbio4.4_sc5_Katz_FD_skewness	0.45+/-0.4(29)	1.55+/-1.9(15)	0.82+/-1.3(44)	0.004
c3_PP_Atrial_rbio4.4_sc5_Nonlinear_Energy_skewness	0.44+/-0.4(29)	1.57+/-1.9(15)	0.83+/-1.3(44)	0.003
c3_PP_Atrial_rbio4.4_sc5_Curve_length_skewness	0.09+/-0.4(29)	0.63+/-0.9(15)	0.27+/-0.7(44)	0.008
c3_PR_Atrial_rbio4.4_sc5_Energy_skewness	0.61+/-0.7(26)	1.73+/-1.7(14)	1.00+/-1.3(40)	0.005
c1_PP_Atrial_rbio4.4_sc10_Peak_Freq_min	3.20+/-1.1(28)	4.10+/-0.9(15)	3.51+/-1.1(43)	0.009
c2_PR_Chest_rbio4.4_sc10_Nonlinear_Energy_mean	0.00+/-0.0(26)	0.00+/-0.0(14)	0.00+/-0.0(40)	0.010
c1_PR_Atrial_rbio4.4_sc15_Spectral_entropy_skewness	0.67+/-0.9(25)	-0.15+/-0.8(14)	0.38+/-0.9(39)	0.008
c1_PR_Atrial_rbio4.4_sc15_Curve_length_skewness	0.64+/-1.2(25)	-0.84+/-1.7(14)	0.11+/-1.5(39)	0.003
c1_PR_Atrial_rbio4.4_sc20_Nonlinear_Energy_skewness	0.75+/-1.1(25)	-0.35+/-1.1(14)	0.35+/-1.2(39)	0.004
c1_PR_Atrial_rbio4.4_sc20_Curve_length_skewness	0.35+/-0.8(25)	-0.73+/-1.4(14)	-0.04+/-1.2(39)	0.004
c2_PR_Atrial_rbio4.4_sc20_Peak_Freq_skewness	1.23+/-3.8(26)	-2.77+/-3.7(13)	-0.10+/-4.1(39)	0.003
c2_PR_Chest_rbio4.4_sc20_Median_Freq_min	4.88+/-1.4(27)	7.04+/-3.0(14)	5.62+/-2.3(41)	0.003
c1_PR_Atrial_rbio4.4_sc25_Nonlinear_Energy_skewness	0.74+/-1.2(25)	-0.27+/-1.0(14)	0.38+/-1.2(39)	0.010
c1_PR_Atrial_rbio4.4_sc25_Peak_Freq_max	5.02+/-2.7(25)	2.61+/-2.5(14)	4.15+/-2.9(39)	0.010
c1_RP_Atrial_rbio4.4_sc30_Peak_Freq_std	0.55+/-0.5(25)	0.19+/-0.1(14)	0.42+/-0.4(39)	0.010
c1_RP_Atrial_rbio4.4_sc30_Peak_Freq_kurtosis	34.61+/-62.6(22)	146.55+/-149.2(11)	71.92+/-111.4(33)	0.005
c4_PP_Atrial_rbio4.4_sc30_Peak_Freq_mean	2.28+/-0.7(24)	1.53+/-0.8(14)	2.00+/-0.8(38)	0.004
c2_PR_Chest_rbio5.5_sc5_Nonlinear_Energy_skewness	6.11+/-5.7(27)	1.49+/-2.1(14)	4.53+/-5.2(41)	0.006
c2_PR_Chest_rbio5.5_sc5_Mean_Freq_std	3.28+/-1.4(27)	2.06+/-0.8(14)	2.86+/-1.4(41)	0.005
c2_PR_Chest_rbio5.5_sc5_Median_Freq_std	2.94+/-1.1(27)	2.02+/-0.4(14)	2.63+/-1.1(41)	0.006
c2_PR_Chest_rbio5.5_sc5_Peak_Freq_max	26.35+/-6.7(27)	18.96+/-9.1(14)	23.83+/-8.3(41)	0.005
c3_PP_Atrial_rbio5.5_sc5_Energy_skewness	0.44+/-0.4(29)	1.52+/-1.8(15)	0.81+/-1.2(44)	0.004
c3_PP_Atrial_rbio5.5_sc5_Katz_FD_skewness	0.48+/-0.4(29)	1.60+/-2.1(15)	0.86+/-1.3(44)	0.006
c3_PP_Atrial_rbio5.5_sc5_Nonlinear_Energy_skewness	0.49+/-0.4(29)	1.69+/-2.1(15)	0.90+/-1.4(44)	0.004
c3_PP_Atrial_rbio5.5_sc5_Curve_length_skewness	0.14+/-0.4(29)	0.68+/-0.9(15)	0.33+/-0.6(44)	0.007
c3_PR_Atrial_rbio5.5_sc5_Energy_skewness	0.62+/-0.5(26)	1.76+/-1.8(14)	1.02+/-1.3(40)	0.005
c1_PP_Atrial_rbio5.5_sc10_Peak_Freq_skewness	-0.13+/-2.2(27)	1.83+/-2.1(15)	0.57+/-2.3(42)	0.007
c2_PP_Atrial_rbio5.5_sc10_Peak_Freq_skewness	0.28+/-1.9(29)	2.55+/-3.7(15)	1.05+/-2.8(44)	0.010
c2_RP_Atrial_rbio5.5_sc10_Peak_Freq_skewness	0.36+/-1.7(27)	3.12+/-3.7(14)	1.30+/-2.8(41)	0.002
c3_RP_Atrial_rbio5.5_sc10_Shannon_Entropy_std	0.04+/-0.0(26)	0.07+/-0.0(14)	0.05+/-0.0(40)	0.002
c4_RP_Atrial_rbio5.5_sc10_Curve_length_kurtosis	3.45+/-1.6(22)	6.32+/-4.2(13)	4.52+/-3.1(35)	0.007
c1_PR_Atrial_rbio5.5_sc15_Spectral_entropy_skewness	0.80+/-1.0(25)	-0.10+/-0.9(14)	0.48+/-1.0(39)	0.007
c1_PR_Atrial_rbio5.5_sc15_Curve_length_skewness	0.73+/-1.4(25)	-0.88+/-1.8(14)	0.15+/-1.7(39)	0.003
c3_PR_Chest_rbio5.5_sc15_Peak_Freq_std	0.67+/-0.4(26)	1.64+/-1.7(14)	1.01+/-1.2(40)	0.009
c1_PR_Atrial_rbio5.5_sc20_Nonlinear_Energy_skewness	0.83+/-1.1(25)	-0.34+/-1.1(14)	0.41+/-1.2(39)	0.003
c1_PR_Atrial_rbio5.5_sc20_Curve_length_skewness	0.42+/-0.9(25)	-0.72+/-1.4(14)	0.01+/-1.2(39)	0.004
c2_PR_Chest_rbio5.5_sc20_Median_Freq_min	4.92+/-1.1(27)	6.93+/-2.8(14)	5.61+/-2.0(41)	0.002
c4_RP_Atrial_rbio5.5_sc20_Peak_Freq_mean	3.89+/-1.4(22)	2.68+/-0.8(13)	3.44+/-1.3(35)	0.008
c1_PP_Atrial_rbio5.5_sc25_Peak_Freq_max	4.86+/-0.8(28)	3.83+/-1.1(15)	4.50+/-1.1(43)	0.002
c1_RP_Atrial_rbio5.5_sc25_Peak_Freq_max	5.08+/-1.1(25)	3.50+/-1.3(14)	4.51+/-1.4(39)	0.000
c1_PR_Atrial_rbio5.5_sc25_Nonlinear_Energy_skewness	0.76+/-1.1(25)	-0.26+/-1.0(14)	0.40+/-1.1(39)	0.006
c1_PR_Atrial_rbio5.5_sc25_Peak_Freq_kurtosis	36.54+/-58.7(24)	172.79+/-176.5(11)	79.36+/-124.9(35)	0.002

c1_PP_Atrial_rbio5.5_sc30_Mean_Freq_max	4.91+/-1.0(28)	3.97+/-1.1(15)	4.58+/-1.1(43)	0.007
c1_PP_Atrial_rbio5.5_sc30_Median_Freq_max	6.66+/-2.0(28)	4.74+/-2.0(15)	5.99+/-2.2(43)	0.005
c1_RP_Atrial_rbio5.5_sc30_Median_Freq_max	7.48+/-2.2(25)	5.34+/-2.6(14)	6.71+/-2.5(39)	0.008
c2_PP_Atrial_rbio5.5_sc30_Shannon_Entropy_kurtosis	5.43+/-5.3(29)	12.75+/-12.0(15)	7.93+/-8.8(44)	0.007
c2_PR_Chest_rbio5.5_sc30_Peak_Freq_std	0.89+/-0.6(27)	0.42+/-0.4(14)	0.73+/-0.6(41)	0.009
c4_RP_Atrial_rbio5.5_sc30_Peak_Freq_mean	2.51+/-1.0(22)	1.33+/-1.2(13)	2.07+/-1.2(35)	0.003
c1_RP_Atrial_rbio6.8_sc5_Shannon_Entropy_max	0.30+/-0.1(25)	0.21+/-0.1(14)	0.27+/-0.1(39)	0.003
c2_PR_Chest_rbio6.8_sc5_Nonlinear_Energy_skewness	6.03+/-6.1(27)	1.44+/-1.9(14)	4.46+/-5.5(41)	0.010
c3_PP_Atrial_rbio6.8_sc5_Energy_skewness	0.40+/-0.4(29)	1.42+/-1.6(15)	0.75+/-1.1(44)	0.002
c3_PP_Atrial_rbio6.8_sc5_Katz_FD_skewness	0.44+/-0.4(29)	1.57+/-1.9(15)	0.83+/-1.3(44)	0.004
c3_PP_Atrial_rbio6.8_sc5_Nonlinear_Energy_skewness	0.45+/-0.4(29)	1.60+/-1.9(15)	0.84+/-1.2(44)	0.002
c3_PP_Atrial_rbio6.8_sc5_Curve_length_skewness	0.07+/-0.4(29)	0.58+/-0.8(15)	0.25+/-0.6(44)	0.007
c3_PR_Atrial_rbio6.8_sc5_Energy_skewness	0.59+/-0.6(26)	1.75+/-1.8(14)	1.00+/-1.3(40)	0.004
c2_RP_Atrial_rbio6.8_sc9_Mean_Freq_kurtosis	4.38+/-2.6(27)	9.74+/-7.9(14)	6.21+/-5.6(41)	0.002
c2_RP_Atrial_rbio6.8_sc9_Median_Freq_kurtosis	3.96+/-3.1(27)	10.70+/-9.0(14)	6.26+/-6.5(41)	0.001
c2_PR_Chest_rbio6.8_sc9_Mean_Freq_std	1.25+/-0.8(27)	0.61+/-0.4(14)	1.03+/-0.8(41)	0.009
c3_PP_Atrial_rbio6.8_sc9_Mean_Freq_min	7.20+/-0.8(29)	6.32+/-0.9(15)	6.90+/-0.9(44)	0.002
c3_RP_Atrial_rbio6.8_sc9_Mean_Freq_min	7.12+/-1.0(26)	6.13+/-1.1(14)	6.77+/-1.1(40)	0.005
c3_RP_Atrial_rbio6.8_sc9_Mean_Freq_mean	10.64+/-2.0(26)	8.84+/-1.6(14)	10.01+/-2.1(40)	0.006
c1_RP_Atrial_rbio6.8_sc13_Peak_Freq_min	3.24+/-1.0(25)	4.14+/-0.8(14)	3.56+/-1.0(39)	0.007
c1_PR_Atrial_rbio6.8_sc13_Curve_length_skewness	0.70+/-1.2(25)	-0.81+/-1.9(14)	0.16+/-1.6(39)	0.004
c4_PR_Chest_rbio6.8_sc13_Shannon_Entropy_kurtosis	3.89+/-3.2(22)	11.47+/-11.8(13)	6.70+/-8.3(35)	0.007
c1_RP_Atrial_rbio6.8_sc17_Mean_Freq_min	3.89+/-0.9(25)	4.71+/-0.9(14)	4.19+/-1.0(39)	0.010
c1_PR_Atrial_rbio6.8_sc17_Nonlinear_Energy_skewness	0.83+/-1.3(25)	-0.39+/-1.1(14)	0.39+/-1.4(39)	0.006
c1_PR_Atrial_rbio6.8_sc17_Curve_length_skewness	0.53+/-1.0(25)	-0.80+/-1.6(14)	0.05+/-1.4(39)	0.003
c2_PR_Atrial_rbio6.8_sc17_Peak_Freq_kurtosis	10.91+/-14.4(25)	51.14+/-53.6(14)	25.35+/-38.7(39)	0.001
c1_PR_Atrial_rbio6.8_sc21_Nonlinear_Energy_skewness	0.73+/-1.0(25)	-0.31+/-1.0(14)	0.35+/-1.1(39)	0.004
c1_PR_Atrial_rbio6.8_sc21_Curve_length_skewness	0.32+/-0.8(25)	-0.73+/-1.3(14)	-0.06+/-1.2(39)	0.005
c2_PR_Chest_rbio6.8_sc21_Median_Freq_min	4.41+/-0.9(27)	6.06+/-2.4(14)	4.97+/-1.8(41)	0.003
c1_PP_Atrial_rbio6.8_sc25_Mean_Freq_skewness	0.24+/-2.0(28)	3.89+/-6.0(15)	1.51+/-4.2(43)	0.005
c1_PR_Atrial_rbio6.8_sc25_Nonlinear_Energy_skewness	0.74+/-1.1(25)	-0.24+/-0.9(14)	0.39+/-1.1(39)	0.008
c2_RP_Atrial_rbio6.8_sc25_Shannon_Entropy_std	0.04+/-0.0(27)	0.02+/-0.0(14)	0.04+/-0.0(41)	0.007
c2_RP_Atrial_gaus1_sc2_Shannon_Entropy_skewness	0.41+/-1.1(27)	-0.82+/-1.4(14)	-0.01+/-1.3(41)	0.004
c2_PR_Chest_gaus1_sc2_Mean_Freq_min	4.47+/-2.0(27)	8.72+/-4.7(14)	5.92+/-3.7(41)	0.000
c2_PR_Chest_gaus1_sc2_Median_Freq_min	6.91+/-3.6(27)	11.56+/-6.3(14)	8.50+/-5.1(41)	0.004
c2_PR_Chest_gaus1_sc2_Peak_Freq_mean	4.83+/-2.6(27)	7.44+/-3.0(14)	5.72+/-3.0(41)	0.007
c3_PP_Atrial_gaus1_sc2_Energy_skewness	0.34+/-0.6(29)	1.58+/-1.7(15)	0.76+/-1.3(44)	0.001
c3_PP_Atrial_gaus1_sc2_Energy_kurtosis	3.80+/-2.1(29)	15.92+/-19.8(15)	7.93+/-12.8(44)	0.002
c3_PP_Atrial_gaus1_sc2_Katz_FD_skewness	0.43+/-0.4(29)	1.50+/-1.8(15)	0.79+/-1.2(44)	0.003
c3_PP_Atrial_gaus1_sc2_Nonlinear_Energy_skewness	0.40+/-0.4(29)	1.46+/-1.9(15)	0.76+/-1.2(44)	0.005
c3_PP_Atrial_gaus1_sc2_Curve_length_skewness	0.10+/-0.4(29)	0.67+/-0.9(15)	0.30+/-0.7(44)	0.006
c3_PR_Atrial_gaus1_sc2_Median_Freq_skewness	0.15+/-0.8(26)	2.55+/-3.4(14)	0.99+/-2.3(40)	0.001
c3_PR_Atrial_gaus1_sc2_Median_Freq_kurtosis	4.42+/-2.7(26)	31.25+/-50.7(14)	13.81+/-32.1(40)	0.010
c1_PR_Atrial_gaus1_sc4_Curve_length_skewness	0.42+/-0.9(25)	-0.81+/-1.9(14)	-0.02+/-1.5(39)	0.009
c3_PP_Atrial_gaus1_sc4_Curve_length_kurtosis	4.10+/-2.2(29)	12.88+/-16.0(15)	7.10+/-10.2(44)	0.005
c4_PR_Atrial_gaus1_sc4_Peak_Freq_kurtosis	4.70+/-7.2(20)	21.63+/-24.5(13)	11.37+/-18.1(33)	0.007
c1_PP_Atrial_gaus1_sc6_Median_Freq_kurtosis	4.16+/-2.9(28)	12.56+/-14.5(15)	7.09+/-9.6(43)	0.005
c1_PR_Atrial_gaus1_sc6_Nonlinear_Energy_skewness	0.70+/-1.3(25)	-0.49+/-1.2(14)	0.28+/-1.4(39)	0.010
c3_PR_Chest_gaus1_sc6_Peak_Freq_mean	4.99+/-3.3(26)	1.99+/-2.4(14)	3.94+/-3.3(40)	0.005
c3_PR_Chest_gaus1_sc6_Peak_Freq_skewness	-0.74+/-3.5(26)	4.30+/-7.6(14)	1.02+/-5.8(40)	0.007
c4_PR_Chest_gaus1_sc6_Peak_Freq_mean	5.12+/-3.1(22)	1.71+/-2.4(13)	3.85+/-3.3(35)	0.002
c2_PR_Chest_gaus1_sc8_Peak_Freq_mean	3.02+/-2.3(27)	0.95+/-1.3(14)	2.31+/-2.2(41)	0.003
c2_PR_Chest_gaus1_sc8_Peak_Freq_skewness	-0.36+/-3.9(24)	4.56+/-6.3(11)	1.19+/-5.2(35)	0.007
c3_PR_Chest_gaus1_sc8_Katz_FD_skewness	0.65+/-1.1(26)	2.17+/-1.8(14)	1.18+/-1.5(40)	0.002
c3_PR_Chest_gaus1_sc8_Katz_FD_kurtosis	7.67+/-9.5(26)	20.20+/-15.8(14)	12.06+/-13.3(40)	0.003
c4_PR_Chest_gaus1_sc8_Peak_Freq_kurtosis	31.81+/-45.9(18)	159.37+/-183.0(8)	71.06+/-120.0(26)	0.009
c3_PR_Chest_gaus1_sc10_Energy_skewness	0.67+/-1.0(26)	2.36+/-2.2(14)	1.26+/-1.7(40)	0.002
c3_PR_Chest_gaus1_sc10_Energy_kurtosis	5.64+/-4.5(26)	21.53+/-26.0(14)	11.20+/-17.3(40)	0.004
c3_PR_Chest_gaus1_sc10_Spectral_entropy_kurtosis	4.82+/-2.7(26)	8.53+/-4.9(14)	6.12+/-4.0(40)	0.004
c3_PR_Chest_gaus1_sc10_Shannon_Entropy_skewness	0.12+/-1.7(26)	-2.42+/-3.5(14)	-0.77+/-2.7(40)	0.003
c4_PP_Atrial_gaus1_sc10_Spectral_entropy_max	3.71+/-2.8(24)	6.89+/-3.9(14)	4.88+/-3.5(38)	0.006
c3_PR_Atrial_gaus1_sc12_Median_Freq_skewness	0.18+/-1.5(26)	1.89+/-2.3(14)	0.77+/-2.0(40)	0.007
c3_PR_Atrial_gaus1_sc12_Median_Freq_kurtosis	5.64+/-5.2(26)	17.34+/-19.2(14)	9.73+/-13.1(40)	0.005
c3_PR_Chest_gaus1_sc12_Energy_skewness	0.76+/-0.9(26)	2.58+/-2.4(14)	1.40+/-1.8(40)	0.001
c3_PR_Chest_gaus1_sc12_Energy_kurtosis	5.39+/-3.3(26)	24.93+/-34.6(14)	12.23+/-22.2(40)	0.006
c4_PP_Atrial_gaus1_sc12_Spectral_entropy_max	4.14+/-3.0(24)	7.42+/-3.8(14)	5.35+/-3.6(38)	0.006
c4_RP_Atrial_gaus1_sc12_Spectral_entropy_max	2.85+/-2.9(22)	6.06+/-3.6(13)	4.04+/-3.5(35)	0.007
c4_RP_Atrial_gaus1_sc12_Spectral_entropy_std	0.29+/-0.3(22)	0.66+/-0.5(13)	0.43+/-0.4(35)	0.005
c4_PR_Chest_gaus1_sc12_Mean_Freq_kurtosis	5.42+/-6.2(22)	14.31+/-11.9(13)	8.72+/-9.6(35)	0.006
c4_PR_Chest_gaus1_sc12_Shannon_Entropy_skewness	-0.48+/-1.2(22)	-2.47+/-2.8(13)	-1.22+/-2.2(35)	0.007
c2_RP_Atrial_gaus2_sc4_Median_Freq_kurtosis	3.38+/-1.7(27)	6.07+/-3.9(14)	4.30+/-2.9(41)	0.003
c2_RP_Atrial_gaus2_sc4_Peak_Freq_skewness	0.72+/-1.4(27)	2.60+/-2.7(14)	1.36+/-2.1(41)	0.006
c4_PP_Atrial_gaus2_sc4_Peak_Freq_min	1.85+/-1.6(24)	0.43+/-0.7(14)	1.33+/-1.5(38)	0.004
c1_PR_Atrial_gaus2_sc7_Curve_length_skewness	0.63+/-1.3(25)	-0.88+/-1.7(14)	0.09+/-1.6(39)	0.003
c3_PP_Atrial_gaus2_sc7_Peak_Freq_mean	3.16+/-1.6(29)	1.91+/-1.0(15)	2.73+/-1.5(44)	0.009
c3_RP_Atrial_gaus2_sc7_Peak_Freq_mean	2.59+/-1.8(26)	1.12+/-1.0(14)	2.08+/-1.7(40)	0.008
c4_PP_Atrial_gaus2_sc7_Peak_Freq_mean	3.30+/-1.4(24)	2.09+/-1.1(14)	2.86+/-1.4(38)	0.010
c4_RP_Atrial_gaus2_sc7_Peak_Freq_mean	2.94+/-1.8(22)	1.28+/-1.4(13)	2.33+/-1.8(35)	0.008
c4_PR_Atrial_gaus2_sc7_Peak_Freq_max	7.61+/-4.2(22)	3.73+/-3.5(13)	6.17+/-4.4(35)	0.009
c1_PR_Atrial_gaus2_sc10_Nonlinear_Energy_skewness	0.72+/-1.1(25)	-0.28+/-1.0(14)	0.36+/-1.2(39)	0.008
c2_PR_Chest_gaus2_sc10_Median_Freq_min	4.28+/-1.1(27)	6.30+/-2.8(14)	4.97+/-2.1(41)	0.002
c4_PP_Atrial_gaus2_sc10_Peak_Freq_mean	2.44+/-1.1(24)	1.30+/-0.9(14)	2.02+/-1.2(38)	0.002
c4_RP_Atrial_gaus2_sc10_Peak_Freq_max	5.45+/-2.8(22)	2.73+/-2.4(13)	4.44+/-3.0(35)	0.006
c4_RP_Atrial_gaus2_sc10_Peak_Freq_mean	2.38+/-1.6(22)	0.89+/-1.1(13)	1.82+/-1.6(35)	0.007
c4_PP_Atrial_gaus2_sc13_Peak_Freq_mean	2.05+/-1.0(24)	1.14+/-0.8(14)	1.72+/-1.0(38)	0.007
c4_PR_Chest_gaus2_sc13_Peak_Freq_min	0.59+/-1.5(22)	2.65+/-2.7(13)	1.36+/-2.2(35)	0.006
c1_PR_Atrial_gaus2_sc19_Peak_Freq_skewness	3.14+/-6.5(16)	-5.41+/-4.8(6)	0.81+/-7.1(22)	0.008
c2_PR_Chest_gaus2_sc19_Mean_Freq_min	3.14+/-1.5(27)	4.61+/-1.7(14)	3.64+/-1.7(41)	0.008
c2_PR_Chest_gaus2_sc19_Median_Freq_min	4.12+/-2.8(27)	6.78+/-3.3(14)	5.03+/-3.2(41)	0.010
c1_RP_Atrial_gaus3_sc4_Shannon_Entropy_max	0.32+/-0.0(25)	0.26+/-0.1(14)	0.30+/-0.1(39)	0.010
c2_PP_Atrial_gaus3_sc4_Mean_Freq_kurtosis	2.79+/-0.8(29)	6.29+/-6.9(15)	3.98+/-4.3(44)	0.010
c2_PP_Atrial_gaus3_sc4_Median_Freq_kurtosis	2.85+/-1.3(29)	6.19+/-6.2(15)	3.99+/-4.0(44)	0.008
c2_RP_Atrial_gaus3_sc4_Mean_Freq_kurtosis	2.73+/-0.8(27)	7.56+/-8.2(14)	4.38+/-5.3(41)	0.004

c2_RP_Atrial_gaus3_sc4_Median_Freq_kurtosis	2.77+/-1.1(27)	6.52+/-6.2(14)	4.05+/-4.0(41)	0.003
c3_PP_Atrial_gaus3_sc4_Peak_Freq_min	4.86+/-2.0(29)	2.90+/-2.1(15)	4.19+/-2.2(44)	0.005
c1_RP_Atrial_gaus3_sc7_Mean_Freq_max	11.11+/-2.8(25)	8.58+/-2.2(14)	10.20+/-2.9(39)	0.006
c1_RP_Atrial_gaus3_sc7_Median_Freq_max	15.00+/-4.1(25)	11.57+/-2.9(14)	13.77+/-4.0(39)	0.009
c2_PR_Atrial_gaus3_sc7_Mean_Freq_mean	7.69+/-1.6(27)	6.18+/-1.0(14)	7.17+/-1.6(41)	0.003
c2_PR_Atrial_gaus3_sc7_Peak_Freq_mean	6.90+/-1.3(27)	5.21+/-1.0(14)	6.32+/-1.5(41)	0.000
c3_PR_Atrial_gaus3_sc7_Mean_Freq_kurtosis	5.91+/-5.4(26)	27.34+/-35.8(14)	13.41+/-23.5(40)	0.004
c1_RP_Atrial_gaus3_sc10_Shannon_Entropy_skewness	0.13+/-2.0(25)	-3.17+/-5.3(14)	-1.06+/-3.8(39)	0.008
c1_PR_Atrial_gaus3_sc10_Nonlinear_Energy_skewness	0.73+/-1.0(25)	-0.39+/-1.1(14)	0.33+/-1.2(39)	0.003
c1_PR_Atrial_gaus3_sc10_Curve_length_skewness	0.28+/-0.8(25)	-0.63+/-1.2(14)	-0.05+/-1.0(39)	0.008
c1_RP_Atrial_gaus3_sc13_Mean_Freq_min	3.29+/-1.1(25)	4.61+/-1.3(14)	3.77+/-1.3(39)	0.002
c1_RP_Atrial_gaus3_sc13_Median_Freq_min	4.25+/-1.8(25)	6.66+/-2.5(14)	5.11+/-2.3(39)	0.001
c1_PR_Atrial_gaus3_sc13_Nonlinear_Energy_skewness	0.67+/-1.0(25)	-0.26+/-1.0(14)	0.34+/-1.1(39)	0.010
c3_PR_Chest_gaus3_sc13_Katz_FD_skewness	0.51+/-1.0(26)	2.35+/-2.4(14)	1.15+/-1.8(40)	0.001
c3_PR_Chest_gaus3_sc13_Katz_FD_kurtosis	6.25+/-6.5(26)	22.30+/-24.7(14)	11.87+/-17.0(40)	0.003
c3_PR_Chest_gaus3_sc13_Shannon_Entropy_skewness	0.18+/-2.0(26)	-2.07+/-3.1(14)	-0.61+/-2.6(40)	0.008
c1_RP_Atrial_gaus3_sc16_Median_Freq_min	3.74+/-2.1(25)	5.74+/-2.0(14)	4.46+/-2.2(39)	0.006
c1_RP_Atrial_gaus3_sc16_Peak_Freq_min	0.96+/-1.0(25)	2.07+/-1.4(14)	1.36+/-1.3(39)	0.008
c4_PP_Atrial_gaus3_sc16_Median_Freq_mean	4.29+/-1.2(24)	5.65+/-1.4(14)	4.79+/-1.4(38)	0.004
c1_PP_Atrial_gaus3_sc19_Peak_Freq_skewness	-0.30+/-2.6(26)	-4.95+/-6.6(15)	-2.00+/-4.9(41)	0.003
c1_RP_Atrial_gaus3_sc19_Mean_Freq_min	2.46+/-0.8(25)	3.30+/-1.0(14)	2.76+/-1.0(39)	0.007
c1_PR_Chest_gaus3_sc19_Median_Freq_kurtosis	5.44+/-4.1(25)	13.03+/-11.6(14)	8.16+/-8.4(39)	0.005
c3_PR_Atrial_gaus3_sc19_Median_Freq_skewness	0.03+/-1.5(26)	1.72+/-2.2(14)	0.62+/-1.9(40)	0.006
c3_PR_Atrial_gaus3_sc19_Median_Freq_kurtosis	5.52+/-5.3(26)	16.45+/-16.6(14)	9.34+/-11.7(40)	0.004
c3_PR_Chest_gaus3_sc19_Spectral_entropy_kurtosis	4.39+/-2.0(26)	12.79+/-14.6(14)	7.33+/-9.5(40)	0.006
c4_PP_Atrial_gaus3_sc19_Spectral_entropy_max	3.73+/-2.8(24)	6.64+/-3.5(14)	4.80+/-3.3(38)	0.008
c4_PP_Atrial_gaus3_sc19_Median_Freq_mean	3.78+/-1.2(24)	4.91+/-1.3(14)	4.19+/-1.3(38)	0.009
c4_RP_Atrial_gaus3_sc19_Spectral_entropy_max	2.58+/-2.6(22)	5.36+/-3.2(13)	3.61+/-3.1(35)	0.009
c4_RP_Atrial_gaus3_sc19_Spectral_entropy_std	0.25+/-0.2(22)	0.58+/-0.4(13)	0.37+/-0.4(35)	0.007
c3_PP_Atrial_gaus4_sc4_Katz_FD_skewness	0.36+/-0.6(29)	1.27+/-1.6(15)	0.67+/-1.1(44)	0.007
c3_PP_Atrial_gaus4_sc4_Nonlinear_Energy_skewness	0.37+/-0.6(29)	1.34+/-1.7(15)	0.70+/-1.2(44)	0.008
c1_PR_Atrial_gaus4_sc10_Spectral_entropy_skewness	0.77+/-0.9(25)	-0.10+/-1.0(14)	0.46+/-1.0(39)	0.009
c1_PR_Atrial_gaus4_sc10_Nonlinear_Energy_skewness	0.90+/-1.4(25)	-0.38+/-1.2(14)	0.44+/-1.5(39)	0.007
c1_PR_Atrial_gaus4_sc10_Curve_length_skewness	0.59+/-1.2(25)	-0.82+/-1.7(14)	0.08+/-1.5(39)	0.003
c2_PR_Chest_gaus4_sc10_Shannon_Entropy_skewness	-1.40+/-2.2(27)	0.83+/-2.7(14)	-0.64+/-2.5(41)	0.006
c1_PR_Atrial_gaus4_sc13_Nonlinear_Energy_skewness	0.72+/-1.0(25)	-0.26+/-0.9(14)	0.37+/-1.1(39)	0.004
c1_PR_Atrial_gaus4_sc13_Curve_length_skewness	0.33+/-0.8(25)	-0.72+/-1.3(14)	-0.04+/-1.1(39)	0.004
c2_PR_Chest_gaus4_sc13_Median_Freq_min	4.30+/-0.6(27)	5.83+/-2.3(14)	4.82+/-1.6(41)	0.002
c1_PP_Atrial_gaus4_sc16_Mean_Freq_skewness	0.05+/-1.8(28)	2.82+/-4.8(15)	1.02+/-3.4(43)	0.010
c2_RP_Atrial_gaus4_sc16_Shannon_Entropy_skewness	-0.26+/-1.3(27)	-2.44+/-3.6(14)	-1.01+/-2.5(41)	0.008
c2_RP_Atrial_gaus4_sc16_Shannon_Entropy_kurtosis	4.04+/-3.1(27)	26.32+/-41.9(14)	11.65+/-26.3(41)	0.008
c2_RP_Atrial_gaus4_sc19_Shannon_Entropy_skewness	0.02+/-1.7(27)	-2.55+/-3.5(14)	-0.85+/-2.7(41)	0.003
c2_PR_Chest_gaus4_sc19_Median_Freq_std	1.23+/-0.7(27)	0.66+/-0.5(14)	1.04+/-0.7(41)	0.009
c2_RP_Atrial_mexh_sc3_Median_Freq_kurtosis	3.26+/-1.5(27)	6.24+/-3.9(14)	4.28+/-2.9(41)	0.001
c2_RP_Atrial_mexh_sc3_Peak_Freq_skewness	0.81+/-1.4(27)	2.71+/-2.9(14)	1.46+/-2.2(41)	0.007
c2_PR_Chest_mexh_sc3_Nonlinear_Energy_mean	0.00+/-0.0(26)	0.00+/-0.0(14)	0.00+/-0.0(40)	0.010
c4_PP_Atrial_mexh_sc3_Peak_Freq_min	1.79+/-1.3(24)	0.43+/-0.7(14)	1.29+/-1.3(38)	0.001
c1_PR_Atrial_mexh_sc5_Nonlinear_Energy_skewness	0.77+/-1.4(25)	-0.52+/-1.3(14)	0.31+/-1.5(39)	0.007
c1_PR_Atrial_mexh_sc5_Curve_length_skewness	0.63+/-1.3(25)	-0.87+/-1.7(14)	0.09+/-1.6(39)	0.003
c3_PP_Atrial_mexh_sc5_Peak_Freq_mean	3.14+/-1.6(29)	1.90+/-1.0(15)	2.72+/-1.5(44)	0.009
c3_RP_Atrial_mexh_sc5_Peak_Freq_mean	2.58+/-1.8(26)	1.12+/-1.0(14)	2.07+/-1.7(40)	0.008
c4_PP_Atrial_mexh_sc5_Peak_Freq_mean	3.26+/-1.4(24)	2.07+/-1.1(14)	2.82+/-1.4(38)	0.009
c4_RP_Atrial_mexh_sc5_Peak_Freq_mean	2.92+/-1.8(22)	1.27+/-1.4(13)	2.31+/-1.8(35)	0.008
c4_PR_Atrial_mexh_sc5_Peak_Freq_max	7.61+/-4.2(22)	3.65+/-3.6(13)	6.14+/-4.4(35)	0.008
c1_PR_Atrial_mexh_sc7_Nonlinear_Energy_skewness	0.75+/-1.1(25)	-0.27+/-1.1(14)	0.38+/-1.2(39)	0.008
c2_PR_Chest_mexh_sc7_Median_Freq_min	4.31+/-1.1(27)	6.34+/-3.0(14)	5.00+/-2.1(41)	0.003
c4_PP_Atrial_mexh_sc7_Peak_Freq_mean	2.46+/-1.1(24)	1.32+/-0.9(14)	2.04+/-1.2(38)	0.002
c4_RP_Atrial_mexh_sc7_Peak_Freq_max	5.59+/-3.1(22)	2.73+/-2.4(13)	4.53+/-3.2(35)	0.007
c4_RP_Atrial_mexh_sc7_Peak_Freq_mean	2.39+/-1.6(22)	0.90+/-1.2(13)	1.84+/-1.6(35)	0.007
c2_PP_Atrial_mexh_sc9_Shannon_Entropy_kurtosis	5.03+/-3.1(29)	17.72+/-22.7(15)	9.36+/-14.5(44)	0.005
c3_PR_Atrial_mexh_sc9_Median_Freq_kurtosis	5.87+/-8.3(26)	22.15+/-28.4(14)	11.57+/-19.3(40)	0.009
c4_PP_Atrial_mexh_sc9_Peak_Freq_mean	2.08+/-1.0(24)	1.13+/-0.8(14)	1.73+/-1.0(38)	0.006
c1_PR_Atrial_mexh_sc13_Peak_Freq_skewness	2.92+/-6.5(16)	-5.67+/-4.9(6)	0.58+/-7.1(22)	0.008
c2_PR_Chest_mexh_sc13_Mean_Freq_min	3.18+/-1.5(27)	4.64+/-1.6(14)	3.68+/-1.7(41)	0.007

References

1. Steinberg, J.S., *Postoperative atrial fibrillation: a billion-dollar problem.* Journal of the American College of Cardiology, 2004. **43**(6): p. 1001-1003.

2. Villareal, R.P., et al., *Postoperative atrial fibrillation and mortality after coronary artery bypass surgery.* Journal of the American College of Cardiology., 2004. **43**(5): p. 742-8.

3. Hakala, T. and A. Hedman, *Predicting the risk of atrial fibrillation after coronary artery bypass surgery.* Scandinavian Cardiovascular Journal., 2003. **37**(6): p. 309-15.

4. Amar, D., et al., *Clinical prediction rule for atrial fibrillation after coronary artery bypass grafting.* Journal of the American College of Cardiology, 2004. **44**(6): p. 1248-1253.

5. Aranki, S.F., et al., *Predictors of Atrial Fibrillation After Coronary Artery Surgery: Current Trends and Impact on Hospital Resources.* Circulation, 1996. **94**(3): p. 390-397.

6. Auer, J., et al., *Risk factors of postoperative atrial fibrillation after cardiac surgery.* Journal Of Cardiac Surgery, 2005. **20**(5 (Print)): p. 425-431.

7. Barnes, B.J., et al., *Risk-Stratified Evaluation of Amiodarone to Prevent Atrial Fibrillation After Cardiac Surgery.* The Annals of Thoracic Surgery, 2006. **82**(4): p. 1332-1337.

8. Chandy, J., et al., *Increases in P-wave dispersion predict postoperative atrial fibrillation after coronary artery bypass graft surgery.* Anesthesia & Analgesia, 2004. **98**(2): p. 303-10.

9. Chang, C.M., et al., *The role of P wave in prediction of atrial fibrillation after coronary artery surgery.* International Journal of Cardiology, 1999. **68**(3): p. 303-8.

10. Crystal, E., et al., *Interventions on Prevention of Postoperative Atrial Fibrillation in Patients Undergoing Heart Surgery: A Meta-Analysis.* Circulation, 2002. **106**(1): p. 75-80.

11. Dagdelen, S., et al., *The value of P dispersion on predicting atrial fibrillation after coronary artery bypass surgery; effect of magnesium on P dispersion.* 2003: p. 162-4, 2003 Jun.

12. Faggiano, P., et al., *Contribution of left atrial pressure and dimension to signal-averaged P-wave duration in patients with chronic congestive heart failure.* American Journal of Cardiology, 1997. **79**(2): p. 219-22.

13. Funk, M., et al., *Incidence, timing, symptoms, and risk factors for atrial fibrillation after cardiac surgery.* American Journal of Critical Care: An Official Publication, American Association of Critical-Care Nurses, 2003. **12**(5 (Print)): p. 424.

14. Hogue, C.W., Jr, et al., *RR interval dynamics before atrial fibrillation in patients after coronary artery bypass graft surgery.* Circulation, 1998. **98**(5): p. 429-434.

15. Kern, L.S., *Postoperative atrial fibrillation: new directions in prevention and treatment.* Journal of Cardiovascular Nursing., 2004. **19**(2): p. 103-15.

16. Klein, M., et al., *Use of P-wave-triggered, P-wave signal-averaged electrocardiogram to predict atrial fibrillation after coronary artery bypass surgery.[see comment]*. American Heart Journal, 1995. **129**(5): p. 895-901.

17. Mathew, J.P., et al., *A multicenter risk index for atrial fibrillation after cardiac surgery.* JAMA, 2004. **291**(14): p. 1720-1729.

18. Osranek, M., et al., *Left Atrial Volume Predicts the Risk of Atrial Fibrillation After Cardiac Surgery: A Prospective Study.* Journal of the American College of Cardiology, 2006. **48**(4): p. 779-786.

19. Passman, R., et al., *Predicting post-coronary bypass surgery atrial arrhythmias from the preoperative electrocardiogram.* American Heart Journal. 142(5):806-10, 2001 Nov.

20. Poli, S., et al., *Prediction of atrial fibrillation from surface ECG: review of methods and algorithms.* Ann Ist Super Sanità, 2003. **39**(2): p. 195-203.

21. Steinberg, J.S., et al., *Value of the P-wave signal-averaged ECG for predicting atrial fibrillation after cardiac surgery.* Circulation, 1993. **88**(6): p. 2618-22.

22. Zaman, A.G., et al., *Atrial Fibrillation After Coronary Artery Bypass Surgery : A Model for Preoperative Risk Stratification.* Circulation, 2000. **101**(12): p. 1403-1408.

23. Heckerman, D., *A Tutorial on Learning With Bayesian Networks*. 1995, Microsoft Research.

24. Opie, L.H., *Heart physiology : from cell to circulation*. 4th ed, Philadelphia: Lippincott Williams & Wilkins.

25. Malmivuo, J. and R. Plonsey, *Bioelectromagnetism: Principles and Applications of Bioelectric and Biomagnetic Fields*. 1995, New York: Oxford Uiversity Press.

26. DRAPER, H.W., et al., *The Corrected Orthogonal Electrocardiogram and Vectorcardiogram in 510 Normal Men (Frank Lead System).* Circulation, 1964. **30**(6): p. 853-864.

27. Lang, S.A. and M.N. Levy, *Effects of vagus nerve on heart rate and ventricular contractility in chicken.* Am J Physiol Heart Circ Physiol, 1989. **256**(5): p. H1295-1302.

28. Dota, C.D., et al., *Inter- and intraday variability in major electrocardiogram intervals and amplitudes in healthy men and women.* Pacing And Clinical Electrophysiology: PACE, 2003. **26**(1 Pt 2 (Print)): p. 361-366.

29. Willems, J.L., P.F. Poblete, and H.V. Pipberger, *Day-to-day variation of the normal orthogonal electrocardiogram and vectorcardiogram.* Circulation, 1972. **45**(5 (Print)): p. 1057-1064.

30. Feinberg, W.M., et al., *Prevalence, age distribution, and gender of patients with atrial fibrillation. Analysis and implications.* Arch Intern Med, 1995. **155**(5): p. 469-473.

31. Podrid, P.J., Kowey, P. R., *Handbook of Cardiac Arrhythmia*. 1996, Baltimore: Williams and Wilkins.

32. Lake, F.R., et al., *Atrial fibrillation and mortality in an elderly population.* Aust N Z J Med, 1989. **19**(4): p. 321-6.

33. Wolf, P., R. Abbott, and W. Kannel, *Atrial fibrillation as an independent risk factor for stroke: the Framingham Study.* Stroke, 1991. **22**(8): p. 983-988.

34. Psaty, B.M., et al., *Incidence of and Risk Factors for Atrial Fibrillation in Older Adults.* Circulation, 1997. **96**(7): p. 2455-2461.

35. Klein, T., *A user's guide to bypass surgery*. 1996, Athens [Ohio]: Ohio University Press. xxii, 170 p.

36. Ad, N., et al., *Histologic atrial myolysis is associated with atrial fibrillation after cardiac operation.* Ann Thorac Surg, 2001. **72**(3): p. 688-93.

37. Wyse, D.G., et al., *A comparison of rate control and rhythm control in patients with atrial fibrillation.* N Engl J Med, 2002. **347**(23): p. 1825-33.

38. Lee, J.K., et al., *Rate-control versus conversion strategy in postoperative atrial fibrillation: trial design and pilot study results.* Card Electrophysiol Rev, 2003. **7**(2): p. 178-84.

39. McKeown, P.P. and D. Gutterman, *Executive Summary: American College of Chest Physicians Guidelines for the Prevention and Management of*

Postoperative Atrial Fibrillation After Cardiac Surgery.. CHEST, 2005. **128**: p. 1S-5S.

40. Weber, U.K., et al., *Selective versus non-selective antiarrhythmic approach for prevention of atrial fibrillation after coronary surgery: is there a need for pre-operative risk stratification?: A prospective placebo-controlled study using low-dose sotalol.* Eur Heart J, 1998. **19**(5): p. 794-800.

41. Shantsila, E., T. Watson, and G.Y.H. Lip, *Atrial fibrillation post-cardiac surgery: changing perspectives.* Current Medical Research And Opinion, 2006. **22**(8 (Print)): p. 1437-1441.

42. Zacharias, A., et al., *Obesity and risk of new-onset atrial fibrillation after cardiac surgery.* Circulation, 2005. **112**(21 (Electronic)): p. 3247-3255.

43. Lamm, G., et al., *Postoperative white blood cell count predicts atrial fibrillation after cardiac surgery.* Journal Of Cardiothoracic And Vascular Anesthesia, 2006. **20**(1 (Print)): p. 51-56.

44. Leitch, J.W., et al., *The importance of age as a predictor of atrial fibrillation and flutter after coronary artery bypass grafting.* J Thorac Cardiovasc Surg, 1990. **100**(3): p. 338-42.

45. Andrikopoulos, G.K., et al., *Increased variance of P wave duration on the electrocardiogram distinguishes patients with idiopathic paroxysmal atrial fibrillation.* Pacing & Clinical Electrophysiology, 2000. **23**(7): p. 1127-32.

46. Buxton, A.E. and M.E. Josephson, *The role of P wave duration as a predictor of postoperative atrial arrhythmias.* Chest, 1981. **80**(1): p. 68-73.

47. Fukunami, M., et al., *Detection of patients at risk for paroxysmal atrial fibrillation during sinus rhythm by P wave-triggered signal-averaged electrocardiogram.[see comment]*. Circulation, 1991. **83**(1): p. 162-9.

48. Hopkins, C.B. and O. Barrett, Jr., *Electrocardiographic diagnosis of left atrial enlargement. Role of the P terminal force in lead V1.* Journal of Electrocardiology, 1989. **22**(4): p. 359-63.

49. Stafford, P., P. Denbigh, and R. Vincent, *Frequency analysis of the P wave: comparative techniques.* Pacing & Clinical Electrophysiology, 1995. **18**(2): p. 261-70.

50. Stafford, P.J., et al., *Reproducibility of the signal averaged P wave: time and frequency domain analysis.* Heart, 1997. **77**(5): p. 412-6.

51. Stafford, P.J., et al., *Signal averaged P wave compared with standard electrocardiography or echocardiography for prediction of atrial fibrillation after coronary bypass grafting.* Heart, 1997. **77**(5): p. 417-22.

52. Stafford, P.J., I. Turner, and R. Vincent, *Quantitative analysis of signal-averaged P waves in idiopathic paroxysmal atrial fibrillation.* American Journal of Cardiology, 1991. **68**(8): p. 751-5.

53. Tukek, T., et al., *Effect of left atrial size and function on P-wave dispersion: a study in patients with paroxysmal atrial fibrillation.* Clinical Cardiology, 2001. **24**(10): p. 676-80.

54. Vassilikos, V., et al., *Can P wave wavelet analysis predict atrial fibrillation after coronary artery bypass grafting?* Pacing & Clinical Electrophysiology, 2003. **26**(1): p. 305-9, 2003 Jan.

55. Kolb, C., et al., *Modes of initiation of paroxysmal atrial fibrillation from analysis of spontaneously occurring episodes using a 12-lead Holter monitoring system.* American Journal of Cardiology, 2001. **88**(8): p. 853-7.

56. Maier, C., M. Bauch, and H. Dickhaus. *Screening and prediction of paroxysmal atrial fibrillation by analysis of heart rate variability parameters*. in *Computers in Cardiology 2001*. 2001.

57. Vikman, S., et al., *Altered complexity and correlation properties of R-R interval dynamics before the spontaneous onset of paroxysmal atrial fibrillation.* Circulation, 1999. **100**(20): p. 2079-84.

58. Bollmann, A., et al., *Frequency analysis of human atrial fibrillation using the surface electrocardiogram and its response to ibutilide.* American Journal of Cardiology, 1998. **81**(12): p. 1439-45.

59. Bollmann, A., et al., *Non-invasive assessment of fibrillatory activity in patients with paroxysmal and persistent atrial fibrillation using the Holter ECG.* Cardiovascular Research, 1999. **44**(1): p. 60-6.

60. Fogel, L.J., O.A. J., and M.J. Walsh, *Artificial intelligence through simulated evolution*. 1966, New York: Wiley.

61. Goldberg, D.E., *Genetic Algorithm in Search, Optimization and Machine Learning*. 1989, Reading, MA: Addison-Wesley.

62. Holland, J.H., *Genetic algorithms.* Scientific American, 1992. **267**: p. 66-72.

63. Haupt, R.L. and S.E. Haupt, *Practical Genetic Algorithms*. 1998, New York, NY: John Wiley & Sons, Inc.

64. Wang, X.-H., et al., *Computer-assisted diagnosis of breast cancer using a data-driven Bayesian belief network.* International Journal of Medical Informatics, 1999. **54**(2): p. 115-126.

65. Neapolitan, R., *Learning Bayesian Networks*. 2004, London: Pearson Printice Hall.

66. Krishnapuram, B., et al., *A Bayesian approach to joint feature selection and classifier design.* Pattern Analysis and Machine Intelligence, IEEE Transactions on, 2004. **26**(9): p. 1105-1111.

67. Bressan, M. and J. Vitria, *On the selection and classification of independent features.* Pattern Analysis and Machine Intelligence, IEEE Transactions on, 2003. **25**(10): p. 1312-1317.

68. Larranaga, P., et al., *Structure learning of Bayesian networks by genetic algorithms: a performance analysis of control parameters.* IEEE Transactions on Pattern Analysis and Machine Intelligence, 1996. **18**(9): p. 912-26.

69. Domingos, P. and M. Pazzani, *On the optimality of the simple Bayesian classifier under zero-one loss.* Machine Learning, 1997. **29**(2-3): p. 103-30.

70. Kahn, C., et al., *Construction of a Bayesian network for mammographic diagnosis of breast cancer.* Comput Biol Med, 1997. **27**(1): p. 19-29.

71. Eisenstein, E.L. and F. Alemi. *A comparison of three techniques for rapid model development: an application in patient risk-stratification*. in *Proceedings of the American Medical Informatics Association Fall Symposium*. 1996.

72. A. Brogini, M.B., D. Slanzi, *Identifying a Bayesian Network for the Problem "Hospitals and Families: The Analysis of Patient Satisfaction with their Stay in Hospital."* in *Applied Bayesian Statistical Studies in Biology and Medicine*, M.D.A. Di Bacco, G. Scalfari, F., Editor. 2004, Kluwer Academic Publishers: Boston. p. 258.

73. Pang, B., et al., *Computerized tongue diagnosis based on Bayesian networks.* Biomedical Engineering, IEEE Transactions on, 2004. **51**(10): p. 1803-1810.

74. *Bayesian Models in Medicine*. in *Proceedings of the European Conference on Artificial Intelligence in Medicine*. 2001. Cascais, Portugal.

75. Zabell, S.L., *W.E. Johnson's 'Sufficientness' Postulate.* The Annals of Statistics, 1982. **10**(4).

76. Altman, D.G., *Practical Statistics for Medical Research* 1991: CRC Press.

77. Metz, C., *Basic principles of ROC analysis.* Semin Nuclear Med 1978. **8**(4): p. 283-298.

78. Swets, J.A., *Measuring the accuracy of diagnostic systems.* Science, 1988. **240**(4857): p. 1285-1293.

79. *Cardiac Surgery Consultants Board Definitions For Collection Form,* http://www1.va.gov/health/cscb/define.htm. 1998, Veterans Health Administration.

80. D'Alessandro, M., et al., *Epileptic seizure prediction using hybrid feature selection over multiple intracranial EEG electrode contacts: a report of four patients.* Biomedical Engineering, IEEE Transactions on, 2003. **50**(5): p. 603-615.

81. Clayton, R.H., A. Murray, and R.W.F. Campbell. *Frequency analysis of self-terminating ventricular fibrillation*. in *Computers in Cardiology 1994*. 1994.

82. Tu, C., Y. Zeng, and X. Yang, *Nonlinear processing and analysis of ECG data.*, in *Technology & Health Care*. 2004, IOS Press. p. 1-9.

83. Gerstenfeld, E.P., et al., *Evaluation of right atrial and biatrial temporary pacing for the prevention of atrial fibrillation after coronary artery bypass surgery.* Journal of the American College of Cardiology, 1999. **33**(7): p. 1981-1988.

84. Gerstenfeld, E.P., et al., *Effectiveness of bi-atrial pacing for reducing atrial fibrillation after coronary artery bypass graft surgery.* Journal of interventional cardiac electrophysiology : an international journal of arrhythmias and pacing, 2001. **5**(3): p. 275-283.

85. Kohler, B.-U., C. Hennig, and R. Orglmeister, *The principles of software QRS detection.* Engineering in Medicine and Biology Magazine, IEEE, 2002. **21**(1): p. 42-57.

86. Laguna, P., G.B. Moody, and R.G. Mark, *Power spectral density of unevenly sampled data by least-square analysis: performance and application to heart rate signals.* Biomedical Engineering, IEEE Transactions on, 1998. **45**(6): p. 698-715.

87. Wiggins, M., et al. *Prediction of Atrial Fibrillation Following Cardiac Surgery Using Rough Set Derived Rules*. in *Proceedings of the 28th Annual International Conference of the IEEE Engineering in Medicine and Biology Society (EMBC '06)*. 2006. New York City, New York, USA.

88. Wiggins, M., et al. *Non-Invasive, Cardiac Risk Stratification Using Wavelet Coefficients*. in *WSEAS Conference and Transaction on Computers*. 2003.

89. Wiggins, M.C., et al., *Electrogram Features are Superior to Clinical Characteristics for Predicting Atrial Fibrillation After Coronary Artery Bypass Graft Surgery.* Journal of the American College of Cardiology (JACC), 2006. **47**(4A): p. 12A-13A.

90. Zhao, L., et al. *Risk Stratification Based on Multiple Features*. in *IEEE International Symposium on Signal Processing and Information Technology*. 2003.

91. Duda, R.O., P.E. Hart, and D.G. Stork. *Pattern Classification* 2000: Wiley-Interscience.

92. Cover, T.M., *The Best Two Independent Measures Are Not the Two Best.* IEEE Transactions on Systems, Man, and Cybernetics, 1974. **SMC-4**(1): p. 116-117.

93. Elashoff, J.D., R.M. Elashoff, and G.E. Goldman, *On the choice of variables in classification problems with dichotomous variables.* Biometrika, 1967. **54**: p. 668-670.

94. Toussaint, G.T., *Note on optimal selection of independent binary-valued features for pattern recognition.* IEEE Transactions on Information Theory, 1971. **IT-17**: p. 618.

95. Theodoridis, S. and K. Koutroumbas, *Pattern Recognition: Third Edition*. 2006: Elsevier.

96. Dawid, P., *Statistical theory. The prequential approach (with discusion).* Journal of the Royal Statistical Society A 1984. **147**: p. 178-292.

97. Houck, C., J. Joines, and M. Kay, *A Genetic Algorithm for Function Optimization: A Matlab Implementation.* NCSU-IE TR, 1995: p. 95-109.

98. Kubat, M. and S. Matwin. *Addressing the Curse of Imbalanced Training Sets: One-Sided Selection*. in *MACHINE LEARNING -INTERNATIONAL WORKSHOP/CONFERENCE*. 1997: MORGAN KAUFMANN PUBLISHERS, INC.

99. True, H.L. and S.L. Lindquist, *A yeast prion provides a mechanism for genetic variation and phenotypic diversity.* Nature, 2000. **407**(6803): p. 477-483.

100. Yamagishi, H., et al., *Impact of Diabetes Mellitus on Worsening of the Left Ventricular Ejection Fraction in Exercise-Gated 201Tl Myocardial Single Photon Emission Computed Tomography in Patients With Coronary Artery Disease.* Circulation, 2003. **67**(10): p. 839-845.